VERY LOW FREQUENCY EMISSIONS FROM THE EXOSPHERE

by R. L. Dowden, M. Sc.

A thesis submitted in fulfillment
of the requirements for the degree of
Doctor of Philosophy
in the University of Tasmania

HOBART
1962

CONTENTS

NOTE: Sections, subsections, and equations are numbered by a "decimal" system according to chapter. Pages, references, figures and tables are numbered serially from the beginning of the thesis.

1. INTRODUCTION

This work describes investigations in a relatively new field: very low frequency radio emissions from the earth's exosphere. It is new in that most of the development has occurred in the last five or six years, though the phenomena has been known for some decades. Two basic types of emissions occur: continuous ("hiss") and discrete. When this work was begun in 1959 comparatively little was known about "hiss", though a considerable amount of information about the discrete emissions was obtained during the I.G.Y. The cause of either of these types was still a mystery, though two theories (shown to be unlikely in this thesis), which seemed to explain some of the features of the discrete emissions, appeared in that year.

The dominant feature of this thesis is the doppler shifted (electron) cyclotron theory, which is shown to explain all types of V.L.F. exospheric emissions. This idea occurred to the author while writing Chapter 4 (review of theories) after all the experimental work and Chapters 2, 4, 5 and 6 had been completed (late 1961). The development of this and other ideas and the general layout of the thesis are given below.

Chapter 1. The present chapter, mainly an outline of the rest of the thesis.

Chapter 2. This brings the reader up to the present state of knowledge of the phenomena. The development of this knowledge is traced from the earliest to the present time. Except for some of the illustrations, the author's contributions have been excluded.

Chapter 3. The author's observations and experimental techniques are presented and discussed in this chapter. Only work on the continuous emissions was performed.

Chapter 4. All the theories proposed (up till about 1961) for the generation of very low frequency emissions as well as some proposed by radio astronomers for high frequency generation are reviewed. The most promising idea seemed to be the travelling wave tube (TWT) process. A new idea suggested itself in discussion of doppler shifted cyclotron radiation from protons. These ideas are developed in later chapters.

Chapter 5. Further development of these ideas first required a model of electron density distributions in the exosphere. A theoretical model based on geomagnetic control is derived in this chapter. Soon after this work was done (1960) experimental confirmation appeared.

Chapter 6. Using this model Gallet's TWT process is treated in the general case and in more detail. It is shown that this process can account for all the relevant characteristics of hiss, though not those of the discrete emissions for which it was originally proposed.

Chapter 7. The idea from Chapter 4, that cyclotron radiation from electrons is permissible if it is shifted down by doppler effect, is developed. It is shown that this process gives the detailed frequency-time characteristics of the discrete emissions. A new emission is predicted.

Chapter 8. Four tests of this electron-cyclotron theory are presented. The most crucial of these was the observation of the

predicted emission with the predicted time characteristics.

Chapter 9. Since the frequency-time characteristics of observed discrete emissions could be accurately matched by suitably choosing the electron parameters (energy, helical pitch, and latitude) it seemed that these parameters could be deduced from observed characteristics. A method of doing this is presented, with examples from published spectrograms of emissions.

Chapter 10. It is shown in this chapter that this electron-cyclotron process can also account for the characteristics of hiss as well as does the TWT process (as developed in Chapter 6). Tests for distinguishing the two theories are proposed.

Chapter 11. A brief resume of the progress achieved is given, further work is suggested, papers published by the author on this work are listed, and acknowledgements are made.

2. HISTORICAL REVIEW

2.1 Introduction

At the audio frequency end of the electromagnetic spectrum there are a number of naturally occurring emissions. These can be heard on a sensitive audio amplifier connected to a large aerial in a quiet site. Two quite distinct classes occur: those produced by lightning discharges ("spherics", "tweeks", and "whistlers"), and those produced (as we will see) in the earth's exosphere by the interaction of fast electrons with the exospheric medium. Only the exospheric emissions will be considered in this work.

There are two, or perhaps three, main types of exospheric emission. The first appears as band limited "white" noise, variously called "hiss", "V.L.F. noise", "geomagnetic noise", and "auroral noise". Spectrograms of hiss are shown in Figures 1, 5 and 8. Amplitude-frequency spectra of hiss are shown in Figure 4A. The second type includes all the "discrete events". Spectrograms of these are shown in Figure 6. The third type, "dawn chorus", is intermediate. Aurally, or on fast spectrograms, chorus appears as a series of short distinct musical tones ("discrete events") often overlapping in time. At times, particularly for some recording devices to be described later, chorus may be indistinguishable from hiss. Spectrograms of chorus are shown in Figure 2.

Exospheric emissions are characterised by association with periods of geomagnetic disturbance and with high geomagnetic latitudes. Audio frequencies are typical but not characteristic. Frequencies as low as 100 c/s and as high as 200 kc/s occur at times.

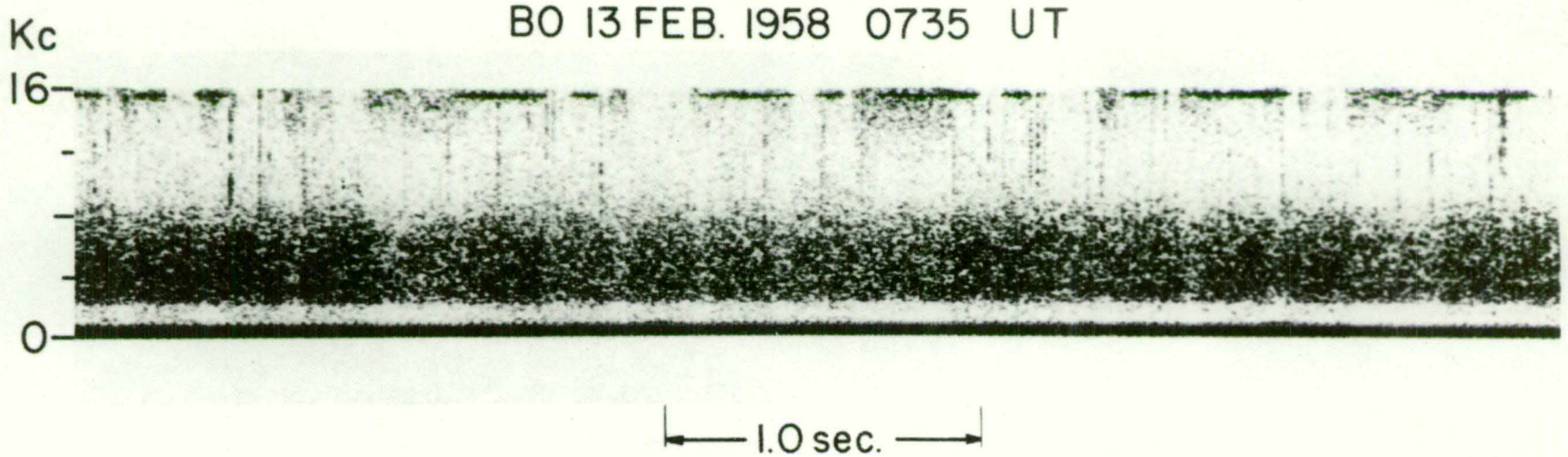

Fig. 1. Spectrogram of hiss recorded at Boulder (after Helliwell and Carpenter [9]).

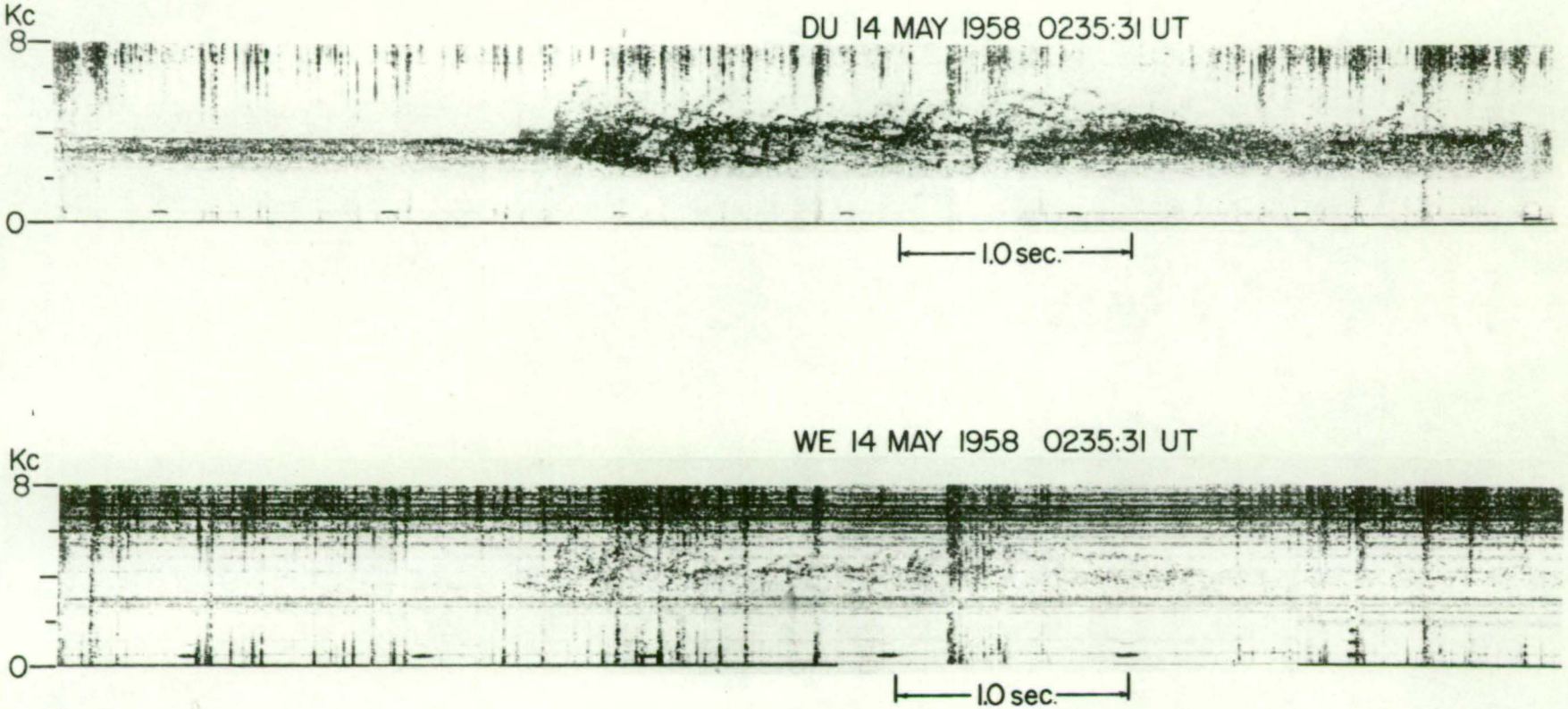

Fig. 2. Spectrograms of dawn chorus recorded simultaneously at Dunedin (DU) and Wellington (WE). (after Helliwell and Carpenter [9]).

2.2 Early Work

Following up observations made by Barkhausen[1] during World War I (which may have included exospheric emissions) Eckersley[2] et al noticed a sound like the warbling of birds. This tended to occur most frequently near dawn and so was named "dawn chorus". Soon after (1933) Burton and Boardman[3] in America observed a "frying sound" which was closely correlated with an auroral display present at the time. This appears to be the first recorded observation of hiss*. In England Eckersley (unpublished, quoted by Storey[4]) also observed hiss, "at a frequency of about 5 kc/s, on a receiver connected to a pair of large direction finding loops and observed that it was coming from a northerly direction".

After this there was little work in this field until Storey[4], who published his work on whistlers in 1953. Storey observed hiss and incidentally used this term. However Storey's main contributions to this field were indirect but much more important. He demonstrated that much higher electron densities existed in the exosphere than were previously thought. Although the densities required for his theory (a few hundred electrons per c.c.) are small by laboratory vacuum standards they made all the difference between empty space and a medium having very interesting properties. By clearing up the mystery of whistlers he opened the door to study of the phenomena not explained by his theory. It seemed likely that these were propagated and guided along magnetic lines of force in the same way as were whistlers, and

---

* In other ways their description seems that of a "swishler" or broad band whistler.

were probably generated in the exosphere. Thus they became known[6] as "exospheric emissions".

Storey further showed that whistlers could be used to probe the exosphere in much the same way as the ionosonde probes the ionosphere. Later discoveries such as the "nose whistler" effect[42,43] and the use of V.L.F. transmitters[44,40] bore this out further. This, and later the extra spur of the IGY-IGC, led a great many workers to begin recording whistlers on magnetic tape. Hiss and other exospheric emissions were automatically recorded on the same tapes. These were later analysed on frequency spectrographs (such as the "sonagraph") along with whistlers (Figures 1 and 2).

2.3 Tape Recorded Observations

Observations made in this way present a view of the phenomena (hiss) somewhat different to those using techniques to be described later on. In view of this, and the fact that over the next five years (from 1953) very few observations were made with these other techniques but a vast amount recorded on magnetic tape (one worker[5] recorded over 350 miles of tape in four years), we consider these observations separately here. All magnetic tape work up to the present time is considered here so that some discoveries after 1958 were preceded by Ellis and his co-workers. Some observations made at a very high latitudes have been left for a later section.

The correlation of hiss and chorus phenomena with magnetic activity was noticed by the early workers mentioned

above and also by Storey[4], Gallet[6] and others[7,8] more recently. Dinger[5] found that hiss and chorus activity was considerably higher during most of 1958 (sunspot maximum) than during corresponding periods in other years. Allcock[7], and Crouchley and Brice[8] showed that chorus is strongly correlated with magnetic disturbance index, though for high latitudes ($\sim 60^{\circ}$ geomagnetic) the latter showed that a "saturation" chorus strength is reached for the magnetic index K~3. For large K, chorus strength actually decreases. Since they also found that chorus strength or occurrence frequency increases with latitude, reaching a peak around G.M. lat. 60° they interpreted this as indicating an equator ward shift of a ten degree wide "chorus zone" with K index. Similar observations covering a greater number of stations were made by Helliwell and Carpenter[9] (Figure 3).

At times of great magnetic activity hiss lasts for a considerable time. Watts[10] at Boulder (G.M. lat. 50°) and Helliwell at Stanford (G.M. lat. 44°) simultaneously observed a "noise storm" lasting 12 hours following a period of $K_p = 7+$. Gallet examined 122 cases of hiss and found an average duration of 1.6 hours though hiss sometimes lasted 10 hours.

From four years of observation Dinger[5] showed that hiss is more common at night with a shallow minimum around noon. A much stronger effect is shown by chorus[2,4,5,7,9]. The maximum occurs around dawn in middle (G.M.) latitudes but occurs progressively later as one observes it at higher latitudes[7,8,12], so that it occurs near noon at about 65° G.M. lat. This is shown in Figure 4.

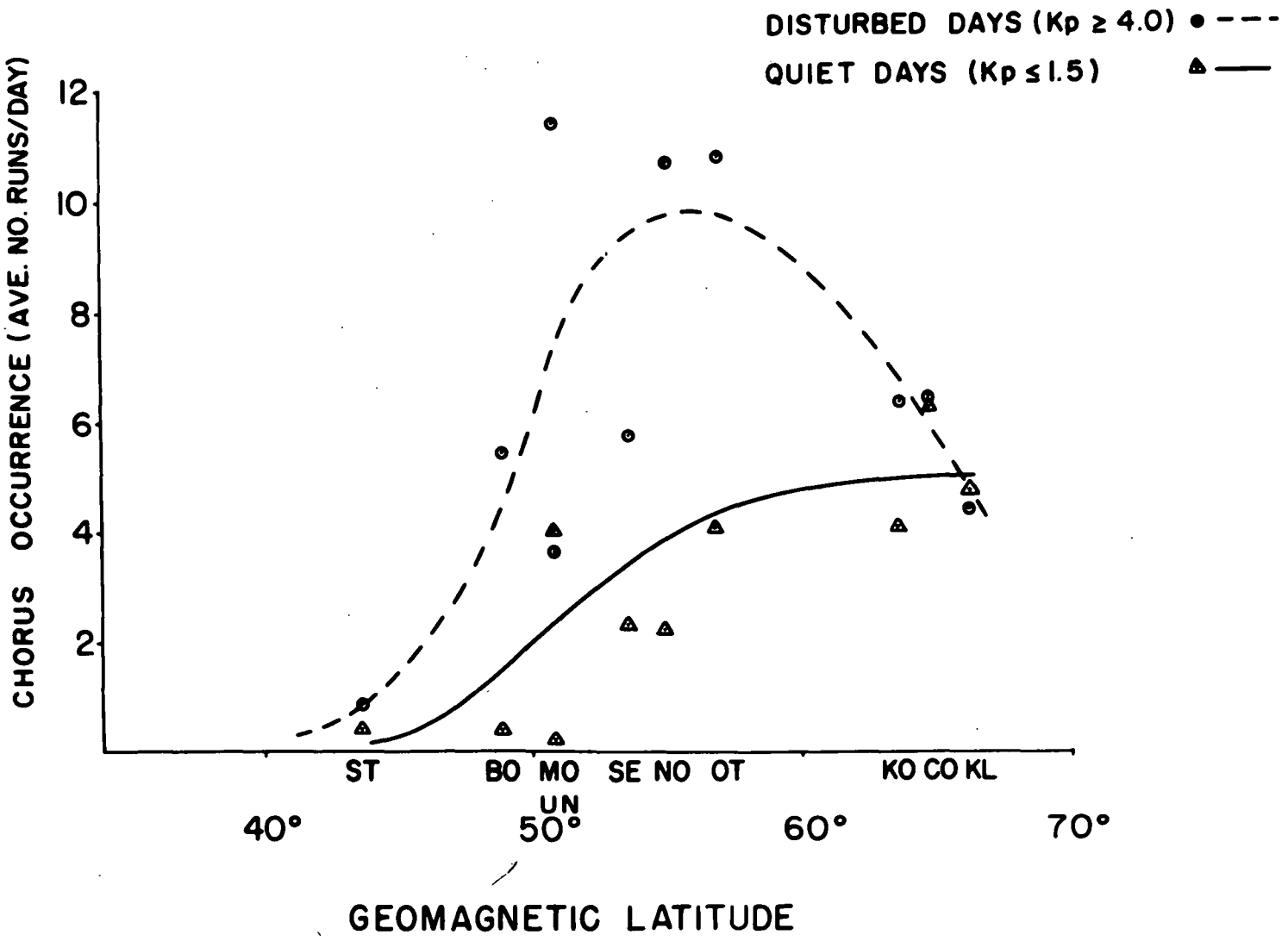

Fig. 3. Variation of chorus occurrence with latitude during magnetically disturbed and quiet periods. (after Helliwell and Carpenter [9]).

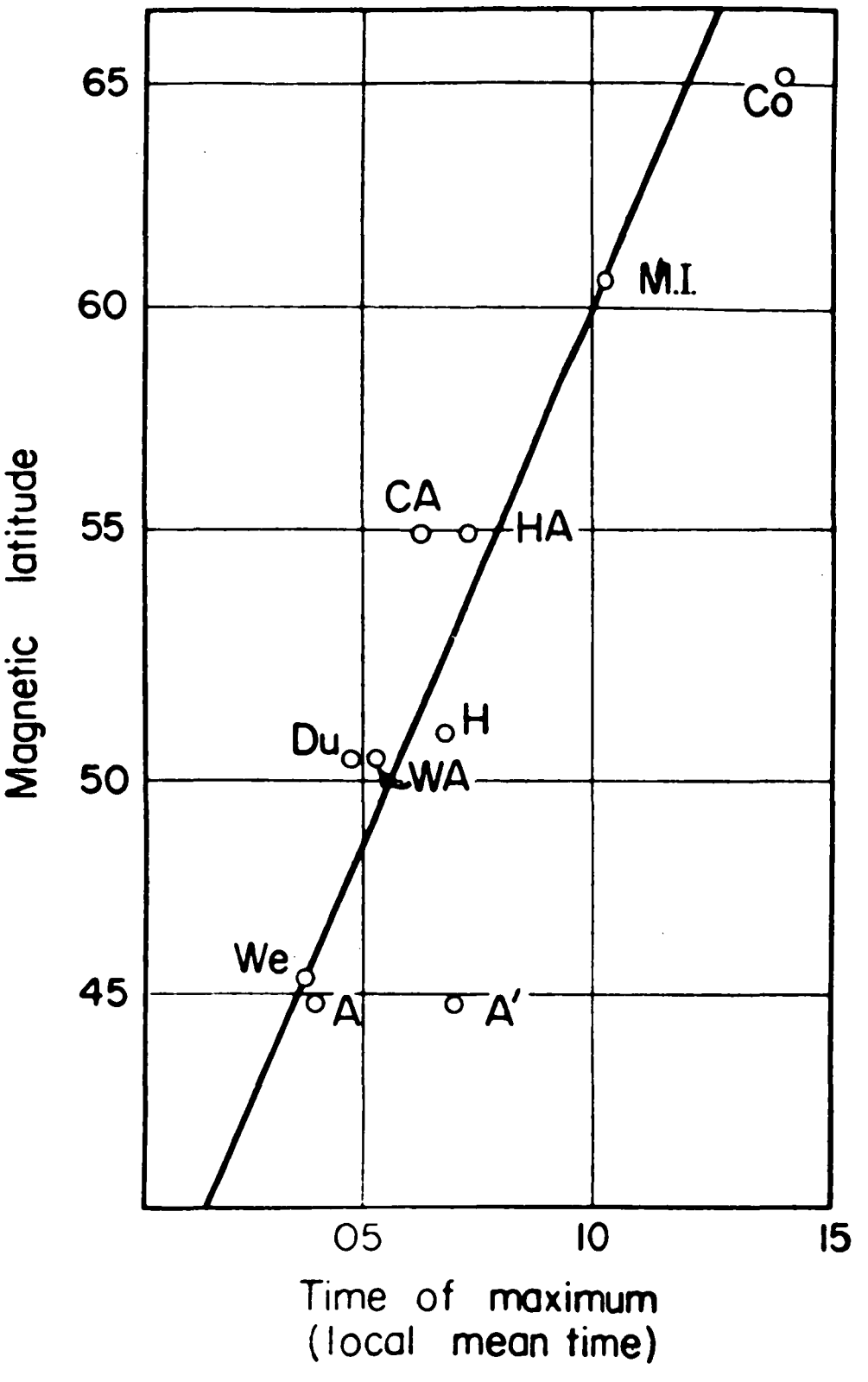

Fig. 4. Variation of time maximum of chorus with geomagnetic latitude. (after Crouchley and Brice [8]).

Allcock[7] finds this in agreement with the hypothesis that chorus signals are initiated by the arrival over the geomagnetic equator of positively charged particles of solar origin.

The noise storm observed by Watts[10] and Helliwell[11] showed a band of hiss from 1 to 10 kc/s. At most times the peak intensity was around 3 kc/s. (Fig. 4A) At times the bandwidth became quite wide (100 c/s to 20 kc/s or so). Helliwell and Carpenter[9] summarize data from ten stations grouped about G.M. lat. $55^{\circ} \pm 10^{\circ}$ (both North and South). They found that hiss occurred in a broad band, or one or more narrow bands (Figures 1 and 8). The narrow bands usually had bandwidths around 1 kc/s, though narrower ones down to 750 c/s occurred. They and other workers[6,10,11] often observed very narrow bands which slowly drifted in frequency, both up and down (rarely both types in the one event[9]), at rates of a few hundred c/s per second. Pope and Campbell[13] observed an intensity modulated form of this which they named "surf" (Figure 5).

Gallet[6] noted that some of the more discrete phenomena, particularly these "gliding tones" appeared to be the fine structure of hiss and suggested that hiss might consist of unresolved phenomena of this type. However, more recently Helliwell and Carpenter[9] pointed out that gliding tones were not very narrow bands of hiss as bandwidths between those of gliding tones (< 150 c/s) and of hiss (> 750 c/s) were not observed.

Chorus, on the other hand, is almost exclusively confined to frequencies from 1 to 5 kc/s[9]. Other forms of discrete events occur[9], mostly with bandwidths less than 150 c/s.. Of these "hooks" (from their appearance on frequency-time spectrograms) are the most

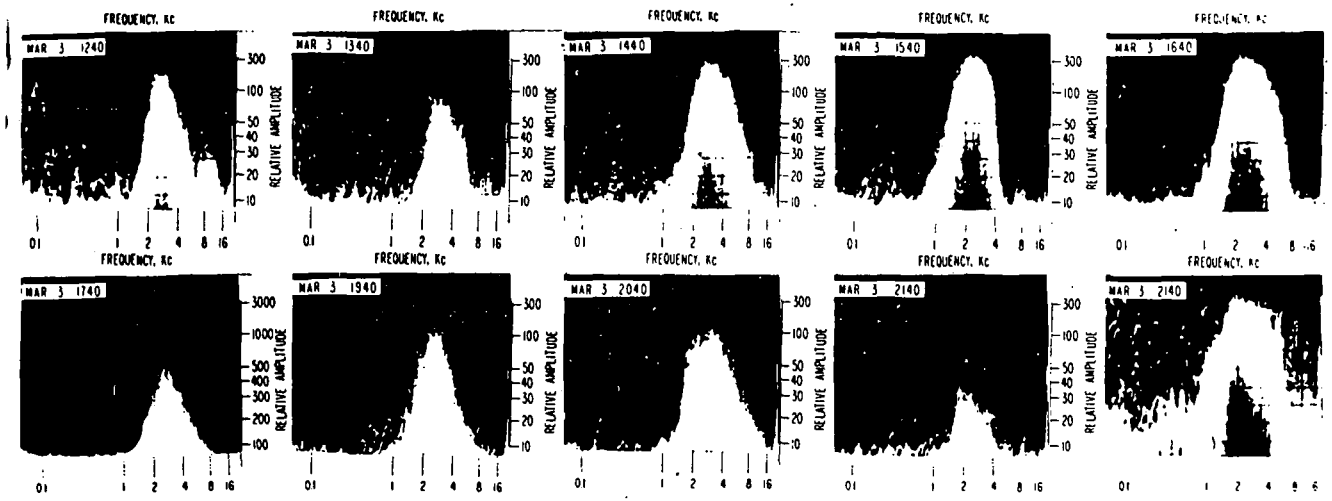

Fig. 4A. Two minute average spectra of hiss recorded on March 3–4, 1956. Note changes of amplitude scale (after Watts [10]).

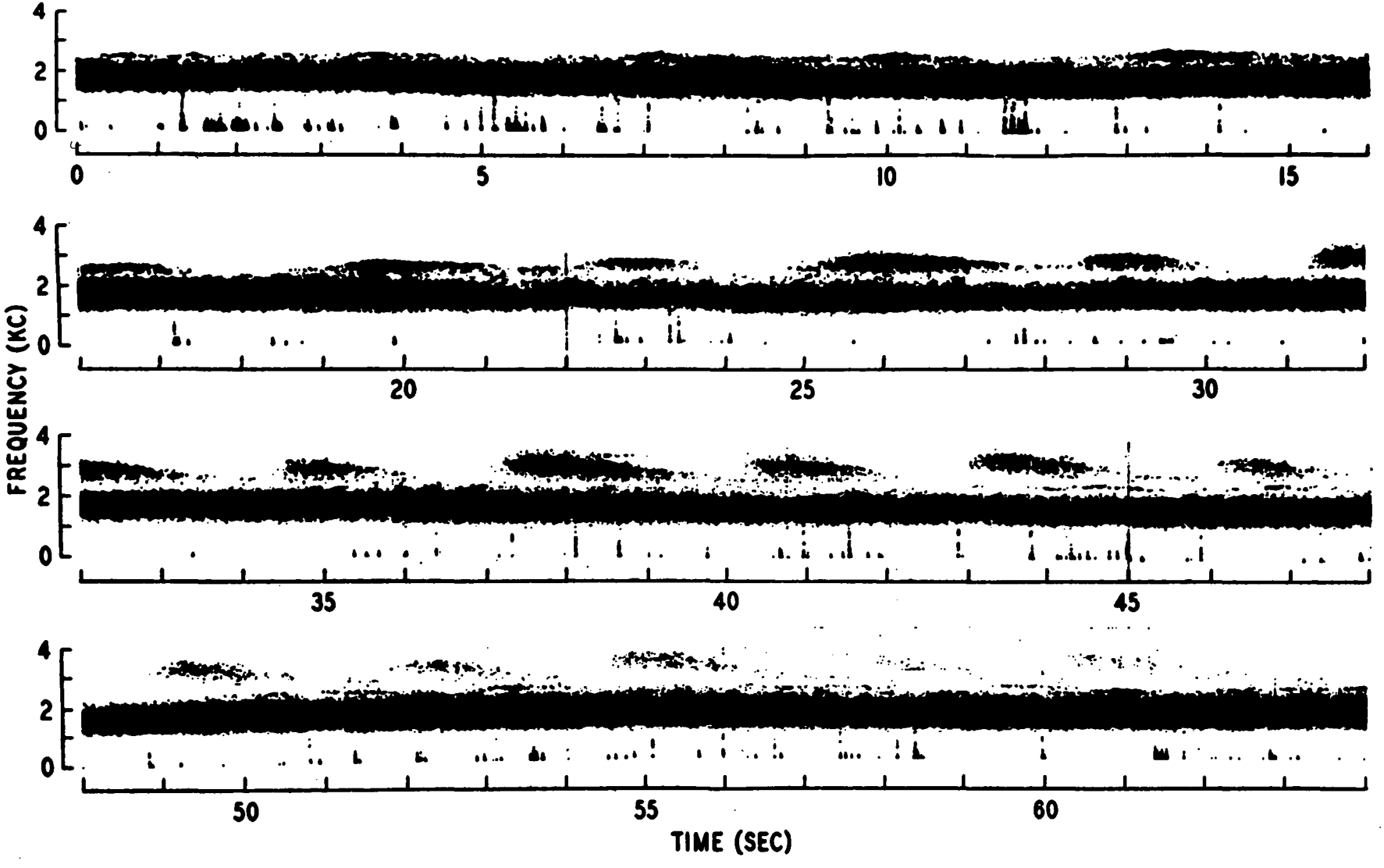

Fig. 5. "Surf" recorded at College, Alaska (after Pope and Campbell [13]).

common. Others are "risers" which are rapid and "falling tones" which are slower and last longer. These might be hooks with the rising or falling parts missing. The remaining forms which occur comparatively frequently, though rarely satisfy the criterion of repeatability, they classed as "unusual events". Later in this thesis it will be shown that many of these "unusual events" are merely special cases of the same general phenomenon. Some examples of these discrete forms (frequency-time spectrograms) are shown in Fig. 6.

The phenomena so far described are those observed at latitudes (G.M.) less than about 65° and generally 50° - 60°. We now discuss observations made from mugh higher latitudes of phenomena presumably occurring within 10 or 20 degrees of latitude of the observer. We will discuss this point later on.

2.4 High Latitude Phenomena

There is some evidence of a downward shift in frequency of phenomena occurring in high latitudes. After a year's observation at Godhavn, Greenland (G.M. latitude 80°N), Ungstrup[14] found that though chorus was observed about 18 per cent of the time around most frequent occurrence (10 - 12 local time), it was almost exclusively confined to the frequency range 500 to 1000 c/s. At lower latitudes, as discussed above[9], chorus is confined to the range 1 to 5 kc/s. If Ungstrup's chorus was not a local phenomenon but had been propagated along the earth-ionosphere wave guide it would have suffered a certain amount of attenuation. Curves given by Watt and Maxwell[15] show the attenuation at these frequencies to be about 6 db per 1000 km.

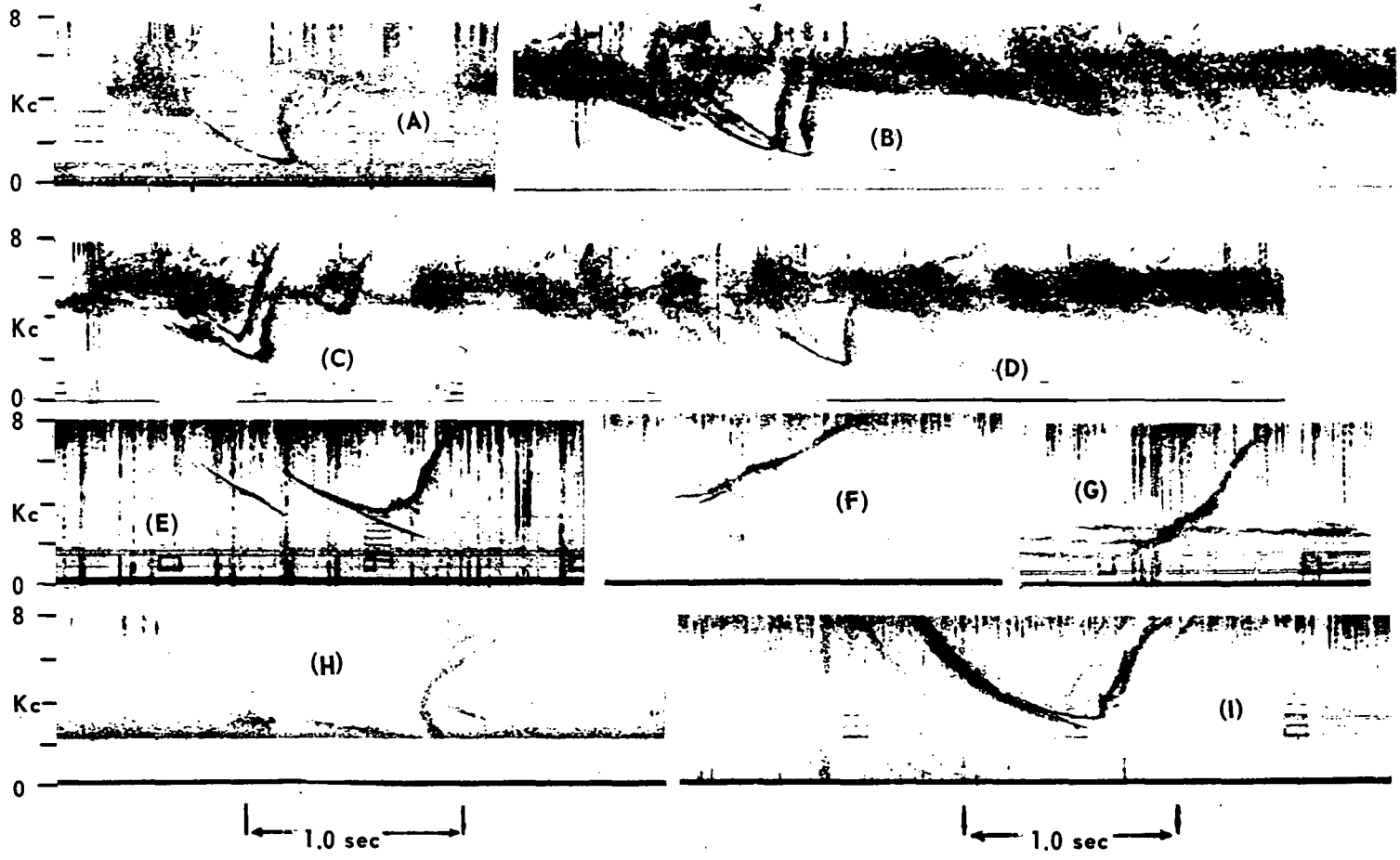

Fig. 6. Spectrograms of discrete V.L.F. emissions (after Helliwell and Carpenter,[9]). "Falling tones" appear in *E*, "quasi-constant tones" in *G*, and "risers" in *F* and *G*. The other forms are probably all "hooks".

Thus this chorus probably occurred at G.M. latitudes of at least 60°.

It is difficult to see similar behaviour for hiss, for we have already seen that it can cover a wide range of frequency. As will be seen later however there is a "quiet" form of hiss, which is narrow band, stable in frequency and amplitude, and often occurs at times of relatively weak magnetic activity. At G.M. latitudes below about 50° this is observed at about 4 kc/s. At Kiruna, Sweden (G.M. latitude 65°N) a stable band appears[20,21] at 750 c/s ± 150 c/s (Figure 7). Higher frequency hiss (1.8 to 4.5 kc/s) of broader bandwidth and less stable in frequency is also observed here. One of these workers[19] also made observations at Tromso, Norway (G.M. latitude 67°N). He observed a similar band at 800 c/s and a broader band normally centred at around 2 or 3 kc/s which sometimes extended from 0.5 to 7 kc/s.

At similar G.M. latitudes in the southern hemisphere the phenomena appears different. Two types of hiss are observed at Byrd, Antarctica[16] (G.M. latitude 70°S). One type, "normal" hiss, is not inconsistent with the observations above. A spectrogram (Figure 8) shows a number of narrow bands (2 kc/s, 1 kc/s, 500 c/s). It only occurs below 4 kc/s (partly by definition) and sometimes extends to below 150 c/s.

The second type, "auroral" hiss receives the main attention in this paper[16]. It occurs above 4 kc/s in a broad band centred at about 8 kc/s (also Figure 8) and shows a close association with aurorae. The intensity and bandwidth vary with ionospheric absorption and may also vary with the intensity of the aurorae. There are some indications that the centre frequency of this auroral hiss band may be related to the type of aurora; in particular, a centre frequency of 9.6 kc/s appears to be

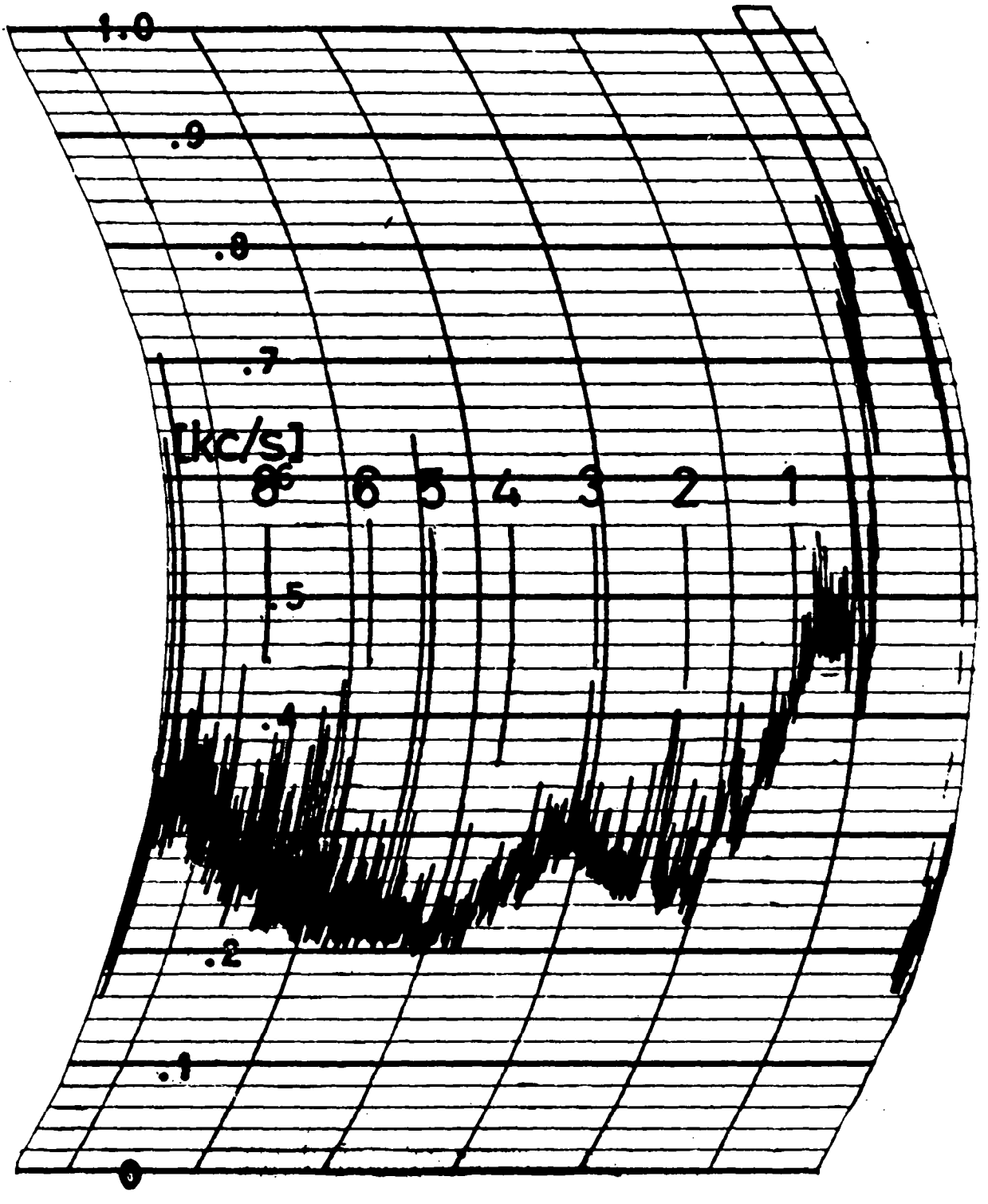

Fig. 7. Intensity – v – frequency recording of hiss at Kiruna (after Aarons, Gustafsson and Egeland [21]). The peak occurs near 750 c.p.s.

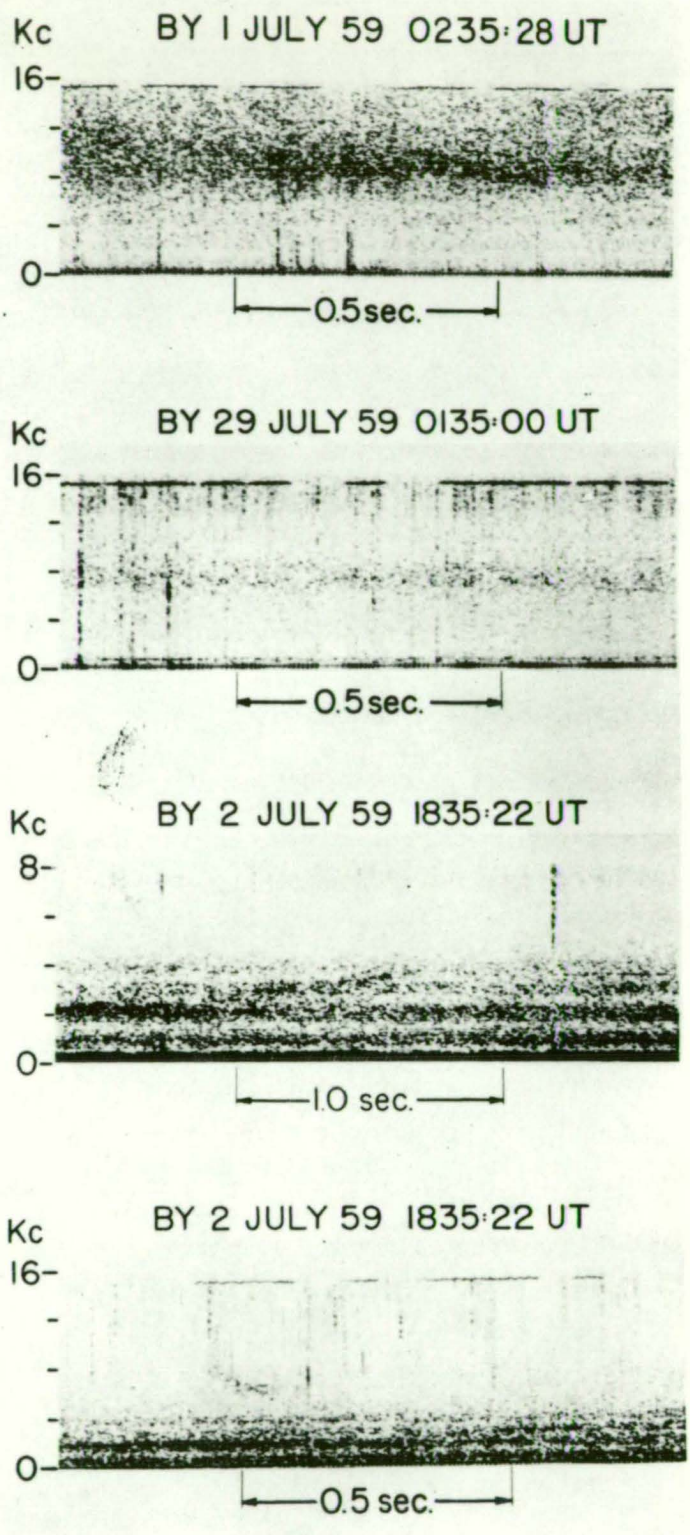

Fig. 8. Narrow bands of "normal" hiss (bottom two spectrograms) and broader bands of "auroral" hiss (top two) recorded at Byrd, Antarctica (after Martin, Helliwell and Marks [16]).

associated with red aurora[16]. This 9.6 kc/s hiss is also observed at the (geographic) South Pole[17] (G.M. latitude 79°S).

It is not impossible that the phenomena observed by the Scandinavian and Antarctic workers were the same. The apparent difference might be ascribed to different interpretations and different interests. The Scandinavians attached considerable importance to the stable 800 c/s band which they considered to be proton gyro radiation[19-21].

2.5 Australian Work

The first successful equipment to be designed, built and operated specially for observations of hiss was due to Ellis[28]. All work using these techniques so far published (late 1961) has been confined to Ellis and other Australian workers influenced by him. All other observations have been made on equipment designed for other applications. The tape recorded work just reviewed showed the spectral characteristics of hiss and some of the long term effects and correlations with other phenomena. These techniques, admirably suitable for whistlers and discrete events are not suitable by intensity and intensity-v.-time observations. On the other hand receivers used for recording V.L.F. atmospherics, though of the intensity-v.-time form, are virtually useless for hiss recording as will be seen later.

The observations described in this section are pen recorded or photographed with chart or film speeds of a few cm. per hour. A day of recording would thus be a manageable two feet or so. However, it is necessary to discriminate against atmospherics and other types of impulsive interference which can be some orders of magnitude stronger

than hiss. On the whistler records reviewed above hiss is observable between the atmospherics because the time resolution (some tens of milliseconds) is much less than the interval between the atmospherics. For slow continuous recordings, having time resolutions of the order of a minute, special techniques are required which are discussed below.

The most direct method is to apply the detected signal to the Y plates of a cathode ray tube and record on slowly moving film. An example of a burst of hiss recorded in this way is shown in Figure 9. The steady noise component is given by the bottom of the filled in trace. This represents the level in between impulses. It is seen that the peak level of the atmospherics is always completely off scale. This is further demonstrated in Figure 10 where it is seen that atmospherics are appreciable even when the gain is decreased by a large factor. An alternative method for recording on a pen and paper system of much slower response utilises the minimum reading circuit described by Ellis[22,23]. This uses a partly unidirectional integrator having a charging time constant of the order of a minute and a discharge time constant of the order of 0.01 seconds (Figure 11). Similar techniques can be used for frequency time recording though generally it was found that hiss could be readily distinguished from atmospherics on the records, as seen in Figure 12.

All other work so far published of continuous recording of noise in the V.L.F. band has been done without discrimination against atmospherics and other impulse noise. Most of these workers[24-27] have been mainly interested in recording atmospherics and some times used peak reading circuits[24]. It is not surprising that these have reported a general lack of correlation between recorded intensities

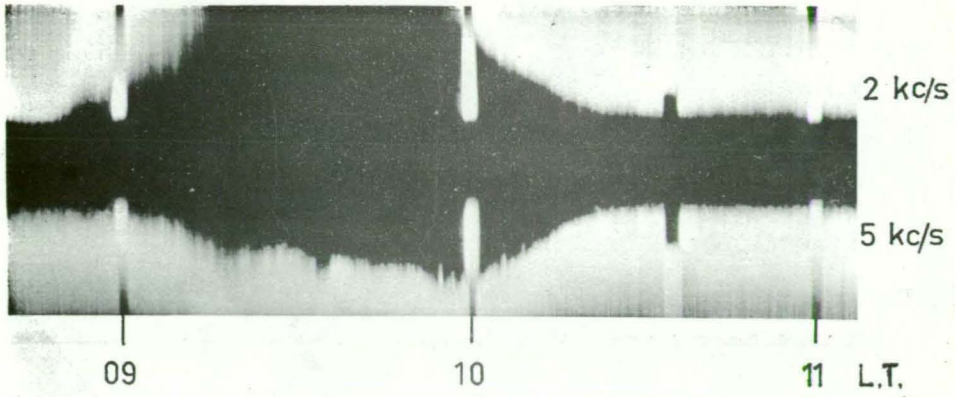

Fig. 9. A burst of hiss recorded at two frequencies by the C.R.T. and film method. The time marks are also zero input levels. Impulsive (atmospheric) noise is superimposed.

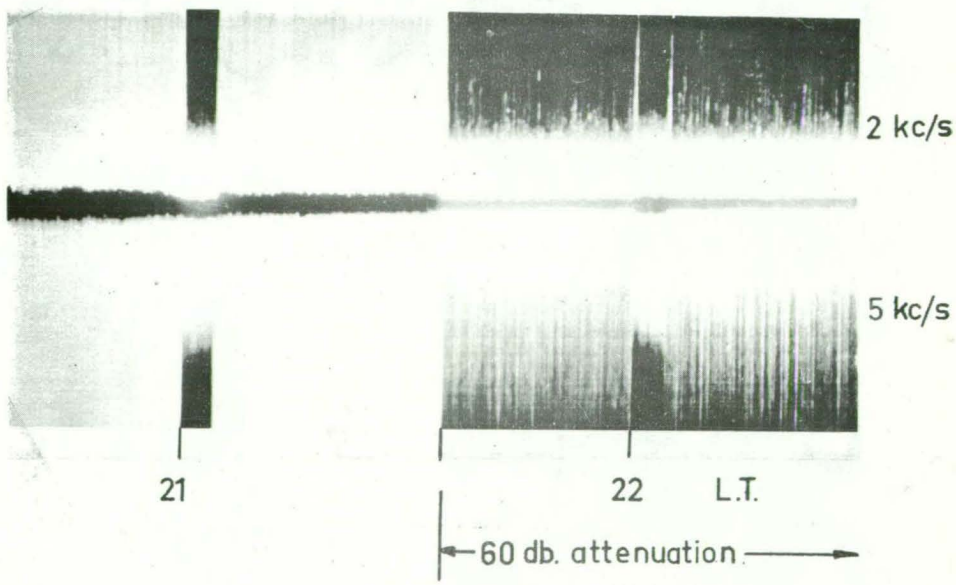

Fig. 10. A period of no hiss but of very strong atmospherics. The latter contribute only a very slight base level. An indication of the strength of these atmospherics is shown in the latter part of the record during which 60 db attenuators were inserted between the antennae and the receivers: many impulses still produce full scale deflection.

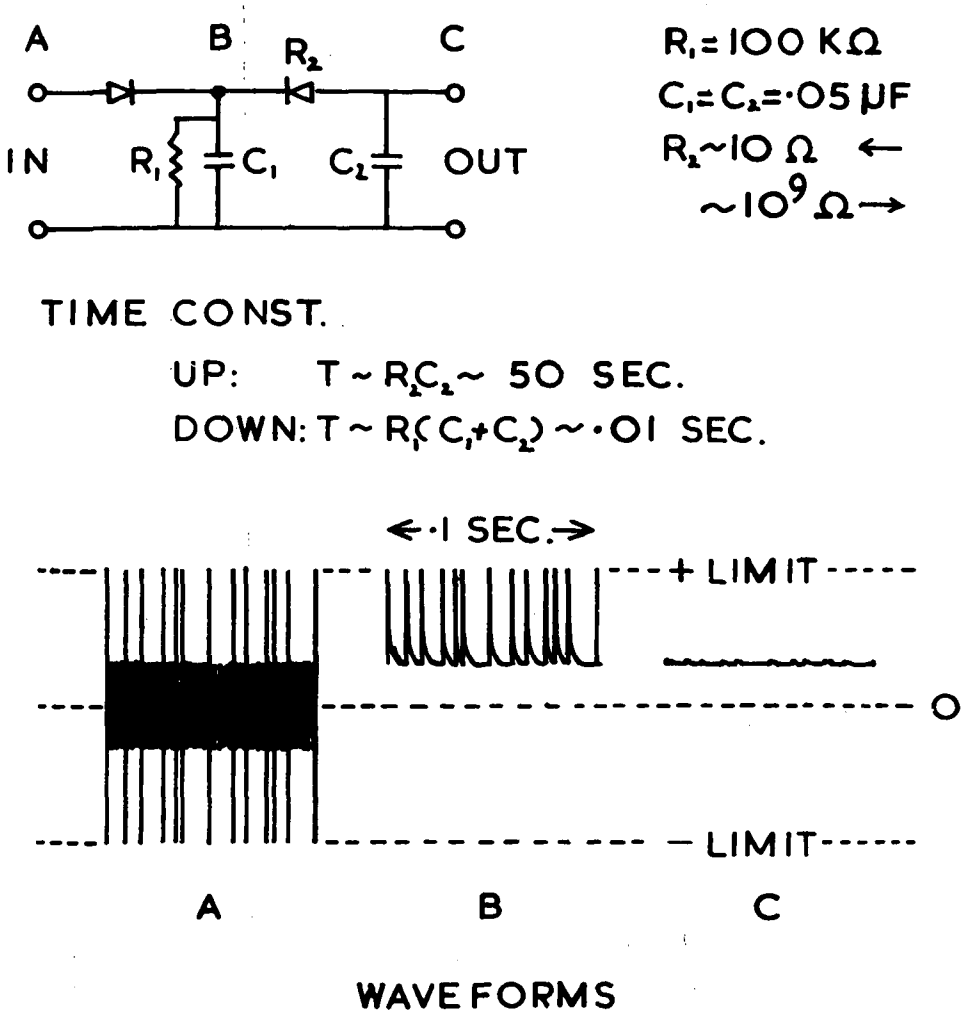

Fig. 11. "Minimum reading" circuit. The input (A) is fed from a low impedance from the last (A.C.) amplifier. The impulses would have overloaded the last amplifier stages. The steady noise and the impulses are seen before (A) and after (B) detection and smoothing. At the output (**c**), which must be fed to a *very* high impedance, only the steady noise level remains. The output level automatically rises to the minimum at B. For any increases above this level at B the second diode (R_2) is reverse biased so that the "up" time constant applies. This illustrates the principle. A practical circuit is shown in Fig. 30.

and geomagnetic disturbances[20], and so concluded that most if not all audio frequency fluctuations originates in thunderstorm activity[25,26]. It is only at high latitudes during ~~stray~~ strong magnetic disturbance, when atmospherics from low and middle latitudes are weak and hiss relatively strong, that hiss is,stronger than atmospherics and so observable on these recording systems. Some of the work discussed above was in this category[20,21] (see Figure 7).

The first continuous recording of hiss was begun by Ellis[28] in June 1958 at Camden. The intensity receiver had a centre frequency of 4.6 kc/s and a bandwidth of about 800 c/s. Continuous measurements were made on a pen recorder using the minimum reading technique described above. The spectrum from 2 to 40 kc/s was also continuously recorded on film using a frequency scanning analyser.

The system proved to be much more sensitive for detecting hiss than the tape recorder systems reviewed above. It was soon found that hiss occurred in bursts lasting some hours. No background of hiss was present in between bursts. (More recent observations over an extended period on a high gain receiver in a very quiet site have not confirmed this (Ellis, unpublished).) Apart from built in electronic discrimination, these bursts of hiss are readily distinguished from man made bursts by their comparatively slow build up and decay (Figure 9). These bursts of hiss can be classified into two main types both from their spectral characteristics and duration. This classification fits other properties discussed later.

The most common type were "isolated bursts". These occurred

well separated from one another and often during magnetically quiet conditions. They were narrow band, usually 1 - 2 kc/s, centred at about 4 kc/s. Both the intensity and spectrum remained constant during these bursts. This is the "quiet" form of hiss mentioned earlier. Isolated bursts lasted about an hour. Figures 9 and 12 are examples.

The second type were extended series of bursts of hiss or "noise storms". These lasted longer (up to 50 hours) and showed considerable intensity and spectrum variations (Figure 13). The frequencies of hiss observed on the spectrum analyser were similar to those reviewed above. However in general the bandwidth increased with magnetic activity, extending over most of the recording range during severe disturbances. All major magnetic storms were accompanied by noise storms. On the average these began about 6½ hours after a magnetic sudden commencement.

A diurnal effect was noticed at Camden[28] showing a peak occurrence around midnight and, initially, no bursts between 1000 and 1400 hours local time. Later observations[37] showed that this was entirely due to propagation (over the surface of the earth) conditions as practically the reverse was true at Hobart (Figure 14). It now appears that the occurrence of bursts is equally probable at all times but those occurring between 0800 and 1200 hours local time (at Hobart) are generally stronger[37].

Bursts showed a strong correlation with red oxygen (6300 Å) airglow on 6 nights. On three occasions hiss and airglow showed the

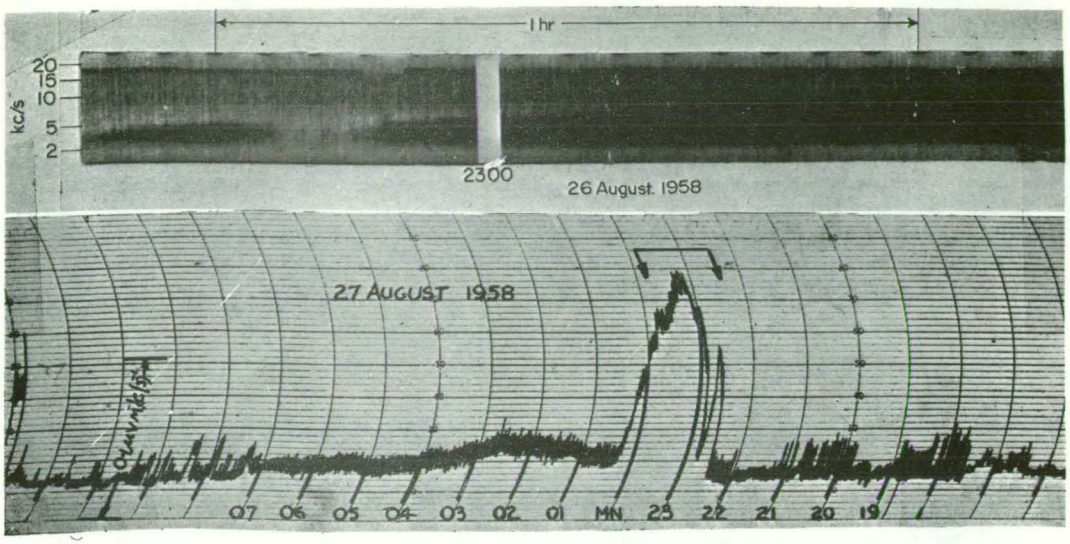

Fig. 12. An "isolated burst". The spectrum is shown for the period between the arrows (after Ellis[28]).

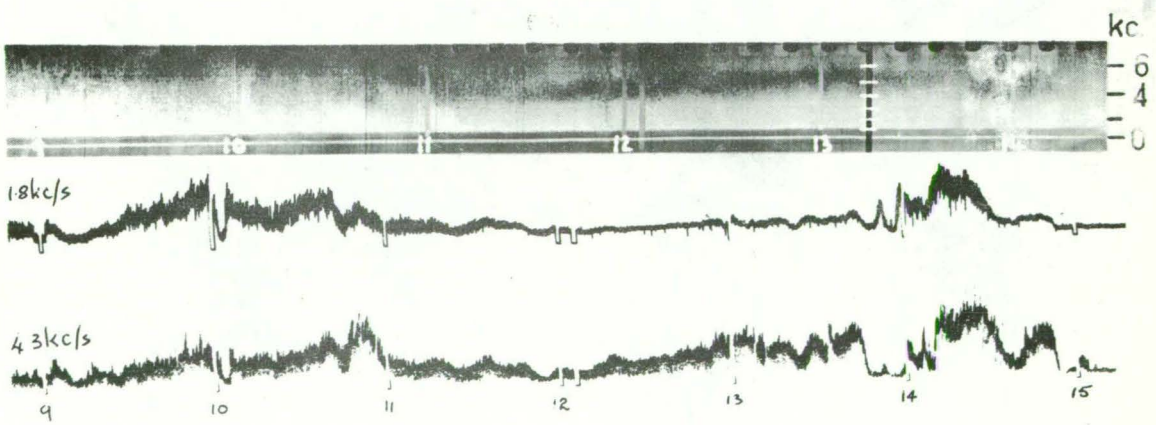

Fig. 13. A moderate "noise storm" recorded at two frequencies. Note the rapid bandwidth variation near 1400 L.T.

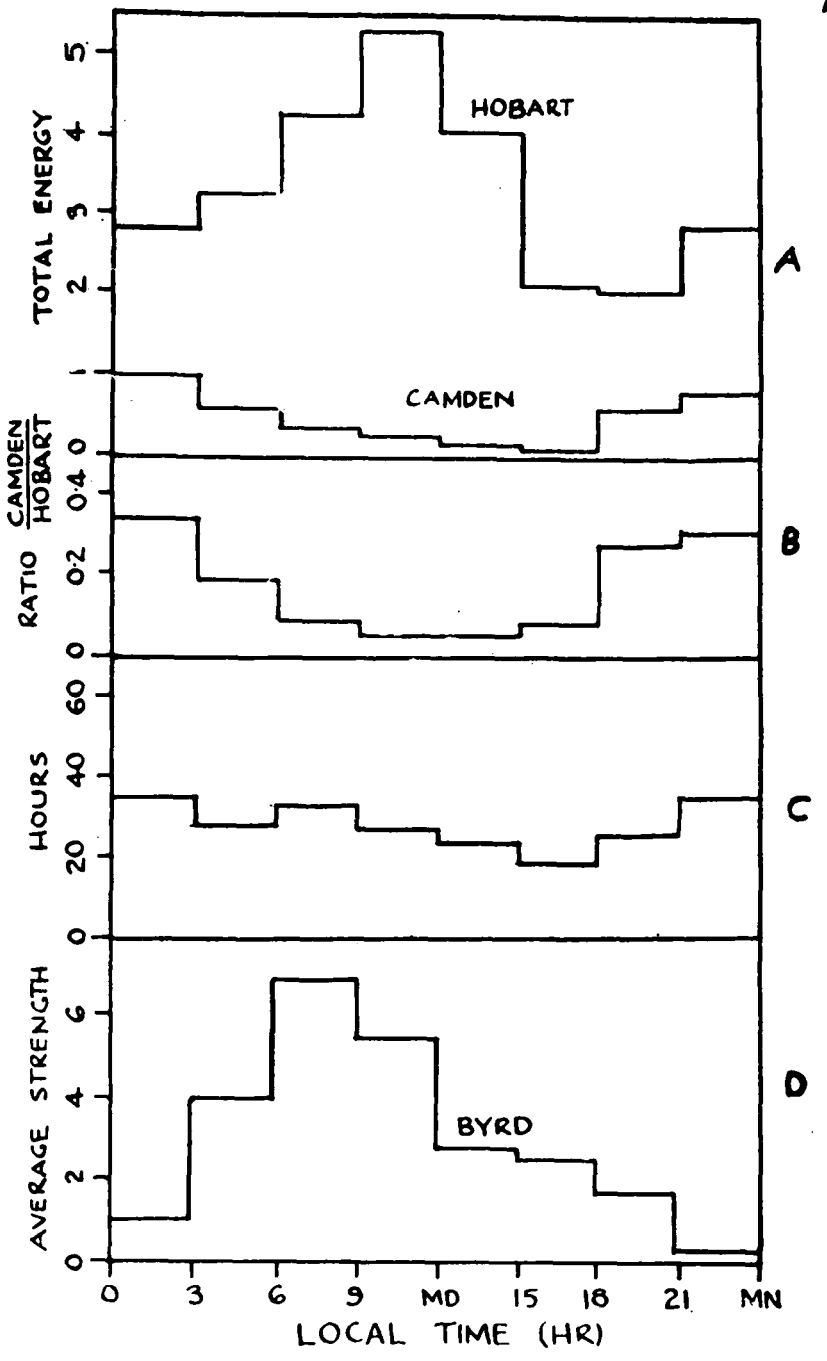

(*a*) The diurnal variation of the average noise energies received in three hourly periods at Hobart and Camden between September 1959 and April 1960. (*b*) Ratio of noise power at Camden and Hobart. (*c*) Total number of hours of noise at Hobart and Camden, September 1959 to April 1960. (*d*) Variation of intensity of radio noise below 4 kc/s at Byrd Base, Antarctica, July 1959 (after *Martin, Helliwell, and Marks*).

Fig. 14. Diurnal effects (after Ellis [37]).

the same minute to minute variation and both hiss and airglow appeared to be coming from the south (Figure 15). Observations at Byrd[16] discussed above showed that ionospheric absorption can prevent observation of hiss during aurora, similarly below horizon airglow or bad seeing conditions could have prevented observation of airglow at Camden. Possibly, then, hiss and airglow always occurred together.

The amplitude fluctuations of a few noise storms have followed a reproducible sequence with a 27 hour interval between a long burst lasting several hours and a much weaker burst[28]. This suggests a source not fully partaking in the movement of the earth's surface but rather almost constant in position in Right Ascension[28]. Later observation confirmed this effect[37,38].

2.6 Source Location

A difficulty which began to be recognized was that phenomena which was observed at a given point did not necessarily "occur" near that point. Phenomena brought about by propagation or generation in the exosphere such as hiss, chorus and whistlers could be channeled down the earth's magnetic field to a point on the earth's surface at a considerable distance from the observer and still be observed[40]. Phenomena observed at a medium latitude station might be predominantly high latitude phenomena and vice versa. Thus whistlers, a relatively low latitude phenomenon, are observed at the South Pole[17]. At least one of these whistlers was traced by Allcock[18] as having originated over 4000 km away. Utilization

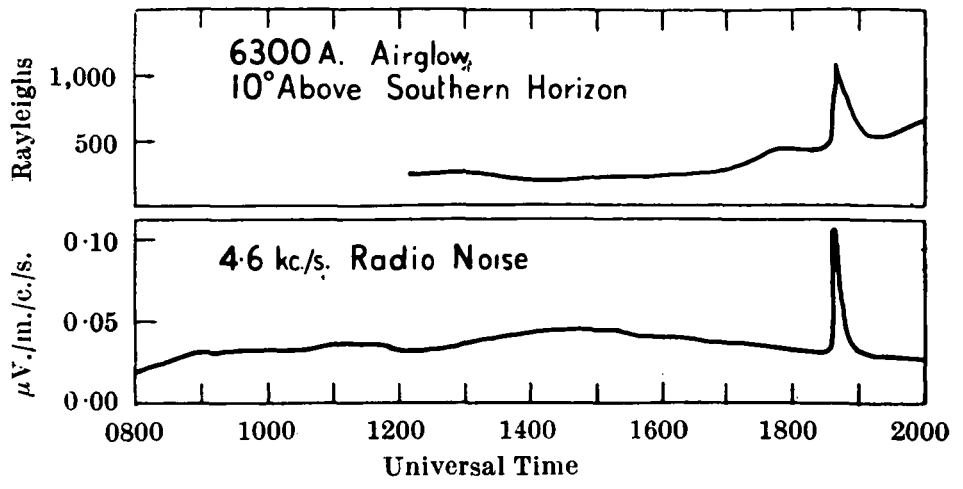

Noise and auroral burst observed on July 21, 1958

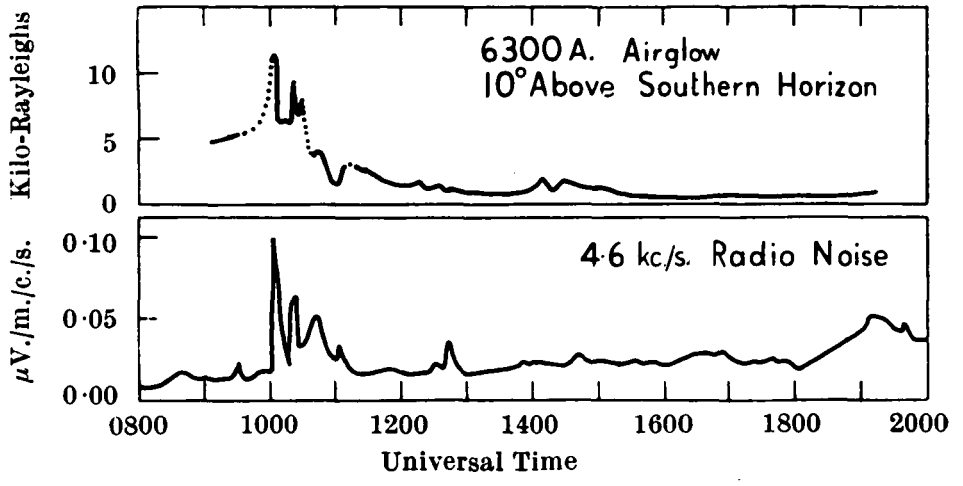

Airglow and noise records for August 27, 1958. No red airglow observations were made during those periods for which the trace is dotted

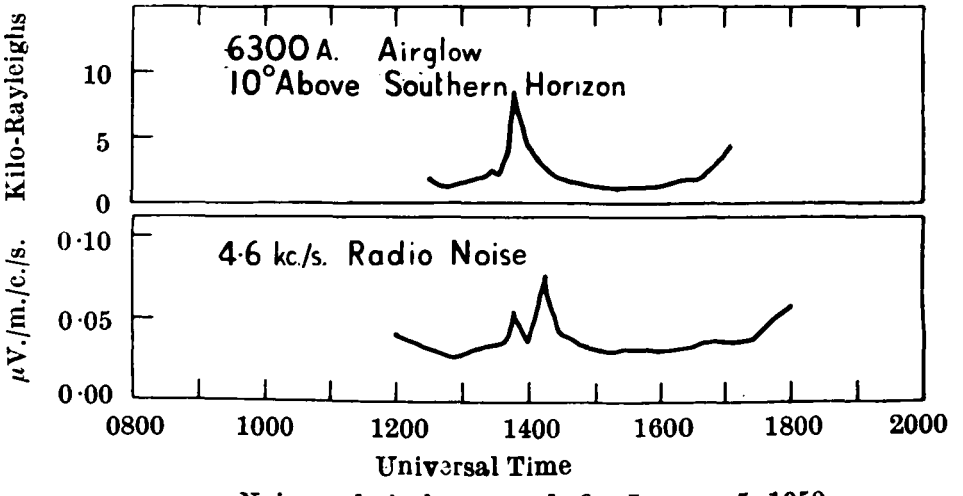

Noise and airglow records for January 5, 1959

Fig. 15. Simultaneous occurrence of airglow and hiss (after Duncan and Ellis [29]).

of the nose effect ~~and V.L.F. transmitters~~ resolved the difficulty for the whistler workers.

Thus an important development was the location of the regions (virtual sources) on the surface of the earth from which hiss appeared to be coming after propagation down to the earth from the actual region of generation above the ionosphere. The first observation of this type appears to have been made by Eckersley[4], as mentioned earlier.

Experiments at Camden[32] at 5 kc/s showed that direction location was possible with rotating loop systems. It was further shown that the angular extent of the virtual source could be estimated from the sharpness of the null[33]. A number of isolated bursts were recorded at 5 kc/s simultaneously on direction finding systems at Camden, Adelaide and Hobart[34]. For those which were reasonably strong at all three stations it was possible to find the locations, sizes and approximate shapes. It was found that most of the bursts came from sources at G.M. latitudes greater than 50° and many of these were too far south to be resolvable. Those resolved were roughly circular in shape, about 500 km in geographical size and came from various geomagnetic latitudes between 45° and 56°.

It was pointed out by Ellis[34] that use of a large network of locating receivers would make possible the construction of a map for any instant of the areas where the radiation emerges from the ionosphere. This map would represent an image on the surface of the earth of the generating regions in the exosphere. Work on whistlers[36]

has shown that guiding along a line of force is even stronger than expected from Storey's theory (field aligned columns of ionization have been suggested as the cause of this effect[35]). Thus the "focus" of the image should be quite sharp.

Thus the observation of images of only a few hundred kilometers extent implies, for these at least, generation in quite narrow magnetic tubes of force. If hiss is generated in the exosphere by low energy charged particles (also guided along the earth's field), then these charged particles must also, at times, be confined to narrow tubes of force. Direct observation by satellite of an "arc" of incoming charged particles coincident with an auroral arc showed narrow streams of particles of widths down to 25 km[41].

Very recently (late 1961) Crary[45] has shown that polarization errors in rotating loop direction location of whistlers can be very serious. Both the null bearing angle and the null sharpness (maximum to minimum ratio) are affected. This casts serious doubt on the validity of the method of estimating source sizes from null sharpness[33]. However, ~~as will be shown later in this thesis,~~ direction finding measurements of hiss should be less subject to bearing angle errors than is the case for whistlers.

Position location is also possible without direction finding if intensity records from three or more stations are available[37]. This system has certain advantages in that the equipment is simpler, position location is continuous and instantaneous, and for a large number of stations it gives more information on position, shape and size of geographically large sources. Ellis[37] observed 43 separate

bursts and one major noise storm at 5 kc/s on a network of four stations extending across southern Australia. The majority of the separate noise bursts appeared to come from geographical large sources far to the south (G.M. latitudes greater than 50°). Two of these appeared to be long narrow sources or "arcs" occurring somewhere between 50° and 60° G.M. latitude. Eight of the separate bursts were small discrete sources randomly distributed between geographic latitudes 38° and 45° (45° - 55° G.M.). Observations during noise storms[37,38] showed the same general amplitude variations at all stations though a considerable difference in the relative amplitudes (Figure 16). This was interpreted[37] as a very large source with fine structure. Some of the peaks in this fine structure appeared progressively later at the western stations, being observed at each station at about their same local time. This suggested[38] that the sources of these were remaining almost constant in position in Right Ascension.

Investigations by Ellis[30] on isolated bursts occurring during periods of weak magnetic activity (K ~ 3) showed that about half (43 out of 97) were associated with positive magnetic bays. The bursts occurred at the same time as the bays. Cartwright[31] obtained evidence that these bursts and bays are also coincident in geographic position. Recent investigations of the ionospheric current systems associated with magnetic bays suggest local precipitation of protons and electrons. Hence it seems likely that these particles also produce the localised bursts of hiss[30].

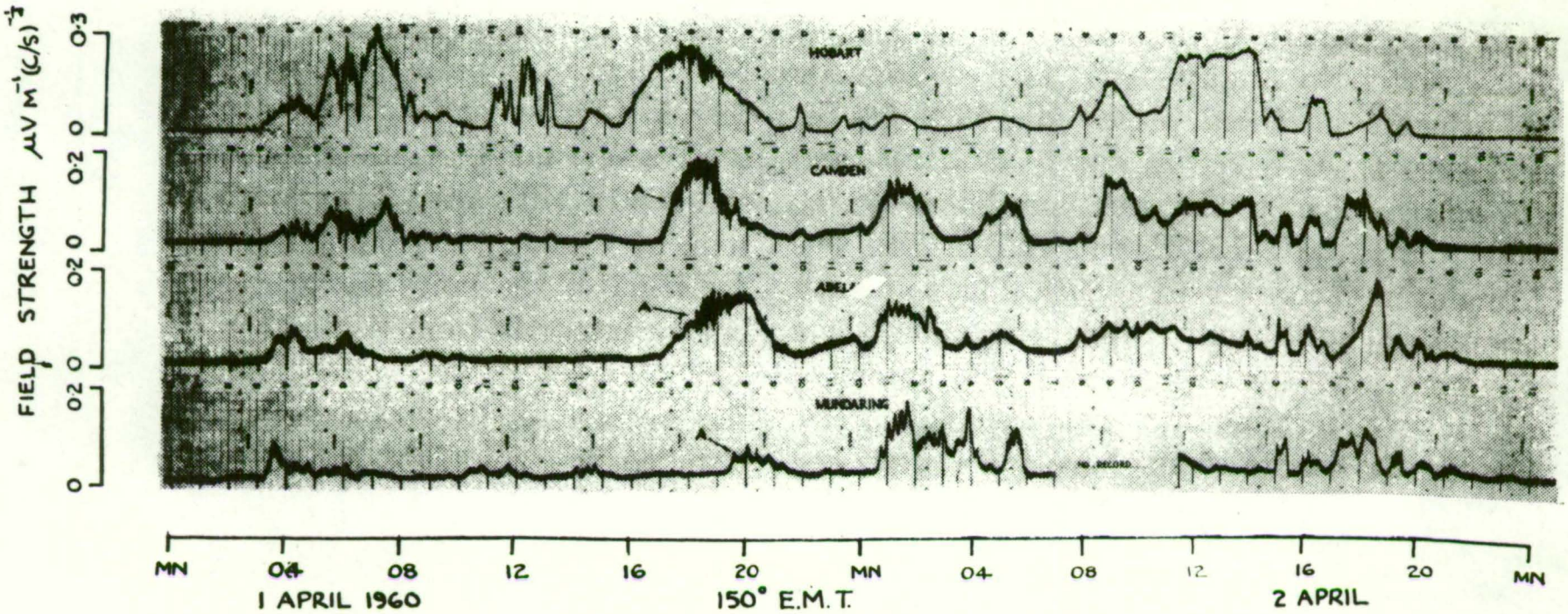

Fig. 16. Noise storm recorded simultaneously at four stations (after Ellis [37]).

3. OBSERVATIONS OF HISS.

3.0.1. Introduction.

The writer's experimental work was confined to observations of hiss. In 1959 when this work was begun a vast amount of data in the form of spectrograms of discrete emissions, chorus and hiss had already been recorded by several groups throughout the world. Complicated and costly equipment was needed to produce high quality spectrograms and essentially new work in this field required more sophisticated experiments and techniques. On the other hand Ellis had just opened up a new field by his techniques for studying the longer term amplitude and frequency variations of hiss. In addition these techniques required only relatively simple equipment.

It should be noted that the definition of the three types of exospheric emissions: "discrete emissions", "chorus" and "hiss", are based on their sound and their appearance on fast spectrograms. The recording techniques used by Ellis and in the work to be described would treat discrete events as impulses, and so reject them. On the other hand chorus consisting of overlapping "discrete emissions" would be treated as hiss.

3.1 WIDE BAND BURSTS

3.1.1 Introduction:

Early observations by Ellis[28] showed that sometimes, particularly at times of strong geomagnetic disturbance, wide band bursts occur spreading from 2 kc/s or less, to at least 30 kc/s. One of the first experimental projects by the writer was to extend the observing range to find out the frequency range of very wide band bursts and how the intensity varied with frequency. Very wide band bursts were observed at frequencies from about 100 c/s to about 250 kc/s. The observed (ground level) intensity in $W\,m^{-2}\,(c/s)^{-1}$ ranged from nearly 10^{-9} at 100 c/s to 10^{-19} at 250 kc/s. However as will be shown here, the intensity at the source region in the exosphere deduced by subtracting the losses suffered in the ionosphere and below the ionosphere, shows a relatively flat spectrum at a level of the order of $10^{-10}\ W\,m^{-2}(c/s)^{-1}$.

Ground level intensities were recorded at several spot frequencies (125 c/s, 240 c/s, 410 c/s, 760 c/s, 1.8 kc/s, 4.3 kc/s, 9.0 kc/s, and 230 kc/s) during wide band bursts observed at Hobart.

Only six recording channels were available so that simultaneous recordings were not made at all eight frequencies mentioned above. However there was sufficient frequency overlap to suggest that the wide band bursts measured mainly at the higher frequencies were similar to those measured mainly at the lower frequencies.

Two sweep frequency analysers covering the ranges 40 c/s to 500 c/s and 400c/s to 6 kc/s, though of less sensitivity and of restricted use for intensity measurement, were used to check the interpretation of the fixed frequency records.

3.1.2 Observations:

In a period of about fifteen months (October 1959 to January 1961), twenty five wide band bursts were recorded. Three of these are shown in Figures 17 to 19. The main wide band burst in Figure 17 (around 1130 local time) is accompanied by a medium bandwidth burst between 10 and 11 local time and several narrow band bursts after local noon. To avoid zero intensities appearing in the statistical analysis, consideration of intensities was restricted to these twenty five for which non zero intensities were recorded on all channels. In general, as in Figure 17, the peak intensity during narrow band bursts ~~at the~~ was of the same order as that during wide band bursts at the

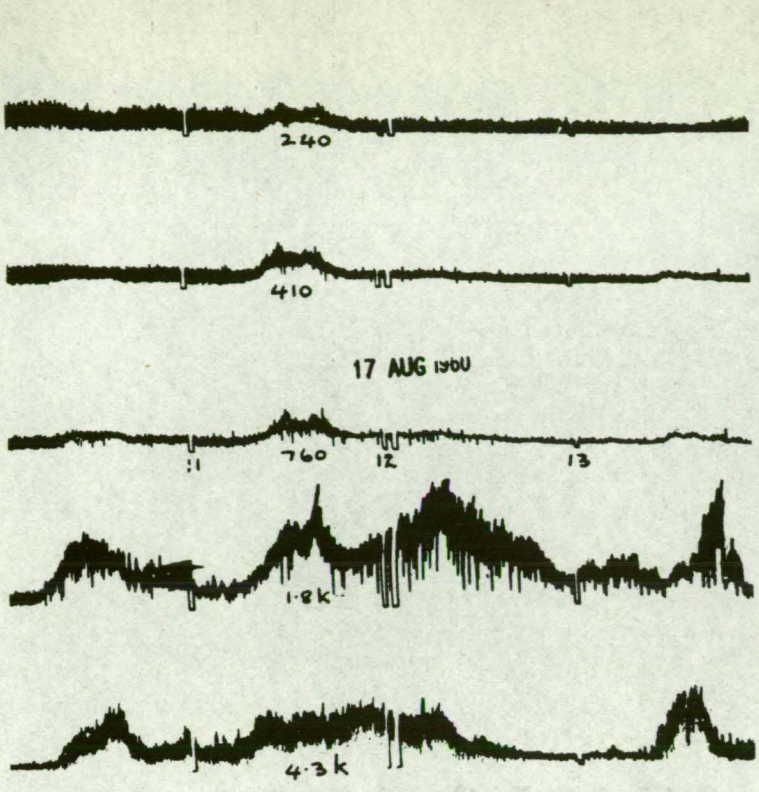

Fig. 17. Wide band (c. 1130 L.T.) and narrow band bursts.

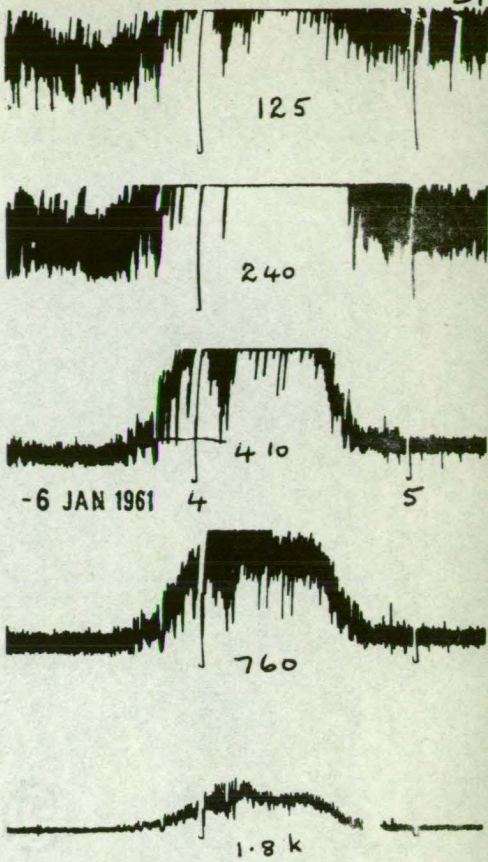

Fig. 18. Wide band burst

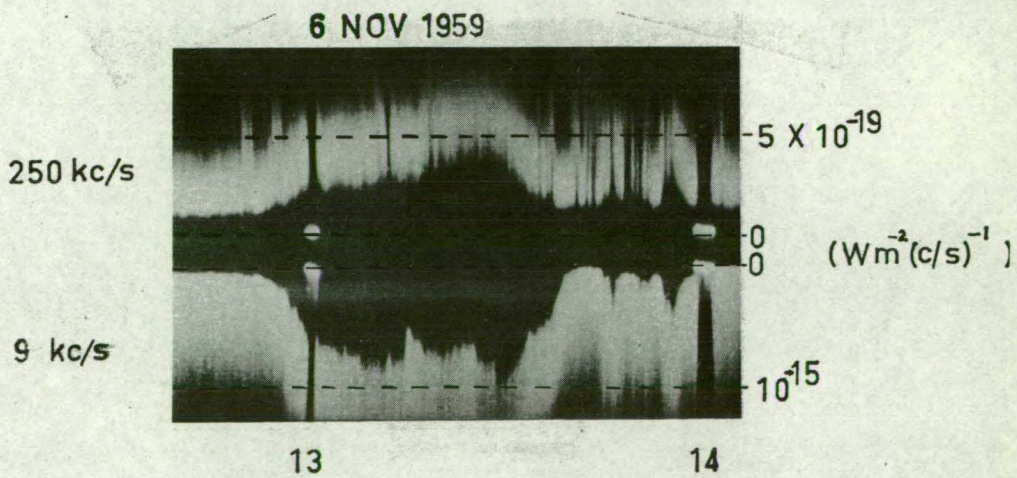

Fig. 19. Wide band burst (only these two channels were operating at the time.).

same frequency. The median intensities and the spread of intensities recorded is shown plotted in Figure 20. Medians for 125 c/s, 9.0 kc/s and 230 kc/s may not be truly representative as less than five values were obtained for each. This occured because these channels were operated for a relatively short period.

It is seen that very wide band bursts covered the full observing range so it seems likely that some extended beyond this range. However the (burst) signal to (background) noise ratio became gradually worse at the very high and very low frequencies so that this was not checked by extending the observing range further.

The most striking feature in Figure 20 is the strong dependence of observed intensity on frequency. We are interested in the source intensity and its variation with frequency, so we will now attempt to find out how much of the observed effect is produced by propagation losses.

3.1.3 Propagation Losses:

Although there is no strong experimental evidence to indicate the level at which V.L.F. noise

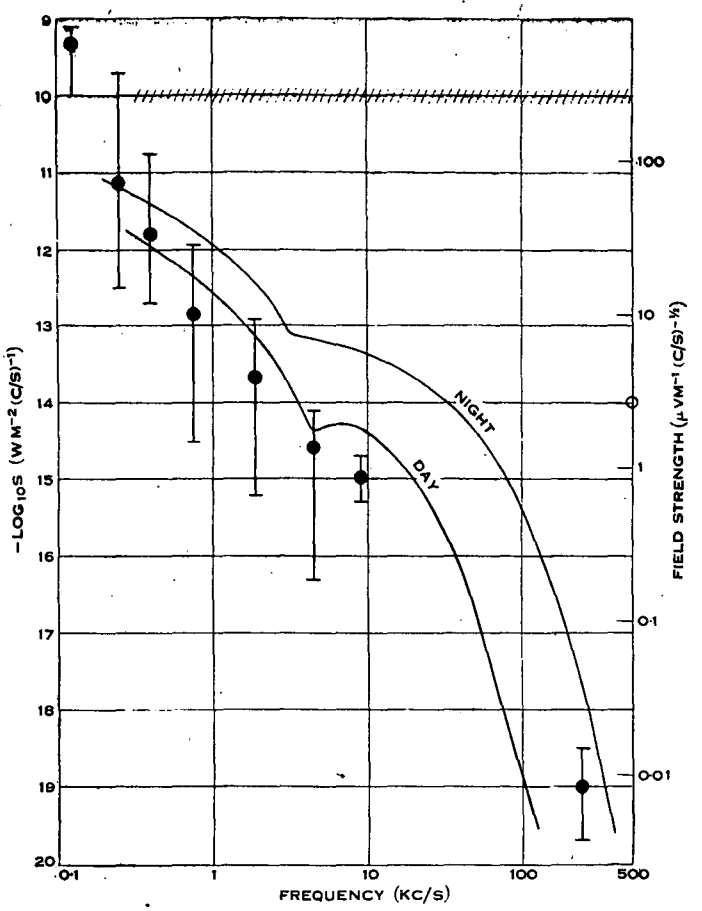

Fig. 20. Medians and spread of peak intensities of observed wide-band bursts. Curves are expected ground intensities for a " white " source above the ionosphere at the hatched level [10^{-10} Wm^{-2} $(c/s)^{-1}$]. The right-hand ordinate is field strength.

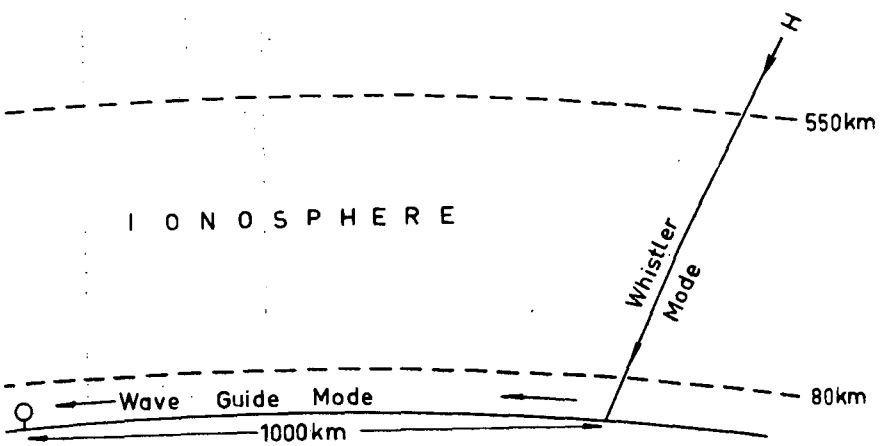

Fig. 21. Path of wave from generation region to receiving antenna.

is produced, we will assume here that it is above most of the ionosphere, that is above, say, 550 km. Directional and spaced observations (Ellis[34]) show that V.L.F. noise bursts often appear to be coming from virtual sources of quite small areas on the earth's surface. Consequently we adopt the model that the burst is generated in a relatively narrow tube of force somewhere above the ionosphere, is then piped down through the ionosphere in the "whistler mode" and radiated out under the ionosphere in the two surface (earth or ocean and ionosphere) wave guide to the observer. This is shown in Figure 21. We require, then, the losses suffered in these two modes.

The earth-ionosphere wave guide losses have been calculated by Watt and Maxwell[78] for frequencies from 1 to 100 kc/s. Curves are given of field strength versus frequency for propagation over daytime and nighttime sea water paths of various distances for a unit "white" point source. In our case the distance between the virtual source and the observing point is not known for each burst but a typical median value can be estimated along the following lines.

Suppose all sources were point sources and that they were randomly distributed about Hobart. We consider an annular area centred on Hobart at distance r, width dr, and area dA. We define the probabilities: $p_s(r, dr)$ of a source occuring within this annular area; $p_o(r, dr)$ of it being observed at Hobart if it did occur; and $p_{os}(r,dr)$ of an observable source occuring within this area (within r and r+ dr). It follows:

$$p_s(r, dr) \propto dA \propto r.dr$$

$$p_o(r, dr) \propto \text{intensity on arrival at Hobart} \propto \frac{e^{-\alpha r}}{r}$$

where α = attenuation coefficient for the earth - ionosphere wave guide mode.

Hence,

$$p_{os}(r,dr) = p_s(r,dr) \cdot p_o(r,dr) = e^{-\alpha r} \cdot dr$$

We define a median range $\bar{r}$ such that

$$\int_0^{\bar{r}} p_{os}(r,dr) = \int_{\bar{r}}^{\infty} p_{os}(r,dr)$$

that is

$$\frac{1}{\alpha}\left[e^{-\alpha r}\right]_{\bar{r}}^{0} = \frac{1}{\alpha}\left[e^{-\alpha r}\right]_{\infty}^{\bar{r}}$$

Hence,

$$e^{-\alpha \bar{r}} = \tfrac{1}{2}$$

6 The attenuation coefficient, α, is strongly frequency dependent, but typical values are around 3 dB per 1000 km (Watt and Maxwell[78]) so that the typical range ($\bar{r}$) will be around 1000 km.

Suppose instead the sources were very large so that everywhere in the vicinity of Hobart was essentially uniformly illuminated by each burst. We consider the same annular area described above. The total power intecepted by this annulus is proportional to its area:

$$dW_s(r) \propto r, \cdot dr,$$

Transmission over distance r to Hobart would decrease this by a factor

$$\frac{e^{-\alpha r}}{r}$$

So that the power observed at Hobart from this area (from the ranges r to r + dr) is then

$$dW_{os}(r) = K.e^{-r}.dr$$

K being a constant of proportionality. We define the median range $\bar{r}$ as that range within which half of the observed power occurs. Then

$$K \int_0^{\bar{r}} e^{-\alpha r}. \, dr = K \int_{\bar{r}}^{\infty} e^{-\alpha r}. \, dr$$

Hence the same argument as the above leads to

$$\bar{r} \sim 1000 \text{ km}.$$

7 Selection of the r = 1000 km. day and night curves of Watt and Maxwell[78] gives us the below-ionosphere losses for the frequency range 1 to 100 kc/s. Those for frequencies outside this range are estimated by extrapolation.

The attenuation for whistler mode propagation through the ionosphere were obtained from curves by Helliwell[11] using a model daytime ionosphere from 80 to 550 km. given by Francis and Karplus[79]. Night time attenuations were estimated from this model by disregarding the ionosphere below 100 km. The attenuations suffered in the successive strata of the ionosphere thus calculated are given in Table 1 below.

Table 1

Power attenuation for whistler mode propagation through successive strata of the ionosphere at the frequencies given.

Ionospheric	Power attenuation (dB) at frequency (kc/s)					
stratum (km)	0.1	0.4	4.5	17	230	500
550 - 140	0.12	0.24	0.8	0.9	8.4	22
140 - 120	0.04	0.08	0.2	0.5	2.2	5
120 - 100	0.24	0.5	1.6	3.0	14	33
100 - 90	0.3	0.6	2.2	4.2	17	42
90 - 80	0.7	1.4	4.2	7.5	20	48
Day 550-80	1.4		9.0	16	60	150
Night 550-100	0.4	0.8	2.6	5	25	60

There is little experimental data to check these calculations, particularly of the lower frequencies. However whistler mode echo observations[80] at 17 kc/s for daytime propagation indicated that the actual attenuation at the time could not have greatly exceeded these figures. Very recent preliminary data[82] from the LOFTI I satellite at 18 kc/s indicate that 80 per cent of the time the attenuation ranged from 33 to 45 dB by day and from 4 to 29 dB by night. A rocket measurement[81] at 512 kc/s showed at least 40 dB attenuation for night time propagation.

The losses for propagation through the ionosphere (whistler mode) and below the ionosphere (wave guide) are combined and graphed in Figure 20 for day and night conditions. We have assumed a "white noise" source of intensity 10^{-10} $Wm^{-2}(c/s)^{-1}$ at a level of 550 km. The curves thus represent the expected intensity at an observing station on the ground about 1000 km from the point immediately below the source. The accuracy of these curves deteriorates towards both ends of the frequency scale. The treatment used above breaks down at the low end because the distances involved approach a wavelength.

At the high frequencies the attenuations are so large that small errors in the estimation of parameters become important. Both ends will suffer from extrapolations.

It is seen from Figure 20 that the expected "ground level" spectrum resulting from this flat or "white" source spectrum fits the observed intensities to an order of magnitude or so, although an intensity proportional to wavelength might give better fit at the low frequency end. The main point emerging from this study is that much of the very strong frequency dependence of observed intensities is accounted for by attenuation.

Intensities of over 10^{-14} $W m^{-2}(c/s)^{-1}$ at 512 kc/s have been observed at a height of 400 km by Mechtly and Bowhill[81] (open circle in Figure 20). This is a lower limit (receivers overloaded) and so consistent with our results. On the other hand at frequencies above 900 kc/s, at times when the ionosphere above Hobart is transparent, ground level intensities (due to Cosmic Noise) of only 2×10^{-19} $W m^{-2}(c/s)^{-1}$ are observed[83]. This is some nine orders of magnitude less than our value. However it must be remembered that very wide band bursts are

rare and occur only during very severe disturbances whereas the ionosphere is transparent at low frequencies only during very quiet conditions. Nevertheless, this does show that, at least at the higher frequencies, a continuous high background level does not exist.

3.1.4 Conclusions:

The important results of this study are: (1) very wide band bursts of hiss occur at times, (2) the peak intensity of these (and narrow band bursts) near the regions of production is around $10^{-10} Wm^{-2} (c/s)^{-1}$ to within a few orders of magnitude, and (3) this intensity is not strongly frequency dependent, and may well be "flat" or frequency independent.

3.2 DYNAMIC CHARACTERISTICS

3.2.1 Amplitude Variations.

The narrow band pass channel at 4.3 kc/s was operated longer than any of the other channels. To show the amplitude variations the original pen recorder (4.3 kc/s channel) charts were redrawn on a compressed time scale. Eight months (June to September 1960 and 1961) processed in this way are shown in Figure 22. Each trace shows a single (local time) day. When these appear as straight lines no hiss was received. The trace was not drawn at times of equipment failure (e.g. 21st June, 1961). In addition the trace is followed by a dot if the 24 hour average (centred at 2200 L.T.) value of Kp exceeded 5. The amplitude scale is such that the separation of successive traces is approximately 0.5 μ volt.

Many of the features reported by Ellis, as described in Chapter 2, can be seen in Figure 22. Both "isolated bursts" and "noise storms" appear. The duration of "isolated bursts" is seen to be of the order of an hour whereas "noise storms" last several hours. Bursts appear at all times of the day but in general hiss activity is strongest in daylight hours. The "noise storms" occur on days of magnetic activity, but "isolated bursts" occur on other days as well.

One effect, also reported by Ellis, shows up quite clearly on this type of presentation: there is a general tendency

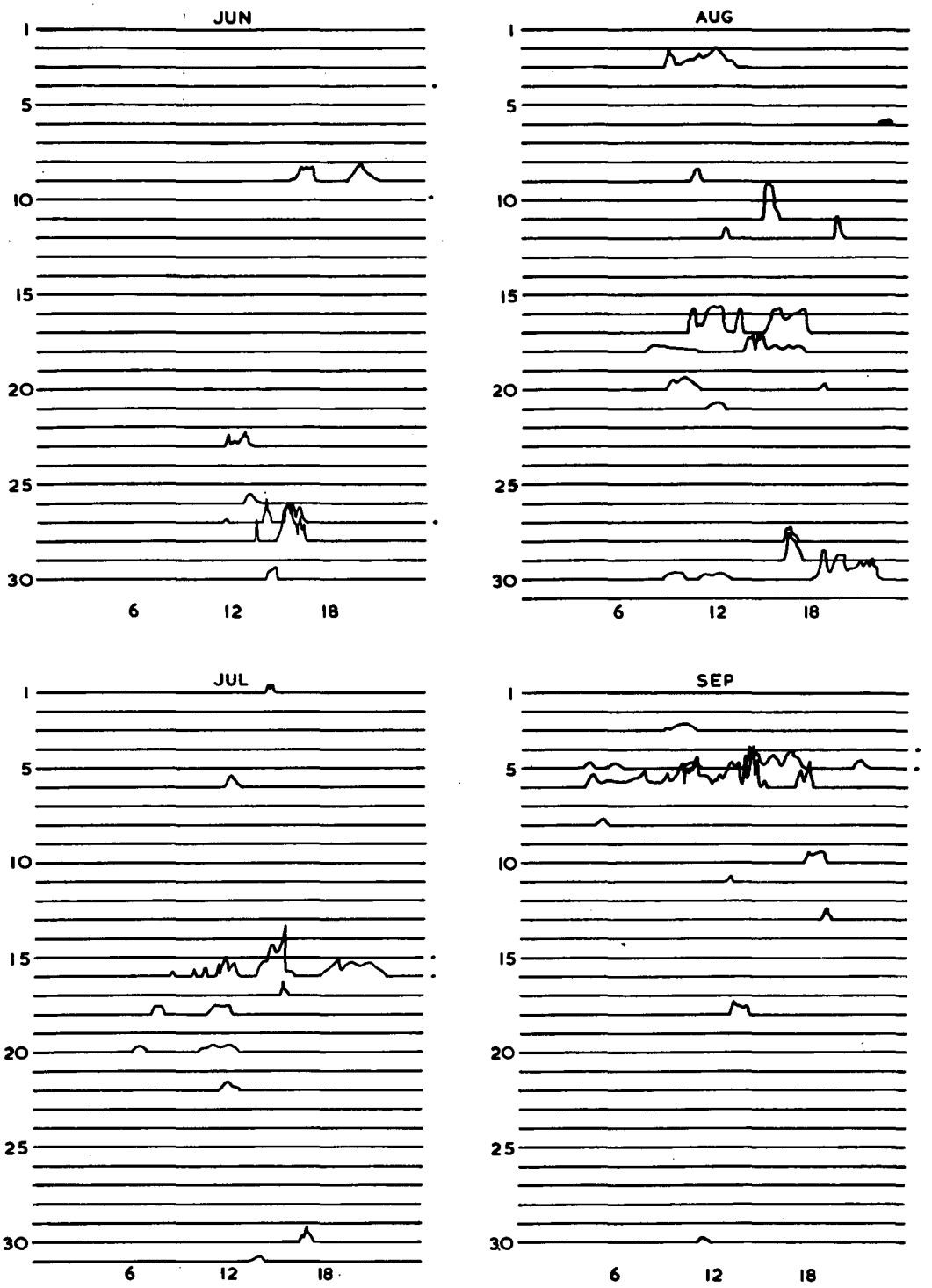

Fig. 22(a). Amplitude records (4.3 kc/s) for four months in 1960.

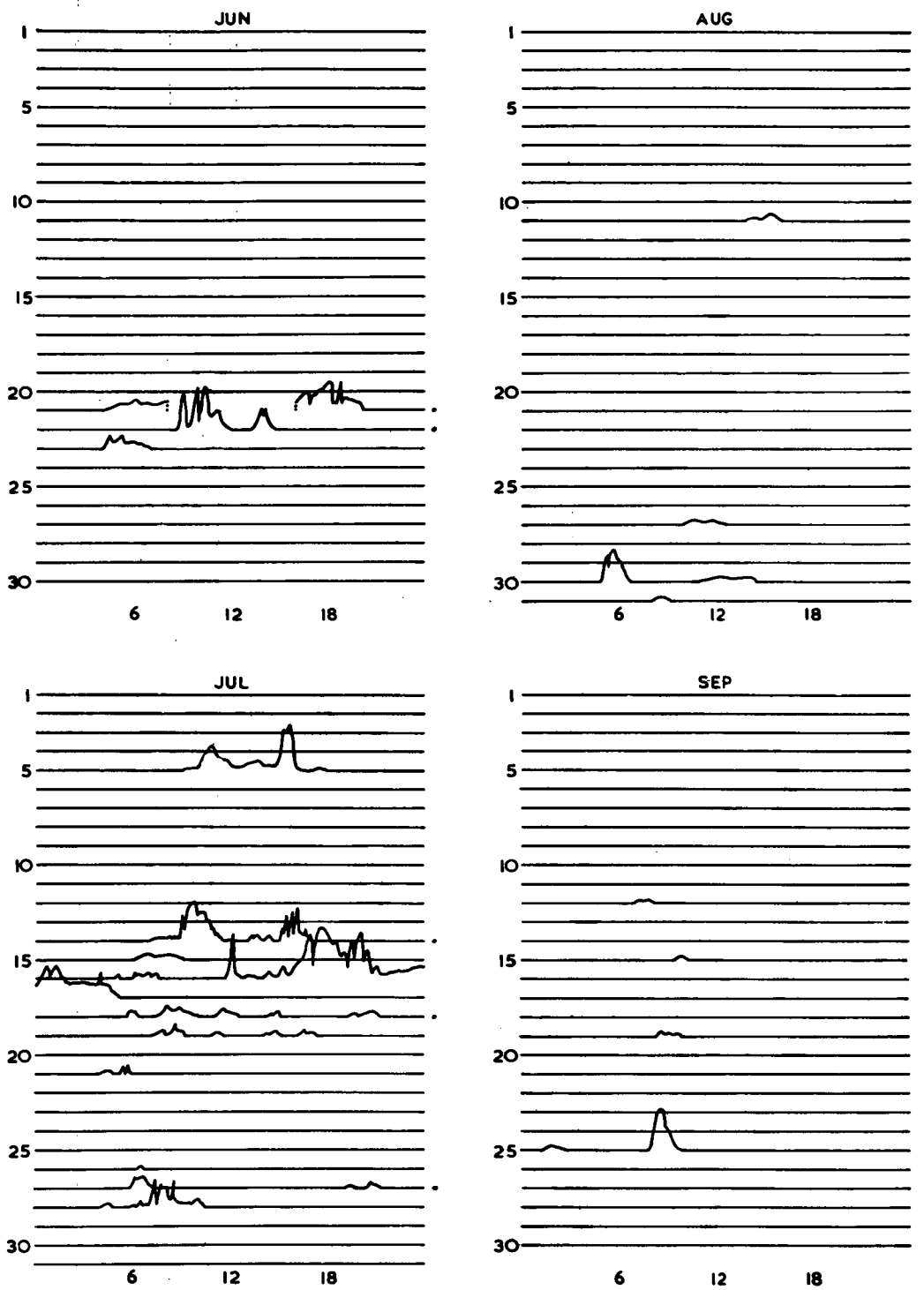

Fig. 22(b). Amplitude records (4.3 kc/s) for same four months in 1961.

for bursts to recur at about the same time on the following day, often with similar sequences of amplitude variations. A good example of this effect occurs in the group of bursts on the 26th June, 1960, to the 1st July, 1960, thus a "rounded" burst at 1310 on the 26th June, a "spiked" burst at 1410 on the 27th June, a triple peaked burst at about 1600 on the 27th June and a "rectangular" or double peak burst at 1330 on the 30th June, are each followed by similarly shaped "echoes" delayed by 22½, 23, 24 and 24 hours respectively. Many other examples are seen in Figure 22. There are some cases of multiple "echoes" having an apparent two day delay in the middle of July, 1960.

A similar effect of long standing appears on magnetic records: Chapman and Bartels[84] show several examples of recurring magnetic bays. In view of the association between magnetic bays and isolated bursts already established (Chapter2), this is not unexpected.

In an attempt to test this effect objectively the following rules were adhered to. The "echo" burst must occur at least twelve and not more than thirty six hours after the "originating" burst. The "echo" should be similar in duration. If two similar "echo" bursts occurred within a few hours of one another, only the first was considered. Only the bursts shown in Figure 22 were considered. A histogram of time delays is shown in Figure 23(a). It is seen that the delays are relatively narrowly distributed about 23-24 hours. To test that this was not entirely

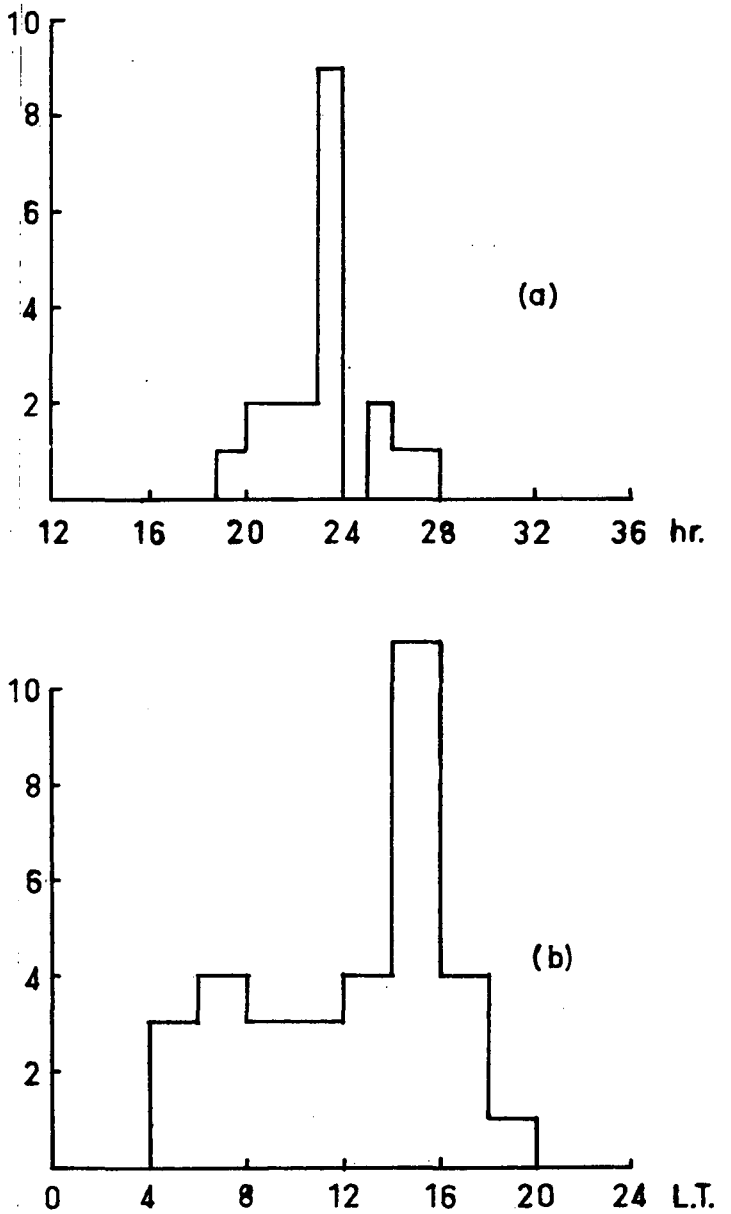

Fig. 23. (a) Histogram of time delays between "originating" and "echo" bursts in Figure 22. (b) Histogram of occurrence time of these bursts. The latter distribution is broader.

due to a diurnal effect, the times of occurrence of all "originating" and "echo" bursts were noted and are shown in the histogram of Figure 23(b). Although this shows a peak, the distribution is broader.

The amplitude variations which occur within a burst or noise storm are generally too diverse to classify into types. This also applies to the onsets and tails of bursts: both fast and slow (and medium) rises and falls occur. On a few occasions, however, a regular variation has been observed. The best example recorded is shown in Figure 24. This appeared as a relatively wide band pulsating burst, having a pulsation period of about two minutes. Magnetic records from Melbourne, Macquarie Island and Mawson for this time (0700-0800 U.T., 6 Sept. 1960) were examined but no phenomena of this period was found.

Another effect which could perhaps be included in this category was observed in a clear cut form on only one occasion. This is shown in Figure 25. At frequencies below about 1 kc/s there was a background noise which increased in intensity with decreasing frequency. The origin of this was not determined. This background level is seen in Figure 25 to be fairly strong at 125 c/s, progressively weaker at the higher frequencies, and steady in amplitude up till about 0850 L.T. At that time a strong (the 4.3 kc/s and 1.8 kc/s channels gains were low) narrow band burst began at about 4 kc/s and simultaneously the background began to decrease to the receiver noise levels. Towards the end of this

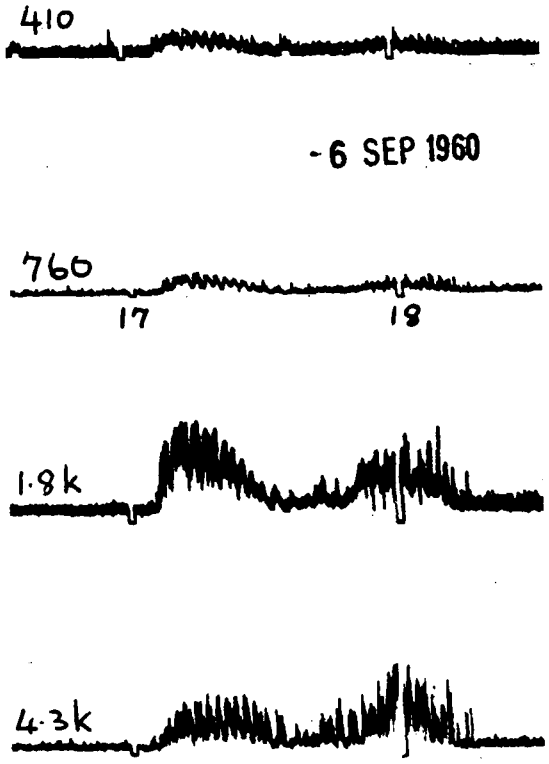

Fig. 24. Pulsating burst.

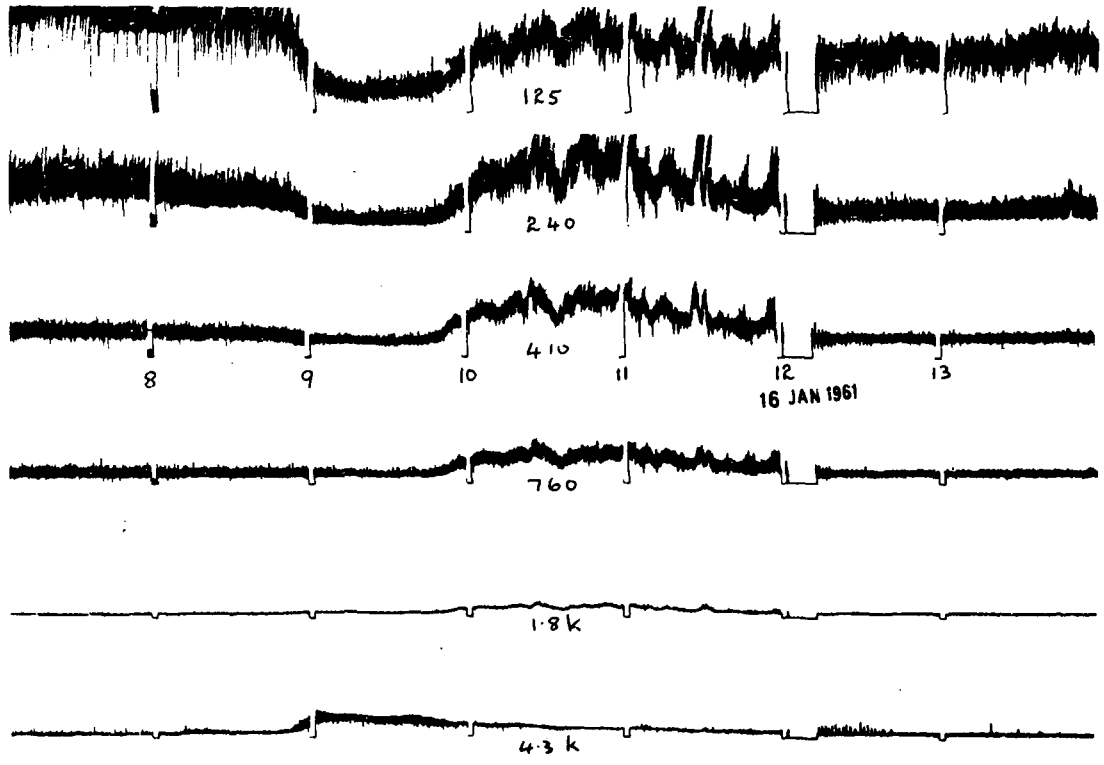

Fig. 25. Blanketing of low frequency (particularly 125 c/s and 240 c/s) background noise associated with 4 kc/s burst.

narrow band burst a wide band ($<$ 125 c/s to $\sim$ 2 kc/s) burst began. Finally the latter died out and the background rose to its previous level.

The important aspect of this event is that the presence of the narrow and wide band bursts in some way inhibited the background noise, either by inhibiting its generation or by inhibiting its propagation (increased attenuation). The latter is perhaps more likely as we have already seen (Section 2.4) that ionospheric absorption is correlated with hiss. Since the bursts were observed despite the increased attenuation, this suggests that the background noise has its origin at greater distances (higher latitudes).

3.2.2 Frequency Variations

The speed of the spectrograms used in studying whistlers and discrete emissions is such that a distance of one second along the time scale is of the order of 10 kc/s along the frequency scale (aspect ratio of 10 kc/s = 1 sec.). These show hiss as a steady band or series of bands of noise (Figures 1, 5 and 8). However, hiss shows pronounced variations of intensity, bandwidth and centre frequency if much slower spectrograms (aspect ratio of 10 kc/s $\approx$ 1 hour) are used. Examples are shown in Figures 26,27 and 28.

As found by Ellis (Chapter 2) "isolated bursts" were typically narrow band and the centre frequency was usually constant. However, some bursts which appeared as short isolated bursts on

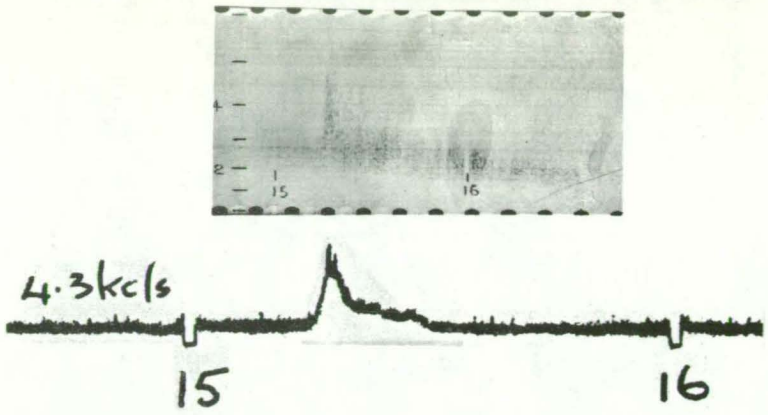

Fig. 26. Burst recorded on 17th July, 1960. Compare this with the burst recorded 24 hours previously (Figure 28.).

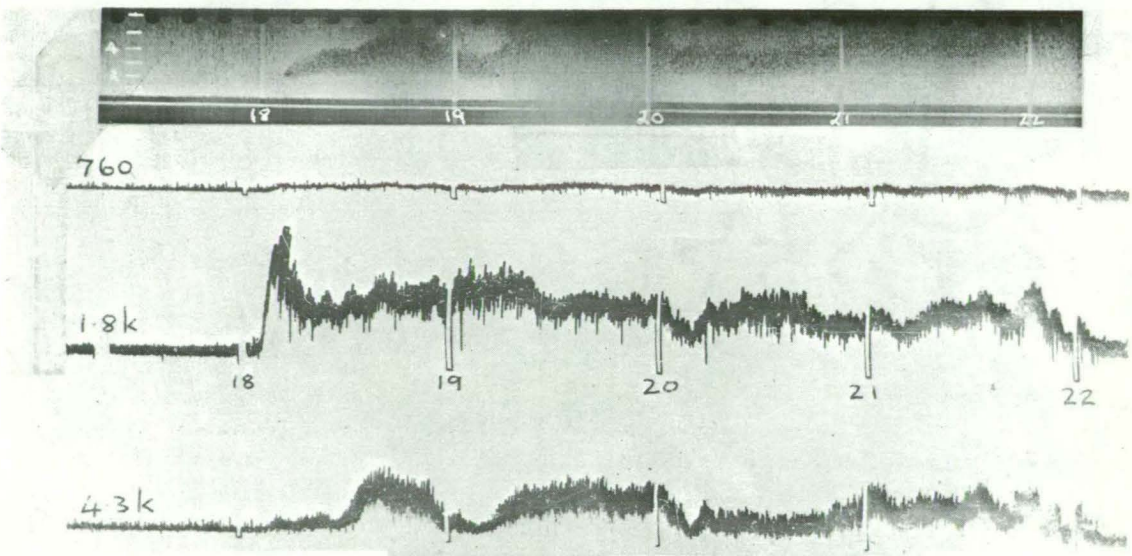

Fig. 27. Noise storm on 30th August, 1960.

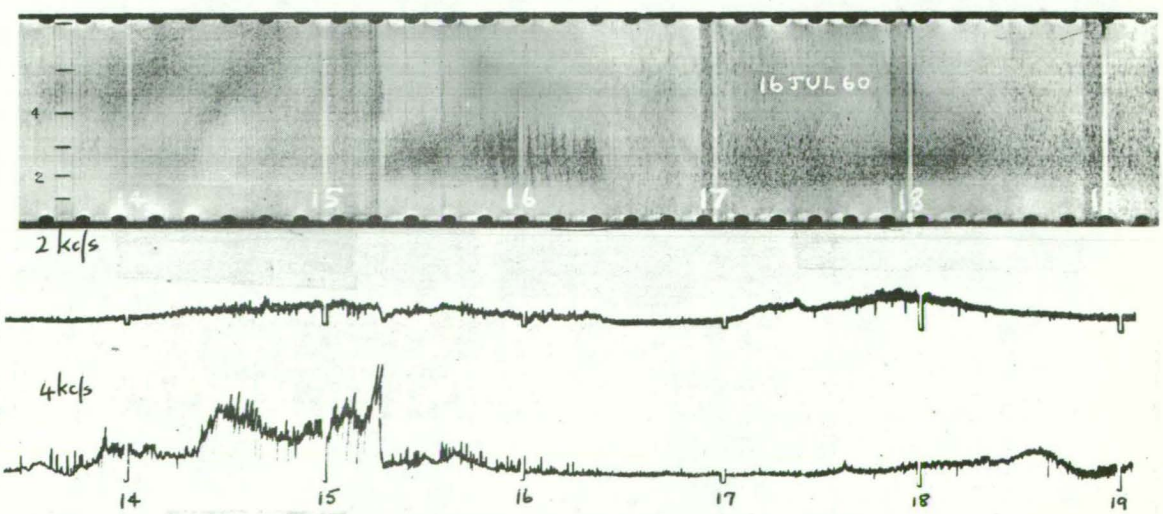

Fig. 28. Noise storm.

amplitude (pen) records showed some variation. That shown in Figure 26 is an example of this. The spectrogram shows that this burst lasted about 1½ hours and was fairly narrow band except for a short time (1515 to 1530 L.T.) when it appeared on the 4.3 kc/s pen channel. It slowly drifted downwards in frequency so that at about 1600 L.T. it became obvious on the 1.8 kc/s pen channel. This burst can also be found in Figure 22 where it appears as an "echo" of a previous noise storm "spike" (see also Figure 28).

During "noise storms" the bandwidth, and to some extent the centre frequency, varied greatly. This is seen in Figures 27 and 28. To some, and perhaps to a large extent, the amplitude variations as observed on a narrow band fixed frequency receiver are caused by these frequency variations. In contrast to the frequency-time traces of discrete emissions (as observed on fast spectrograms), the frequency-variations of hiss during "noise storms" do not show repeatable forms. However, the variations are not erratic and are rarely discontinuous. Wide band noise thus appears to grow out from narrow band noise, though it may extend mainly to higher frequencies as in Figure 27 or mainly to lower frequencies as in Figure 25.

As was seen in Section 3.1, the frequency extent of wide band hiss can be very large (some eleven octaves). Thus, at times, hiss has been observed at Hobart at frequencies from about 100 c/s to over 200 kc/s. On the other hand, whenever narrow band

hiss occurred, both during "isolated bursts" in magnetically quiet periods and during "noise storms" in severely disturbed periods, its centre frequency was usually around 3kc/s. It was never less than 2 kc/s or greater than about* 8 kc/s.

* The upper limit is not well known as it was outside the range of the spectrum analyser. On rare occasions hiss occurred on the 9.0 kc/s pen channel which did not appear on the 4.3 kc/s channel.

3.3 TECHNIQUES.

3.3.1 General

A block diagram of the complete receiving system is shown in Figure 29. Two vertical loop antennae were used. The low frequency ($<$ 10 kc/s) loop had six turns of hook up wire. The high frequency loop had two turns made from standard 300 ohm ribbon transmission line. Both loops were triangular (40 ft. base, 20 ft. height) and of area 40 sq. metres. In both cases the signal was fed into wide band pre-amplifiers situated near the loops, The pre-amplifier outputs were fed into the remainder of the equipment by coaxial cable. This equipment was housed about a hundred metres from the loop antennae to minimise power supply pick up.

For the highest two frequencies (70 kc/s and 230 kc/s) standard communications receivers (R1155) were used. The frequencies chosen were comparatively free from communication interference. The detector outputs of these receivers were amplified and applied to the deflector plates of a twin beam cathode ray tube. This was recorded on 35mm film moving continuously at a rate of one or three inches per hour.

Two systems were used for the lower frequencies (100 c/s to 10 kc/s). Originally, as shown in Figure 29, the pre amplifier output was further amplified (W.B.A.) and then fed through cathode followers to seven fixed-frequency tuned amplifiers and two sweep-frequency spectrum analysers. The bandwidth of the fixed tuned amplifiers was approximately one tenth of the operating frequency.

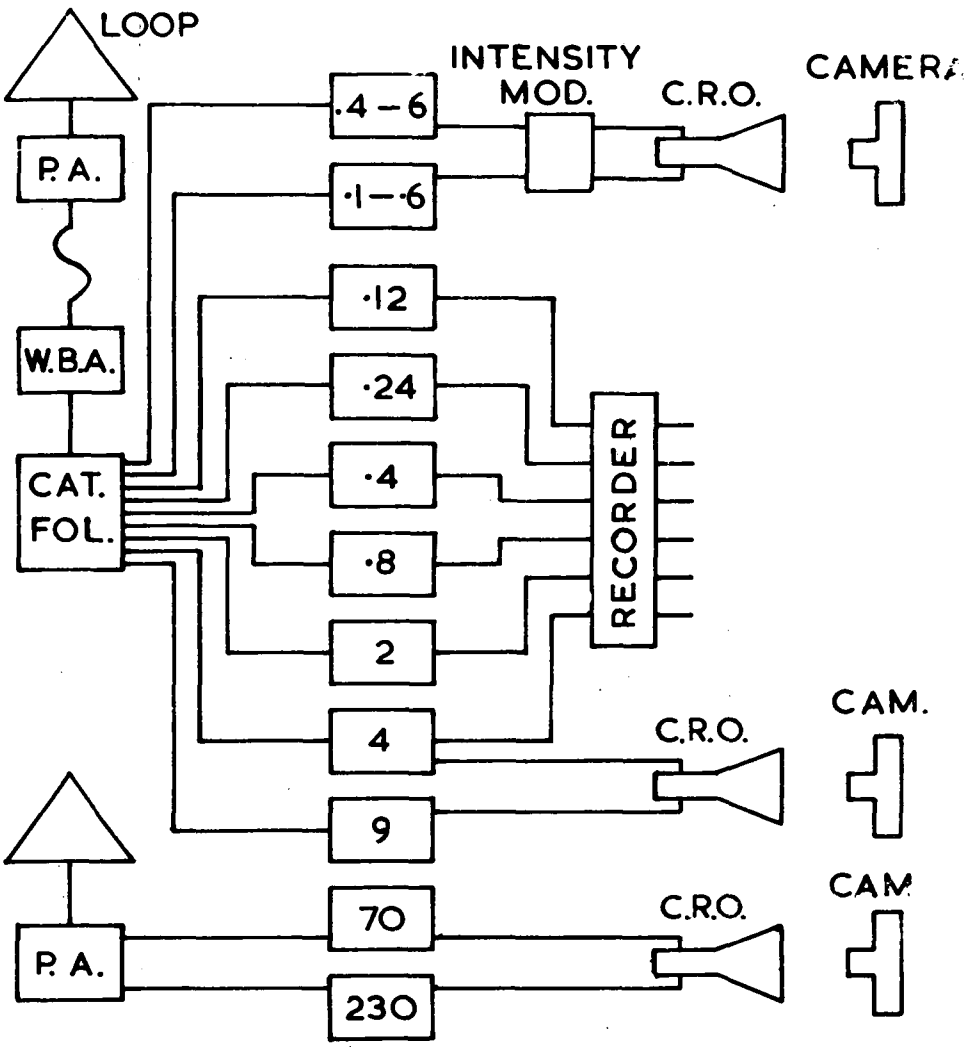

Fig. 29. Block diagram of receiving system.

A minimum reader circuit similar to that shown in Figure 11 was used for pen recording.

The system so far described used standard techniques and so will not be described in greater detail. A later system used separate complete receivers for each channel. A circuit diagram is shown in Figure 30. This is a slight modification of that designed by Ellis, which is fully described elsewhere[23].

The two channel sweep-frequency spectrum analyser used standard heterodyne techniques. The high frequency (400 c/s to 6 kc/s) channel had a local oscillator mechanically swept (motor driven cam) from 20 kc/s to 26 kc/s. Its intermediate frequency amplifier had a centre frequency of 20 kc/s and bandwidth of 40 c/s. The low frequency limit (400 c/s) was set by local oscillator break through. The sweep rate was 4 sweeps per minute. The low frequency channel (100 c/s to 600 c/s) was basically similar: L.O. sweep from 2.0 kc/s to 2.6 kc/s, I.F. of 2.0 kc/s with 10 c/s band width, and sweep rate of 2 s.p.m. The outputs of these channels modulated the intensity of two in-line traces on a twin beam C.R.T. A circuit diagram of the intensity modulator is shown in Figure 31, and is discussed below.

In the quiescent state current through V1 and hence R1 produces a potential difference across R1 and hence between grid and cathode of V3 sufficient to keep V3 cut off. A sufficiently strong (negative) signal on the grid of V1 will cut off V1 and thus allow V3 to conduct and ascillate. The output of this

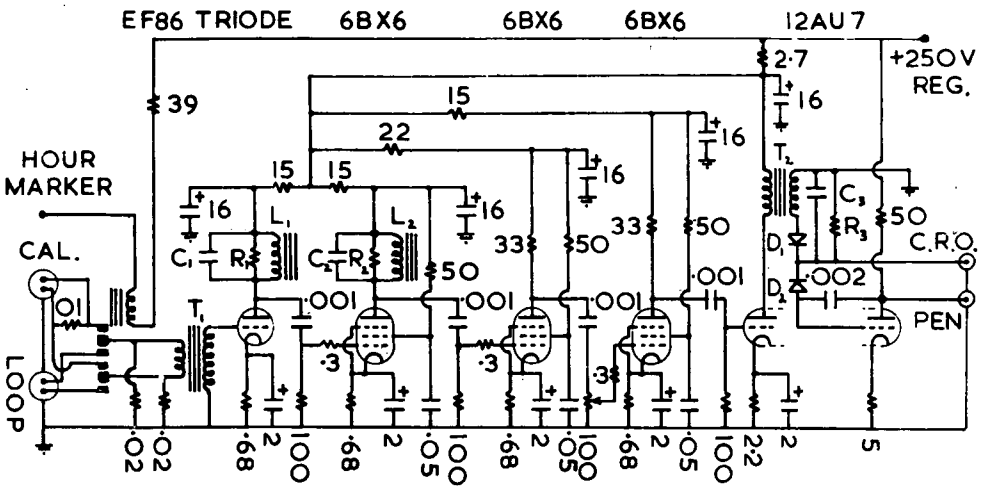

Fig. 30. Circuit of complete (single channel) receiver for hiss. Resistance units are kilohms and capacitance units are microfarads. Transformers T_1 and T_2 are ferroxcube potcores wound with 30:3000 and 1000:2000 turns respectively. Diodes D_1 and D_2 are 0A202's (silicon). The values of the tuning and detector integrator components depend on the centre frequency and bandwidth required.

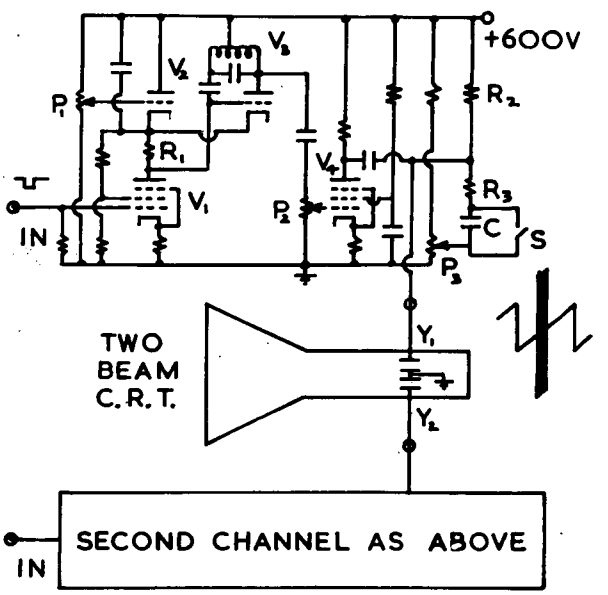

Fig. 31. Two channel intensity modulator.

oscillator is amplified by V4 and applied to the Y1 deflector plate of a twin beam C.R.T. Also applied to Y1 is a time base voltage (B2 and C) and a shift voltage (P3). Thus in the absence of a strong input signal the C.R.T. spot moves across the screen at a constant rate in step with the frequency sweep. When a strong signal input triggers the oscillator the C.R.T. spot has impressed on it an additional very strong and very rapid movement. This tends to make the spot invisible. This effect is augmented by the characteristics of the C.R.T. screen phospher and the photographic emulsion. The second channel operates in precisely the same way and its output is applied to Y2. The net effect is two separate in-line traces which can have different amplitudes and time bases and which can be intensity modulated independently. Incidentally this intensity modulation is "direct coupled", i.e., it has full response down to zero frequency.

3.3.2 Calibration

Two basic methods of intensity calibration were used. In the first the loop antennae was replaced by a signal generator or standard noise generator of the same impedance. Intensities of hiss were then deduced from this receiver sensitivity calibration and the effective height of the loop antenna calculated from measurement of its physical dimensions. The second method gave direct calibration by generating a known field strength in the vicinity of the antenna from a remote auxiliary loop[85]. This method has the other advantages that the receiving system is not disturbed and that the calibration signal has to compete with interference (atmospherics) in the same way as does the hiss signal. Both these methods

gave consistent results. The calibration and reading accurancy (about 10%) was more than adequate for the arguments presented in this thesis.

In addition to manual "absolute" intensity and frequency calibrations, several calibrations were applied automatically. At the beginning of every hour a time mark was applied to all channels for about two minutes. At first this was done by removing the output from the preamplifiers, but later by replacing the loop antennae by dummy loads (as in Figure 30). This second method also provided a zero level. An additional time mark was applied at noon and midnight (local time). Later on this was replaced by an automatic noise generator calibration (using a silicon diode[86]). Two frequency calibrations at harmonics of 200 c/s and 1 kc/s (using a multivibrator) were applied to the spectrum analyser each hour for about one minute.

The timing for these operations was derived from synchronous motors (the power frequency in Tasmania is quite stable). All recording devices such as the film and paper chart drives were motor driven from the A.C. mains supply. To avoid ambiguities in timing arising from a power failure, and in particular a series of power failures, a relay operated by the first power failure transferred the timing to a clock work system. This relay was reset manually along with the synchonous timers.

4. REVIEW OF THEORIES OF GENERATION OF V.L.F. EMISSIONS.

4.1 Early work. Many of the early ideas on generation of V.L.F. emissions were borrowed from solar radio astronomy. When work in this field began, solar radio astronomy had already made over a decade of progress in observations and theoretical work. However, it should be noted that the earliest of the ideas discussed here is ~~are~~ less than five years old. Because this whole field is so new the development of ideas from crude to sophisticated does not fit a strictly chronological pattern.

The sun's corona is in many ways similar to the earth's exosphere. Some writers have in fact referred to the exosphere as the terrestrial corona. The exosphere is much smaller, colder and less dense and the magnetic field is weaker. The last two points also amount to a scaling down (from H.F. to V.L.F.) of the natural resonance frequencies, these gyro and plasma frequencies. Another difference is that the magnetic field of the sun is highly complex while that of the earth is fairly closely dipole.

Nevertheless it is surely significant that in both regions electro-magnetic phenomena are produced at frequencies of about the same order of magnitude of these natural resonance frequencies. Thus many of the processes which account for H.F. emissions from the solar corona might well account for V.L.F. emissions from the earth's exosphere. There is an essential difference, however. In the solar case only processes allowing outward propagation from the region of generation to interplanetary space and ultimately to the earth can account for observations made here on the earth. Quite the reverse is true for V.L.F. emissions from

../2.

the earth's exosphere: inward propagation is necessary for observation on the earth's surface. This point rules out many of the processes which work in the solar case.

Some of the processes which apply in the solar case are synchrotron radiation, cyclotron radiation, and plasma oscillations. The first two are related to the particle gyro frequency given by

$$h = B \frac{e}{m}$$

where e is the particle* charge
m is the particle* mass
B is the magnetic intensity

Synchrotron radiation is produced by relativistic electrons at multiples of the (particle) gyro frequency. For very energetic particles most of the energy is radiated at the high harmonics. Cyclotron radiation is produced by non relativistic particles at the gyro frequency only. Ellis [28] suggested that the narrow band 4kc/s hiss which he observed might be cyclotron radiation. The (electron) gyro frequency has this value at about 6 earth radii from the centre of the earth[28]. This is the region where particle streams from the sun should be stopped by the geomagnetic field[28].

Plasma oscillations occur at the frequency

$$p^2 = N e^2 / \pi m$$

where N is the particle density.

.../3.

---

* We are mainly concerned with electrons here. When we consider protons we will use H and M for the proton gyro frequency and mass.

Plasma oscillations are excited by fast particles, but it is not these particles which radiate as in the synchrotron and cyclotron case, but the medium itself, the plasma.

We will now see if any of these processes allow downward propagation at V.L.F. from the exosphere through the ionosphere to the earth's surface. The only propagation mode allowable is the "whistler mode": the longitudinal extraordinary mode below the gyro frequency. The refractive index of this mode (n) is given by :-

$$n^2 = 1 + \frac{p^2}{f\,(h-f)} \qquad (4.1)$$

where f is the frequency of the wave being propagated and p and h refer to electrons.

Since propagation is not possible for $f > h$, synchrotron radiation from electrons will not be observable (except possibly at the fundamental f=h). At f=h the refractive index becomes infinite and the attenuation very large. Thus even cyclotron radiation (from electrons) will be severely inhibited. As we will see in chapter 5, the electron density in the exosphere is approximately proportional to the magnetic field strength, thus

$$p^2/h \simeq \text{constant} \; (\approx 1 \text{ Mc/s}) \qquad (4.2)$$

Since, in the exosphere $h < 1$Mc/s then $p > h$. Consequently, electron plasma oscillations cannot propagate down to the earth.

However, the exosphere must be electrically neutral so that in all regions the electrons must be balanced by an equal charge of ions. These will be almost entirely protons. The presence of these protons has relatively little effect on the refractive index as calculated on the electron component alone[46], but it does present the possibility of proton emission processes.

,...4/-

The proton gyro frequency H is given by :-

$$H = h\frac{m}{M} \sim h/2000$$

The highest proton gyro frequencies will occur near the earth's surface and near the poles. Even there it is only about 800c/s. Thus although allowable as far as downward propagation is concerned, cyclotron radiation from protons would occur at frequencies too low for most of the V.L.F. emissions discussed in Chapter 2. Adrons and co-workers [19,20,21] suggest that their narrow band emission at 750 c/s was proton cyclotron radiation. On the other hand synchrotron radiation at multiples of H produced by highly relativistic protons might resolve this difficulty. At a given point in the exosphere a series of tones separated by H (a few cycles per second, generally) would be produced. Since these tones would be rising the net result would probably be indistinguishable from wide band noise. However, there are probably not enough relativistic protons to provide observable intensities even if most of the energy of these protons is converted into electro-magnetic energy in the V.L.F. band.

Allcock[7] suggested proton plasma oscillations as a possible mechanism for dawn chorus. He pointed out that a cloud of incoming fast particles might excite oscillations at decreasing levels in sequence. This would appear as a series of rising tones to an observer on the earth. A similar process was thought to produce Type III solar radio bursts. The proton plasma frequency (P) is given by :-

$$P^2 = \frac{m}{M} p^2 \sim p^2/2000$$

Thus $P^2/h \sim 500$ c/s

Consequently downward propagation [redacted] proton plasma oscillators could occur for all regions for which h $>$ 500c/s. This probably includes all of what we will descri[redacted] as the earth's exosphere.

.../5.

The much greater mass of protons make them very poor radiators compared with electrons. It is doubtful if any of these proton processes could produce an observable amount of radiation. This and a more sophisticated proton process will be discussed in a later section.

4.2 Cerenkov Radiation. This is produced when a charged particle travels in a medium at a velocity greater than the phase velocity of electromagnetic waves in that medium. Radiation is produced at all frequencies for which this condition holds. It has been observed and studied in the visible light region for several decades. It was proposed as a mechanism for the generation of most of the non-thermal radio emission from the sun by Marshall[47]. Noting this Ellis[48] showed that Cerenkov radiation would also be produced in the exosphere at V.L.F. From (4.1) and (4.2), even for $h \gg f$, the (phase) refractive index is greater than 10 for $f < 10$ kc/s. The refractive index will also be high near the gyro frequency ($h-f$ small). Thus in both cases V.L.F. emission would be produced even from relatively slow particles (0.1 c.). The emission would generally be broad band hiss.

At first it appeared that the amount of radiation produced would not be sufficient to produce the observed intensities. However, rocket[49] and satellite[41] measurements showed that streams of incoming particles were stronger than previously supposed. Also Jelley[50] pointed out that small (of dimensions much less than a wave length) irregularities would radiate coherently, so that the radiated power from each irregularity would be proportional to the square of the number of particles it contained. Quite a small amount of irregularity or "bunching" suffices to explain the observed intensities.

.../6.

In a sense it is the medium which radiates rather than the particle or "bunch". In a magneto active plasma such as the exosphere or the solar corona the process is much more complicated than in the simple media for which the Cerenkov expressions were originally derived. A vigorous theoretical treatment of Cerenkov emission produced by a single electron moving in a magneto active plasma is given by Eidman[51].

4.3 T W T Amplification. The ideas discussed above have been borrowed from solar radio astronomy. We now consider an idea borrowed from laboratory U.H.F. techniques. [illegible] In the travelling wave tube (TWT) amplifier an electron beam and an electro magnetic wave travel down the axis of the tube. A slow wave structure reduces the phase velocity of the wave to a value considerably less than the free space velocity C. The longitudinal component of the electric field of the wave can interact with the electrons in the beam. When the electron velocity (or component along the axis of the tube if magnetic focusing is used) is equal to the phase velocity of the wave, electrons lose energy to the wave so that the wave grows exponentially. Gallet and Helliwell[52] suggested that the same process might occur in the exosphere. The slow wave structure of the laboratory TWT is replaced by the high refractive index of the whistler mode in the exosphere. Both streams of electrons and V.L.F. waves in the exosphere will tend to travel down a magnetic field line and thus be confined to a magnetic tube of force. A substantial longitudinal component of electric field of the wave will exist for interaction with the electron stream[52]. When the velocity of the electrons (assumed to travel exactly down the field line), βc, equals the phase velocity

of a wave, c/n, at frequency f, then amplification is produced at these frequencies.

Thus from the condition :-

$$n\beta = 1$$

And from (4.1), assuming $n^2 >> 1$, they found

$$f = \frac{h}{2}\left[1 \pm \left(1 - \frac{4\pi^2 p^2}{h^2}\right)^{\frac{1}{2}}\right]$$

It is seen that two frequencies (f^+ and f^-) are amplified. The Cerenkov condition discussed above is

$$n\beta > 1$$

Thus Cerenkov radiation is produced in two bands covering the frequencies c to f^- and f^+ to h. If we impose the restriction on Cerenkov radiation that emission is only allowable in a direction along the field line then Cerenkov radiation is also only allowable at these two frequencies, f^+ and f^-.

The attraction of the TWT process (or restricted Cerenkov emission) is that at a given small region only two frequencies are produced. If the electrons in the stream all have much the same velocity and if the length of the stream along the field line is short (a few hundred kilometers) then only two narrow bands will be amplified at a given time. As the stream progresses down the field line the centre frequencies of these bands will vary. To an observer on the earth these will appear as time varying tones. Gallet and Helliwell[52] showed that the frequency - time sequence of one of these narrow bands (f^-) agrees closely with that observed for some types of discrete emissions ("hooks", "quasi constant tones"). Typically the frequency (f^-) is fairly constant while the stream is in the exosphere but rises rapidly when the

stream enters the upper ionosphere.

If amplification is restricted to the exosphere where the f^- is fairly constant then a long stream of monoenergetic electrons should produce narrow band hiss. It seems reasonable that greater amplification would be produced in regions and for electron velocities for which the frequency of amplification is slowly varying. Some further observation and theoretical developments have made this theory more attractive. For these reasons this idea is much further developed in Chapter 6.

4.4 Doppher Shifted Cyclotron Radiation. This is presented at this point because these ideas followed (and perhaps were stimulated by) the TWT paper by Gallet and Helliwell. Mac Arthur[53] pointed out that protons gyrating at frequency H will appear at the doppler shifted and thus much higher frequency f if they are rapidly approaching the observer, where

$$f = \frac{H}{1 - n\beta_d}$$

where $c\beta_d$ is the velocity component of the protons in the direction of the magnetic field (and direction of propagation). He showed that this approximated the TWT expression given above. Essentially this is because for $H/f << 1$, $n\beta_d \approx 1$. The same process was also considered by Murcray and Pope. However, they used the refractive index at frequency H rather than that at f and consequently obtained a different (and erroneous) expression.

Murcray and Pope[54, 56] pointed out an advantage of the proton gyration theory over the TWT theory: a quantitative estimate of radiation can be made. On the other hand such an estimate made by Santirocco[55] indicated that proton radiation would be much too small for detection. Murcray

../9.

and Pope[56] countered this by showing that sufficient radiation would be produced if the protons radiated coherently. There are a number of flaws in Santirocco's arguement but his conclusions are correct. It is unrealistic to suppose that enormous numbers of protons would radiate coherently.

While working on this review an idea occurred to the writer which would resolve this difficulty. Santirocco gave an expression for radiated power which shows that this is inversely proportional to the square of the particle mass. Thus one would expect the radiated power from gyrating electrons to be greater than three million times that from protons, other factors being the same. But only radiation emitted at frequencies less than the electron gyro frequency can propagate down to the surface of the earth. Thus we require a downward doppler shift of the frequency h. This would happen if the electrons travelled away from the observer. This idea is developed in Chapter 7. ~~The argument used there to show that the resulting intensity from gyrating electrons would be adequate to explain observed intensities of discrete emissions can also be used (by making the appropriate substitutions in particle mass) to show the inadequacy of proton radiation.~~

4.5 Conclusions. All the mechanisms for production of V.L.F. emissions in the exosphere so far published (late 1961) have been reviewed above. The most promising ideas appear to be the TWT amplification process (mainly for hiss) and doppler shifted cyclotron radiation, at least for electrons (~~for discrete emissions~~). Before these ideas (particularly the former) can be further developed it is necessary to obtain an expression for the variation of electron density in the exosphere along a geomagnetic field line. This is derived in the next chapter.

5. ELECTRON DENSITY DISTRIBUTION ALONG A GEOMAGNETIC FIELD LINE IN THE EXOSPHERE.

5.1 Introduction.

Over the last few years whistler (and to some extent, micropulsation) studies have yielded considerable information about electron densities in the exosphere out to several earth's radii. However the measured quantities (delay times) are the result of an intergration over the whole path along the field line. The important contribution to this integral occurs at the equatorial plane where the electron density and magnetic field are least for the path. The value of this integral is relatively insensitive to the way in which the electron density varies along the path. Thus whistler work has produced fairly accurate estimates of electron density in the equatorial plane but relatively little information as to how the electron density varies along the path (field line). It is this manner of variation which we require for the discussions in chapters 6 and 7.

An assumption often made is that the electron density is distributed with spherical symmetry about the centre of the earth. This would be logical in the

absence of any magnetic field as any local discontinuities would tend to diffuse over a sphere. In the presence of a magnetic field, however, charged particles are fairly well confined to a magnetic tube of force so that diffusion would take place along the magnetic field lines. Some workers[52] have adopted a gyro frequency model, that is, the electron density is everywhere proportional to the magnetic field strength or gyro frequency. As it turns out in this chapter, this is a good approximation. However no theoretical argument justifying this has been given previous to this work (1960).

This chapter is an attempt to make this effect into account and derive the distribution along a field line on the assumption that the tubes of force are supplied with charged particles (electrons and protons) from the upper ionosphere. The particles will move in helical orbits along the field line (Figure 32). Since the cross-section of the tube of force rapidly increases towards the equatorial plane and since the pitch of the helices decreases (i.e. opens out) in this direction we would expect the density to decrease rapidly. Collisions are neglected except in the source regions near the earth's surface. Here

down coming particles which are scattered and "lost" are replaced (assuming equilibrium) by an equal number of up-going ones.

Thus the distribution of the thermal particles (electrons and protons) which make up the medium is derived on the assumption of injection near the earth's surface (upper ionosphere). The distribution of the faster particles which produce aurora and airglow and presumably V.L.F. emissions is derived on the assumption that these particles are injected into the tubes in regions farthest from the earth, that is near the equatorial plane. Finally, for completeness, the distributions for injection at any point is derived. This latter is briefly discussed with regard to the outer Van Allen belt.

If the source distributions, both along the field lines and across the field lines, were known, it would be possible to find the particle densities at any point in the exosphere. This is done in the case of the thermal particles making up the medium by taking a simplified model of source region electron density variation with geomagnetic latitude.

5.2 Theory.

The various equations describing the dipole magnetic field, a line of force and a tube of force are given (Alfven[56], Chapman and Sugiura[58],):

$$R = R_o \cos^2 \ell$$

$$R_o = \sec^2 \lambda$$

$$B = \eta B_o$$

$$BA = B_o A_o \text{ hence } A = A_o/\eta$$

$$\frac{ds}{d\ell} = R_o \phi \cos \ell$$

where:

R = radius vector in earth radii } polar coordinates

ℓ = latitude angle } polar coordinates

λ = geomagnetic latitude at which the line of force cuts the earth's surface

L = latitude of injection point

B = intensity of the earth's magnetic field

η = $\phi \sec^6 \ell$

ϕ = $(1 + 3 \sin^2 \ell)^{\frac{1}{2}}$

A = cross section area of tube of force

s = distance along line of force.

Some of these definitions are illustrated in Figure 32. Subscript "o" denotes values for which $\ell = 0$ (i.e. in equatorial plane), and subscript "L" values for which $\ell = L$, subscript "λ" values for which $\ell = \lambda$ (earth's surface), We note immediately that:

$$\eta_o = \phi_o = 1.$$

We consider one of the particles spiralling along the line of force determined by "λ". At the point determined by "ℓ", let its pitch angle be "ψ" and its speed "v". Equations governing its motion (Gold[59]), are:

$$v = v_o \text{ (constant)}$$

$$B/\sin^2\psi = B_o/\sin^2\psi_o$$

Hence: $\sin^2\psi = \eta \sin^2\psi_o$

The velocity of the "guiding centre" of the spiralling particle is:

$$\frac{ds}{dt} = v\cos\psi = v(1 - \sin^2\psi)^{\frac{1}{2}}$$

$$= v(1 - \eta\sin^2\psi_o)^{\frac{1}{2}}$$

The probability of finding this particle at position "ℓ" is proportional to $\frac{dt}{d\ell}$

Now $\frac{dt}{d\ell} = \frac{dt}{ds}\cdot\frac{ds}{d\ell} = R_o\phi\cos\ell\left[v(1 - \eta\sin^2\psi_o)^{\frac{1}{2}}\right]^{-1}$

If we consider a large number of such particles (ℓ, ψ_o, v) the density (cm^{-3}) will be given by

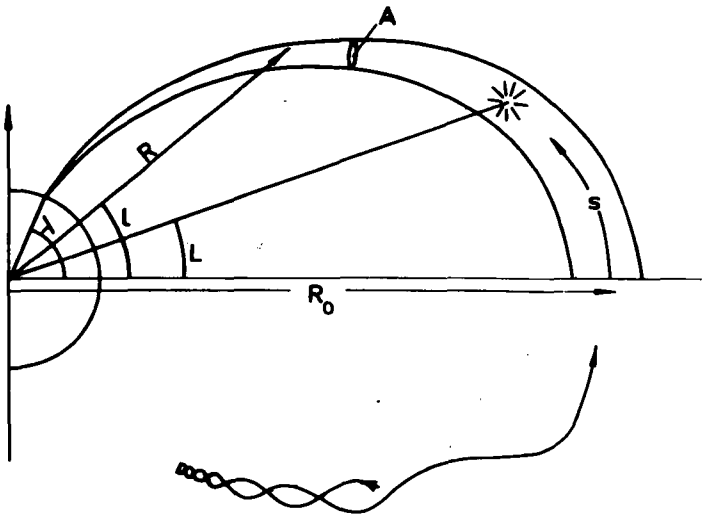

Fig. 32. Definition of coordinate system.

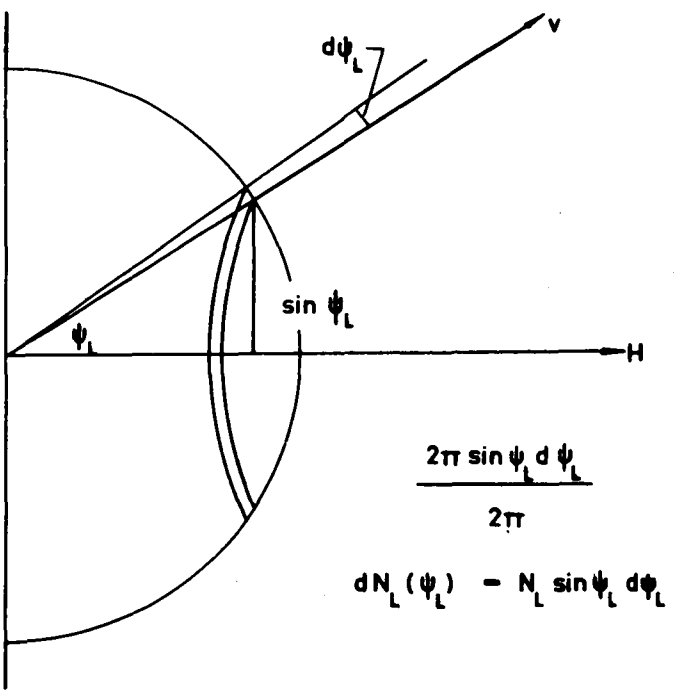

Fig. 33. Pitch distribution for isotropic injection.

$$\mathcal{N}(\psi_0, v) \propto \frac{dt}{dl} / A$$

$$= \frac{k R_0}{A_0 v} \cdot \eta \phi \cos l \, (1 - \eta \sin^2 \psi_0)^{-\frac{1}{2}}$$

where k is a constant of proportionality.

In the equatorial plane:

$$\mathcal{N}(\psi_0, v) = \frac{k R_0}{A_0 v} (1 - \sin^2 \psi_0)^{-\frac{1}{2}} = \frac{k R_0}{A_0 v \cos \psi_0}$$

Hence

$$\mathcal{N}(\psi_0) = \mathcal{N}_0(\psi_0) \, \eta \phi \cos l \cos \psi_0 \, (1 - \eta \sin^2 \psi_0)^{-\frac{1}{2}} \qquad (5.1)$$

We first consider the simpler case of a source of particles in the equatorial plane ($L = 0$). If the source is isotropic (no preferred particle direction) simple geometrical considerations (see Figure 33) show that the distribution of pitch angles will be given by

$$d N_0(\psi_0) = N_0 \sin \psi_0 \, d\psi_0 \qquad (5.2)$$

where the expression on the left hand side represents the density (at $l = 0$) of particles having pitch angles in the range ψ_0 and $\psi_0 + d\psi_0$.

Substituting this for $\mathcal{N}_0(\psi_0)$ in equation (5.1):

$$d N(\psi_0) = N_0 \eta \phi \cos l \sin \psi_0 \cos \psi_0 \, (1 - \eta \sin^2 \psi_0)^{-\frac{1}{2}} d\psi_0$$

The total density at point l, λ is given by integration over all allowable values of ψ_0 from $\psi_0 = 0$ to ψ_0 = its maximum value Ψ_0 given by $\eta \sin^2 \Psi_0 = 1$.

Particles which had pitch Ψ_0 will have pitch $\psi = \frac{\pi}{2}$

at this point (magnetic mirror point). Particles of greater pitch will have been removed by magnetic reflection before reaching this point.

Hence

$$N = N_0 \eta \phi \cos l \int_0^{\Psi_0} \sin\psi_0 \cos\psi_0 (1 - \eta \sin^2\psi_0)^{-\frac{1}{2}} d\psi_0$$

Putting

$$y^2 = 1 - \eta \sin^2\psi_0$$

$$N = N_0 \eta \phi \cos l \frac{1}{\eta} \int_0^1 dy = N_0 \phi \cos l \qquad (5.3)$$

The expression $\phi \cos l$ is unity at $l = 0$ and at $\sin^2 l = 2/3$ ($l \sim 55°$). It has its maximum value (1.15) for $\sin^2 l = 1/3$ ($l \sim 35\frac{1}{2}°$). Simple computation shows it to be within 15% of unity for $l < 60°$

Hence this distribution which probably applies to the case of solar particles injected into the tube of force during magnetic storms gives a practically constant density along a line of force for all lines (λ) up to $\lambda = 60°$

The thermal particles which make up the background medium are probably supplied where ionization is taking place, i.e. in the ionosphere. Accordingly we consider an isotropic source at $L = \lambda$ The distribution of pitch angles is given (as in Equ. 5.2) by

$$d N_\lambda(\psi_\lambda) = N_\lambda \sin\psi_\lambda \, d\psi_\lambda \qquad (5.4)$$

We relabel these same particles by the pitch angles (ψ_0) they would have on reaching the equatorial plane, where

$$\sin^2\psi_\lambda = \eta_\lambda \sin^2\psi_0 \qquad (5.5)$$

Differentiating:

$$2\sin\psi_\lambda\cos\psi_\lambda\, d\psi_\lambda = 2\eta_\lambda \sin\psi_0\cos\psi_0\, d\psi_0$$

Hence

$$\sin\psi_\lambda\, d\psi_\lambda = \eta_\lambda \frac{\sin\psi_0\cos\psi_0}{\cos\psi_\lambda}\, d\psi_0$$

$$= \eta_\lambda \sin\psi_0\cos\psi_0 (1-\eta_\lambda\sin^2\psi_0)^{-\frac{1}{2}}\, d\psi_0$$

Relabelling Equ.(5.4) and substituting:

$$dN_\lambda(\psi_0) = N_\lambda \eta_\lambda \sin\psi_0\cos\psi_0 (1-\eta_\lambda\sin^2\psi_0)^{-\frac{1}{2}}\, d\psi_0 \qquad -(5.6)$$

From Equ.(5.1) we have:

$$\mathcal{N}_0(\psi_0) = \mathcal{N}_\lambda(\psi_0)\frac{(1-\eta_\lambda\sin^2\psi_0)^{\frac{1}{2}}}{\phi_\lambda\,\eta_\lambda\cos\psi_0\cos\lambda}$$

Replacing $\mathcal{N}_0(\psi_0)$ **by** $dN_0(\psi_0)$ **and** $\mathcal{N}_\lambda(\psi_0)$ **by** $dN_\lambda(\psi_0)$**:**

$$dN_0(\psi_0) = \frac{N_\lambda \sin\psi_0}{\phi_\lambda\cos\lambda}\, d\psi_0$$

Integrating from $\psi_0 = 0$ **to** $\psi_0 = \Psi_0$ **where** $\sin^2\Psi_0 = 1/\eta_\lambda$ **(hence** $\cos\Psi_0 = (1-1/\eta_\lambda)^{\frac{1}{2}}$ **):**

$$N_0 = \frac{N_\lambda}{\phi_\lambda\cos\lambda}\int_0^{\Psi_0}\sin\psi_0\, d\psi_0$$

$$= \frac{N_\lambda}{\phi_\lambda\cos\lambda}\left[1-(1-1/\eta_\lambda)^{\frac{1}{2}}\right]$$

$$= \frac{N_\lambda}{\phi_\lambda\cos\lambda}\, \xi\left(\frac{1}{\eta_\lambda}\right) \qquad (5.7)$$

Hence

$$dN_0(\psi_0) = \frac{N_0}{\xi\left(\frac{1}{\eta_\lambda}\right)}\sin\psi_0\, d\psi_0 \qquad (5.8)$$

We can now find N at any point "l" as in the previous argument by replacing the pitch distribution given in Equ.(5.2) by that in Equ.(5.8) except that the upper limit is now given by $\sin^2 \Psi_0 = 1/\eta_\lambda$.

$$\text{i.e.} \quad N = \frac{N_0}{\xi(\frac{1}{\eta_\lambda})} \phi \cos l \left[(1 - \eta \sin^2 \psi_0)^{\frac{1}{2}} \right]_{\Psi_0}^{0} \qquad (5.8a)$$

$$= N_0 \phi \cos l \; \xi\left(\frac{\eta}{\eta_\lambda}\right) / \xi\left(\frac{1}{\eta_\lambda}\right) \qquad (5.9)$$

where $\xi(\frac{\eta}{\eta_\lambda}) = 1 - (1 - \frac{\eta}{\eta_\lambda})^{\frac{1}{2}}$ and use has been made of Equ. (5.5)

An approximation can be obtained by noting

$$\xi(\delta) \approx \tfrac{1}{2}\delta + \tfrac{1}{8}\delta^2$$

Hence for $\eta_\lambda \gg 1$ and $\eta_\lambda \gg \eta$:

$$N \propto N_0 \eta \phi \cos l \qquad (5.10)$$

This approximation is good to within about 10% provided $\eta_\lambda/\eta > 2\frac{1}{2}$ or $\sec^2\lambda/\sec^2 l > 2$ or $R > 1.25$.

It is easy to generalise these expressions for the case of injection at any point $l = L$. The argument from equation (5.4) to equation (5.8a) applies if the subscripts λ are replaced by subscripts L. However the limit of integration Ψ_0 at the point l, λ depends on whether this point is on the earth side or the other side of the injection point L, λ. All the injected particles can reach points at $l < L$,

, but some cannot reach points for $\ell > L$.

Thus Ψ_o is given by:

$$\sin^2 \Psi_o = 1/\eta_L \quad \text{for} \quad \ell \leq L$$
$$= 1/\eta \quad \text{for} \quad \ell \geq L$$

Substituting in equation (5.8a), where subscript λ is replaced by subscript L:

$$\left.\begin{aligned} N &= N_o \phi \cos\ell \cdot \xi\left(\frac{\eta}{\eta_\lambda}\right) / \xi\left(\frac{1}{\eta_\lambda}\right) && \ell \leq L \\ &= N_o \phi \cos\ell && \ell \geq L \end{aligned}\right\} \quad (5.9a)$$

A discontinuity in high order derivatives occurs in $N(\ell)$ because the injections itself is a discontinuity. If a number of injection points or a smooth distribution of injection exists then the resulting density distribution would be a summation or integration of density distributions as given in equation (5.9a).

The distributions derived have been expressed in terms of N_o since for the thermal particles, this quantity (as a function of R_o or λ) is the one most readily found from whistler and pulsation studies. However, the $N_o(\lambda)$ distribution is derivable if we assume a distribution of injection as a function of λ. We take this to be equal to N_λ, the electron density in the upper ionosphere. A simplified model of the

variation of this electron density with geomagnetic latitude is :

$$N_\lambda = N_E \cos\lambda$$

where N_E is the density above the equatore($\lambda = 0$)

Substituting in equation (5.7)

$$N_o = \frac{N_E}{\phi_\lambda} \xi\left(\frac{1}{\eta_\lambda}\right)$$

$$\approx N_E / 2\,\phi_\lambda \eta_\lambda \qquad \text{for} \quad \lambda > 25^\circ$$

Or in terms of R_o ($R_o > 1.25$):

$$N_o \approx \frac{N_E}{2R_o^3\,(4 - 3/R_o)} \qquad (5.11)$$

Substitution of these expressions for N_o into equation (5.10), we get N for any point ℓ, λ :

$$N \approx \frac{N_E}{2} \cdot \frac{\eta\,\phi}{\eta_\lambda\,\phi_\lambda} \cdot \cos\ell$$

Or in terms of ℓ, R :

$$N \approx \frac{N_E}{2R^3} \cdot \frac{\phi^2 \cos\ell}{4 - \frac{3}{R}\cdot\cos^2\ell}$$

Transposing we get the equation of an isopyc (surface of constant N) in a form suitable for computation:

$$R^3 \approx \frac{N_E}{2N} \cdot \frac{\phi^2 \cos\ell}{4 - \frac{3}{R}\cdot\cos^2\ell} \qquad (5.12)$$

5.3 Assumptions. The main purpose of this chapter is the derivation of the electron density distribution along a field line as given in

equations (5.9) and (5.10). The derivation is valid provided (i) that the geomagnetic field is approximately dipole, (ii) that collisions and (iii) gravitational forces can be neglected, and (iv) that the electrons (and protons) are supplied mainly from near the earth's surface ($L \approx \lambda$). We will consider each of these assumptions separately.

Recent data[60] from the space probe Pioneer V indicates that the field extends out to about 14 earth's radii. Vestine and Sibley[61] find that the field lines connecting the auroral zones ($R_o \sim 6$) are not seriously distorted by solar streams, even during auroral displays. Thus the magnetic field is probably a dipole one out to about 10 radii.

As pointed out in section 5.1, collisions in the region of highest collision frequency, the source regions, are effectively taken into account by the theory. In an exosphere of protons and electrons only collisions of electrons with protons are important since elastic collisions between like particles involve only

velocity exchange and the much heavier protons are not greatly affected by collisions with electrons. Assuming a temperature of about 10,000°K in the source regions, the thermal velocity of an electron would be around 10^8 cm/sec. The time taken for one trip along even a very long field line such as $\lambda = 70^\circ$ would be about 100sec. The effective average density $\bar{N}$ given by

$$\bar{N}s = \int N\,ds$$

along this line is about 80 cm^{-3} so that at this temperature the effective collision frequency will be about 2×10^{-4} sec^{-1}. Thus the probability of an electron suffering a collision during a single trip would be about 1 in 50.

Gravitational forces can also be neglected if the maximum gravitational potential energy is much less than the kinetic energy of the particles. This condition is met for temperatures in the source regions of about 2°K for electrons and about 4000°K for protons. Thus the temperatures of 10,000K assumed above would be adequate.

When this chapter was first prepared (1961) there was some controversy about

the temperature of the source regions. In 1959 Chapman[62] suggested that the temperature of the exosphere would range from 30,000°K at heights around 1000 km. to about 200,000°K where the exosphere merges into interplanetary space. On the other hand satellite drag data[63] give temperatures of 1000-1500°K at heights around 400 - 700 km. Although the latter temperatures refer to the neutral particle gas which predominates at these levels, Johnson[64] pointed out (in 1960) that the electron temperatures would be the same. However the situation has since changed. Direct electron temperatures measurements[65] using the "dumb-bell" electrostatic probe installed in rockets[87], show that electron temperatures are about twice as high as neutral particle temperatures at heights up to about 300 km. Electron temperatures deduced from nose whistler attenuation[88] are of the order of 250,000°K at about 4-4.5 earth's radii. Recent theoretical considerations[89] show that electron temperatures in the ionosphere may exceed neutral particle temperatures by a factor of three or more. Thus in the source regions (height of about 1000km) the electron temperature may well be of the order of (or more than) 10,000°K, but direct measurements at these

heights have yet to be reported.

Several complications arise if the source region temperature is low. At 1500°K collision frequencies would be some twenty times greater than those for 10,000°K. The probability of an electron suffering a collision during a single trip would be then about one in two or three. Collisions would tend to randomise the electron pitch distributions. Thus we might expect that the electron density distrbutions along a field line would consequently fall off less rapidly than as given by equations (5.9) and (5.10). On the other hand the much heavier protons will be little affected by collisions and since the conductivity of the exosphere is very high the electron density must be everywhere equal to the proton density. The protons, however, will now be appreiably affected by gravitational forces. If the exosphere rotates with the earth these will be cancelled out by geocentrifugal forces at around 6 earth's radii (in the equatorial plane).

Johnson[66] has shown that the electrons etc. making up the exosphere must be of telluric

(terrestrial) rather than solar origin . Hence the ultimate source must be the ionosphere where appreciable ionization is taking place. Equations (5.9) and (5.10) are derived on the basis of injection at $\ell = \lambda$, that is, at the earth's surface. However even if the injection level is quite high, equation (5.9a) shows that the approximation (5.10) is unaltered.

5.4 Computed Distributions. The distributions along the field lines $\lambda = 40^{\circ}$ and $\lambda = 60^{\circ}$ were computed from equation (5.9) using values of N_o of 10,000 cm^{-3} and 100 cm^{-3} respectively taken from the Allcock- Obayashi curve in Figure 35. These are shown in Figure 34 together with distributions computed from this experimental curve for a spherically symmetrical distribution. The dashed portions of the curves correspond to extrapolations into regions within the upper ionosphere (within 1000 km of the earth's surface). The fact that the discrepancies between the two types of distributions change sign between $\lambda = 40^{\circ}$ and $\lambda = 60^{\circ}$ suggests that the spherical symmetry distribution may be a reasonable approximation within this range of λ .

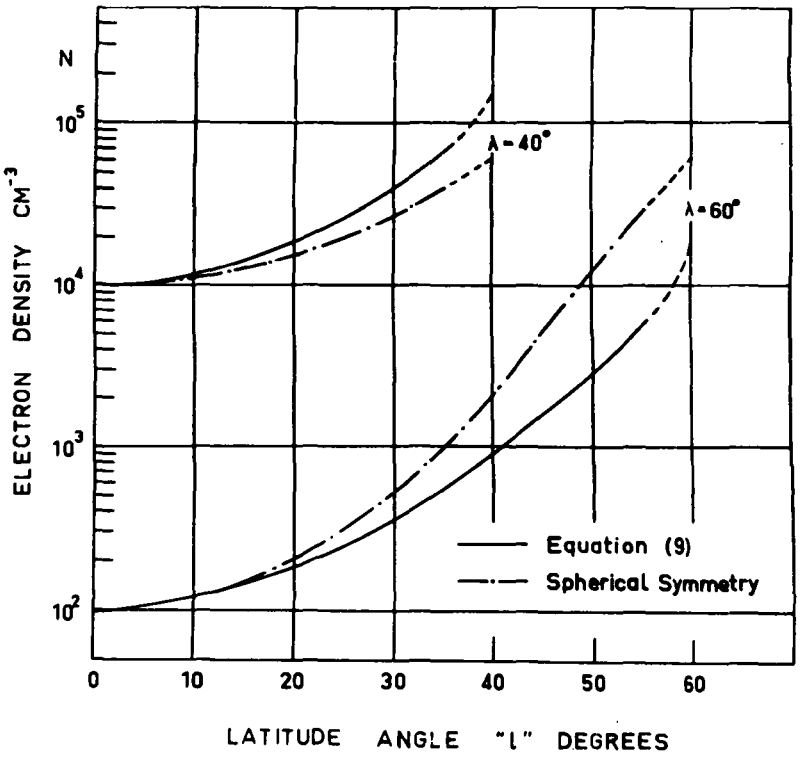

Fig. 34. Electron density along a line of force.

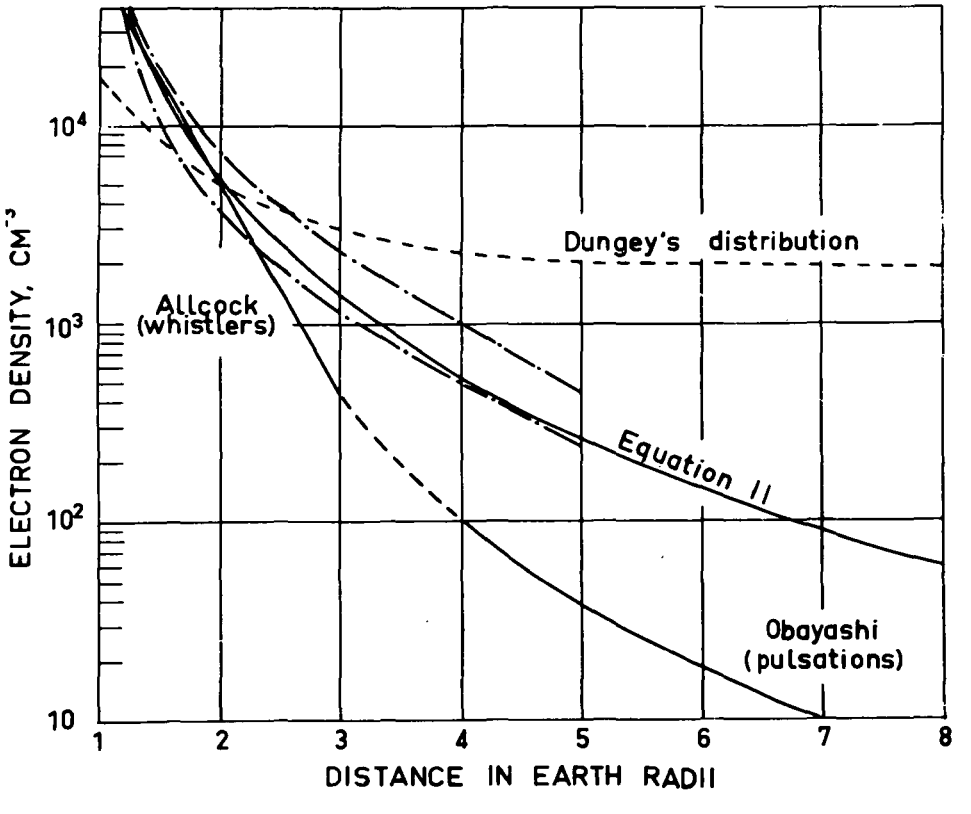

Fig. 35. Electron density along a radius in the equatorial plane. The two dot-dash curves are from Smith[43].

The electron density in the equatorial plane (N_o) computed from equation (4.11) as function of radial distance (R_o) is shown in Figures 35. Also shown is Dungey's[67] theoretical distribution $N \propto exp(2.5/R)$, a composite experimental curve by Allcock[68] (from whistler data) and Obayashi[69] (pulsations), and two curves by Smith[43] from nose whistler data. These have been scaled to the Allcock- Obayashi curve to agree at $R_o = 2$. Smith's nose whistler data (published after this work was done) is considered the most accurate. Obayashi's work has since been questioned. The two curves by Smith correspond to two periods of observation some six months apart. For agreement with Allcock's data at $R_o = 2$, we require $N_E = 2 \times 10^5$ cm^{-3} in equation (5.11). Very good agreement with Smith's data at all points is reached for $N_E = 6 \times 10^4$ cm^{-3}. Both of these values of N_E are consistent with experimental measurements[70] of the noon maximum density of the ionosphere (N_{max}) at the equator of 20×10^5 cm^{-3} and values[71] of N/N_{max} of about 0.2 at around 800 km (source region?) found by satellite experiments.

Values of electron density (N) were computed for a large number of points (λ, ℓ)

for field lines up to $\lambda = 80^{o}$ from values of N_o taken from the experimental $N_o(R_o)$ Allcock-Obayashi curve. For $\lambda > 65^{o}$ values of <u>effective</u> N_o were obtained by extrapolation. Resulting contours of electron density or <u>isopycs</u> are shown in a plane containing the geomagnetic axis in Figure 36. The field line $\lambda = 70^{o}$ is shown for reference. This suggetts considerable extensions of electron density in the direction of the axis.

~~After this work was done (1960) Obayashi's datawas shown to be questionable data was published.~~ Since Smith's data[43] fits equation (5.11) so well the assumptions involved in the derivation of (5.11) and (5.12) must be reasonable. Contours were then calculated from equation (5.12) for $N_E = 6 \times 10^4$ cm^{-3} as shown in Figure 37. The anomalous features in Figure 36 due to use of Obayashi's data disappear. The polar dip shown in Figure 37 should not be taken too seriously since N_λ at the poles is not zero. In any case this type of treatment cannot be applied at very high latitudes as the magnetic field will not be dipole. The curve labelled "h" in Figure 37 is one of constant magnetic field strength or gyro frequency and is shown here for comparison.

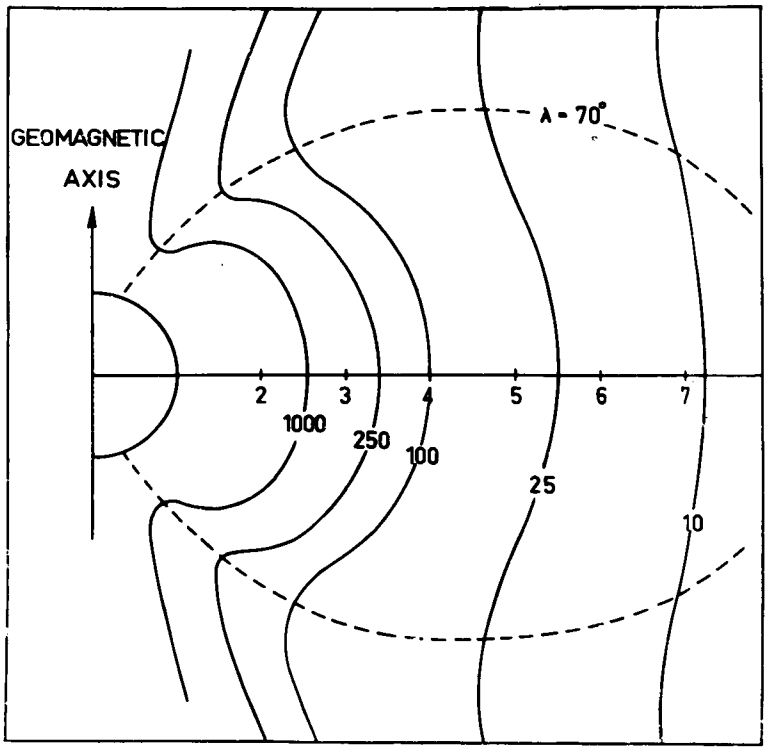

Fig. 36. Electron density contours derived from the experimental N_o (R_o) curve of Allcock and Obayashi (Fig. 35).

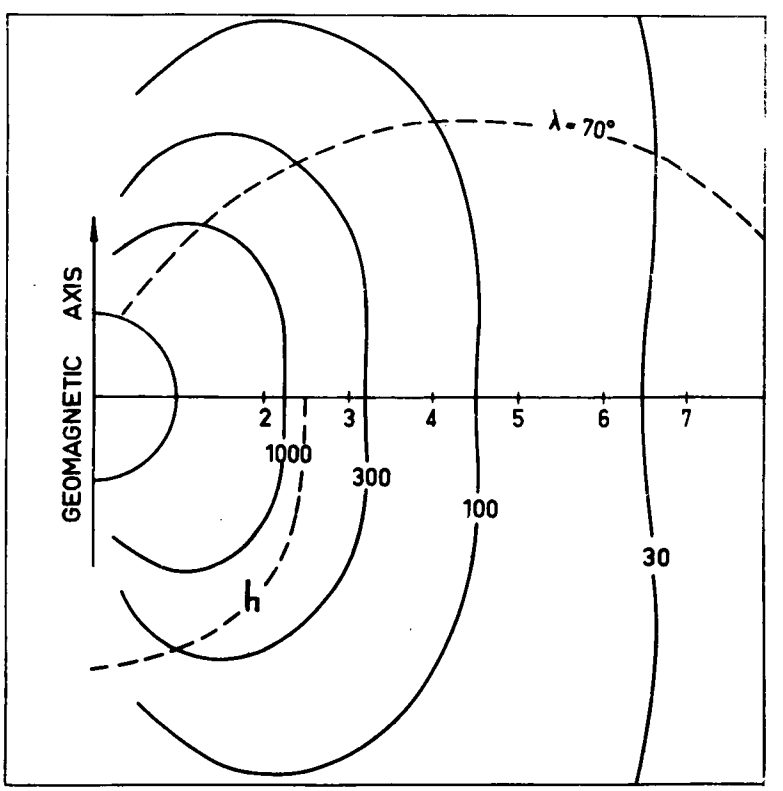

Fig. 37. Electron density contours calculated from equation (5.11).

The process of calculating a density distribution from a source distribution can be reversed. Thus some idea of the injection points can be obtained for a given density distribution. This was done for published[72] count rate contours of the outer Van Allen belts. It was assumed that the count rate would be directly proportional to density. Count rates as a function of (ℓ, λ) taken from contours are shown as the solid curves in Figure 38. The calculated curves (dashed) were found in the following way. It was assumed that the outer Van Allen belts are filled from isotropic point sources (one for each field line) in a short time at time t = 0. After a time interval t, long compared with this filling time, the original density distribution N(0) calculated from equation (5.9a) will have decayed through collisions with neutral particles to N, where

$$N = N(0)\ e^{-\rho t}$$

where ρ is proportional to the neutral particle density as given by Singer[73].

The injection points for calculated density distributions which give the best fit

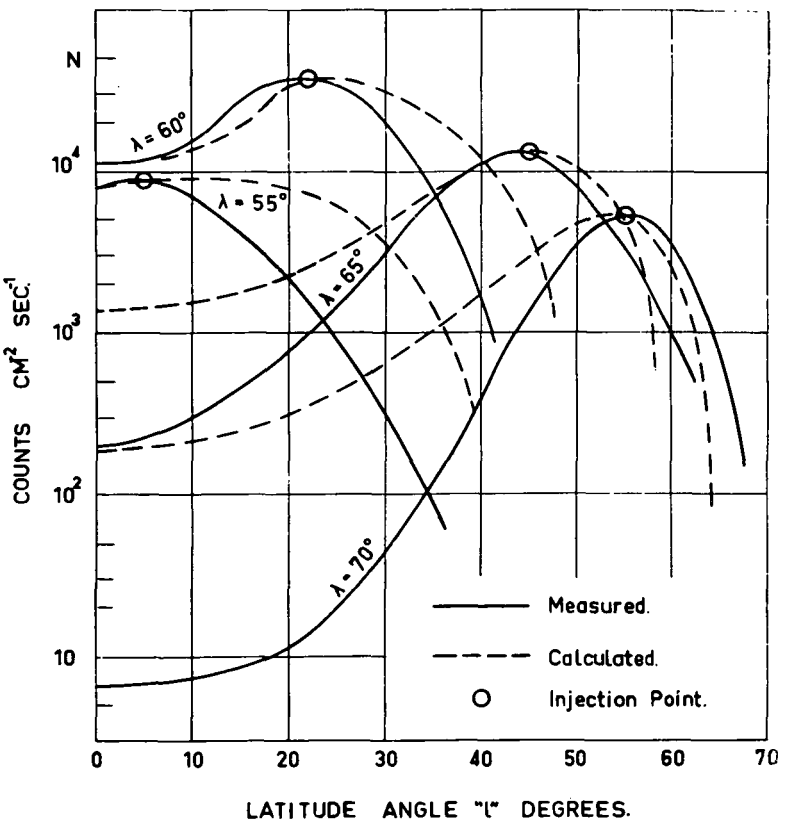

Fig. 38. Flux of fast particles along a line of force.

are shown by the small circles in figure 38. The agreement is not close. The "measured" densities (count rates) decrease too rapidly towards the equatorial plane for $\lambda = 65^{\circ}$ and $\lambda = 70^{\circ}$. No injection distribution could produce this effect. However it appears that the experimental data is not sufficiently accurate to draw any conclusions from this.

5.5 "Scale frequency" of the exosphere.

A further approximation ($\phi \cos l \sim 1$) of (5.10) gives $N \sim N_0 \eta$ or $N \propto B$. Since $N \propto p^2$ and $B \propto h$, where p and h are the plasma and gyro frequencies, this can be expressed as:

$$p^2 = ah \qquad (5.13)$$

The constant of proportionality, a, has the dimensions of frequency and so might be called the "scale frequency" of the exosphere. It is typically around 1 Mc/s (as deduced from Smith's work[43]).

To the extent that the "gyro-frequency model" ($N \propto B$) fits the real exosphere, the scale frequency is constant. However for any other model of the exosphere the scale frequency can be considered a varying parameter defined

by (5.13). Thus (5.9) becomes:

$$a = a_0 \phi \cos l \cdot \xi\left(\frac{\eta}{\eta_\lambda}\right)\left[\eta\, \xi\left(\frac{1}{\eta_\lambda}\right)\right]^{-1}$$

which for $\eta_\lambda \gg 1$ and $\eta_\lambda \gg \eta$, becomes:

$$a \simeq a_0 \phi \cos l \sim a_0$$

Since these equations and Smith's data[43] show that the scale frequency is at least quasi-constant than variations in space and time could be sensitively expressed by it. Scale frequencies can be deduced from whistler measurements of nose frequency (f_n) and time delay at this frequency (t_n).

It has been shown[90] that for a wide range of exospheric models the nose frequency dispersion ($D_n = t_n f_n^{\frac{1}{2}}$) is related to the "low frequency" ($f \to 0$) dispersion, D(0), by:

$$D_n = 1.456\, D(0)$$

where $$D(0) = t f^{\frac{1}{2}} = \frac{1}{2c} \int_{path} \frac{b}{h^{\frac{1}{2}}}\, ds$$

To the extent that the scale frequency is constant along a field line:

$$D(0) = a^{\frac{1}{2}}\, s/c$$

where s is the half length of a field line.

Thus we have

$$a = \underline{N}(f_n)\, t_n^2\, f_n^{5/3} \qquad (5.14a)$$

where $$\underline{N}(f_n) = (1.456\, f_n^{1/3}\, s/c)^{-2} \qquad (5.14b)$$

Since both s and f_n are functions of latitude λ,

then s can be expressed in terms of f_n. Thus $\underline{N}$ is a function* of f_n only. In this particular form, $\underline{N}$ is a slowly varying function. A nomogram based on (5.14) and given in Chapter 9 (see Figure 53) enables quick evaluation of "a" from f_n, t_n data.

* Do not confuse the function $\underline{N}$ with the electron density symbol N.

6. THEORY OF GENERATION OF CONTINUOUS V. L. F. NOISE ("HISS") FROM THE EXOSPHERE.

6.1. Introduction.

As discussed in Chapter 4 the TWT process was proposed by Gallet and Helliwell[52] to account for the frequency time characteristics of the discrete emissions. However, as we will see, this process can give qualitative agreement with only one or two types of discrete emissions: "quasi-constant tones" and those "hooks" which are preceded by a quasi-constant tone. Furthermore, this process is inefficient for the production of rapidly varying tones. On the other hand, it is well suited for the production of hiss. In this chapter, by taking into account the spiral motion of electrons travelling in the magnetic field, the interaction distance for which amplification at any frequency can occur, and the slowing down of the stream electrons by the wave amplification, it is shown that all the important characteristics of hiss can be produced by the TWT process.

Gallet and Helliwell made the simplifying assumption that both the electrons of the stream and the amplified wave travelled exactly along the

direction of the magnetic field. Since their work it has been established by several workers that field aligned columns of ionisation occur in the exosphere[43] and these produce a strong wave guide action in the very low frequency range[35]. Thus the second assumption is well justified. The first assumption requires modification. In general the electrons will spiral down the field lines. The pitch at any position is determined as in chapter 4. For the low energy particles required for this process (at most a few k.e.v.) the radii of gyration will be much smaller than the extent of the wave front. Thus it is the component of particle velocity down the field line or "guiding centre" velocity which must be equated to the wave phase velocity.

The analogy of this process with the travelling wave tube is perhaps closer than envisaged by Gallet and Helliwell. A longitudinal magnetic field is often introduced into travelling wave tubes to focus the electron beams, and it is the guiding centre velocity of the electrons which determines the amplification. As the case of the laboratory TWT a (signal) longitudinal electric field is required for interaction with the stream. As pointed out by Gallet and Helliwell a substantial longitudinal component of electric field will exist in the

exospheric TWT. It is the phase velocity of this component which is important, but for simplicity we will assume that this is c/n, where n is the refractive index of the medium for strict longitudinal propagation in the extraordinary mode below the gyro frequency ("whistler mode"). Thus for guiding centre velocity $\beta_d c$ the condition for amplification is

$$n\beta_d = 1$$

In addition to this we assume that, as in the case of the laboratory TWT, the amplification in decibels or nepers is proportional to the distance in wavelengths along the field line for which amplification is possible at any one frequency. In the treatment given below the physical processes of amplification are not cosidered further.

6.2. Amplified frequencies.

Replacing β by β_d in the necessary condition for amplification to occur, we find the amplified frequencies

$$f = \frac{h}{2}\left[1 \pm \left(1 - \frac{4\beta_d^2 p^2}{h^2}\right)^{\frac{1}{2}}\right]$$

This is essentially the expression derived by Gallet and Helliwell as given in chapter 4. If a model of the exosphere is assumed this expression can be put in a form where, for a given line of force, the latitude angle co-ordinate is the only variable. To do this we assume that at least along the lines of force considered here the magnetic field is dipole and the electron density varies as derived in chapter 5.

Thus:

$$h = \eta h_o$$

$$p^2 = p_o^2 \eta \, \emptyset \cos l \quad \text{for } R > 1.25$$

$$\beta_d^2 = \beta^2 \, (1 - \eta \sin^2 \psi_o)$$

Substitution of these expressions we find

$$f = \frac{\eta h_o}{2\emptyset} \left\{ 1 \pm \left[1 - \frac{4\beta^2 p_o^2}{h_o^2} \cos^7 l \, (1 - \eta \sin^2 \psi_o) \right]^{\frac{1}{2}} \right\} \quad \ldots (6.1)$$

It will be seen later that the frequency given by the minus sign is the more interesting. This can be put in a form containing relatively slowly varying functions which is more suitable for computation. We define:

$$\underline{a} = \frac{4\beta^2 p_o^2}{h_o^2}$$

$$z = a \cos^7 l \, (1 - \eta \sin^2 \psi_o)$$

$$\nu = \frac{2}{\pi}\left[1 - (1 - z)^{\frac{1}{2}}\right]$$

Then:

$$f^- = \frac{\eta\, h_o}{2}\left[1 - (1 - z)^{\frac{1}{2}}\right]$$

$$= \frac{\beta^2 p_o^2}{h_o}\, \nu \cdot \phi \cos\ell\, (1 - \eta \sin^2 \psi_o) \qquad \ldots (6.2)$$

Frequencies as a function of the latitude angle ℓ have been computed for particles of various speeds and pitch angles travelling along the line of force which terminates at geomagnetic latitude 50°. A smooth join to an ionosphere similar to that used by Gallet and Helliwell[52] has been made at a height of 2000 km above the surface of the earth. The results of this are shown in Figure 39. Except for the effect of the ionosphere the shape of these curves would be very similar for lines of force terminating at other latitudes. Only a change in frequency scale is required. The important parameter affecting the shape is a*. It is seen that in many cases the amplified frequency is fairly constant over great distances. This follows from (6.2), for $\phi \cos\ell$ stays within 15 per cent of unity for $\ell < 60°$, ν rapidly approaches unity for small values of z, and the term containing the pitch angle is fairly constant except near the mirror points.

*not to be confused with scale frequency (a), which is not used in this chapter.

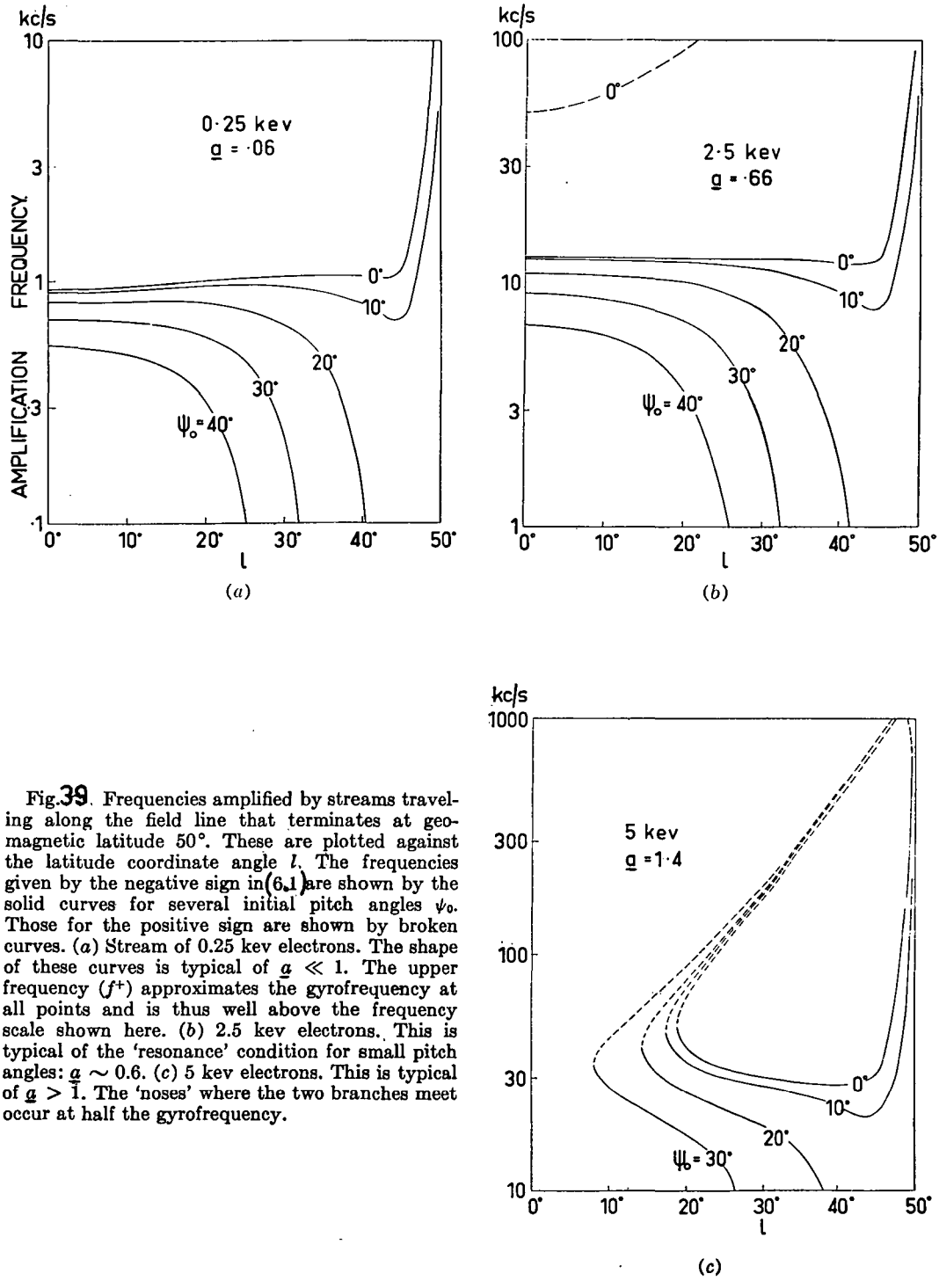

Fig. 39. Frequencies amplified by streams traveling along the field line that terminates at geomagnetic latitude 50°. These are plotted against the latitude coordinate angle l. The frequencies given by the negative sign in (6.1) are shown by the solid curves for several initial pitch angles ψ_0. Those for the positive sign are shown by broken curves. (*a*) Stream of 0.25 kev electrons. The shape of these curves is typical of $g \ll 1$. The upper frequency (f^+) approximates the gyrofrequency at all points and is thus well above the frequency scale shown here. (*b*) 2.5 kev electrons. This is typical of the 'resonance' condition for small pitch angles: $g \sim 0.6$. (*c*) 5 kev electrons. This is typical of $g > 1$. The 'noses' where the two branches meet occur at half the gyrofrequency.

6

Of even greater interest are those regions for which variation of these terms nearly cancels out producing very nearly constant frequencies over great distances. At these frequencies amplification will be great. We will consider this in greater detail.

6.3 Interaction distance. For appreciable interaction at any one frequency we require not only that the wave phase and particle guiding centre velocities be equal, but that this condition should hold effectively over some appreciable distance s.

Suppose that initially (s = 0) the condition $n\beta_d = 1$ holds exactly at some frequency but further on due to changes in the guiding centre velocity of the medium the particle stream slowly overtakes the wave. The stream (guiding centre) velocity relative to the wave is thus:

$$\Delta v = \frac{c}{n}(n\beta_d - 1)$$

In time dt

$$d(\Delta s) = \Delta v.dt, \quad ds = \frac{c}{n}.\ dt$$

Therefore $d(\Delta s) = (n\beta_d - 1)\ ds$

Now $$(n\beta_d - 1) = \int_o^s (n\beta_d)' \ .\ ds$$

where $$(n\beta_d)' = \frac{\partial}{\partial s}\ (n\beta_d)\ \ f \text{ const.}$$

Hence $$\Delta s = \int_o^s \int_o^s (n\beta_d)' \ .\ ds\ .\ ds$$

~~In the region of interest, then it~~ On one of the curves defined by (6.1) the condition $n\beta_d = 1$ holds at all points - changes in the medium or stream velocity being exactly balanced by changes in frequency f.

Thus $$\frac{d}{ds}\ (n\beta_d) = 0$$

Hence $$\frac{\partial}{\partial s}\ (n\beta_d)_{f \text{ const.}} = -\frac{\partial}{\partial s}\ (n\beta_d)_{f \text{ varying}}$$

Now $$n\beta_d = p\beta_d\left[f(h - f)\right]^{-\frac{1}{2}} \text{ for } \beta^2 \ll 1 \ (n^2 \gg 1)$$

Therefore $$-\frac{\partial}{\partial s}\ (n\beta_d)_{f \text{ varying}} = \frac{\frac{1}{2}p\beta_d\left[f(h - f)\right]^{-\frac{1}{2}} \ .\ (h\ .\ \frac{df}{ds} - 2f\ .\ \frac{df}{ds})}{f(h - f)}$$

Hence $\frac{\partial}{\partial s}(n\beta_d)_{f\,const} = \frac{1}{2f}\cdot\frac{h-2f}{h-f}\cdot\frac{df}{ds}$ since $n\beta_d = 1$

Since Δs must be small (at least $< \frac{\lambda}{2}$) throughout the interaction distance s, then s is given by:

$$\frac{\lambda}{2} > \Delta s = \int_0^s\int_0^s (n\beta_d)'ds\,ds = \frac{1}{2}\int_0^s\int_0^s \left(\frac{1}{f}\cdot\frac{h-2f}{h-f}\cdot\frac{df}{ds}\right)ds\,ds \qquad (6.3)$$

where λ is the wave length*.

This shows that amplification will not be appreciable at the frequency given by the plus sign (f^+) in (6.1) for two reasons. Firstly because $\frac{df}{ds}$ is usually large (Figure 39) and secondly because $(h - f)$ is generally quite small. At the points where the two curves join (Figure 39c) $h - 2f$ is zero but also $\frac{df}{ds}$ is infinite. Consequently the high frequency branch will not be considered further.

Thus considering only the low frequency branch, we differentiate (6.1) with respect to l:

$$f = \frac{\eta h_0}{2}\left\{1 - \left[1 - \underline{a}\cos^7 l\,(1 - \eta\sin^2\psi_0)\right]^{\frac{1}{2}}\right\} \qquad (6.1)$$

$$\frac{df}{dl} = \frac{h_0}{2}\{\}\frac{d\eta}{dl} + \frac{\eta h_0}{2}\left\{-\frac{1}{2}[\,]^{-\frac{1}{2}} \times\right.$$

$$\left. \times - \left[7\underline{a}\cos^6 l(-\sin l)(1 - \eta\sin^2\psi_0) + \underline{a}\cos^7 l\left(-\frac{d\eta}{dl}\cdot\sin^2\psi_0\right)\right]\right\}$$

*use of λ = G.M. latitude is avoided in this chapter.

$$= \frac{f}{\eta} \cdot \frac{d\eta}{dl} - \frac{\eta h_o}{4}\left[\ \right]^{-\frac{1}{2}} \underline{a} \cos^7 l \left[7 \tan l + \eta \sin^2 \psi_o \left(\frac{1}{\eta}\frac{d\eta}{dl} - 7\tan l\right)\right]$$

$$\text{Now } \frac{1}{\eta}\frac{d\eta}{dl} = \left[\ 6 + \frac{3\cos^2 l}{\phi^2}\ \right]\tan l$$

$$\text{Thus } \frac{1}{f}\frac{df}{dl} = \left\{ 6 + \frac{3\cos^2 l}{\phi^2} - \frac{\frac{1}{2}\underline{a}\cos^7 l\left[7+\eta\left(\frac{3\cos^2 l}{\phi^2}-1\right)\sin^2\psi_o\right]}{\underline{a}\cos^7 l(1-\eta\sin^2\psi_o) - \frac{2f}{\eta h_o}} \right\}\tan l$$

Making the ν substitution:

$$\frac{1}{f}\cdot\frac{df}{dl} = \left\{ 6 + \frac{3\cos^2 l}{\phi^2} - \frac{7+\eta\left(\frac{3\cos^2 l}{\phi^2}-1\right)\cdot\sin^2\psi_o}{(1-\eta\sin^2\psi_o)(2-\nu)} \right\}\tan l$$

$$= Q \qquad (6.4)$$

This expression is shown in Figure 40 as Q - v - l for several values of ψ_o and $\underline{a}$. Note that for ψ_o small and $\underline{a} \sim 0.6$ the function Q is close to zero for a large range of l .

From the line of force equations for a dipole field

$$\frac{ds}{dl} = R_o \phi \cos l \qquad (6.5)$$

The resulting expression containing s can be simplified by noting that $\phi\cos l \sim 1$ for $l < 60^o$ and in the region of interest (high amplification) the term

$$\frac{h - 2f}{h - f}$$

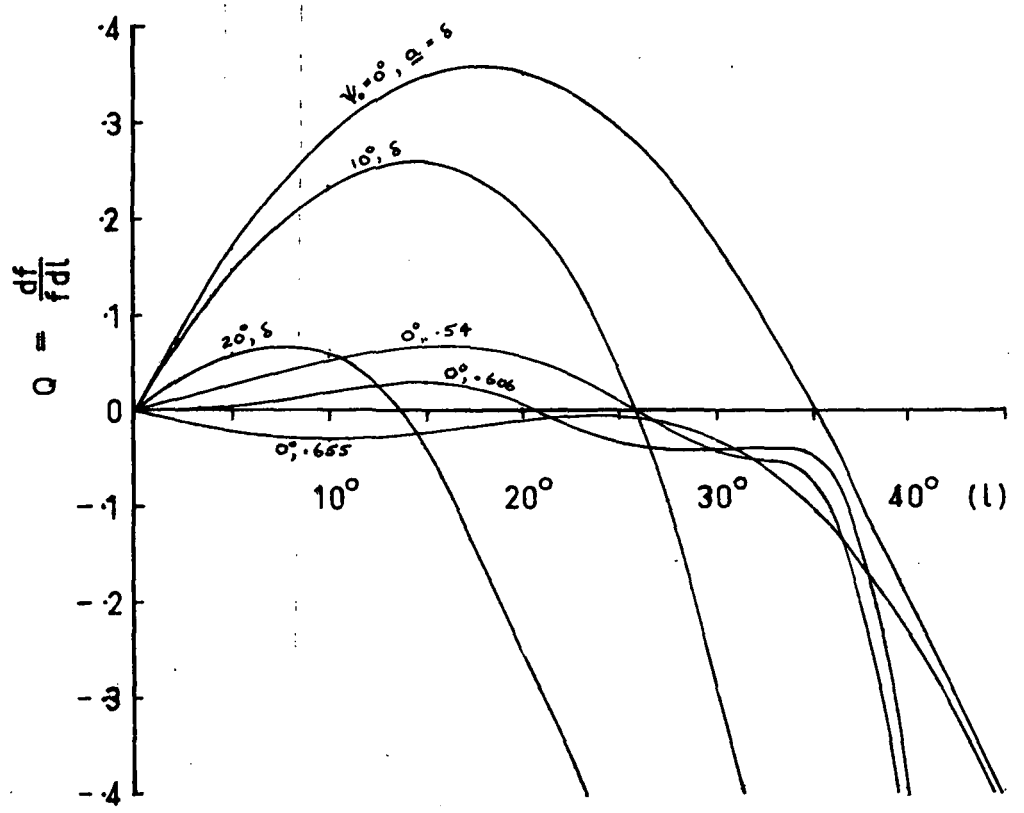

Fig. 40. Fractional rate of change of amplified frequency (Q) as a function of the latitude angle coordinate (l). Amplification will be large when Q stays close to zero for an appreciable range of (l), as in the case $\underline{a} \sim 0.6$.

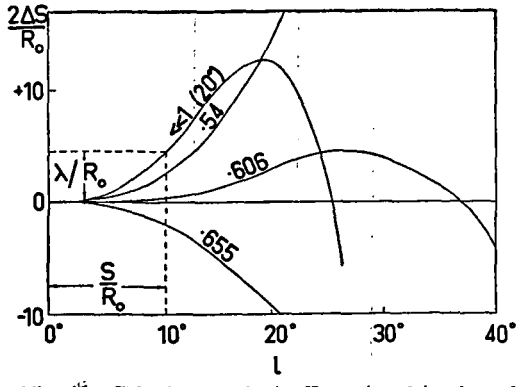

Fig. 41. Calculation of s/λ. Equation 6 is plotted for three values of $\underline{a}$ near 0.6 for $\psi_0 = 0$, and for $\underline{a} \ll 1$ for $\psi_0 = 20°$.

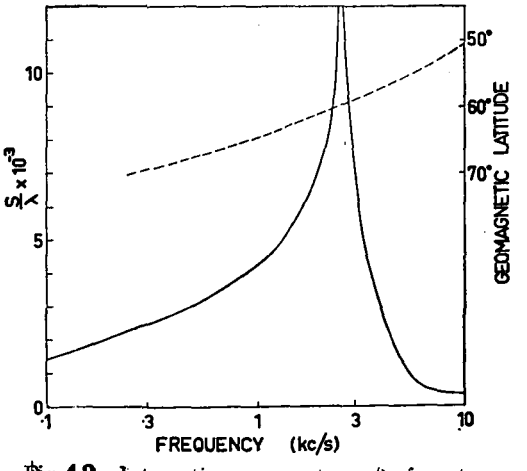

Fig. 42. Interaction parameter s/λ for stream particles of small pitch guided along the field line terminating at geomagnetic latitude 60°. At other latitudes frequencies will scale so that maximum s/λ occurs at the frequency given by the dashed curve.

is also close to unity. Thus from (6.3), (6.4), and (6.5) we have

$$\frac{2\Delta s}{R_o} \simeq \int_{l_1}^{l_2}\int_{l_1}^{l} Q \, dl \, dl \qquad (6.6)$$

$$\frac{s}{R_o} \simeq l_2 - l_1$$

We assume that, as in the TWT process, the amplification (in db. or nepers) is proportional to the interaction distance measured in wavelengths, s/λ. In those cases for which s is sufficiently small, The integration range $l_2 - l_1$ is also small so that over this range the integral Q in (6.6) will be approximately constant. Thus

$$\frac{2\Delta s}{R_o} \simeq Q \cdot \tfrac{1}{2}(l_2 - l_1)^2$$

$$= \frac{\lambda}{R_o} \text{ in the limiting case } \left(\Delta s = \frac{\lambda}{2}\right)$$

Then, since $\lambda = \frac{c}{nf} = \frac{\beta_d c}{f}$

$$\left(\frac{s}{\lambda}\right)^2 \simeq \frac{2f}{\beta_d c} \cdot \frac{R_o \phi \cos l}{Q} \qquad (6.7)$$

However in the more interesting cases where s is large (6.6) must be integrated. Curves giving $2\Delta s/R_o$ as a function of l are shown in Fig. 41 for some of the cases which give relatively large values of s. For a given curve the value s/λ is found by selecting a range of l which has a range of

$2\Delta s/R_o$ equal to λ/R_o. This range of l is then s/R_o as shown in Figure 41. Itis seen that for very small pitch angles the highest values of s/λ are found for $\underline{a} \sim 0.6$. For larger pitch angles these are found at lower values of $\underline{a}$. No particles of pitch angles ψ_o much greater than 20^o have large s/λ values.

The parameter s/λ as a function of frequency for particles of very small pitch angles travelling along the line of force terminating at geomagnetic latitude 60^o is shown in Figure 42. Particles of greater pitch angle will have a s/λ curve showing a smaller and broader maximum occuring at lower frequencies. For other lines of force the essential change in the s/λ curve is the frequency ssale, the maximum occuring (from(6.2)) at:

$$f \approx \tfrac{1}{4} \underline{a}\, h_o \sim 0.15\, h_o$$

This relation is also shown in Figure 42.

The theory derived so far shows that provided a particle strem is confined to a narrow tube of force and provided this stream is "weak" so that very high amplification is required, a narrow band of noise(?hiss") can be produced even though the stream contains a wide spectrum of particle velocities and pitch angles. This occurs because

only a very narrow range of particles' velocities and pitches can give the necessary amplification. Thus we have explained the observed occurrence of narrow band, "quiet", isolated bursts. The theory further predicts that the frequency at which these bursts occur is a function of the terminating latitude of the line of force. There is not sufficient experimental evidence as yet to prove this one way or the other, though those observations discussed in Section 2.4 seem to indicate that lower frequencies occur at higher latitudes as predicted.

6.4. Energy Loss: On the other hand, if the stream is "strong" so that a high rate of amplification occurs, considerable energy will be transferred from the stream particles to the wave within distances appreciably less than the "no-loss" interaction distances calculated above. The stream particles will thus be slowed down by the wave and synchronism will be lost after some distance which is the effective interaction distance. All "no-loss" interaction distances greater than this will be limited by this effective value so that a wide band of frequencies will be amplified by roughly the same amount.

This process is closely analogous to a sensitive narrow band amplifier having a frequency response as in Figure 42. For a very low level input of very wide band noise a narrow band output is obtained. However, for progressively higher levels of noise the amplifier reaches the overload condition. From that point on, higher levels of input noise cannot produce a higher output level but only a wider band of output noise. We consider this process in more detail.

We assume that the amplification (in nepers) is proportional to s/λ . Thus the amplified power is

$$W = b \exp\left(\alpha \frac{s}{\lambda}\right) \qquad (6.8)$$

where b and α are constants. The constant "b" is thus the power before amplification or at least that initially produced for s very small. We will not consider its precise physical significance. If we put b in the form of <u>intensity</u> ($Wm^{-2}\ (c/s)^{-1}$) then W will also be in this form. The constant controlling the amplification rate is probably strongly dependent on the stability or density fluctuation of the particle stream.

The kinetic power of the particle stream K can be expressed as

$$K = k\beta^2$$

where k is constant during the amplification process. The power gained by the wave is equal to the power lost by the stream.

$$\Delta K = \Delta W$$

We assume that $\Delta K/K$ is small, though $\Delta W/b$ may be very large.

Thus

$$2K \cdot \frac{\Delta\beta}{\beta} = b\left[\exp\left(\alpha \frac{s}{\lambda}\right) - 1\right] \qquad (6.9)$$

The velocity $\Delta\beta.c$ is the velocity of the wave relative to the stream. After the stream has travelled a distance s this finite relative velocity will have caused the stream to lag behind the wave by distance Δs. We again use the criterion that when $\Delta s = \lambda/2$, amplification ceases.

Now $$\Delta s = \int_0^s \Delta\beta c \frac{dt}{ds} \cdot ds$$

Substituting from (6.9) and assuming That the change in K is small over the integration

$$\Delta s = \frac{b}{2K}\left\{\frac{\lambda}{\alpha}\left(e^{\alpha\frac{s}{\lambda}} - 1\right) - s\right\}$$

We are interested in cases where the amplification is appreciable, so that

$$\exp\left(\alpha \frac{s}{\lambda}\right) \gg \frac{s}{\lambda} \gg 1$$

Thus $$\Delta s \simeq \frac{b}{\alpha K} \cdot \frac{\lambda}{2} \exp\left(\alpha \frac{s}{\lambda}\right)$$

Using the criterion for maximum Δs we find the

maximum power attainable is thus

$$W_m = \alpha K \qquad (6.10)$$

Thus amplification continues until the wave power reaches some fraction α of the stream power. Amplification then ceases at this frequency because the particles are no longer synchronised with the wave.

The kinetic power K used above refers only to those particles capable of producing some amplification. We seek it in the form of intensity: watts per square meter per unit frequency interval of the amplified band. From (6.2), neglecting terms usualy close to unity

$$f \approx \beta^2 p_o^2 / h_o$$

Nose whistler data[43] show that p_o^2 / h_o is effectively constant in the exosphere and is approximately 1 mc/s. For electrons β^2 denotes an energy $E = 250\beta^2$ k.e.v. so that

$$f \approx 4E \times 10^3 \text{ c/s} \qquad (6.11)$$

McIlwain[49] has measured the flux and energy spectrum of an electron stream which was observed to produce a quiescent auroral glow. We will assume this to be typical of streams producing our process. He found that the particle flux could be expressed as (E in k.e.v.)

$$J\ (>E) = 1.5 \times 10^{10} \exp(-E/5)\ \text{sec}^{-1}\text{cm}^{-2} \qquad (6.12)$$

The energy flux in watts per square meter per unit energy interval (k.e.v.) is then

$$E\frac{dJ}{dE} = 4.8 \times 10^{-3}\ E \exp(-E/5)$$

From (6.11)

$$\frac{dE}{df} = 2.5 \times 10^{-4} \text{ k.e.v. per (c/s)}$$

So from this and (6.11) we find K for electrons (o.5 k.e.v.)* producing amplification around 2 kc/s:

$$K = 6 \times 10^{-7}\ \text{Wm}^{-2}\ (\text{c/s})^{-1}$$

It should be noted that all the particles of such a stream must have had the small initial pitch angles (ψ_o) required for appreciable amplification, otherwise they would not have been able to get to within a few hundred kilometers of the earth where the above measurements[49] were made. We have expressed K as an intensity also. This introduces an apparent difficulty because all such intensities will increase towards the earth. This occurs because both the stream and the amplified wave are confined to a tapering

---

* this involves considerable extrapolation as McIlwain's expression (6.12) was only observed to apply for the range 3 to 30 k.e.v.

magnetic tube of force. We avoid this difficulty by referring all intensities to the values they would have near the earth's surface.

An estimate of the initial intensity b is required. As will be pointed out later a rough order of magnitude estimate will suffice. Suppose, then, that this is produced by the Cerenkov process. The specific power per electron (Marshall[47]) is given by

$$w = \beta cf \times 10^{-45} \; W(c/s)^{-1}$$

For frequencies around 2 kc/s and electrons which produce amplification at these frequencies (o.5 k.e.v.), $w = 3 \times 10^{-33}$. We suppose that the stream density is uniform initially so that radiation from a large number of electrons will add incoherently. We require b in the form of intensity referred to the earth's surface so we take a tube of force having a cross-section area of one square meter at the earth's surface. From (6.12) the stream density near the earth's surface for 0.5 k.e.v. electrons is about $10 \; cm^{-3}$. Throughout the length of the tube the linear density is thus approximately 10^7 electrons per meter. If 2 kc/s Cerenkov radiation can be produced over a distance of around 10,000 km, the total number of electrons involved is 10^{14}. Thus

$$b \simeq 3 \times 10^{-19}\ \mathrm{Wm}^{-2}(\mathrm{c/s})^{-1}$$

We consider various streams all described by (6.12) but having different values of the parameter α. We assume that this is possible, that is, that α is influenced by some factors not described by (6.12). We will not consider its precise physical significance though it is reasonable to suppose that streams occurring during disturbed conditions might have larger density fluctuations or less stability leading to higher values of α. In which case α would be a disturbance index.

If we assume a value for α, we find for s/λ (given in Figure 42) greater than a critical value, the noise intensity is the "overload" value given by (6.10). For s/λ less than critical the intensity is given by (6.8). Thus we have a plateau region of maximum intensity with quite steep (exponential) sides. At the critical value both (6.8) and (6.10) apply so that

$$\left(\frac{s}{\lambda}\right)_{\mathrm{crit.}} = \frac{1}{\alpha}\log_e\left(\frac{\alpha K}{b}\right) \qquad (6.13)$$

The two frequencies defining the plateau region are those for which s/λ is critical. These frequencies can be read off the curve in Figure 42.

The interesting characteristics of noise are the peak intensity and the frequency

range. The important parameter is α. The peak intensity is independent of b, though this enters into calculation of critical s/λ and thus frequency range. However for strong amplification, say $\alpha\frac{s}{\lambda} \sim 20$, an error of even three orders of magnitude in estimation of b will change critical s/λ by only 35 per cent. In Table 2 estimates of these characteristics are given for several values of α.

Table 2 Peak intensity (at 2 kc/s for wide band hiss), frequency range and bandwidth of hiss produced by electron streams of flux $J(>E) = 1.5 \times 10^{10} \exp(-E/5)$ electrons sec^{-1} cm^{-2} (E in k.e.v.), and of various α.

Disturb. Index ($\alpha \times 10^3$)	Peak Intensity ($W m^{-2} (c/s)^{-1} \times 10^{10}$)	Crit. s/λ ($\times 10^{-3}$)	Frequency Range* (kc/s)	Bandwidth (kc/s)
1	6	21	2.6	0.15
2	12	11	2.6	0.20
5	30	4.6	1.1 - 3.4	2.3
10	60	2.4	0.3 - 4.3	4.0
20	120	1.2	0.1 - 5.2	5.1
50	300	0.5	0.1 - 7.0	6.9
100	600	0.26	0.1 -(100)	100

* The first two entries are centre frequencies.

These have been chosen to show the bandwidth characteristics. The values of peak intensity then follow from (6.10).

6.5 Discussion. The noise characteristics as derived from this theory and listed in Table 2 agree well with those observed. A large range of bandwidths is possible. It is seen that there is a range of α, probably corresponding to quiet magnetic conditions, which produces narrow band bursts. This is followed by a transition region for which the bandwidth increases rapidly and then tapers off. This is typical of the observed behaviour during magnetic storms[28]. Finally for large α (severe magnetic disturbances) very wide band bursts are predicted as observed[28](Chapter 3). Short streams some 1000 km long in the direction of the field, having high values of α and a narrow spectrum of velocities, would amplify the frequencies along one of the curves in Figure 39 in sequence. These might produce the "quasi constant tones" and perhaps the TWT "hooks" as proposed by Gallet and Helliwell[52]. However the latter ("hooks") would occur in regions of rapid frequency change and so require very short streams and very high α values for appreciable amplification.

The predicted peak intensities in Table2

are somewhat greater than those deduced from observations (around $10^{-10} Wm^{-2}(c/s)^{-1}$) after correction for propagation losses in the ionosphere and earth-ionosphere wave guide (Chapter 3). However the errors involved in the propagation loss correction could easily account for this discrepancy, so that quantitative agreement is probably quite good.

Narrow band noise at a given latitude at frequencies other than those given in Figure 42 (dashed curve) can be produced by narrow energy (velocity) or pitch distributions of electrons in the stream. McIlwain[49] found that a stream which produced a strong visible aurora consisted of practically monoenergetic electrons. In this way more than one narrow band can be produced as is sometimes observed (Figure 8). Multiple narrow bands can also be produced if several streams occur in slightly different latitudes simultaneously. Thus, as seen from Figure 42 (dashed curve), centre frequencies differing by a factor of two can be produced by streams less than 5° of latitude ($\sim$ 500km) apart. In the same way the finite width of streams would set a limit to the narrowness of the amplified band. However, satellite measurements[41] at a height of a few hundred kilometres show that some

streams are as narrow as 25 km (traversed by the satellite in 3 seconds).

It may appear to the reader that this theory rests on the assumption that detailed expressions can be extracted from a theoretical model which might not be truly representative of the real exosphere. However, provided the electron density along the field line varies smoothly in a manner not greatly different from the model used, the essential qualitative results of this theory should still hold. Similarly the qualitative results may not be greatly affected should subsequent study of the exospheric TWT mechanism require some modification to the amplification condition $n\beta_d = 1$.

A very different theory, based on the process to be discussed in the next chapter, is presented in Chapter 10. This new theory also explaines all the features discussed in this section. However new experiments (proposed in Chapter 10) are needed to find out whether this new process or the one (TWT) presented above (or both) actually produces the hiss we observe.

7. DOPPLER SHIFTED CYCLOTRON RADIATION FROM ELECTRONS : A THEORY OF DISCRETE* V.L.F. EMISSIONS FROM THE EXOSPHERE.

7.1 Introduction. As mentioned in Chapter 4, electrons which spiral away from the observer will produce a downward doppler shift of the electron gyro frequency. Further, since electrons are much better radiators than protons, the intensity of the radiation should be easily observable without presupposing enormous numbers of particles radiating coherently, as is required for protons.

7.2 Theory. Suppose an electron (or rather a small bunch of electrons) is travelling in a helix about a line of force of the earth's magnetic field. Suppose it is travelling away from the observer's hemisphere with velocity component along the line of force of $\beta_d c$. Thus the rotating electron (or bunch) is an oscillator of frequency h moving away from the observer at velocity $\beta_d c$ in a medium for which the observed frequency f travels at velocity c/n.

Thus

$$f = \frac{h}{1 + \beta_d n}$$

where

$$n^2 \approx \frac{p^2}{f(h-f)} \qquad n^2 \gg 1$$

Then, using the "scale frequency" a, defined in section 5.5, we have :

$$(h - f)^3 = a \beta_d^2 f h \qquad (7.1)$$

* This chapter is only concerned with the discrete emissions, but it will be shown later (Chapter 10) that this process can also explain the detailed features of chorus and hiss.

This is difficult to evaluate algebraically except for $f << h$ when

$$f \approx \frac{h^2}{a\beta_d^2} \qquad (7.2)$$

However (5.1) can be put in the form

$$\frac{(1 - f/h)^3}{f/h} = \frac{a\beta_d^2}{h} \qquad (7.3)$$

A plot of $a\beta_d^2/h$ versus f/h enables f to be found, given β_d^2 and h. This shown in Figure 43. The approximation (7.2) is seen to be valid only for $a\beta_d^2/h > 20$.

Values of f have been found from Figure 43 for electrons of energies 5, 10, 25 and 50 k.e.v. travelling along the line of force terminating at geomagnetic latitude 60°. The position of a point on this field line is determined by the latitude angle l. The emitted frequency as a function of latitude angle is shown in Figure 44. The helical pitch (ψ_o) of all these electrons is 20° in the equatorial plane, so that mirror points occur in each hemisphere at $l = 41^\circ$. The parameter β_d is calculated for invariance of magnetic moment (as in Chapter 5) :

$$\beta_d^2 = \beta^2(1 - \eta \sin^2 \psi_o)$$

Suppose these electrons make one trip from the mirror point in the observer's hemisphere to the mirror point in the opposite hemisphere. We require to find how frequency would vary with time as observed on the earth's surface at the base of this line of force. Such frequency-time curves can be found by summing the time delay due to the finite velocity of the electron (t_e) and that due to the finite group velocity of the wave (t_g).

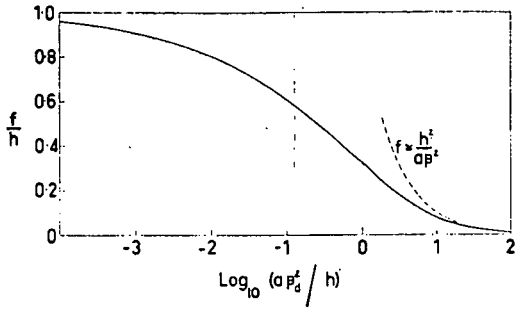

Fig. 43. Graph of equation 3 for finding emitted frequency.

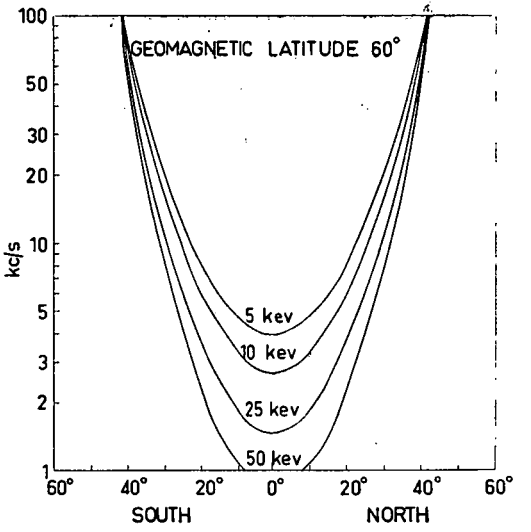

Fig. 44. Frequency emitted by an electron of the energies shown as a function of position (latitude angle). All four electrons have mirror points at 41°.

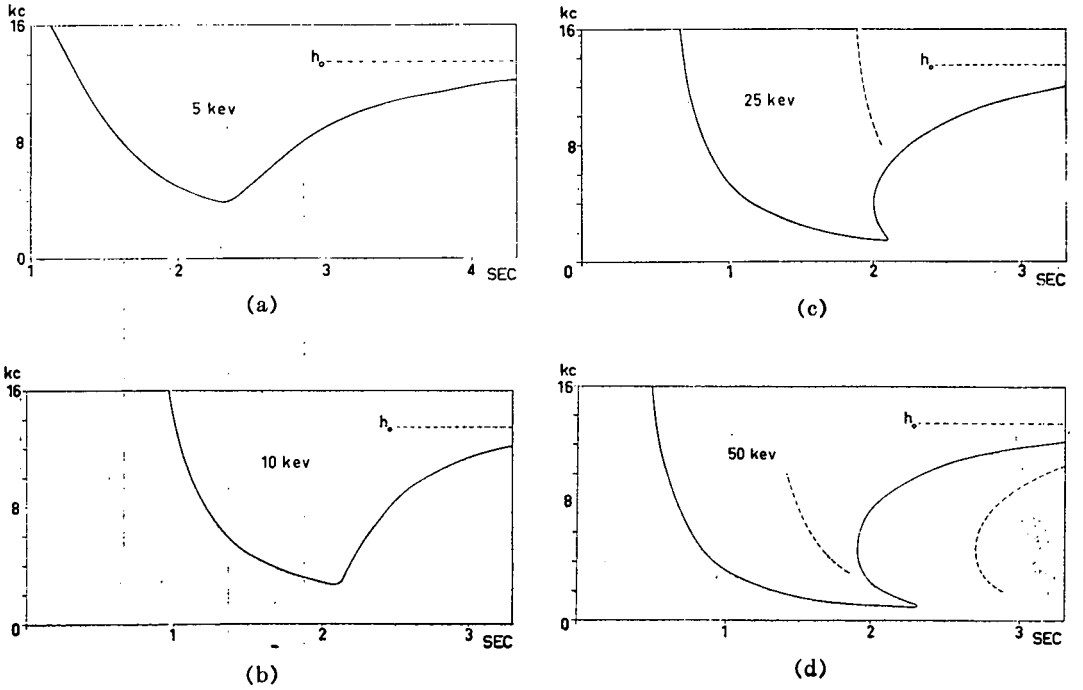

Fig. 45. Frequency time (dispersion) curves for the electrons considered in Fig. 44. These should be compared with the observed spectrograms in Fig. 6.

$$t = t_e + t_g$$

where $$t_g = \int \frac{ds}{v_g} = \frac{a^{\frac{1}{2}}}{2cf^{\frac{3}{2}}} \int \frac{h^{3/2}}{(h-f)^{3/2}} \cdot ds + \frac{D(\text{ionosphere})}{f^{\frac{1}{2}}}$$

and $$t_e = \int \frac{ds}{v_e} = \frac{1}{\beta c} \int \frac{ds}{(1 - \eta \sin^2 \psi_e)^{\frac{1}{2}}}$$

The two parts of the first (t_g) integral correspond to exospheric and ionospheric delays respectively. Smith[43] gives a value of 5 $sec^{\frac{1}{2}}$ for the ionospheric "dispersion" D, calculated for a simple one layer parabolic model of the ionosphere. For a = constant as used here, the exospheric integral becomes[43] an elliptic function. However Smith[43] found that the calculated frequency-time shape of a nose whistler is almost independent of the exospheric model used. Consequently we will use the quasi-constant electron density model, also given by Smith[43], which gives an algebraic solution. If the integration is taken from the level $h = h_e$ (equatorial plane) to $h = h$, the exospheric delay is then

$$t_g(\text{ex.}) = \frac{3.02\, a^{\frac{1}{2}}}{f^{\frac{1}{2}} h_e^{1/3}} \cdot \frac{1 - h_e/h}{1 - f/h_e} \cdot (1-f/h)^{-\frac{1}{2}} \qquad (7.4)$$

in seconds where a is in Mc/s and f, h in kc/s.

The second integral (t_e) cannot be solved directly. However, except near the mirror points, the integrand is slowly varying. In this region a graphical method (planimeter) is adequate. As the mirror points are approached the integrand goes to infinity. In this region an approximation[74] can be used :

$$t_e = \frac{R_e}{\beta c} \cdot \sqrt{\frac{2}{3}} \cdot \frac{\phi \cos l_m}{\sin l_m} \cdot \cos^{\frac{1}{2}} l_m (\cos l - \cos l_m)^{\frac{1}{2}} \qquad (7.5)$$

where l_m is the latitude angle of the mirror points and t_e is the time taken for the electron to travel from l to l_m.

In each case integration is carried out over the appropriate paths. The resulting frequency-time curves are shown in Figure 45. The time t = 0 is defined as that instant the electron passes through the equatorial plane towards the observer's hemisphere. It could thus be the time of injection into the line of force. Note that for the 5 k.e.v. electron the time scale starts one second after this.

7.3 Spectra. The frequency-time curves in Figure 45 show good agreement with the observed hooks in Figure 6. If the electron bunch only makes half of the mirror to mirror trip, which might happen if the source of the bunch (probably near the equatorial plane) is also a sink, then only half of the full hooks will be observed. If this half trip was confined to the observer's hemisphere only the falling part ("falling tone") would be observed. This might be mistaken for a whistler in some circumstances. Trips confined to the opposite hemisphere would give rise to the other half: "risers" (f and g in Figure 6) and "pseudo noses".

On the other hand, at times, several complete trips might take place before the bunch is lost. This would give rise to a series of hooks or similar shape separated in time by the period of oscillation of the bunch between mirrors. For the faster particles in Figure 45 this is indicated by the curved dashed lines. The oscillation periods are given in Table 3. An observer in the opposite hemisphere near the conjugate point would observe the same

Table 3.

Mirror oscillation periods of the electrons considered in Figure 44.

Energy (k.e.v.)	Period (sec.)
5	2.56
10	1.82
25	1.28
50	0.81

series of hooks, but since radiation is observed only when the bunch is travelling away from this observer he will observe this series shifted in time by half a period. Thus a northward going bunch sends a hook to the southern observer then when returning on its southward trip sends a hook to the northern observer. This conjugate point test of the theory was suggested to the writer by Professor G.R.A. Ellis.

The cases described above are illustrated in Figure 46. A bunch will tend to be scattered by turbulent magnetic fields in the source region (probably near the equatorial plane) and be absorbed by collisions near the mirror points. Thus we would expect the relative frequency of occurrence of the various types of emission to decrease with the number of mirrors and source region transits required for each type. Thus "risers" which are required to survive no such hazards should be the most common. In Table 4 the number of hazards for each type (as listed in Figure 46) is compared with the observed relative frequency of occurrence (from

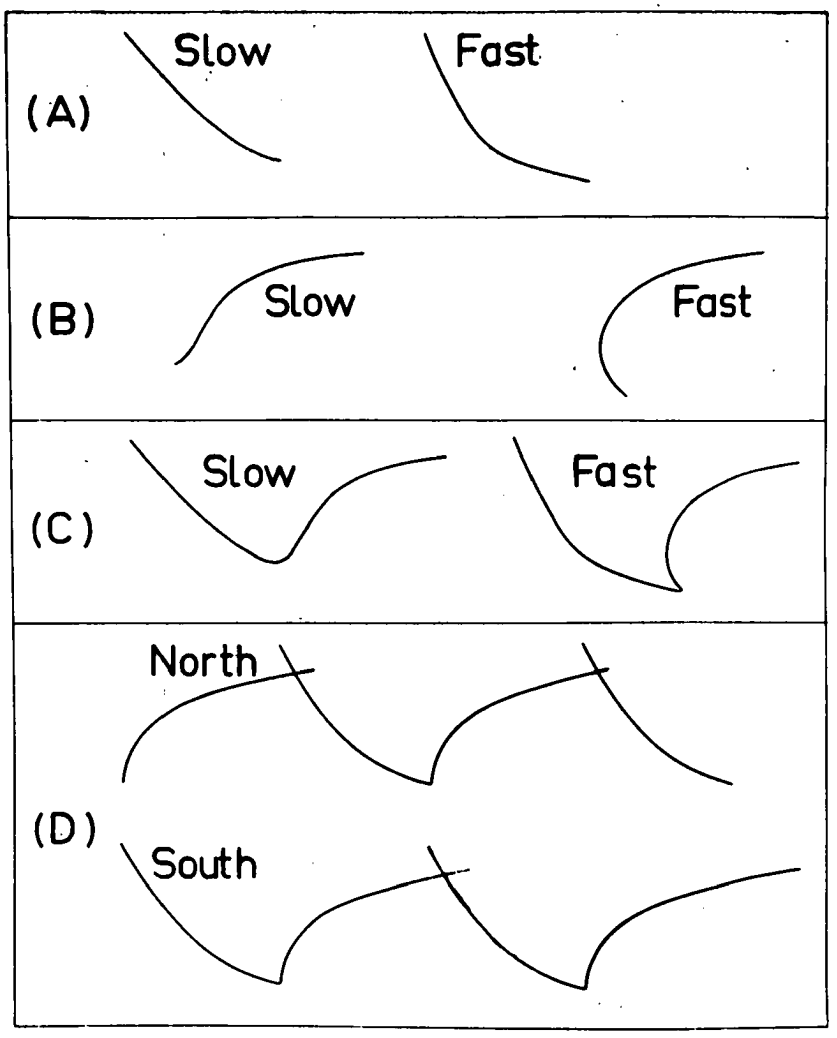

Fig. 46. Types of discrete emission which can be produced by this process. (A) Bunch injected at midpoint (equatorial plane), mirrored in *observer's* hemisphere and scattered at midpoint ("falling tone" or "pseudo whistlers"). (B) Bunch injected at midpoint and either absorbed near the mirror in the *opposite* hemisphere or mirrored, and scattered at the midpoint ("riser" for slow bunch, "pseudo nose" for fast). (C) Bunch injected at midpoint, mirrored in observer's hemisphere, survived one transit through midpoint to pass into opposite hemisphere ("hook"). (D) Medium speed bunch injected at midpoint, mirrored in southern hemisphere, then northern, southern, northern and finally scattered at the midpoint. In the northern hemisphere a "riser" a "hook" and a "falling tone" are observed; in the southern, two "hooks". Synchronised spectrograms from conjugate points would look like this.

McInnes[75],). Nosed forms seem to be relatively rare. This is probably because low particle speeds occur more frequently than high. The observed order of abundance is otherwise as expected.

Table 4.

Hazards and Relative Occurrence

Class and Types (see Fig. 46)	Hazards: Mirrors	Hazards: Source region Transits	Observed * Relative Abundance
(B) "risers"	0	0	178
"p. noses"	1		7
(A) "falling tones"	1	0	21
(C) "hooks"	1	1	15
(D) Multiple forms	2 or more	1 or more	-

* from McInnes[75]

7.4 Intensity Estimates. One of the advantages claimed[55] for this type of theory is that quantitative estimates of intensity can be made. If we assume that each electron radiates independently (i.e. incoherently) then the calculated intensity from reasonable numbers of electrons will be some orders of magnitude too low. On the other hand if small bunches of electrons radiated coherently the radiated power from the bunch would be proportional to the square of the number of the electrons in the bunch. For reasonable densities of the radiating electrons[49, 76] bunch sizes of the order of a few tens of metres would suffice.

However, without independent knowledge of such bunching effects, detailed estimates of intensity are pointless.

Suffice to say that on the simple theory of cyclotron radiation from charged particles in a vacuum the radiated power is inversely proportional to the square of the particle mass. Thus radiation from electrons would be some three million times that from protons, other factors being the same.

7.5 Conclusions. The qualitative frequency-time form of many exospheric discrete emissions is explained by this theory. Further it does not require ionospheric effects to explain part of this form as does the TWT type mechanism. In addition to explaining characteristics already observed it predicts further points which would provide a test for the theory. Since radiation is only produced from electrons travelling away from the observer local precipitation effects (aurora, absorption, X rays) will tend to occur in the hemisphere opposite to that from which the radiation is observed. Observation of more than one similar hook produced by bunches making more than one trip would show firstly that the hooks were generated in a region where mirroring is possible (exosphere) and secondly give an independent measure of particle velocity to check the theory. Simultaneous observations at both ends of a line of force (conjugate point experiment) would be useful for checking this.

8. TESTS OF THE CYCLOTRON THEORY.

8.1 Spectrogram matching. It was shown in Chapter 7 that the doppler shifted cyclotron radiation from receding electrons would give the observed frequency-time shapes of discrete V.L.F. emissions. A more exacting test of this theory would be to take a well defined and complicated hook as observed on a frequency-time spectrogram and attempt to match it in shape and scale with one calculated according to the theory. Such a hook is shown in Figure 47. This was observed[9] at Seattle on September 23, 1957. It also appears in Figure 6(A).

It will be shown in the next chapter that four parameters (two frequencies and two times) scaled from the observed hook is sufficient to allow calculation of electron energy (E), initial helical pitch angle (ψ_o), geomagnetic field line of occurrence (λ) and scale frequency (a). Thus for the hook in Figure 47 the location of three points in the frequency-time plane umambiguously requires E = 150 k.e.v., $\psi_o = 68.6^\circ$, $\lambda = 61.4^\circ$ and a = 527 kc/s. To test the theory, 25 points were calculated from first principles (Chapter 7) using this information and assuming a dipole magnetic field and an exosphere of constant (along a field line) scale frequency. The curve though these points is shown vertically above the observed hook in Figure 47. Comparison shows excellent agreement.

8.2 Symmetry of Emission. One of the features of the theory is that the sequence of emitted frequencies is spatically symmetric

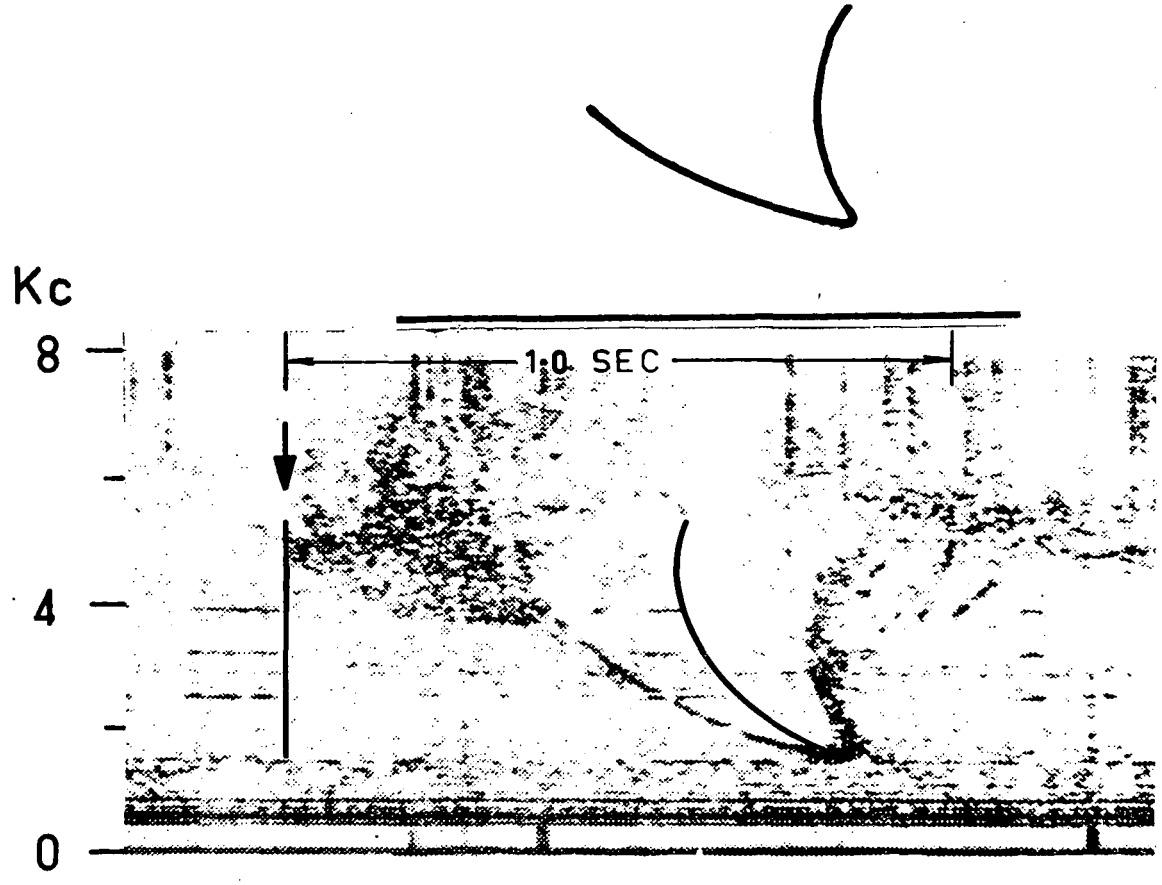

Fig. 47 Hook recorded at Seattle on 23rd Sept. 1957 at 2035 : 28 U.T. (after Helliwell and Carpenter[9]). Above this is the hook calculated from the theory for F = 150 k.e.v., $\psi_0 = 68.6^\circ$, $\lambda = 61.4^\circ$ and a = 527 kc/s. Superimposed on the observed hook is drawn a computed nose whistler originating from a hypothetical impulse at the equatorial plane at the instant shown by the arrow. Note that this computed curve is in the centre of the hook at all frequencies.

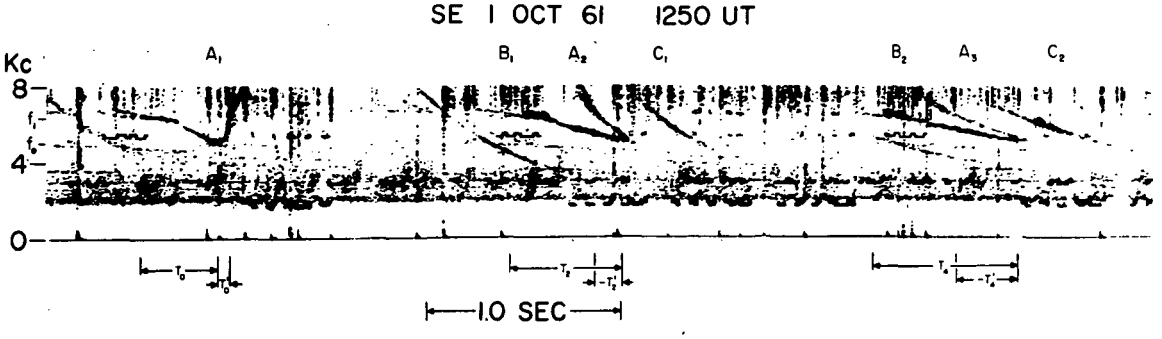

Fig. 48 "Hooks, (A_1, A_2 A_3) and whistlers (B_1, B_2 and C_1, C_2) echoing in the whistler mode over the same path". (Figure with caption after Brice[92]). The notation used here is Brice's, not that used in Chapter 9.

about the equatorial plane (provided that this is a symmetry plane for the magnetic field and electron density distribution). Thus the frequency emitted at the point (λ , ℓ) is the same as that at the point (λ , $-\ell$). This was illustrated in Figure 44. As will be shown in the next chapter (equation 9.9), one consequence of this symmetry feature is that the observed frequency-time distribution of a hook should be symmetrically spaced (in time) about a half-dispersed nose whistler. In other words, at any frequency the mid-point in time between the two branches of a hook should lie on a curve corresponding to the whistler mode dispersion of a hypothetical wide band impulse originating at the top of the field line at the instant of generation of the lowest frequency. This is also the instant at which the emitting electron bunch passes through this point.

Consider the hook shown in Figure 47. Super-imposed on this is drawn the nose whistler originating from a hypothetical impulse at the top of the field line at the instant shown by the arrow. The frequency-time shape of this nose whistler was calculated from a function given by Smith and Carpenter[90] which, they have shown, accurately represents this shape. The frequency-time scale adopted corresponds to a nose frequency (f_n) of 4.60 kc/s (latitude of end point 61.4°) and a short whistler delay time (t_n) at this frequency of 1.64 seconds. This (f_n, t_n) is typical of moderately disturbed conditions (Carpenter[91]) when generation of hooks is likely. Careful measurement of Fig. 47 shows that this curve is accurately in the centre of the hook at all frequencies as predicted.

A different test of the symmetry feature was proposed by Brice[92]. He considered whistler mode reflections of hooks measured at the minimum frequency f_o and some other frequency f_1. By denoting the propagation times for these two frequencies from the top of the path (equatorial plane) to the observer by τ_o and τ_1 respectively, Brice showed (using Brice's notation) :

$$T_1 - T_o = 2(\tau_o - \tau_1) = T_o - T_o' \qquad (8.1)$$

where T_o and T_o' are the times between the observation of the first appearance of f_1 and f_o and of f_o and the second appearance of f_1 respectively. These times refer to the "zero order" or non-reflected hook. The times T_1 and T_1' are the corresponding times for the "first order" or once reflected hook. These definitions are illustrated in Figure 48. He generalised (8.1) for an 'n' hop echo :

$$T_n - T_o = n(T_o - T_o') = T_o' - T_n' \qquad (8.2)$$

From this he derived his testing parameters :

$$\frac{n(T_o - T_o')}{T_n - T_o} = \frac{n(T_o - T_o')}{T_o' - T_n'} = 1 \qquad (8.3)$$

If the hook and echoes are observed at only one station, an ambiguity exists (as Brice pointed out) because one would not know* whether the first hook observed was the zero order or non-reflected hook or the first order or once reflected hook. In the latter case the non-reflected hook would only be observable at the conjugate point. In which case the testing parameter becomes :

---

* As explained in the next chapter (Section 9.5) this ambiguity can be removed if the true nose frequency is measurable - not the case in Figure 48.

$$\frac{n-1}{3} \cdot \frac{T_1 - T_1'}{T_n - T_1} = \frac{n-1}{3} \cdot \frac{T_1 - T_1'}{T_1 - T_n} = 1 \qquad (8.4)$$

Brice considered the series of hooks shown in Figure 48 as well as three other series observed simultaneously at conjugate stations (spectrograms of these were not given). He used the interpretation appropriate to (8.3) for all these because the conjugate ones indicated this. His tabulated results[92] are reproduced in Table 5.

TABLE 5.

f_1	f_o	n	T_n	T_n'	$\frac{n(T_o - T_o')}{T_n - T_o}$	$\frac{n(T_o - T_o')}{T_o' - T_n'}$
kc/s	kc/s		sec.	sec.		
6.5	5.1	0	.39	.05		
		2	.57	-.14	3.8	3.6
		4	.75	-.31	3.8	3.8
4.5	3.8	0	.16	.03		
		1	.22	-.03	2.2	2.2
5.0	3.8	0	.35	.02		
		1	.42	-.97	4.7	3.7
4.4	3.8	0	.17	.02		
		1	.22	-.03	3.0	3.0

As can be seen in Table 5 Brice's testing parameter is of the order of three and quite significantly not unity. Brice[92] concluded

that the theory therefore cannot explain these hooks.

Now, using Brice's notation, it can easily be shown from (8.2) that for symmetrical generation the theory predicts:

$$T_n - T_n' = (2n + 1)(T_o - T_o') \qquad (8.5)$$

If these difference times are calculated from his Table 5 it will be seen that they are clearly not in the predicted ratio 1 : 5 : 9 for the first sequence and 1 : 3 for the other three.

On the other hand it is rather striking that these ratios are none the less in a logical order. They are quite close to 3 : 7 : 11 for the first sequence and 3 : 5 for the other three. This suggests that in each sequence the first trace observed by Brice was not the zero order or non-reflected hook but the first order or once reflected hook. In which case each of Brice's tabulated values of n should be increased by one. Now we can resolve this by measuring the times between any two traces in a sequence at f_1 and f_o. These are the propagation times for the appropriate number of complete hemisphere to hemisphere hops. Thus using the first and third of the traces in Fig. 48 we find $8\tau_o = 4.10$ sec. and $8\tau_1 = 3.72$ sec. Thus from (8.1), $T_o - T_o' = 2(\tau_o - \tau_1) = .095$ sec. This is approximately one third of the value tabulated by him. Consequently for the first sequence at least we have clearly demonstrated that the first trace observed is the first order or once reflected hook. Thus for this sequence Brice's tabulated values of n should be increased by one and his testing parameters should be calculated from equation (8.4). This is shown in Table 6.

TABLE 6.

n	T_n sec.	T_n' sec.	$T_n - T_n'$ sec.	Predicted $T_n - T_n'$ ratios	$\frac{n-1}{3} \cdot \frac{T_1 - T_1'}{T_n - T_1}$	$\frac{n-1}{3} \cdot \frac{T_1 - T_1'}{T_1' - T_n'}$
0	(not observed)		.095	1		
1	.39	.05	.34	3		
3	.57	-.14	.71	7	1.3	1.2
5	.75	-.31	1.06	11	1.3	1.3
0	(not observed)		*	1		
1	.16	.03	.13	3		
2	.22	-.03	.25	5	.7	.7
0	(not observed)		*	1		
1	.35	.02	.33	3		
2	.42	-.07	.49	5	1.6	1.2
0	(not observed)		*	1		
1	.17	.02	.15	3		
2	.22	-.03	.25	5	1.0	1.0

* these missing values could be obtained from the original spectrograms.

Without having recourse to the original spectrograms for the other three sequences we cannot here make similar statements about these other three. Brice's statement[92] that "this ambiguity is

removed if the hook and echo are observed at conjugate stations" is not strictly true. Although the zero order signals must have been reflected somewhere near one of the conjugate stations they could have been missing from the spectrograms or at least not recognised as such for a variety of reasons.

However we can say that Brice's first sequence unambiguously demonstrates the symmetry aspect of the theory in both the predictions that the $T_n - T_n'$ ratios should be close to 1 : 3 : 7 : 11 (from equ. 8.5) and that his testing parameter should be close to unity. The other three sequences fit the theory if the same interpretation of n applies to these also (Table 6.) Furthermore this can easily be checked from the spectrograms as shown above for the first sequence. It should be noted that the remaining discrepancies in $T_n - T_n'$ and his testing parameter values are easily accounted for by errors in scaling the times T_n and T_n' of about.01 to .02 sec. This is quite reasonable since the widths of the traces are some .05 to .1 sec. as seen in Fig. 48.

8.3 Re-generated Hooks. It was predicted in Section 7.3 that a bunch of electrons which makes several complete hemisphere to hemisphere trips between magnetic mirror points will generate a new hook on each trip. This would give rise to a series of similar hooks separated by the bounce period of the electrons. It is readily distinguished from whistler mode echoes of a single hook since successive hooks are not progressively more dispersed according to their order in the sequence. Since the observable radiation is unidirectional the hooks are received in opposite hemispheres alternately,

that is the sequence observed in one hemisphere is displaced half a bounce period from that observed in the other. This effect distinguishes the predicted emission from some other effect such as periodic injection of electrons.

Observation of this predicted emission showing a bounce period consistent with E, ψ_o, and λ scaled from the shape would be a crucial test of the theory both qualitatively and quantitatively.

A sequence which was probably of this type is shown in Figure 49 (with original caption[77]). The two spectrograms were observed at approximately conjugate stations and the times were accurately synchronised. This was interpreted[77] as a sequence of six noise bursts in the 5-6 kc/s frequency region observed at both Knob Lake, Canada (68°N, geomagnetic) and at Byrd Station, Antarctica (70°S, geomagnetic), the sequence beginning at Knob Lake 0.8 ± 0.1 sec. before it began at Byrd.

However, close inspection of Fig. 49 indicates that in each case the sequence is not six separate bursts but a pair of bursts seen three times. In support of this it will be noticed that the shapes and separation of the two bursts in each pair are similar and in each case the first burst occurs at a slightly higher frequency than the second. Furthermore the time separation between successive pairs (using the time scale provided) is 1.6 ± 0.1 sec. which is just twice the delay between Knob Lake and Byrd. Thus at intervals of 0.8 sec. this pair of bursts appeared alternately at Knob Lake and Byrd.

Since only a narrow frequency band was observed the progressive dispersion criterion cannot be applied. However, as

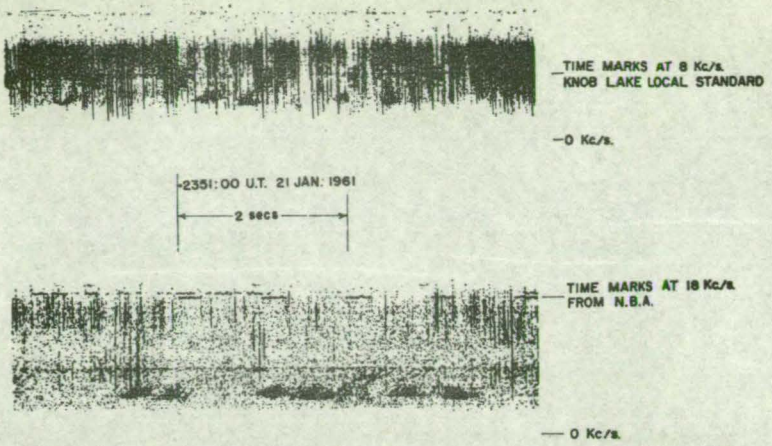

Fig. 1. Six bursts of noise in the 5–6 kc.p.s. frequency region appearing at Knob Lake (above), and at Byrd Station about 0·8 sec. later (below)

Fig. 49 Re-generated bursts or echoes? (After Lokken *et al.*[77])

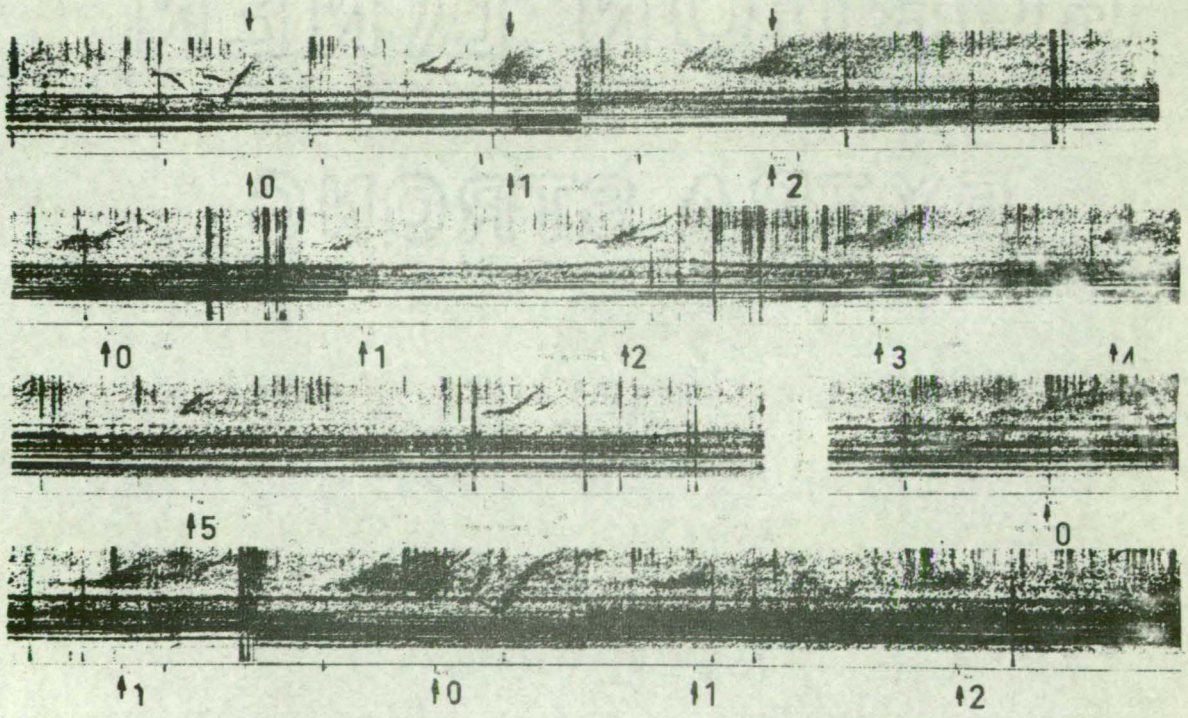

Fig, 50 Four trains of re-generated hooks observed in Alaska (after Gallet[6]). The first hook of each train in marked "0". Progressive dispersion (as in Figure 48) is clearly absent.

pointed out in this paper[77] whistler observations in these latitudes show 5 kc/s propagation times between 1.5 and 2.5 sec. for a single hemisphere to hemisphere trip, i.e. two or three times the observed recurrence period. On the other hand the complete oscillation period of 1.6 sec. would correspond to 60 k.e.v. electrons (for $\psi_o = 20^o$) if the guiding field line was that connecting the two observing stations or 15 k.e.v. (see Table 3) if the guiding field line was typical of those ($\lambda \sim 60^o$) producing nose whistlers observed at Byrd[43]. These electron energies are of the order of those used in Chapter 7 and those measured in the next chapter (Table 8).

The above was published in a letter to Nature[93]. In reply[93] Helliwell agreed with the interpretation that the phenomenon was a pair of bursts seen three times but pointed out that occasionally whistler delay times can be sufficiently small during severe magnetic storms so that in this case the echo possibility cannot be ruled out. In any case this is not the crucial test we would like as the full shape of a hook does not appear so that independent (of the bounce period) estimates of E, ψ_o and λ cannot be made.

Later a much better example (four trains of re-generated hooks) was noticed in a sequence of spectrograms published by Gallet[6]. This is shown in Figure 50. In each of these there is a striking lack of progressive dispersion despite the considerable frequency extent of the hooks and the relatively large number of separate hooks (six, in one sequence). Gallet[6] remarked on this at the time. Table 7 shows E, ψ_o, λ deduced from the shape of one of

TABLE 7. Comparison of observed recurrence period with that calculated from E, ψ_o, λ deduced from the frequency-time shape.

Sequence No.	Number of hooks in each sequence.	Energy E. (k.e.v.)	Helical Pitch ψ_o	Geomag. Latitude λ	Calculated Period (sec.)	Observed Period (sec.)
1	3	14	70°	59°	1.2	1.6
2	6	8	62°	59°	1.7	1.6
3	2	15	72°	59°	1.1	1.6
4	3	5	48°	59°	2.1	1.6

the hooks for each sequence. The expected bounce periods calculated from E, ψ_o, and λ and the observed periods (as measured by Gallet) are shown. The spectrograms (Figure 50) as published[6] are rather small and lack contrast for accurate scaling so that the probable error in the calculated periods is rather large. However the general agreement is quite good.

8.4 Conclusions. We have seen that the electron cyclotron theory gives excellent agreement with the detailed frequency-time characteristics of observed discrete emissions. Two quite different tests of the symmetry aspect of the theory give agreement limited only by scaling errors. In addition the predicted periodic emission (re-generated hooks) is shown to occur and with periods reasonably close to those predicted. Verification of the theory justifies the use of spectrograms of emissions for finding information about the electrons which produce them. A method of doing this is given in the next chapter.

9. METHOD OF MEASUREMENT OF ELECTRON ENERGIES AND OTHER DATA FROM SPECTROGRAMS OF V.L.F. EMISSIONS.

9.1 Introduction. The parameters which affect the frequency-time shape, scale and position of the complete transverse emission ("hook") as observed on the earth are: the energy (E) and helical pitch (ψ) of the emitting electrons, the terminal geomagnetic latitude (λ) of the field line which guides them, the instant (t_o) of their passing through the top of this field line, and the "scale frequency" (a) of the electron density of the medium. If these are suitably chosen a theoretical frequency-time trace can be calculated to give an effectively exact fit to any observed hook. This has been demonstrated with a relatively complex hook. The observed trace contains the effects of these parameters so that it may be possible to deduce these parameters from the observed trace.

It will be shown here that the scaling of only two frequencies (f_n and f_o) and two times (T^+ and T^-) is sufficient for complete and unambiguous evaluation of the parameters cited above.

9.2 Energy. The general expression (51) for the doppler shifted cyclotron frequency from an electron spiraling along a field line is:

$$f = h\left[\gamma\ (1 \pm \beta_d\, n \cos\theta)\right]^{-1} \qquad (9.1)$$

where h is the local gyro frequency, γ is the relativistic correction $(1 - \beta^2)^{-1/2}$, n is the refractive index of the medium at the frequency f, β_d is the longitudinal component of velocity in

units of the velocity of light, and θ is the angle between the field and the direction of emission.

The minus sign in (9.1) refers to forward doppler shift and so need not be considered here. The angle θ in (9.1) also appears in the general Appleton-Hartree expression for the refractive index. For the terrestrial case of backward doppler shifted emission the general expression for f obtained by substituting this refractive index n (θ) into (9.1) is found[94] to be almost independent of θ. If it were otherwise we would not expect such narrow band V.L.F. emissions as are observed. Consequently we consider only the case $\theta = 0$.

Making the appropriate substitutions as in Section 7.2, we have:

$$(h - f)\,(h/\gamma - f)^2 = a\beta_d^2 hf$$

$$= a\beta^2 hf\,(1 - \eta \sin^2 \psi_o) \qquad (9.2)$$

This more general expression reduces to that obtained previously (equ. 7.1) for $\gamma = 1$.

At the equatorial plan ($\ell = 0$) we have:

$$(h_o - f_o)\,(h_o/\gamma - f_o)^2 = a\beta^2 \cos^2 \psi_o\, h_o f_o \qquad (9.3)$$

Making the substitution $x = h_o/f_o$ and $\beta^2 = (\gamma^2 - 1)/\gamma^2$ we get

$$\frac{\gamma^2 - 1}{\gamma^2} = \frac{f_o}{a \cos^2 \psi_o} \cdot \frac{(x-1)^3}{x} \cdot \left[\frac{x/\gamma - 1}{x - 1}\right]^2 \qquad (9.4)$$

The kinetic energy of an electron is given by

$$E = 500\,(\gamma - 1)\ \text{k.e.v.} \qquad (9.5)$$

As we will find later nearly all emissions are produced by electrons

of energies for which relativistic effects are very small ($\gamma \approx 1$). For these we can write

$$E^1 = 250 \beta^2 = \frac{250 f_o}{a \cos^2 \psi_o} (x - 1)^3/x \text{ k.e.v.} \qquad (9.6)$$

From (9.4), (9.5) and (9.6) we find

$$E^1 = E (1 + E \times 10^{-3}) \left[\frac{x - 1}{x - \gamma}\right]^2 \qquad (9.7)$$

From (9.6) we would generally expect high energies to be associated with large values of x. In which case the term containing x is close to unity and (9.7) is in a convenient form for applying relativistic corrections to a nomogram energy scale. This is shown in Figure 54.

Of the quantities in (9.6) required for evaluation of the electron energy only f_o is measurable in an obvious manner from spectrograms of complete emissions ("hooks"). This is the minimum or cusp frequency of the hook (for $\gamma \approx 1$). We now consider methods of deducing the other parameters.

9.3 Latitude λ and parameter x. Suppose we assume that the energy lost (radiated) by the bunch during one hemisphere to hemisphere traverse is negligible. Then the observed emission frequencies will be symmetric with respect to the geomagnetic equatorial plane. That is, the frequency produced by the bunch at latitude angle l in the northern hemisphere will be the same as that produced when this bunch is at the same latitude angle in the southern hemisphere.

Consider the hook in Figure 51 as observed in the northern hemisphere. We require the times T_1 and T_2 for some frequency f.

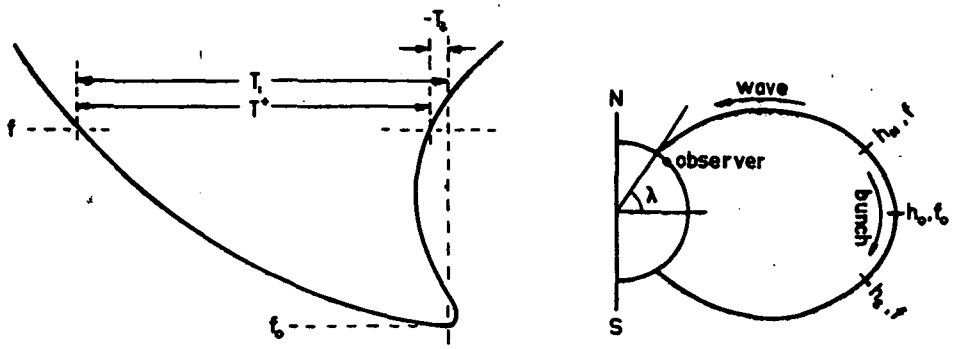

Fig. 51 A hook and the path of the electron bunch which generated it. Definitions.

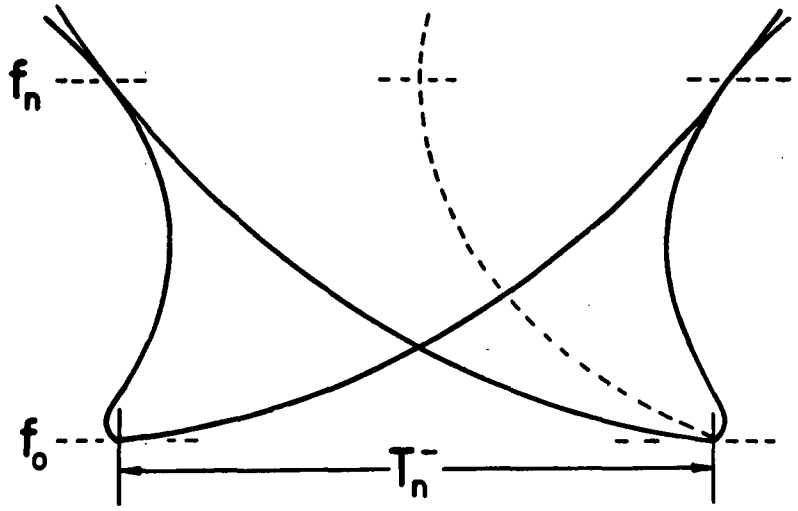

Fig 52 Method of scaling the nose frequency and difference time at this frequency. The midpoint locus (broken curve) has the shape of a nose whistler.

These times, which define the shape of the hook, are made up of group propagation times (t_g) of waves of frequency f and f_o and electron bunch travel times (t_e). We can specify a point on a given line of force by the gyro frequency at that point. Suppose that, at the two points (one in each hemisphere) where the frequency f is produced, the gyro frequency is h. The equatorial plane is then denoted by h_o and the earth's surface by h_λ . Propagation times along the surface of the earth to the observer do not involve dispersion and so do not change the shape of the hook.

Consequently the time T_1 is the time taken for the electron bunch to travel from the point h_N in the northern hemisphere where frequency f is produced to the equatorial plan (h_o) plus the difference between the propagation times for frequency f_o to travel from the equatorial plan (h_o) to the earth's surface ($h_{\lambda N}$) in the northern hemisphere and that for frequency f to travel from point h_N to $h_{\lambda N}$. Putting this in symbolic form:

$$T_1 = t_e\,(h_N \rightarrow h_o) + t_g\,(f_o,\ h_o \rightarrow h_{\lambda N}) - t_g\,(f,\ h_N \rightarrow h_{\lambda N})$$

In a similar way we find:

$$T_2 = t_e\,(h_o \rightarrow h_s) + t_g\,(f,\ h_s \rightarrow h_{\lambda N}) - t_g\,(f_o,\ h_o \rightarrow h_{\lambda N})$$
$$= t_e\,(h_o \rightarrow h_s) + t_g\,(f,\ h_s \rightarrow h_o) + t_g\,(f,\ h_o \rightarrow H_N)$$
$$+ t_g\,(f,\ h_N \rightarrow h_{\lambda N}) - t_g\,(f_o,\ h_o \rightarrow h_{\lambda N})$$

We can drop the N, S subscripts if we always refer to the shortest distance. Taking the sum and difference times T^+ and T^- we find:

$$T^+ = T_1 + T_2 = 2\,t_e\,(h_o \rightarrow H) + 2\,t_g\,(f,\ h_o \rightarrow h) \qquad (9.8)$$

$$T^{-} = T_1 - T_2 = 2\, t_g\,(f_o,\ h_e \rightarrow h_\lambda) - 2\, t_g\,(f,\ h_e \rightarrow h_\lambda) \quad (9.9)$$

We will discuss (9.8) later. Consider now the difference time T^{-} given by (9.9). This contains only wave propagation times. Furthermore, if we consider T^{-} as a function of frequency f then (9.9) is the general (nose) equation of a "short" whistler centred on the time ($T^{-} = 0$) for which $f = f_o$. The frequency for which T^{-} is maximum is then the nose frequency f_n of the equivalent nose whistler. Measurement of f_n defines the line of force in which the hook is produced and along which the electron bunch is guided. A function given by Smith[43] enables h_e and λ to be found from f_n.

A simple but accurate way of measuring f_n is shown in Figure 52. The frequency-time shape of the hook is traced on transparent paper. This tracing is turned over on to the original hook so that the frequency scales still correspond. By moving the tracing in the time direction a position will be found where the descending part of the traced hook just touches the ascending part of the original hook and vice versa. The frequency at which this occurs is then the "true" nose frequency f_n. Note that this is always higher than the pseudo nose which sometimes appears on the ascending part of the hook (Figure 52).

The nose frequency difference time (T_n^{-}) can be found at the same time as shown in Figure 52. We have shown that $T^{-}(f)$ defines the exact shape of a whistler and so should provide electron density information. Smith and Carpenter[90] have shown that if the time delays (t) and frequencies (f) of whistlers are normalised to

nose values (t_n and f_n) then the resulting curves of t/t_n versus f/f_n all closely fit a single "universal whistler dispersion function" which they have calculated. Our T_n^- is then

$$T_n^- = t_o - t_n$$

i.e. $$T_n^- / t_n = S(f_o/f_n) - 1 \qquad (9.10)$$

where t_o is the short whistler time delay at frequency f_o, and S is the Smith-Carpenter dispersion function. The double sided scale shown in Figure 53 which has been constructed from this function allows calculation of t_n. Note that we can also find the time $\frac{1}{2} t_o$ which is the time between the instant the electron bunch passes through the equatorial plane (where frequency f_o is emitted) to the instant of reception on the earth of the cusp or minimum frequency of the hook.

It is interesting to consider here an alternative method of finding f_n and T_n^- which illustrates some of the points made above. The mid point of a line drawn from some frequency f on one branch of the hook to the same frequency on the other branch is given by

$$T_1 - \tfrac{1}{2}T^+ = \tfrac{1}{2}T^-$$

Thus the locus of the mid point is the whistler which would be observed if a wide band impulse occurred at the instant the electron bunch passed through the equatorial plane. This "half whistler" is shown in Figure 52. This alternative method is useful for finding f_n when the hook does not extend to this frequency by using the Smith-Carpenter techniques, particularly if the scale frequency (discussed below) is known from other data.

Having found t_n, f_n by the methods outlined above, or more accurately perhaps by the use of real nose whistlers, we can now find the scale frequency a. This is given by (5.14). A nomogram for solving this equation is given in Figure 53. The function $N(f_n)$ has been built into the f_n scale.

9.4 Helical Pitch. The sum time T^+ is the time width of the hook at any given frequency as shown in Figure 51. From (9.8) we see it contains both wave propagation times and electron bunch travel times. Thus T^+ will be dependent on ψ_o so that it should be possible to use T^+ as a measure of ψ_o.

Suppose we measure T^+ at frequency $f = 2f_o$. For a dipole field we have

$$2t_e = 2 \int_0^l \frac{R_o \cdot \eta \cos^7 l \, dl}{\beta c (1 - \eta \sin^2 \psi_o)^{\frac{1}{2}}}$$

The radial distance to the top of the field line (R_o) can be expressed in terms of h_o, β is given by (9.6) and $h_o = f_o x$. Thus

$$2 t_e = 12.82 \, a^{\frac{1}{2}} f_o^{-5/6} \cos \psi_o \, x^{1/6} (x-1)^{3/2} \int_0^l \frac{\eta \cos^7 l \, dl}{(1 - \eta \sin^2 \psi_o)^{\frac{1}{2}}} \quad (9.11)$$

in seconds where a is in Mc/s and f_o in kc/s.

For the propagation time we have

$$2t_g = \frac{2}{2c \cdot 2f_o} \int_0^l \frac{p \, h \, d \, s}{(h - 2 f_o)^{3/2}}$$

From (7.4) this becomes :

$$2 t_g = 4.28 a^{\frac{1}{2}} f_o^{-5/6} x^{7/6} \frac{\eta^{\frac{1}{2}}(1 - 1/\eta)}{x - 2} (\eta x - 2)^{-1/2} \quad (9.12)$$

In (9.11) and (9.12) the integration limit l and η refer to values at the level for which $f = 2f_o$ (and $h = \eta h_o$). At this

level we have from (9.2) for the non-relativistic case:

$$(\eta h_o - 2 f_o)^3 = a \beta^2 2 f_o \cdot \eta h_o (1 - \eta \sin^2 \psi_o)$$

at the equatorial plane ($f = f_o$) we have:

$$(h_o - f_o)^3 = a \beta^2 f_o h_o \cos^2 \psi_o$$

Dividing and making the x substitution:

$$\left[\frac{\eta x - 2}{x - 1}\right]^3 = \frac{2\eta\left[1 - \eta \sin^2 \psi_o\right]}{\cos^2 \psi_o} \qquad (9.13)$$

We can now find η from (9.13) and l from η and substitute these into (9.11) and (9.12). Then from (9.8) we have

$$T^+ = a^{\frac{1}{2}} f_o^{-5/6} F(x, \psi_o) \qquad (9.14)$$

where F is a function of x and ψ_o but not of η. For a given value of F which can be calculated from observed values of T^+, a, and f_o, then ψ_o is a function of x only. This is shown by the family of curves of constant F in Figure 54. In this nomogram (Figure 54) a point on the x scale is found from f_o and f_n and a point in the F scale from f_o and T^+ (for a = 1 Mc/s). With the help of the nose shaped curve the appropriate F curve is selected. This curve will intercept the previously found x value at the ψ_o value given by the top scale.

The highest frequency observed on the rising part of a hook is about .5 to .6 h_o. This effect is well known in whistler studies[43] and is caused by high attenuation[88] in the vicinity of the gyro frequency. Thus measurement of T^+ at $f = 2f_o$ is not possible for hooks of $x < 3$ or 4. Also it will be noted from Figure 54 that the F curves become nearly horizontal for low values of x. For

such hooks we use an alternative method based on T^+ measurement at $f = f_n$ or in general at $f = gh_e$.

Equation (9.13) becomes

$$\left(\frac{\eta - g}{x - 1}\right)^3 = \frac{\eta g (1 - \eta \sin^2 \psi_o)}{x^2 \cos^2 \psi_o}$$

Rearranging:

$$\frac{x^2}{(x-1)^3} = \frac{\eta g (1 - \eta \sin^2 \psi_o)}{(\eta - g)^3 \cos^2 \psi_o} = X_1 \qquad (9.15)$$

From (9.6) and (9.15) we find

$$\beta^2 = \frac{h_o}{a} \cdot \frac{(\eta - g)^3}{\eta g (1 - \eta \sin^2 \psi_o)}$$

Substituting this into the integral for $2t_e$ we find

$$2t_e = 8.4\, a^{1/2} h_e^{-5/6} \frac{g^{\frac{1}{2}} \eta^{1/2}}{(\eta - g)^{3/2}} (1 - \eta \sin^2 \psi_o)^{1/2} \int_o^{\ell} \frac{\eta \cos^{-7} \ell}{(1 - \eta \sin^2 \psi_o)^{1/2}} d\ell$$

Note that this does not contain x. Also to the extent that

$$\frac{(1 - \eta \sin^2 \psi_e)^{1/2}}{\ell} \int_o^{\ell} \frac{\eta \cos^{-7} \ell \cdot d\ell}{x (1 - \eta \sin^2 \psi_e)^{1/2}} = 1 \qquad (9.16)$$

and using the approximation for small values of ℓ :

$$\ell \approx \sqrt{\frac{2}{3}} (\eta - 1)^{1/2}$$

We have :

$$2t_e = 3.96\, a^{1/2} h_o^{-5/6} g^{1/2} \eta^{1/2} \frac{(\eta - 1)^{1/2}}{(\eta - g)^{3/2}} \qquad (9.17)$$

Using the same quasi constant model of electron denisty and referring all frequencies to h_o we find

$$2\, t_g = \frac{6.06}{g^{1/2}(1-g)}\, a^{1/2}\, h_o^{-5/6}\, \frac{\eta - 1}{\eta^{1/2}}\, (\eta - g)^{-1/2} \qquad (9.18)$$

So that from (9.8) we have:

$$T^+(g) = a^{1/2}\, h_o^{-5/6}\, G(g, \eta) \qquad (9.19)$$

where G is given by (9.17) and (9.18).

The error introduced into t_e by assuming the validity of (9.16) is very small at low frequencies (near f_o) where $t_e > t_g$. It becomes larger at the higher frequencies but there $t_g > t_e$ so that the resulting error in T^+ is never appreciable. It may seem surprising then that G which does not contain ψ_o explicitly can be used to find ψ_o. However we can obtain η by inverting G and then, solving (9.15) for ψ_o, we have:

$$\sec^2 \psi_o = \frac{1}{\eta - 1}\left[\eta - \frac{X_1 (\eta - g)^3}{\eta g}\right] \qquad (9.20)$$

9.5 Use of Nomograms. We have obtained expressions for the electron parameters E, ψ_o, λ, t_o and a in terms of the quantities f_o, f_n, T_n^- and T^+ which can be ~~selected~~ scaled from spectrograms of hooks as explained above. We now discuss techniques of evaluation of these parameters using the nomograms of Figures 53, 54 and 55.

The scale frequency a is found from the nomogram of Figure 53. The f_n, t_n data may be taken from (i) the hook to which one is to apply the scale frequency value for calculation of other parameters, (ii) a nearby hook, or (iii) a nose or "near-nose" whistler. In the first two cases t_n is deduced from f_e, f_n and T_n

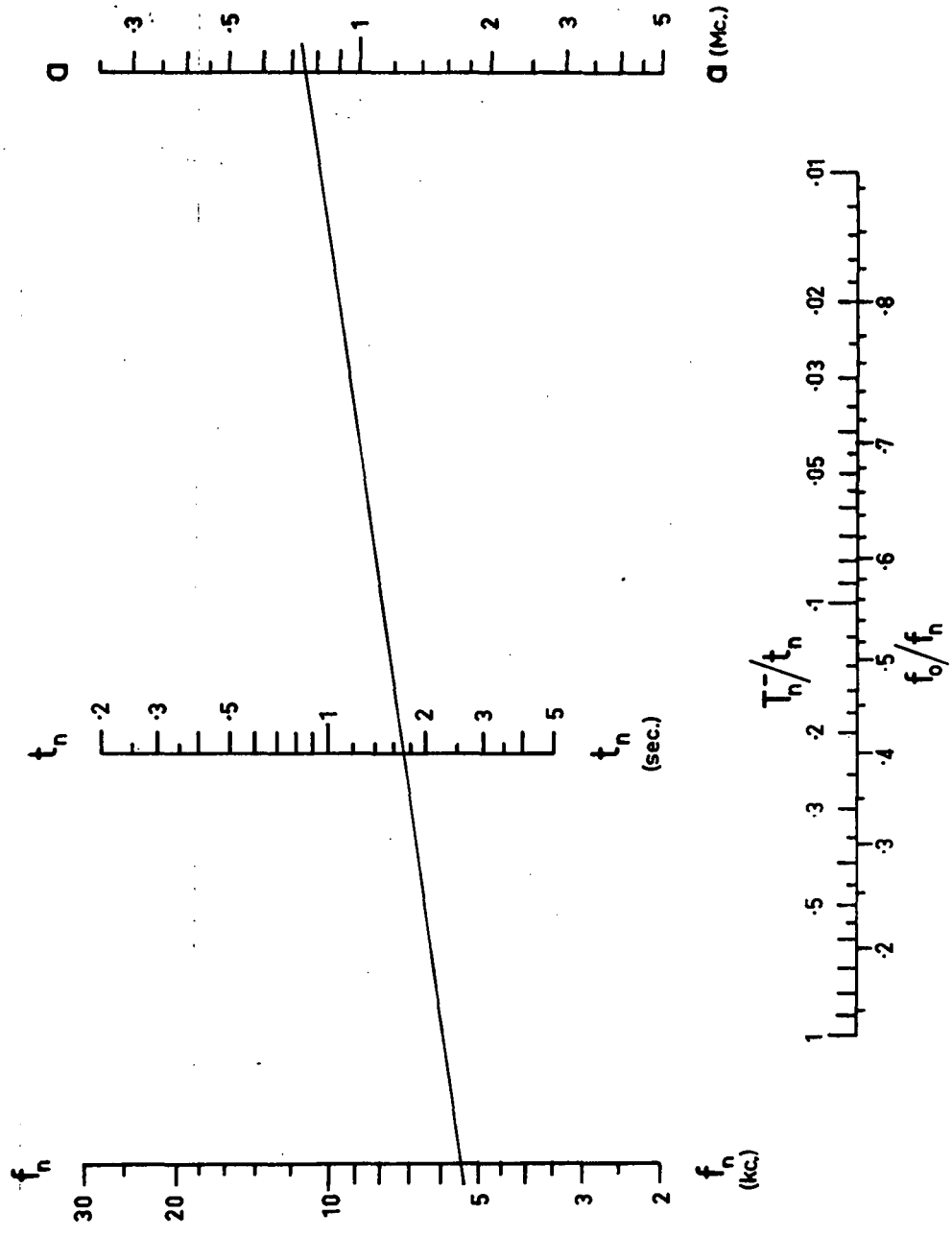

Fig. 53 Nomogram for calculation of scale frequency (a).

by use of the double sided scale in Figure 53. It will be seen from this scale that for reasonable accuracy we require a hook for which $f_n \gtrsim 2f_o$. In general whistler measurements will be more accurate. However in both cases (ii) and (iii) we may be measuring scale frequency in a different field line (if f_n is different). This could introduce an error of 40 per cent[43].

For evaluation of the other parameters T^+ is measured at $f = 2f_o$ and the nomogram of Figure 54 is used provided $f_n \gtrsim 2f_o$. Otherwise T^+ is measured at $f = f_n$ or $f = \frac{3}{4}f_n$ and Figure 55 is used. In both cases the terminating geomagnetic latitude of the field line is immediately obtained from the f_n — λ scale.

Consider the first case (Figure 54). The f_o scale is graduated and scaled logarithmically in f_o. The f_n — λ scale is scaled (but not graduated) logarithmically in h_o. A straight line through appropriate values of f_o and f_n gives the position of x on the x reference line. This scale is not graduated as the actual value is not required. Similarly the position of F on the F reference line can be found from f_o and $T^+ / \sqrt{a}$. The curve labeled X_2 is the function

$$X_2 = (x - 1)^3/x$$

The position of X_2 on the X_2 reference line corresponding to x found above is obtained by drawing a horizontal line through the x point and a vertical line through the X_2 point such that these intersect on the X_2 curve. A horizontal line drawn through the F

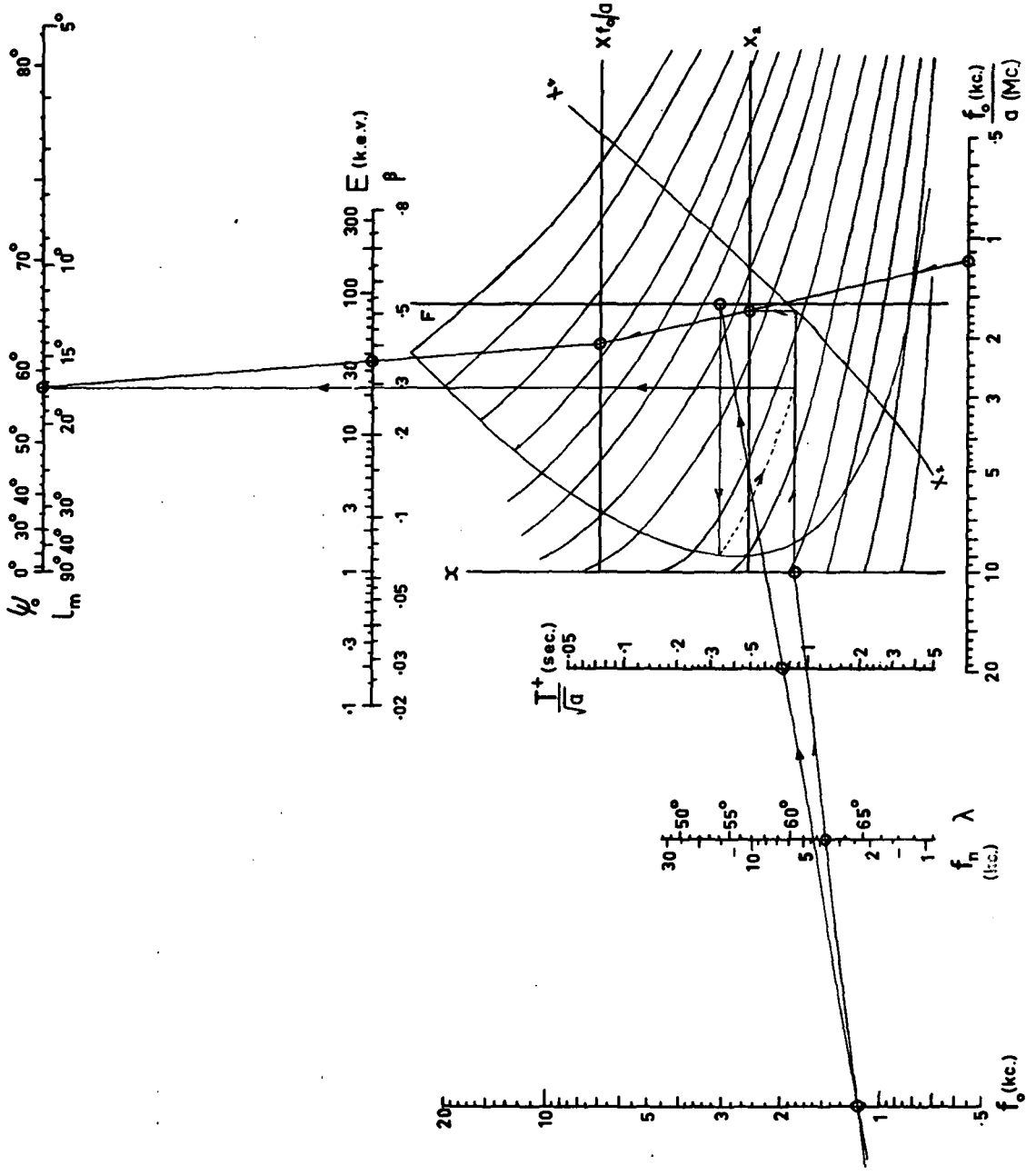

Fig. 54 Nomogram for complete calculation of λ, ψ_o and E when T^+ is measured at the frequency $2f_o$. The scale frequency (a) must be in units of Mc/s as given in Figure 53. In the example calculation shown, meaningful intercepts are marked with circles.

point will intersect the nose shape curve at a point which lies on the appropriate constant F curve of the family. This curve will intersect the horizontal line through x at the value of ψ_o given by (vertical line) the $\psi_o - l_m$ scale of the top of Figure 54. This scale is graduated in degrees for ψ_o and l_m (latitude angle of mirror point) but scaled logarithmically in $\sec^2 \psi_o$. The energy (E) and β are then found from f_o / a, the position X_2, and $\sec^2 \psi_o$ nomographically. This part of the nomogram expresses equation (9.6). The E — β scale is scaled logarithmically in E^1 but graduated according to the relativistic correction given in (9.7).

This procedure is illustrated by the example shown in Figure 54. Only certain combinations of scales bear nomographic relationships so meaningful intercepts are marked with small circles. It is, of course, unnecessary to draw any of these lines or curves. All scales and reference lines are parallel or perpendicular so that set squares can be used for the graphical parts. It should be noted that the scale frequency (a) must be used in units of Mc/s as obtained in Figure 53.

If $f_n < 2f_o$ measurement at $f = 2f_o$ may be impossible. In this case the nomogram of Figure 55 is used. The value of η is found from the f_n and $T^+ / \sqrt{a}$ scales. The η scale is logarithmically scaled in the function G of equation (9.19) but graduated in η for two values of g. As will be seen later the terminal latitude (λ) of the field lines in which hooks are generated appear to be confined to a narrow range about 60°. For

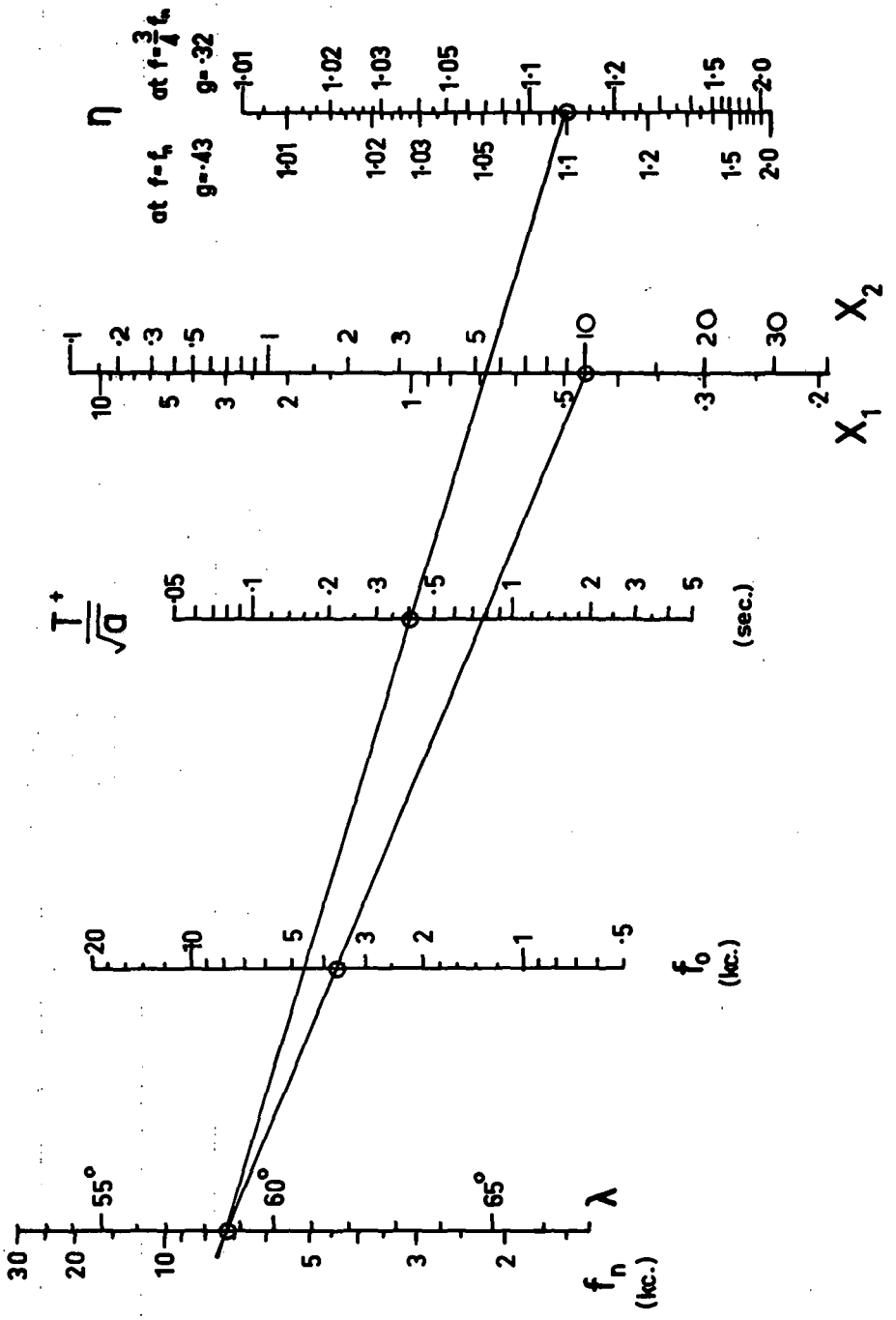

Fig. 55 Nomogram for calculation of η, X_1 and X_2 for T^+ measured at the nose frequency or three quarters of this frequency. Energy and helical pitch are then obtained from the expressions (9.6) and (9.20). This method entails some simple artihmetic and slide rule calculations.

this range these two values correspond to $f = f_n$ and $f = \frac{3}{4}f_n$. The time T^+ can be measured at either of these frequencies provided the corresponding side of the η scale is used. The $X_1 - X_2$ scales are scaled logarithmically in x and so these values are obtained from the f_n and f_o scales as shown in Figure 55. Then E, β and ψ_o must be calculated from equations (9.20) and (9.6).

Since this case ($f_n < 2f_o$) corresponds to low values of x which is generally associated with low energies we do not require a relativistic correction. The simpler form of this nomogram is offset by the necessity of additional slide rule and arithmetical calculations.

The discussion so far has been limited to "original" or non-echoed hooks. However the electromagnetic energy or signal may be reflected near the earth back along the field line once (and so be observable near the conjugate point) or perhaps several times. Such echoed hooks can also be used for evaluation of electron parameters. The frequencies f_o and f_n will be unchanged. From (9.8) we see that T^+ also will be unchanged. On the other hand the midpoint locus $\frac{1}{2}T^-$ for a non-echoed hook is the dispersion of a single trip from the equatorial plane to the earth's surface. For a once-echoed hook the dispersion path is three times this so that T_n^- for such a hook is three times that of the original hook. Since a once-reflected hook is not easily recognised as such (see Section 8.2) calculation of scale frequency from T_n^- by Figure 53 would lead to a value nine times too large. Fortunately, however, such an ambiguity can usually be resolved. Carpenter[91] measured f_n, t_n of

over 250 whistlers. If these are converted to scale frequencies about 75 per cent lie in the range 0.5 to 2 Mc/s. The highest was about 4 Mc/s and for nose frequencies less than about 10 kc/s there was none above 2 Mc/s. Consequently apparent values of $a > 2$ or 3 as obtained from T_n^- is evidence of echoed hooks. This ambiguity is completely removed if more than one echo is observed as t_n can then be measured directly (provided f_n is measurable).

In general the treatment given above can only be applied to complete emissions or hooks. Incomplete forms such as "falling tones" and "risers" only provide f_o, and T_1 or T_2. If the nose and scale frequencies are known from other data the missing parts could be supplied from the midpoint locus $\frac{1}{2}T^-$. This would be the case if identifiable echoes were observed.

The theory of this treatment is based on the assumption of a dipole magnetic field and a constant scale frequency along the field line within the region of generation of the observed frequencies. Some departures in the T^+ curve over that calculated from the theory have been noticed. As these occur at the high frequency end it is perhaps advisable to measure T^+ at the lower of the frequencies f_n and $2f_o$. These departures do not seem to occur in the T^- curve indicating that any perturbations are symmetrical about the equatorial plane.

9.6 Some Examples. As an example of the method fourteen hooks were scaled from spectrograms published by Gallet[6] and by Helliwell and Carpenter[9]. These published spectrograms had the usual aspect ratio

of 10 kc/s range being equivalent to one second interval which is ideal for our purposes. The size, contrast, and definition of these spectrograms as published were not really suitable for accurate scaling but useful results were obtained as shown in Table 8. The first five of these hooks were taken from Gallet and the remaining nine from Helliwell and Carpenter.

The sum time T^+ was measured at $2f_o$ for each hook and at f_n as well for six of these hooks. These times are shown in Table 8 as $T_{2o}{}^+$ and $T_n{}^+$ respectively. For these six hooks both methods were used for energy and helical pitch calculation. The two sets of these values are shown in Table 8. There is reasonable agreement between them. What discrepancies there are could be explained by either scaling errors or the simplifying assumptions used in deriving the alternative (f_n) method.

The scale frequency a as calculated from Figure 53 for each hook is shown in Table 8. However for the value adopted for energy and pitch calculation, use was made of the fact that hooks often occur in groups. For instance the last seven hooks all occurred within thirty seconds or so of 0135 U.T. on October 6, 1959. Also hooks 2 and 3 both occurred at 0635 U.T. on February 15, 1958. It seems reasonable to assume that the scale frequency would not change in such a short time. Thus a weighted average value was adopted in such cases.

This sample is too small for statistical analysis. It seems that relatively few spectrograms of hooks have been actually

Table 8. Electron data deduced from hooks.

MEASURED						DEDUCED						
No.	f_o kc.	f_n kc.	T_n^- sec	T_n^+ sec	T_{2o}^+ sec	$\frac{1}{2}t_o$ sec	a* Mc.	λ	ψ_o	E kev	ψ_o^{**}	E** kev
1	3.3	9.6	.40	.57	.33	.85	1.3	57°	64°	85	62°	78
2	3.3	5.7	.22	.56	.70	1.3	1.8	60°	74°	47	70°	31
3	3.7	7.1	.23	.70	.75	1.0	1.5	59°	58°	23	63°	29
4	2.7	5.3	.35	.78	.80	1.5	1.7	60°	64°	26	66°	26
5	3.9	10.4	.40	-	.53	1.0	2.1	57°	56°	37	-	-
6	1.6	4.6	.48	-	.31	1.0	.50	61°	68°	150	-	-
7	4.2	8.0	.28	.42	.49	-	2.8	58°	50°	47	57°	60
8	2.7	7.5	.28	-	.43	.65	.53	58°	38°	55	-	-
9	1.6	6.5	.61	-	.36	.95	.59	59°	41°	70	-	-
10	2.0	6.5	.44	-	.42	.85	.56	59°	48°	68	-	-
11	2.3	6.5	.44	-	.38	1.0	.82	59°	58°	83	-	-
12	2.1	6.5	.35	-	.38	.70	.40	59°	56°	80	-	-
13	3.2	7.1	.28	.56	.48	.95	1.1	59°	52°	51	56°	57
14	1.9	6.3	.50	-	.38	.95	.63	59°	55°	88	-	-

*Deduced from the hook. The value used for energy and pitch calculation may differ from this.

**Calculated by the alternative method (Figure 55).

published though since seven of the fourteen considered here occurred in an interval of half a minute one would expect that enormous numbers would have been recorded during the I.G.Y. However some interesting preliminary conclusions can be drawn from the few we have here.

Table 8 shows that the generation of these hooks was confined to a narrow range of field line latitudes. The last seven were observed at Seattle (geomagnetic latitude 54°N) but barely or not at all at Stanford (44°N) as shown in Helliwell and Carpenter[9]. This indicates an observing range for any one event (produced by propagation under the ionosphere) of some ten degrees of latitude. Thus we would predict from this that the occurrence rate of observations as a function of receiving station latitude should show a broad maximum in the vicinity of 59°. The observed[9] (Figure 3) occurrence rate of "chorus" for days of $K_p \geq 4$ shows such a maximum at approximately 58°. Although the average latitude of the field lines of generation can be deduced from such analyses of occurrence rate of observations the method given here for the first time gives the latitude of individual emissions. The method also gives the time of generation of the centre (t_o) of the hooks. From Table 8 we see that this occurred about one second before observation.

If the electron bunches which produce these hooks were all injected into the field line near the equatorial plane and if there were no preferred direction of injection, one would expect the median of the equatorial pitch angle (ψ_e) values of a large

number of bunches to be 60°. This is approximately so for the fourteen hooks in Table 8. The latitude angles of the mirror points (l_m) corresponding to these values of Ψ_o range from about 8° to 30° as seen from the top scale of Figure 54. The latitude angles of the points at which the frequency f_n was generated was found from η for the six hooks for which T_n^+ was scaled. These ranged from 7° to 14°. Thus most of the observed frequency range is generated within some ten to twenty degrees of the equatorial plane. It is important to note that since f_n is the highest frequency at which measurements are made, the assumptions of constant scale frequency and dipole magnetic field need only apply within this region.

Probably the most important parameter is the electron energy. The energies shown in Table 8 are of the order of a few tens of kilo electron volts. Thus typical values of β are around 0.3 to 0.5. Relativistic effects are very small at these velocities so that the rough correction formula (9.7) which was applied to the energy scale of Figure 54 should be sufficiently accurate.

10. ELECTRON - CYCLOTRON GENERATION OF EXOSPHERIC V.L.F. NOISE ("HISS").

10.1 Introduction. Over the last three chapters (7, 8 and 9) the doppler-shifted electron-cyclotron theory of discrete V.L.F. emissions has become well established. Since by definition "dawn chorus" is made up of discrete emissions, then it is also explained by this theory. Thus we have a well known and very common class of emissions which are explained in terms of the cyclotron theory and which can be very similar to hiss (see Section 2.1, Figure 2 and Ref. 9). This suggests that perhaps hiss is only a type of unresolved dawn chorus produced by the cyclotron process by a sufficiently large number of small electron bunches or a continuous stream of electrons. This merely explains the continuous or white noise nature of hiss. However it will be shown in this Chapter that all of the other characteristics of hiss which are explained by the TWT process of Chapter 6 can be equally well explained by the doppler shifted electron-cyclotron process.

10.2 Frequency band Limits. It is clear that a sufficiently large number of overlapping and unresolved "discrete emissions" could produce white noise. However an essential feature of hiss is that it is band limited and that the band width is often quite small, whereas at first sight one might expect only broad band noise from unresolved "discrete emissions" produced by the cyclotron process. But two effects limit the upper and lower frequencies respectively.

The highest frequency emitted (equ. 7.1) is the gyro frequency at the mirror point. However there is a propagation cut off much below this limit caused by attenuation near the local gyro frequency. It is very sharp: Liemohn and Scarf[88] found that in the vicinity of this cut off the attenuation increased from 5 db to 50 db in a three per cent interval of frequency. Smith[43] found that the upper cut off frequency of all nose whistlers he analysed never exceeded 0.55 to 0.6 times the minimum gyro frequency along the whistler path. Choosing the lower frequency, for example, the highest observable frequency from emissions generated in the hemisphere opposite that of the observer will be $0.55\ h_o$. For emissions generated in the observer's hemisphere, however, the lowest gyro frequency along the path from the emission point to the observer occurs at the emission point. Thus the highest observable frequency (f_m) will be $0.55\ h_m$ where h_m is the gyro frequency at the point at which f_m is generated. Substituting into (7.1).

$$(h_m - 0.55\ h_m)^3 = 0.55\ a\ \beta^2\ h_m^2\ \cos^2\psi_m$$

From the principle of invariance of magnetic moment we can express the pitch (ψ) in terms of its value at the equator:

$$\cos^2\psi = 1 - (h / h_o)\ \sin^2\psi_o$$

Consequently:

$$f_m = 0.55\ h_m = 0.55 \left[0.17/a\ \beta^2 + \sin^2\psi_o/h_o \right]^{-1} \quad (10.1)$$

These points are illustrated in Figure 56. The rising parts (right hand side of broken curve) are produced in the hemisphere opposite that of the observer and so are limited to

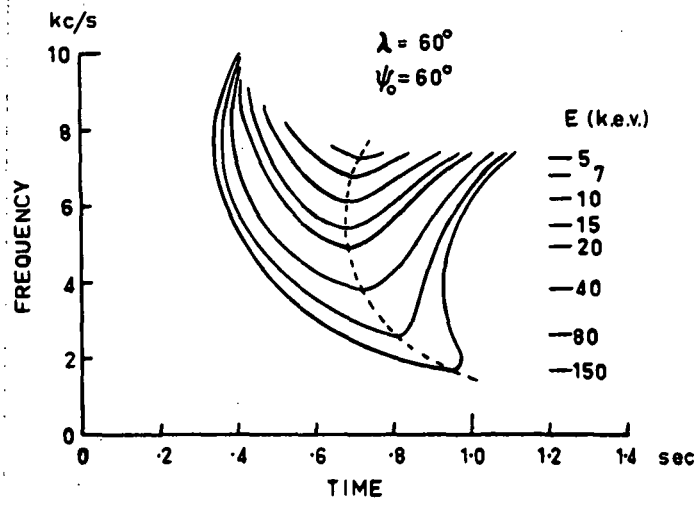

Fig. 56 A family of hooks calculated for electron bunches of minum pitch angle $\psi_0 = 60^\circ$ and several energies as shown travelling in an exosphere of scale frequency $a = 500$ kc/s along the (dipole) field line $\lambda = 60^\circ$. At time $t = 0$ each bunch passed through the equatorial plane from the observer's hemisphere to the opposite hemisphere.

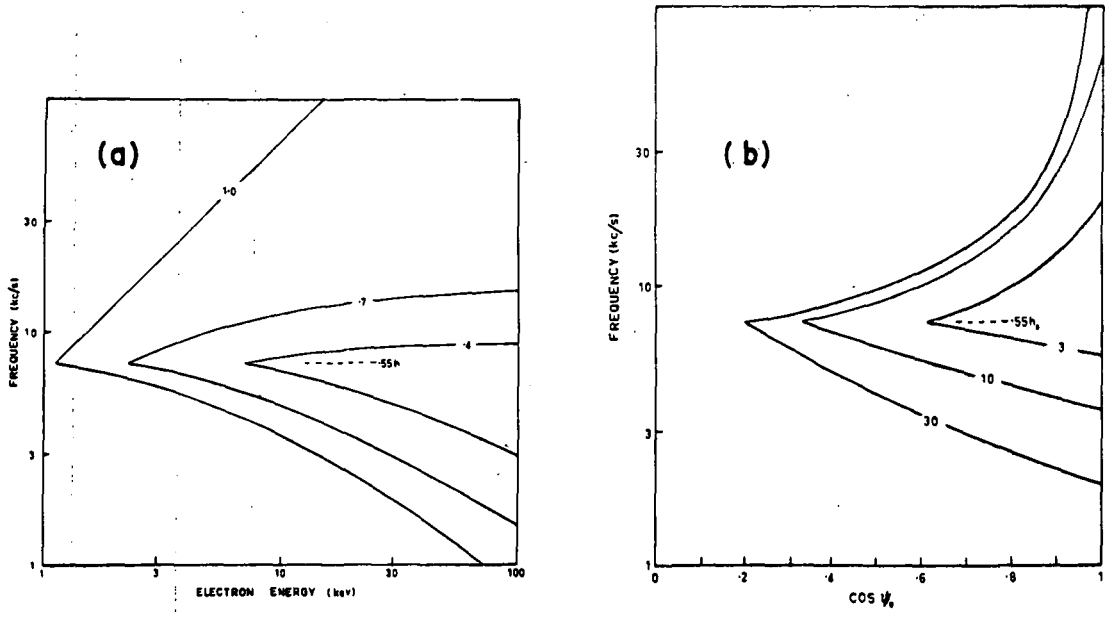

Fig. 57 Upper and lower frequency limits of hiss generated in the field line $\lambda = 60$. (a) Curves f(E) for discrete values of cos ψ_0. (b) Curves $f(\psi_0)$ for discrete E.

$0.55\ h_o$ = 7.4 kc/s. The upper limits of the falling parts are given by (10.1). At any given frequency only energies above some limit can produce radiation. At frequencies below the whistler cut off ($0.55\ h_o$) radiation from both hemispheres can be observed. If the stream is confined to the hemisphere opposite that of the observer the upper limit will be the whistler cut off. This is another way of saying that if the hiss consists entirely of unresolved "risers" and "pseudo noses" (no unresolved "hooks" or "falling tones") the upper frequency limit will be $0.55\ h_o$. This is perhaps likely at times since rising type discrete emissions are about five times as common as hooks and falling tones (Table 4).

The upper and lower limits as a continuous function of energy for discrete pitch angles and of pitch angle for discrete energies are shown in Figure 57. These are drawn for the field line terminating at latitude $\lambda = 60^\circ$. The same curves can be applied at any other latitude if the frequencies and energies are scaled in proportion to h_o. A constant scale frequency of 500 kc/s has been assumed but a definite model of magnetic field is not required (provided it is monotonic) except for obtaining field line latitude λ from minimum gyro frequency h_o. Note that narrow band noise can be produced by a range of energies for any given pitch angle, but for large pitch angles this energy range is larger. Wide and very wide band noise will be produced by electrons of low pitch and high energy. During magnetic storms electron streams reach down to the ionosphere to produce aurorae.[49] At high latitudes ($\sim 60^\circ$) this requires pitch angles (ψ_o) less than about 5°. We

might also expect higher energies during storms and thus wide and very wide band noise as observed (Section 3.1).

10.3 Amplitude - frequency spectra. In considering bandwidths of hiss produced by streams of electrons of various energies and minimum pitch angles we have assumed mono energetic, mono pitched streams. This is not an unreasonable assumption since it is observed that the bandwidths of individual discrete emissions rarely exceed 150 c/s at any instant.[9] This could not happen unless the electrons in the bunches which produce these emissions had narrow ranges of energy and pitch. One would expect the same to hold true of streams. Also mono energetic electron streams have been observed.[49] Pitch angle measurements of electrons in streams have not been reported. However we will show that the main features of hiss can be produced even if the electrons of the streams have wide energy and pitch distributions.

Two energy spectra of electron streams as measured by McIlwain[49] will be considered. Both were measured by rockets fired into visible aurora. The first was observed inside a quiescent auroral glow of intensity I. It showed an integral number energy spectrum proportional to exp (-E/5) electrons/sec cm^2 over the range 3 to 30 kev. The second was observed in a bright active auroral arc. This stream consisted of practically mono energetic electrons of energy 6 kev.

We will consider a pitch angle distribution produced by isotropic injection at the equatorial plane given by equ. (5.2).

Satellite measurements[95] of the low energy (500 kev) electrons in the outer radiation zone indicate such a pitch distribution. Preliminary measurements from hooks (Section 9.6) indicate that the pitch distribution of the electron bunches (but not of the electrons in an individual bunch) is also of this type.

The power radiated by an electron travelling along a helical path in a plasma with superimposed magnetic field has been given by Eidman.[51] For our purpose a crude approximation of his expression will suffice.

$$w = kf^{\frac{3}{2}} E \qquad (10.2)$$

where k is assumed constant. This is the power radiated by a single electron. From Figure 57 we see that a given frequency f requires electrons of energy equal to or greater than some minimum value $E_n(\psi_o)$, which is a function of ψ_o. We will assume that the power radiated by the electron stream at this frequency is proportional to the number of electrons fulfilling this condition, weighted by their energy as in (10.2). If the number of electrons having energies within dE of E is dN(E) and if the pitch distribution is given by (5.2), then the power radiated by the stream at frequency f is given by (arbitrary units):

$$W(f) = f^{\frac{3}{2}} \int_0^{\psi_0} \left(\int_{E_n}^{\infty} E \, d\,N(E) \right) \sin \psi_o \, d\,\psi_o \qquad (10.3)$$

For McIlwain's first stream the integral number energy spectrum is given by

$$J\,(>E) \propto \exp(-E/5) \text{ electrons/sec cm}^2$$

The number energy spectrum per energy interval is then:

$$\frac{dJ}{dE} \propto \exp(-E/5)$$

The density of the electrons in this energy interval dE is given by:

$$dN(E) \propto dJ/\beta c \propto E^{-\frac{1}{2}}\, dJ$$

$$\propto E^{-\frac{1}{2}} \exp(-E/5)\, dE$$

For McIlwain's monoenergetic stream we take:

$$dN(E) = 1 \quad \text{for } E = 6 \text{ kev}$$

$$= 0 \quad \text{for all other values of E.}$$

Amplitude-frequency spectra of hiss generated by these two streams as calculated from (10.3) for streams confined to the field line terminating at latitude $\lambda = 60^{\circ}$ are shown in Figure 58. Note the similarity in shape of the two spectra. The peak or average amplitudes are not comparable, they have been arbitrarily chosen for best clarity. The bands limits of the hiss generated by the monoenergetic stream are approximately given by the $\cos \psi_0 = 1$ curve of Figure 57(a). Thus the hiss spectrum from the first stream (exponential energy distribution) could be approximated in shape, amplitude and bandwidth by one generated by a mono energetic stream of 15 kev electrons. Hiss spectra from two hypothetical mono energetic streams at latitude $\lambda = 63.5^{\circ}$ are shown in Figure 59. From what has been said above we would expect similar spectra from streams having energy distributions $J(>E) \propto \exp(-E/E_0)$ if E_0 is appropriately chosen.

An amplitude discontinuity occurs at the whistler cut off frequency $0.55\, h_e$. Above this frequency only hiss generated in

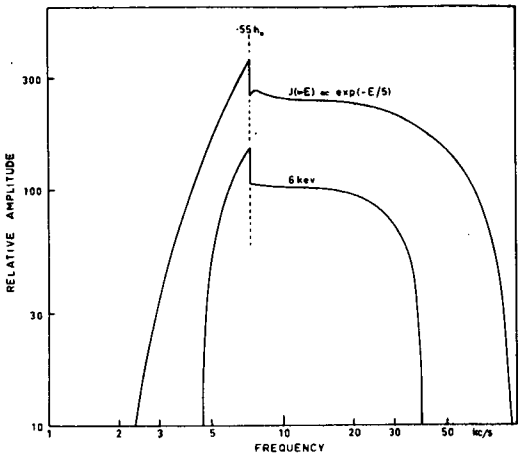

Fig. 58 Amplitude-frequency spectra of hiss generated in the field line $\lambda = 60^{o}$ by electrons having the pitch distribution given by (5,2) and energy distributions as in the streams observed by McIlwain. A finite stream width would smooth out the discontinuity at $0.55\ h_{o}$.

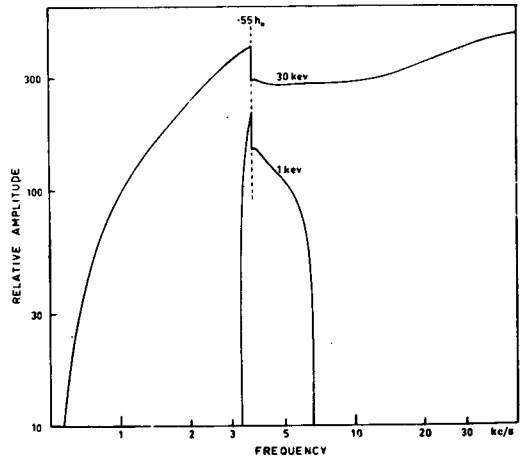

Fig. 59 Amplitude-frequency spectra of hiss generated in the field line $\lambda = 63.5^{o}$ by two mono energetic electron streams having pitch distributions given by (5.2) . Compare these with the observed spectra in Figure 4A .

the observer's hemisphere can be observed, whereas below this frequency hiss from both hemispheres can be observed (see Figure 56). For hiss consisting entirely of unresolved "hooks", or of "hooks" plus equal amounts of "risers" and "falling tones" the discontinuity will be a factor of two in power or of root two in amplitude as shown here. If the hiss consists entirely of "falling tones" the discontinuity will disappear, but if it consists entirely of "risers" and "pseudo noses" the high frequency side ($f > 0.55\ h_o$) will not be observed at all. In all cases the low frequency side could be further augmented by whistler mode reflections near the earth of previously generated hiss. In any case the sharpness of the discontinuities will be considerably rounded by finite attenuation at cut off and finite stream width (field line latitude ranges of a few tenths of a degree would suffice).

Figure 4A shows amplitude-frequency spectra of hiss observed by Watts[19] during a magnetic storm. These show similar shapes to those of Figures 58 and 59 if the discontuities are rounded off. The observed spectra will have been modified by attenuation in propagation through and under the ionosphere. As it is the comparison indicates that the frequency $0.55\ h_o$ is about 2 kc/s. This would correspond to a field line of generation of about latitude 65^o.

10.4 Discussion. This cyclotron theory of hiss can account for the observed characteristics of hiss listed in Chapter 2. From Figures 58 and 59 and equations (9.3) and (10.1) we see that narrow and

medium band width hiss occurring at frequencies less than 10 kc/s would be produced at geomagnetic latitudes of 60° or higher. Very wide to narrow bandwidths can be produced by this process even for wide pitch angle and energy distributions provided the high energies are fairly sharply cut off (power law or exponential) as observed.[49] Wide bandwidths will be produced by higher energy electrons which we might expect to be associated with magnetic activity.

From our present state of knowledge, the cyclotron process explains the observed features of hiss as well as does the TWT process (see Chapter 6). In addition the cyclotron process already explains the much more detailed features of the discrete emissions and dawn chorus. However the two processes are not mutually exclusive. Both may operate, possibly even at the same time and in the same electron stream, though one may dominate. It should be possible to distinguish between these three possibilities (cyclotron, or TWT, or both), if not from present data, at least from new experiments based on predictions of the two theories.

The TWT process requires a stream travelling towards the observer whereas the cyclotron process requires the reverse. Unfortunately hemisphere to hemisphere electron and wave travel times are of the order of seconds whereas time variations of hiss are of the order of minutes or hours[28]. Thus whistler mode reflections of hiss and magnetic reflections of electrons would make the original stream and emission directions very difficult to detect.

Although both theories predict that the centre frequency of narrow band bursts will be proportional to the minimum gyro frequency (h_o), the constants of proportionality are different. For the TWT theory this frequency is 0.15 h_o, whereas for the cyclotron theory it is 0.55 h_o. For typical 4 kc/s narrow band hiss the corresponding field line latitudes are 55.5° and 63.5°. In addition the TWT process can produce narrow band hiss not obeying this relation if the stream is mono energetic and narrow pitched. This effect is difficult to detect on the earth because propagation under the ionosphere allows observation of hiss generated in a wide range of field line latitudes. On the other hand a satellite travelling just above the ionosphere (or higher) will receive only radiation generated in the field line through which it is passing. In addition, since there would be no ionospheric losses to contend with, the intensity would be several orders of magnitude greater and the observed amplitude-frequency spectra would be as generated. For similar reasons such a satellite would be very useful for work on discrete emissions and whistlers.

10.5 Conclusions. Doppler shifted cyclotron radiation from receding electrons which already explains the detailed frequency-time shapes of discrete emissions can also explain the observed characteristics of hiss. However the amplified cerenkov (TWT) process also explains these characteristics and it is difficult to distinguish between the two theories for hiss on present data. Observations from a satellite of the variation of frequency of narrow band hiss with geomagnetic latitude could resolve this.

11. CONCLUDING REMARKS.

11.1 General. The relevant (emission) properties of V.L.F. emissions described in Chapters 2 and 3 are explained. Either or both of two quite different processes might produce "hiss", but only the electron-cyclotron process can explain the detailed features of the "discrete emissions". Furthermore this latter process can explain the other types of discrete emissions ("chorus" and "hiss"). Not only does this clear up a mystery of long standing but provides a new tool (Chapter9) for the investigation of fast electrons in the exosphere.

Other properties not relevant to the emission process are not dealt with in the theoretical treatment. These include the westerly drift of noise sources mentioned in Section 2.6, the 24 hour "echo" bursts and the dynamic variations of amplitude and frequency of hiss described in Chapter 3. These and other long term effects reflect the properties of the sources of the electrons which generate the emissions. However the establishment of the emission process and the techniques (chapter 9) for finding the energy, pitch and latitude of these electrons provide a basis for investigation of these sources.

11.2 Suggestions for Further Work.

(i) The techniques derived in Chapter 9 would provide very interesting information if used on a sufficiently large number of hooks. Although few spectrograms of hooks of suitable aspect ratio (1 sec. = 10 kc/s) have been published, the vast amount of tape recorded during the IGY years (Section 2.3) should contain ample. These techniques should prove as useful for the fast electrons as whistler measurements have been for the thermal electrons (density[43] and temperature[88]).

(ii) Experiments to test the frequency-v-latitude variations of narrow band hiss as predicted by the electron-cyclotron and TWT theories should be carried out, as outlined in Chapter 10.

(iii) As mentioned at the end of Section 9.5, the high frequency parts of hooks sometimes show significant departures (T^+ too large) from the predicted shapes. The cause of this may lie in the assumptions of an unperturbed dipole magnetic field, a constant scale frequency and $\Theta = 0$ (Section 9.2).

11.3 Published Work. Much of this work has been published in appropriate journals. A list of these papers together with the sections of the thesis in which similar material appeared is given below. Reprints of those marked with an asterisk will be found in an envelope at the back of this thesis.

1. R. L. Dowden*, "L. F. radio noise from the aurora", Nature, 184, 803 (1959) (Section 3.1).

2. R. L. Dowden*, "Geomagnetic noise at 230 kc/s", Nature, 187, 677-678 (1960) (Section 3.1).

3. R. L. Dowden*, "Wide band bursts of V.L.F. radio noise ('hiss') at Hobart" Australian J. Phys. 15, 114-119 (1962) (Section 3.1).

4. R. L. Dowden*, "Simultaneous observations of V.L.F. noise ('hiss') at Hobart and Macquarie Island," J. Geophys. Res. 66, 1587-1588 (1961) (not discussed).

5. R. L. Dowden*, "A theoretical model of electron density along a geomagnetic line of force in the exosphere", J. Atmos. Terr. Phys., 20, 122-130 (1961) (Chapter 5).

6. R. L. Dowden*, "'Scale frequency' of the exosphere", Nature, 195, 984-985 (1962) (Section 5.5).

7. R. L. Dowden*, "Theory of generation of exospheric V.L.F. noise ('hiss')" J. Geophys. Res., 67, 2223-2230 (1962) (Chapter 6).

8. R. L. Dowden*, "Doppler shifted cyclotron radiation from electrons : a theory of V.L.F. emissions from the exosphere" J. Geophys. Res., 67, 1745-1750 (1962) (Chapter 7).

9. R. L. Dowden,* "Cyclotron theory of V.L.F. discrete emissions," Nature, 195, 1085-1086 (1962) (Sections 8.1 and 8.3).

10. R. L. Dowden,* "Authors reply to the preceding discussion," J. Geophys. Res., 67, 4900-4902 (1962) (Section 8.2).

11. R. L. Dowden,* "Very-low-frequency discrete emissions received at conjugate points," Nature, 195, 64 (1962)(Section 8.3).

12. R. L. Dowden, "Method of measurement of electron energies and other data from spectrograms of V.L.F. emissions", Australian J. Phys., 15, 490-503 (1962) (Chapter 9).

13. R. L. Dowden, "Doppler shifted cyclotron generation of exospheric V.L.F. noise ('hiss')" Planet, space sci. (in the press, 1962) (Chapter 10).

11.4 Acknowledgments. I am indebted to Prof. G. R. A. Ellis, my supervisor for most of this work, for much encouragement, criticism and advice. In particular Prof. Ellis suggested the investigation of Gallet's TWT process (chapter 6), the conjugate point test of the cyclotron theory (sections 7.3 and 8.3), and the possibility that the cyclotron theory could also explain hiss (chapter 10). I also wish to thank Prof. G. Newstead, my supervisor for the first year, for criticism and advice, and Mr. G. T. Goldstone who built and operated the equipment described in Section 3.3.

Apart from those acknowledged above and in the body of this thesis, all the observations and ideas are my own.

During the period of these investigations I was employed by the Ionospheric Prediction Service of the Commonwealth of Australia. This work was carried out at the University of Tasmania and the I.P.S. Field Station at Llanherne.

R L Dowden.

(R. L. DOWDEN).

November, 1962.

12. REFERENCES

1. H. Barkhausen, Phys. Zeit., 20, 401-403 (1919).

2. T. L. Eckersley, Nature, 122, 768 (1928).

3. E. T. Burton and E. M. Boardman, "Audio-frequency atmospherics", Proc IRE, 21, 1476-1494 (1933).

4. L. R. O. Storey, "An investigation of whistling atmospherics" Phil. Trans. Royal Soc. A. 246, 113-141 (1953).

5. H. E. Dinger, "A four-year summary of whistler activity at Washington, D.C. "J. Geophys. Res., 65, 571-575 (1960).

6. R. M. Gallet, "The V.L.F. emissions generated in the earth's exosphere," Proc. IRE, 47, 211-231 (1959).

7. G. McK. Allcock, "A study of the audio-frequency radio phenomenon known as 'dawn chorus'", Australian J. Phys. 10, 286-298 (1957).

8. J. Crouchley and N. M. Brice, "A study of 'chorus' observed at Australian stations, "Planet, Space Sci., 2, 238-245 (1960).

9. R. A. Helliwell and D. L. Carpenter, "Whistlers-West IGY-IGC synoptic program," SEL Final Report, March 20, 1961, Stanford University.

10. J. M. Watts, "An observation of audio-frequency electromagnetic noise during a period of solar disturbance," J. Geophys. Res., 62, 199-206 (1957).

11. R. A. Helliwell, "Low frequency propagation studies, part I : Whistlers and related phenomena". SEL Final Report (revised, May 28, 1958) Stanford University.

12. J. H. Pope, "Diurnal variation in the occurrence of 'dawn chorus'," Nature, 180, 433 (1957).

13. J. H. Pope and W. H. Campbell, "Observation of a unique V.L.F. emission", J. Geophys. Res., 65, 2543-2544 (1960).

14. Eigil Ungstrup, "Observations of 'whistlers' and very low frequency phenomena at Godhaun, Green-land," Nature, 184, 806-807 (1959).

15. A. D. Watt, and E. L. Maxwell, "Characteristics of atmospheric noise from 1 to 100 kc," Proc. IRE, 45, 787-794 (1957).

16. L. H. Martin, R. A. Helliwell, and K. R. Marks, "Association between aurorae and V.L.F. hiss observed at Byrd station, Antarctica," SEL Report No. 1, April 29, 1960, Stanford University.

17. L. H. Martin, "Observations of 'whistlers' and 'chorus' at the South Pole", Nature 187, 1018-1019 (1960).

18. G. McK. Allcock, "Propagation of whistlers to polar latitudes", Nature, 188, 732-733 (1960).

19. Alv Egeland, "An investigation of the microstructure of the perturbations in the geomagnetic field in the auroral zone," Inst. Theoretical Astrophysics Blindern, Oslo, Report No. 6, (June, 1959).

20. Georg Gustafsson, Alv Egeland, and Jules Aarons, "Audio-frequency electromagnetic radiation in the auroral zone", J. Geophys. Res., 65, 2749-2758 (1960).

21. J. Aarons, G. Gustafsson, and A. Egeland, "Correlation of audio-frequency electromagnetic radiation with auroral zone micropulsations," Nature, 185, 148-151 (1960).

22. G. Reber and G. R. Ellis, "Cosmic radio-frequency radiation near one megacycle," J. Geophys. Res., 61, 1-10 (1956).

23. G. R. A. Ellis, "A receiver for observation of V.L.F. noise from the outer atmosphere," Proc. IRE, 48, 1650-1651 (1960).

24. J. B. Wilcox and Elwood Maple, "Audio-frequency fluctuations in the geomagnetic field," J. Geophys. Res., 65, 3261-3271 (1960).

25. J. B. Wilcox, and E. Maple, "Audio-frequency fluctuations of the geomagnetic field", Nav Ord Rept. 4009, U.S. Naval Ordnance Laboratory, Silver Spring, Maryland, July (1957).

26. R. E. Holzer and O. E. Deal, "Low audio-frequency electromagnetic radiation of natural origin," Nature, 177, 536-537 (1956).

27. J. R. Heirtzler, D. L. Nichols, and R. A. Santirocco, "Some observations of the geomagnetic fluctuation spectrum at audio frequencies" J. Geophys. Res., 65, 2545-2547 (1960).

28. G. R. A. Ellis, "Low frequency electromagnetic radiation associated with magnetic disturbances," Planet, Space Sci., 1, 253-258 (1959).

29. R. A. Duncan and G. R. Ellis, "Simultaneous occurrence of sub-visual aurorae and radio noise bursts on 4.6 kc/s", Nature, 183, 1618-1619 (1959).

30. G. R. A. Ellis, "Geomagnetic disturbances and 5 kilocycles per second electromagnetic radiation", J. Geophys. Res., 65, 1705-1710 (1960).

31. D. G. Cartwright, "The geographical pattern of V.L.F. emissions and associated geomagnetic phenomena", Conference on the Sun-Earth Environment, Brisbane (1961).

32. G. R. A. Ellis and D. G. Cartwright, "Directional observations of radio noise from the outer atmosphere," Nature, 184, 1307 (1959).

33. D. G. Cartwright, "Direction - finding on diffuse sources of electromagnetic radiation", Australian J. Phys., 13, 712-717 (1960).

34. G. R. A. Ellis, "Directional observations of 5 kc/s radiation from the earth's outer atmosphere", J. Geophys. Res., 65, 839-843 (1960).

35. R. L. Smith, R. A. Helliwell, and I. W. Yabroff, "A theory of trapping of whistlers in field-aligned columns of enhanced ionization", J. Geophys. Res., 65, 815-823 (1960).

36. R. A. Helliwell, J. H. Crary, J. H. Pope, and R. L. Smith, "The 'nose' whistler - a new high latitude phenomenon, J. Geophys. Res., 61, 139-142 (1956). See also ref. 43).

37. G. R. A. Ellis, "Spaced observations of the low frequency radiation from the earth's upper atmosphere," J. Geophys. Res., 66, 19-23 (1961).

38. G. R. A. Ellis, D. G. Cartwright, and J. R. V. Groves, "Spaced observations of radio noise from the outer atmosphere, Nature, 184, 1391 (1959).

39. R. A. Duncan, "The cause of magnetic storms and bays," J. Geophys. Res., 65, 3589-3592 (1960) (see also Corrigenda, J.G.R. 66, 1319 (1961).

40. R. L. Dowden, "'Whistler mode' echoes remote from the conjugate point", Nature, 183, 385-386 (1959).

41. B. J. O'Brien, J. A. Van Allen, F. E. Roach, and C. W. Gartlein," Correlation of an auroral arc and a subvisible monochromatic 6300 A arc with outer-zone radiation on November 28, 1959," J. Geophys. Res., 65, 2759-2766 (1960).

42. G. R. Ellis, "On the propagation of whistling atmospherics," J. Atmos. Terr. Phys. 8, 338-344 (1956).

43. R. L. Smith, "The use of nose whistlers in the study of the outer ionosphere," SEL Technical Report No. 6, July 11, 1960, Stanford University.

44. R. A. Helliwell and E. Gehrels, "Observation of magneto-ionic duct propagation using man-made signals of very low frequency", Proc. IRE, 46, 785-787 (1958).

45. J. H. Crary, "The effect of the earth-ionosphere wave guide on whistlers", SEL Technical Report No. 9, July 17 (1961), Stanford University.

46. C. O. Hines, "Heavy ion effects in audio frequency radio propagation", J. Atmos. Terr. Phys., 11, 36-42 (1957).

47. L. Marshall, "Production of the sun's non thermal radio emission by cerenkov radiation", Astrophysical J., 124, 469-475 (1956).

48. G. R. Ellis, "Low frequency radio emission from aurorae", J. Atmos. Terr. Phys., 10, 302-306 (1957).

49. Carl E. McIlwain, "Direct measurement of particles producing visible auroras," J. Geophys. Res., 65, 2727-2747 (1960).

50. J. V. Jelley, "Cerenkov radiation and its applications", Pergamon Press, London (1958).

51. V. Ia. Eidman, "The radiation from an electron moving in a magnetoactive plasma, " J. Exptl., Theoret. Phys. USSR, 34, 131-138 (1958), Soviet Phys. JETP, 7, 91-95 (1958).

52. R. M. Gallet and R. A. Helliwell, "Origin of very low frequency emissions," J. Research NBS 63D, 21-27 (1959).

53. J. W. MacArthur, "Theory of the origin of the very low frequency radio emissions from the earth's exosphere," Phys. Rev. Letters, 2, 491-492 (1959).

54. W. B. Murcray and J. H. Pope, "Doppler shifted cyclotron frequency radiation from protons in the exosphere", Phys. Rev. Letters, 4, 5-6 (1960).

55. R. A. Santirocco, "Energy fluxes from the cyclotron radiation model of V.L.F. radio emission", Proc. Inst. Radio Engrs., 48, 1650 (1960).

56. W. B. Murcray and J. H. Pope, "Energy fluxes from the cyclotron radiation model of V.L.F. radio emission," Proc. Inst. Radio Engrs., 49, 811-812 (1961).

57. H. Alfvén, "Cosmical Electrodynamics" p. 4, Clarendon Press, Oxford (1950).

58. S. Chapman and M. Sugiura, "Arc-lengths along the lines of force of a magnetic dipole", J. Geophys. Res., 61, 485-488 1956).

59. T. Gold, "Origin of the Van Allen belts," Nature, 183, 355 (1959).

60. P. J. Coleman, C. P. Sonnett, D. L. Judge and E. J. Smith, "Some preliminary results of the Pioneer V magnetometer experiment," J. Geophys. Res., 65, 1856-1857 (1960).

61. E. H. Vestine and W. L. Sibley, "Lines of force of the geomagnetic field in space", Planet, Space Sci., I, 285-290 (1959).

62. S. Chapman, "The outermost ionosphere" J. Atmos. Terr. Phys., 15, 43-47 (1959).

63. I. Harris and R. Jastrow, "An interim atmosphere derived from rocket and satellite data" Planet, Space Sci., 1, 20-26 (1959).

64. F. S. Johnson, private communication (1960).

65. K. W. Champion, during discussion at "Sun-Earth Environment" Conference, Brisbane (1961).

66. F. S. Johnson, "Telluric origin of the whistler medium", Nature, 184, 1787-1788 (1959).

67. J. W. Dungey, "The Physics of the Ionosphere", p. 229, Physical Society, London.

68. G. McK. Allcock, "The electron density distribution in the outer ionosphere from whistler data" J. Atmos. Terr. Phys. 14, 185-199 (1959).

69. T. Obayashi, "Geomagnetic storms and the earth's outer atmosphere", Report Ionos. Res. Japan, 12, 301-335 (1958).

70. S. Croom, A. Robbins, and J. O. Thomas, "Variation of electron density in the ionosphere with magnetic dip", Nature, 185, 902-903 (1960).

71. O. K. Garriott, "The determination of ionospheric electron content and distribution from satellite observations", J. Geophys. Res., 65, 1139-1157 (1960).

72. J. A. Van Allen and L. A. Frank, "Van Allen radiation belt", IGY Bull., Trans. A.G.U., 40, 75-78 (1959).

73. S. F. Singer, "Properties of the upper atmosphere and their relation to the radiation belts of the earth", Planet. Space Sci., 2, 165-173 (1960).

74. B. Ross, and S. Olbert, "Notes on particles and fields in outer space", Lecture course 8.56 (1961).

75. B. A. McInnes, "A study of ionospherics at Macquarie Island," Australian J. Phys., 14, 218-233 (1961).

76. A. J. Dessler, "Penetrating Radiation", (Chapter II of "Satellite Environment Handbook", Ed. F.S. Johnson) Dec. 1960.

77. J. E. Lokken, J. A. Shand, C. S. Wright, L. H. Martin, N. M. Brice, and R. A. Helliwell, "Stanford - Pacific Naval Laboratory conjugate point experiment", Nature 192, 319 (1961).

78. A. D. Watt and E. L. Maxwell," Characteristics of atmospheric noise from 1 to 100 kc/s," Proc. Inst. Radio Engrs., 45, 787-794 (1957).

79. W. E. Francis, and R. Karplus, "Hydromagnetic waves in the ionosphere," J. Geophys. Res., 65, 3593-3600 (1960).

80. (Ref. 40).

81. E. A. Mechtlg, and S. A. Bowhill, "Measured noise intensities on 512 kc/s frequency," J. Geophys. Res., 65, 3501 (1960).

82. J. P. Leiphart, R. W. Zeek, L. S. Bearce and E. Toth "Penetration of the ionosphere by very-low-frequency radio signals - Interim results of the LOFTI 1 experiment," Proc. Inst. Radio Engrs., 50, 6-17 (1962).

83. G. R. Ellis, " Cosmic radio-noise intensities below 10 Mc/s", J. Geophys. Res., 62, 229-234 (1957).

84. S. Chapman and J. Bartels, "Geomagnetism" p. 340, Clarendon Press, Oxford (1951).

85. M. G. Scroggie, "Radio and Electronic Laboratory Handbook", p. 394, Iliffe Books Ltd., London (1961).

86. "The Radio Amateur's Handbook", p. 522, A.R.R.L., West Hartford, Conn. (1960).

87. N. W. Spencer, L. H. Brace, and G. R. Carignan, "Electron temperature evidence for non-thermal equilibrium in the ionosphere", J. Geophys. Res., 67, 157-175 (1962).

88. H. B. Liemohn and F. L. Scarf, "Exospheric electron temperatures from nose whistler attenuation", J. Geophys. Res., 67, 1785-1789 (1962).

89. S. Kato, "Joule heating and temperature in the upper atmosphere", Planet. Space Sci. (in the press, 1962).

90. R. L. Smith and D. L. Carpenter, " Extension of nose whistler analysis", J. Geophys. Res. 66, 2582-2586 (1961).

91. D. L. Carpenter, "New experimental evidence of the effect of magnetic storms on the magneto-sphere," J. Geophys. Res., 66, 2582-2586 (1961).

92. N. M. Brice, "Discussion of paper by R. L. Dowden, 'Doppler-shifted cyclotron radiation from electrons: A theory of very low frequency emissions from the exosphere'", J. Geophys. Res., 67, (November, 1962).

93. R. L. Dowden (and reply by R. A. Helliwell) "Very-low-frequency discrete emissions received at conjugate points" Nature, 195, 64 (1962).

94. G. R. A. Ellis,"External radio emission from the earth's exosphere" (to be published).

95. T. A. Farley and N. L. Sanders, "Pitch angle distributions and mirror point densities in the outer radiation zone", J. Geophys. Res., 67, 2159-2168 (1962).

13. SYMBOLS

All symbols are defined in the body of the thesis where they first occur. Those which are used extensively and which may occur away from their definitions are also listed here. Where appropriate the reader is referred to a Section or Figure for further information. Note that a different notation (Brice's) is used in Section 8.2 and in Figure 48.

$a = p^2/h$ = scale frequency (Section 5.5)

$\underline{a} = 4\beta^2 p_o^2/h_o^2$ (used only in Chapter 6)

B = geomagnetic field intensity

c = velocity of light in free space

$D = tf^{\frac{1}{2}}$ = whistler "dispersion".

E = energy

f = signal or emission frequency

f^+, f^- = upper and lower TWT amplified frequencies (Section 6.2)

f_n = whistler nose frequency

$g = f/h_o$

h = electron gyro frequency

$J(>E)$ = flux of particles of energy > E

ℓ = latitude angle coordinate (Fig. 32)

ℓ_m = latitude coordinate of mirror point.

p = electron plasma frequency

n = refractive index

N = electron density

R = radius vector (in earth radii)

s = distance along a field line (Fig. 32)

t = delay time

T_1, T_2 = times related to hooks (Fig. 51)*

$T^+ = T_1 + T_2$ = time "width" of a hook

$T^- = T_1 - T_2$ (= equivalent nose whistler delay)

v = velocity

$x = h_o/f_o$

$X_1 = x^2/(x-1)^3$

$X_2 = (x-1)^3/x$

α = attenuation (or amplification) constant

$\beta = v/c$

$\gamma = (1-\beta^2)^{-\frac{1}{2}}$

$\eta = \phi \sec^6 \ell$

θ = angle between directions of emission and magnetic field.

λ = geomagnetic latitude at which a field line cuts the earth's surface (Fig. 32)

$\phi = (1 + 3\sin^2 \ell)^{\frac{1}{2}}$

ψ = helical pitch angle ($\cos\psi = v_d/v$)

Subscript o = value at $\ell = 0$ (equatorial plane)

Subscript λ = value at $\ell = \lambda$ (earth's surface)

Subscript d = component in the direction of the magnetic field

---

* Used with a different meaning (Brice's) in Section 8.2 and Figure 48.

Subscript m = maximum value (Section 10.2)

Subscript n = value at $f = f_n$

Subscript e = electron component (Section 7.2)

Subscript g = wave group component (Section 7.2)

(*Reprinted from Nature, Vol.* 195, *No.* 4845, *pp.* 984–985, *September* 8, 1962)

'Scale Frequency' of the Exosphere

WHISTLER measurements of nose frequency (f_n) and time delay at this frequency (t_n) give a f_n, t_n distribution well fitted by a 'gyrofrequency' model of electron density in the exosphere[1]: one for which the electron density is everywhere proportional to the magnetic field strength or gyrofrequency (f_H). Since the electron density is directly proportional to the square of the plasma frequency (f_0) and uniquely determined by it we can express this model by the relation:

$$f_0^2 = f_a f_H$$

The constant of proportionality, f_a, has the dimensions of frequency and so might be called the 'scale frequency' of the exosphere. It is typically around one megacycle per second (as deduced from Smith's work[1]).

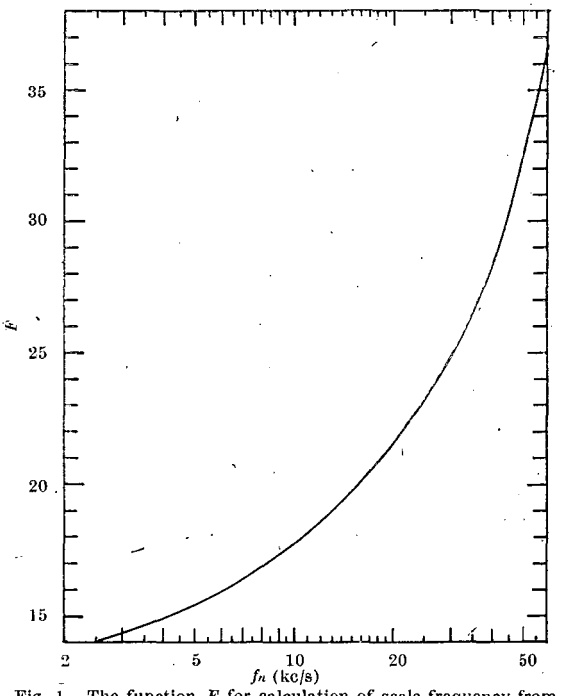

Fig. 1. The function F for calculation of scale frequency from nose frequency and nose delay time

To the extent that the gyrofrequency model fits the real exosphere the scale-frequency is constant. But the point I wish to make in this communication is that, regardless of this fit, the parameter, 'scale frequency', is a very useful one in exospheric studies. It is in the same form (frequency) as the other parameters (f_0, f_H, f) describing emission and propagation in the exosphere. The low-frequency dispersion $D_0 = f^{1/2}t$ becomes $D_0 = s f_a^{1/2}$ where s is the half-length of the field line in light-time units (light-seconds). For f_a constant along a field line the nose whistler integral can be solved analytically[1]. Since whistler data show that the scale frequency is at least quasi-constant then variations in space and time can be sensitively expressed by it. This would be particularly useful in discussing magnetic disturbance effects.

Scale frequencies are readily deduced from f_n, t_n data from nose whistlers. A recent extension of whistler analysis[2] makes it possible to obtain f_n and t_n from perhaps all well-defined whistlers even when the nose is not directly observable. In this work[2] it was shown that the nose frequency dispersion (D_n) is related to the low-frequency dispersion (D_0) as:

$$D_n = 1{\cdot}456\, D_0$$

Thus:

$$t_n f_n^{1/2} = 1{\cdot}456\, s\, f_a^{1/2}$$

Since the field line (and length s) is uniquely determined by the nose frequency, a function of f_n can be substituted for s. Thus:

$$f_a = F\, t_n^2\, f_n^{5/3} \text{ kc/s}$$

$$F = (1{\cdot}456\, s\, f_n^{1/3})^{-2}$$

where t_n is measured in seconds, f_n in kc/s and the slowly varying function F is shown in Fig. 1.

It is interesting to note that a theoretical model[3] of electron density in the exosphere based on the premise that the electrons are controlled by the Earth's magnetic field rather than gravity gives a quasi-constant scale frequency. Thus, this is largely a consequence of geomagnetic control of exospheres just as a quasi-constant scale height in the Earth's atmosphere is a consequence of gravity control.

R. L. Dowden

Ionospheric Prediction Service,
University of Tasmania,
Hobart.

[1] Smith, R. L., Ph.D. dissertation, July 11, 1960, *S.E.L. Tech. Rep.* 6, Stanford University.

[2] Smith, R. L., and Carpenter, D. L., *J. Geophys. Res.*, **66**, 2582 (1961).

[3] Dowden, R. L., *J. Atmos. Terr. Phys.*, **20**, 122 (1961).

Printed in Great Britain by Fisher, Knight & Co., Ltd., St. Albans.

(Reprinted from Nature, Vol 811 pp. 803, September 12, 1959)

Low-frequency (100 kc./s.) Radio Noise from the Aurora

EXTRATERRESTRIAL radio 'noise' has been intensively studied during the past decade. The steady background radiation or 'cosmic noise' from interstellar space has been observed[1] at frequencies down to about 1 Mc./s. and an intensity of about 10^{-19} watts per square meter per cycle per second (W.m.$^{-2}$ (c./s.)$^{-1}$). Ellis[2] later showed that cosmic noise at lower frequencies could not penetrate the earth's magneto-ionic upper atmosphere. Reber[3], however, reported observations of steady noise of intensity 10^{-22} W.m.$^{-2}$ (c./s.)$^{-1}$ at frequencies of 520 kc./s. and 140 kc./s. This appeared to be correlated with sidereal time and so was claimed to be cosmic noise.

Recently[4] extraterrestrial continuous ('white') noise has been studied in the audio-frequency band. This normally shows peak intensity (10^{-16} W.m.$^{-2}$ (c./s.)$^{-1}$) at around 4 kc./s. It appears to be generated in the upper atmosphere by auroral particles[5], it is highly correlated with auroral airglow[6], and it has been designated 'hiss'.

I have also carried out observations of 'hiss' at Hobart, Tasmania, to provide a comparison with those of Ellis at Sydney. Results appeared broadly similar but the intensity at Hobart is much higher (10^{-15} W.m.$^{-2}$ (c./s.)$^{-1}$). In view of Reber's observations (and similar observations of mine[7] at 450 kc./s. at Macquarie Island) it was decided to operate on five frequency channels simultaneously, covering the gap from the normal 'hiss' frequencies to the controversial 100 kc./s. band. The centre frequencies of these channels were 4·6, 9·6, 27, 70 and 180 kc./s. For the loop antenna and amplifiers used the sensitivity increased with frequency, so at the lower two channels it was about 10^{-17} W.m.$^{-2}$ (c./s.)$^{-1}$ and for the higher two it was around 10^{-21} W.m.$^{-2}$ (c./s.)$^{-1}$. It was found that the intensity of both the 'back-ground' radiation and the usual 'bursts' showed a general decrease with frequency so that normally nothing was observed at 70 and 180 kc./s.

On one occasion, however (April, 1959) a number of bursts were observed which showed deep fading. When the records of the five channels were examined together it was found that strong noise was present on all channels. Moreover, the fades on each channel showed a strong one-to-one correspondence and were

simultaneous to the limit of reading ($\sim$ 10 seconds). The noise level of these bursts at the lower frequencies was fairly typical of the more usual bursts (10^{-15} W.m.$^{-2}$ (c./s.)$^{-1}$ at 4·6 kc./s.) but at 70 and 180 kc./s. the noise power was at least two or three orders of magnitude greater than normal (to about 10^{-19} W.m.$^{-2}$ (c./s.)$^{-1}$).

Unfortunately it is not known exactly on what day this occurred nor whether a notable geomagnetic event took place at the same time, for the research station together with the equipment and records was destroyed by fire on May 24, 1959. It is probably a rare event as it only occurred on one occasion in about two months observing. It is none the less established that 'hiss' can sometimes occur at frequencies up to 180 kc./s. at least, suggesting that extraterrestrial noise much below a megacycle might be 'hiss' (that is generated in the upper atmosphere) rather than 'cosmic noise'.

My thanks are due to Mr. G. T. Goldstone, who built and operated much of this equipment and assisted in the observations, and to Dr. G. R. A. Ellis, Upper Atmosphere Section, C.S.I.R.O., who provided part of the equipment and circuits and who suggested the 4·6 kc./s. and 9·6 kc./s. observations.

R. L. Dowden

Commonwealth Ionospheric Prediction Service,
Hobart, Tasmania.
Aug. 19.

[1] Reber, G., and Ellis, G. R., *J. Geo. Res.*, **61**, 1 (1956).
[2] Ellis, G. R., *J. Atmos. Terr. Phys.*, **9**, 51 (1956).
[3] Reber, G., *J. Geo. Res.*, **63**, 109 (1958).
[4] Ellis, G. R., Plan. Space Sci. (in the press).
[5] Ellis, G. R., *J. Atmos. Terr. Phys.*, **10**, 302 (1957).
[6] Duncan, R. A., and Ellis, G. R., *Nature*, **183**, 1618 (1959).
[7] Dowden, R. L., *J. Atmos. Terr. Phys.* (in the press).

Printed in Great Britain by Merritt & Hatcher Ltd., London & High Wycombe

(*Reprinted from Nature, Vol.* 187, *No.* 4738, *pp.* 677–678, *August* 20, 1960)

Geomagnetic Noise at 230 kc./s.

GEOMAGNETIC radio noise or 'hiss' usually occurs only in the audio region. During severe magnetic storms it has been reported up to 30 kc./s. on a sweep frequency analyser[1] and at 70 and 180 kc./s. on fixed tuned channels[2]. The latter report[2] was written after the records had been destroyed in a fire. New observations at up to 230 kc./s. are described here.

Observations were made simultaneously at the four frequencies 4, 9, 70 and 230 kc./s. (using two dual-beam cathode-ray oscillographs and photographic recording) over the period mid-September to mid-November, 1959. Geomagnetic noise was observed on three occasions only: 2245 U.T., October 31; 0430 U.T., November 3; and around 0330 U.T., November 6. The planetary magnetic index (k_p) ranged from 4 to 6 at these times. The noise burst observed on November 6 is reproduced in Fig. 1. This shows 9 and 230 kc./s. only, since the camera recording 4 and 70 kc./s. jammed on this occasion.

The general appearance of the noise burst—relatively gradual rise and decline of intensity (as distinct from the sharp 'on' and 'off' of man-made interference) and impulsive noise component superimposed on a steady or 'white' noise-level—is typical of geomagnetic noise bursts observed at audio-frequencies. The maximum noise-levels are seen to be $0{\cdot}8\ \mu V.m.^{-1}\ (c./s.)^{-\frac{1}{2}}$ at 9 kc./s. and $16\ m\mu V.m.^{-1}\ (c./s.)^{-\frac{1}{2}}$ at 230 kc./s., corresponding to intensities of about $10^{-15}\ W.m.^{-2}\ (c./s.)^{-1}$ at 9 kc./s. and $3 \times 10^{-19}\ W.m.^{-2}\ (c./s.)^{-1}$ at 230 kc./s. The intensities observed at 4 and 9 kc./s. at these times were typical of strong bursts at these frequencies. The 70 and 230 kc./s. intensities were of the same order as previously reported[2]. A striking feature of Fig. 1 is the close correspondence of amplitude fluctuations at the two frequencies. These appear simultaneous to the limit of reading of the time scale (~ 10 sec.).

A probable mechanism for generation of this noise is Čerenkov radiation from small clouds of charged particles travelling through the ionosphere and exosphere[1,3,6]. Radiation is produced at all frequences for which the velocity of the particle clouds exceeds the group velocity of the radiation (Čerenkov condition). The close correspondence between the two

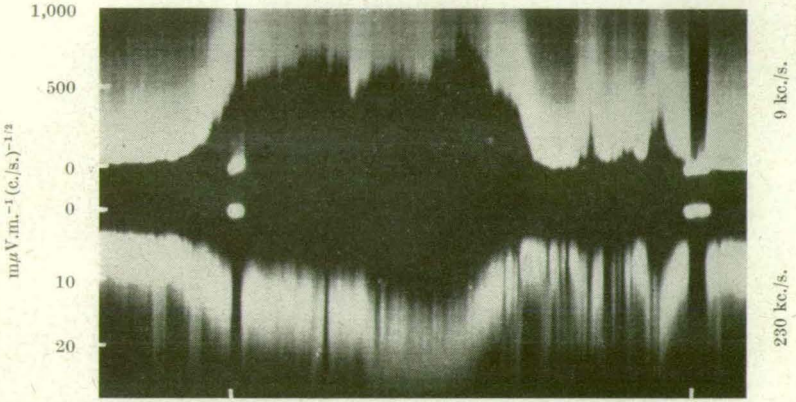

Fig. 1

frequency components observed suggests production by the same particle clouds and in the same geomagnetic tube of force since moving charged particles are effectively constrained to a tube of force.

Accordingly the tube of force ending at Hobart (geomagnetic lat. 52° S.) was considered, and the group velocities of 9 and 230 kc./s. radiation call culated[4] as a function of distance along this tube of force. Electron density as a function of radia- distance was obtained from whistler data[5]. The assumption was made that the electron density in the exosphere is spherically distributed. At 9 kc./s. it was found that the group velocity would be everywhere less than 0·12 c. from the ionosphere to the equatorial plane (total distance 15,000 km.). At 230 kc./s. only radiation produced below the gyro-level is observable on the ground. From the ionosphere to the gyro-level (a distance of about 5,000 km.) the 230 kc./s. group velocity would be everywhere less than 0·17 c. Consequently, particle clouds travelling down this tube of force at 0·2 c. (say) could produce Čerenkov radiation at both frequencies. Since the travel-time even of 9 kc./s. radiation produced at 15,000 km. would be less than a second, bursts of radiation at the two frequencies would arrive at the ground simultaneously to our limit of reading.

Estimates of absolute intensities to be expected from the Čerenkov process depend too strongly on unknown factors (for example, size and number of clouds and cloud density) to be meaningful. But we can make an order-of-magnitude estimate of the relative intensities based on reasonable assumptions. If these unknown factors were the same for both frequencies we would find that the ratio of intensities produced at 9 and 230 kc./s. would be proportional to the path-length in wave-lengths for which the Čerenkov condition holds[3]. This indicates that the intensity produced at 230 kc./s. should be nearly ten times that at 9 kc./s. However, this ratio will be modified by the ear trumpet effect of the converging tube, giving enhancement proportional to the tube cross-section, which is in turn inversely proportional to the field-strength or gyro-frequency. For the tube of force under consideration this will enhance the ratio in favour of 9 kc./s. by a factor of five. Also if the attenuation in regions of high collision frequency is taken into account (from Helliwell's curves[4]) we find that 230 kc./s. will be attenuated by about eight times as many decibels as 9 kc./s. Agreement with the ratio of intensities observed at Hobart (3×10^3 or 35 db.) is reached for an assumption of about 5 db. for 9 kc./s. and hence about 40 db. for 230 kc./s.

Consideration of tubes of force ending farther south of Hobart require attenuations of 9 kc./s. considerably less than this, in keeping with observations of multi-echo whistler trains. Thus estimates based on this mechanism give reasonable agreement with observations of wide-band noise bursts for frequencies from a few kc./s. to a few hundred kc./s.

It is interesting to note that for this mechanism wide-band bursts will only be observed if the electron density distribution along a line of force is such that the plasma frequency is always greater than the gyro frequency for the range of frequencies observed. Since the electron density in the equatorial plane is obtained from whistler data this gives a lower limit to electron density at each point along the line of force.

My thanks are due to Mr. G. T. Goldstone, who built much of the equipment and assisted in the observations, and to Mr. P. S. Bowling who provided housing for the equipment in the field.

R. L. Dowden

Commonwealth Ionospheric Prediction Service,
Hobart, Tasmania. June 10.

[1] Ellis, G. R., *Plan. Space Sci.*, **1**, 253 (1959).
[2] Dowden, R. L., *Nature*, **184**, 803 (1959).
[3] Marshall, L., *Astrophys. J.*, **124**, 469 (1956).
[4] Helliwell, R. A., "Low Frequency Propagation Studies, Part 1", ASTIA Document No. *AD*110184 (1958).
[5] Maeda, K., and Kimura, I., *Rep. Ionos. Res. Japan*, **10**, 105 (1956).
[6] Ellis, G. R., *J. Atmo. Terr. Phys.*, **10**, 302 (1957).

Printed in Great Britain by Fisher, Knight & Co., Ltd., St. Albans.

Journal of Atmospheric and Terrestrial Physics. 1961, Vol. 20, pp. 122 to 130. Pergamon Press, Ltd. Printed in Northern Ireland

A theoretical model of electron density distribution along a geomagnetic line of force in the exosphere

R. L. DOWDEN
Ionospheric Prediction Service, Hobart, Tasmania, and the University of Tasmania

(*Received* 17 *August* 1960)

Abstract—By consideration of charged particles spiralling in geomagnetic tubes of force, particle densities are derived for a source of particles filling the tubes at (i) the equatorial plane or (ii) the earth's surface (ionosphere). The first case gives a distribution of roughly constant density for geomagnetic latitudes (λ) up to 60° and the second to one of density roughly proportional to magnetic field strength for $\lambda < 60°$ and $R < 1{\cdot}25$ earth's radii.

1. INTRODUCTION

OVER the last few years whistler and micropulsation studies have yielded information about electron densities in the exosphere out to several earth's radii. So far this information has not been sufficient to determine whether or not the electron density varies with latitude. In studies of propagation of radio and hydromagnetic waves along the geomagnetic lines of force and of the generation of v.l.f. radio noise, dawn chorus, etc., it is necessary to assume a distribution of electron density along the line of force. The assumption usually made is that electron density is distributed with spherical symmetry about the centre of the earth. This would be logical in the absence of a magnetic field as any local discontinuities would tend to diffuse over a sphere. In the presence of a magnetic field, however, charged particles are mainly confined to a tube of force so that diffusion would take place along the magnetic field lines.

This paper is an attempt to take this effect into account and derive the distribution along a line of force on the assumption that the tubes of force are supplied with charged particles (electrons, protons, etc.) from near the earth's surface (e.g. the upper ionosphere). The particles will move in helical orbits along the line of force. Since the cross-section of the tube of force rapidly increases towards the equatorial plane and since the pitch of the helices decreases (i.e. opens out) in this direction we would expect the density to decrease. Collisions are neglected except in the source regions near the earth's surface. Here down-coming particles which are "lost" are replaced (assuming equilibrium) by an equal number of up-going ones.

The density distribution of the faster particles which produce v.l.f. radio noise and possibly aurora during magnetic storms is also derived on the assumption that these particles are injected into the tubes in regions farthest from the earth, that is near the equatorial plane.

Finally the electron density at any point in space is derived on the rough assumption that the electron density in the source regions (ionosphere) varies with geomagnetic latitude (λ) as cos λ.

In all cases symmetry about the geomagnetic axis is assumed. Hence the relatively slow drift of charged particles in longitude has been neglected.

2. Theory

The various equations describing the dipole magnetic field, a line of force and a tube of force are given (Alfvén, 1950; Chapman and Sugiura, 1956):

$$R = R_0 \cos^2 l$$

$$R_0 = \sec^2 \lambda$$

$$H = \eta H_0$$

$$HA = H_0 A_0 \text{ hence } A = A_0/\eta$$

$$\frac{ds}{dl} = R_0 \phi \cos l$$

where:

R = radius vector in earth radii
l = latitude angle
} polar coordinates

λ = geomagnetic latitude at which the line of force cuts the earth's surface
H = intensity of the earth's magnetic field
$\eta = \phi \sec^6 l$
$\phi = (1 + 3 \sin^2 l)^{1/2}$
A = cross section area of tube of force
s = distance along line of force

Subscript "0" denotes values for which $l = 0$ (i.e. in equatorial plane) and subscript "λ" values for which $l = \lambda$ (earth's surface). We note immediately that:

$$\eta_0 = \phi_0 = 1.$$

We consider one of the particles spiralling along the line of force determined by λ. At the point determined by "l", let its pitch angle be ψ and its speed v. Equations governing its motion (Gold, 1959) are:

$$v = v_0 \text{ (constant)}$$

$$H/\sin^2 \psi = H_0/\sin^2 \psi_0$$

Hence $\sin^2 \psi = \eta \sin^2 \psi_0$.

The velocity of the "guiding centre" of the spiralling particle is:

$$\frac{ds}{dt} = v \cos \psi = v(1 - \sin^2 \psi)^{1/2}$$

$$= v(1 - \eta \sin^2 \psi_0)^{1/2}.$$

The probability of finding this particle at position "l" is proportional to dt/dl. Now,

$$\frac{dt}{dl} = \frac{dt}{ds} \cdot \frac{ds}{dl} = R_0 \phi \cos l [v(1 - \eta \sin^2 \psi_0)^{1/2}]^{-1}.$$

If we consider a large number of such particles (l, ψ_0, v) the density (cm^{-3}) will be given by

$$n(\psi_0, v) \propto \frac{dt}{dl}/A = \frac{KR_0}{A_0 v} \cdot \eta\phi \cos l \,(1 - \eta \sin^2 \psi_0)^{-1/2}$$

where K is a constant of proportionality.

In the equatorial plane:

$$n_0(\psi_0, v) = \frac{KR_0}{A_0 v}(1 - \sin^2 \psi_0)^{-1/2} = \frac{KR_0}{A_0 v \cos \psi_0}.$$

Hence

$$n(\psi_0) = n_0(\psi_0)\eta\phi \cos l \cos \psi_0 (1 - \eta \sin^2 \psi_0)^{-1/2}. \tag{1}$$

We first consider the simpler case of a source of particles in the equatorial plane. If the source is isotropic (no preferred particle direction) simple geometrical considerations show that the distribution of pitch angles will be given by

$$dN_0(\psi_0) = N_0 \sin \psi_0 \, d\psi_0 \tag{2}$$

where the expression on the left hand side represents the density (at $l = 0$) of particles having pitch angles in the range ψ_0 and $\psi_0 + d\psi_0$. Substituting this for $n_0(\psi_0)$ in (1):

$$dN(\psi_0) = N_0 \eta\phi \cos l \sin \psi_0 \cos \psi_0 (1 - \eta \sin^2 \psi_0)^{-1/2} \, d\psi_0.$$

The total density at point l, λ is given by integration over all allowable values of ψ_0 from $\psi_0 = 0$, to $\psi_0 =$ its maximum value Ψ_0 given by $\eta \sin^2 \Psi_0 = 1$. Particles which had pitch Ψ_0 will have pitch $\psi = \pi/2$ at this point (magnetic mirror point). Particles of greater pitch will have been removed by magnetic reflection before reaching this point.

Hence

$$N = N_0 \eta\phi \cos l \int_0^{\Psi_0} \sin \psi_0 \cos \psi_0 (1 - \eta \sin^2 \psi_0)^{-1/2} \, d\psi_0.$$

Putting $x^2 = 1 - \eta \sin^2 \psi_0$,

$$N = N_0 \eta\phi \cos l \frac{l}{\eta} \int_0^1 dx = N_0 \phi \cos l. \tag{3}$$

The expression $\phi \cos l$ is unity at $l = 0$ and at $\sin^2 l = 2/3$ ($l \sim 55°$). It has its maximum value (1·15) for $\sin^2 l = 1/3$ ($l \sim 35\frac{1}{2}°$). Simple computation shows it to be within 15 per cent of unity for $l < 60°$.

Hence this distribution which probably applies to the case of solar particles injected into the tube of force during magnetic storms gives a practically constant density along a line of force for all lines (λ) up to $\lambda = 60°$.

The thermal particles which make up the background medium are probably supplied where ionization is taking place, i.e. in the ionosphere. Accordingly we

consider an isotropic source at $l = \lambda$. The distribution of pitch angles is given [as in (2)] by

$$dN_\lambda(\psi_\lambda) = N_\lambda \sin \psi_\lambda \, d\psi_\lambda. \tag{4}$$

We relabel these same particles by the pitch angles (ψ_0) they would have on reaching the equatorial plane, where

$$\sin^2 \psi_\lambda = \eta_\lambda \sin^2 \psi_0. \tag{5}$$

Differentiating:

$$2 \sin \psi_\lambda \cos \psi_\lambda \, d\psi_\lambda = 2\eta_\lambda \sin \psi_0 \cos \psi_0 \, d\psi_0.$$

Hence

$$\sin \psi_\lambda \, d\psi_\lambda = \eta_\lambda \frac{\sin \psi_0 \cos \psi_0}{\cos \psi_\lambda} d\psi_0$$

$$= \eta_\lambda \sin \psi_0 \cos \psi_0 (1 - \eta_\lambda \sin^2 \psi_0)^{-1/2} \, d\psi_0.$$

Relabelling (4) and substituting:

$$dN_\lambda(\psi_0) = N_\lambda \eta_\lambda \sin \psi_0 \cos \psi_0 (1 - \eta_\lambda \sin^2 \psi_0)^{-1/2} \, d\psi_0. \tag{6}$$

From (1) we have:

$$n_0(\psi_0) = n_\lambda(\psi_0) \frac{(1 - \eta_\lambda \sin^2 \psi_0)^{1/2}}{\phi_\lambda \eta_\lambda \cos \psi_0 \cos \lambda}.$$

Replacing $n_0(\psi_0)$ by $dN_0(\psi_0)$ and $n_\lambda(\psi_0)$ by $dN_\lambda(\psi_0)$ as given in (6):

$$dN_0(\psi_0) = \frac{N_\lambda \sin \psi_0}{\phi_\lambda \cos \lambda} d\psi_0.$$

Integrating from $\psi_0 = 0$ to $\psi_0 = \Psi_0$ where $\sin^2 \Psi_0 = 1/\eta_\lambda$ [hence $\cos \Psi_0 = (1 - 1/\eta_\lambda)^{1/2}$]:

$$N_0 = \frac{N_\lambda}{\phi_\lambda \cos \lambda} \int_0^{\Psi_0} \sin \psi_0 \, d\psi_0$$

$$= \frac{N_\lambda}{\phi_\lambda \cos \lambda} \left[1 - \left(1 - \frac{1}{\eta_\lambda} \right)^{1/2} \right]$$

$$= \frac{N_\lambda}{\phi_\lambda \cos \lambda} \zeta \left(\frac{1}{\eta_\lambda} \right). \tag{7}$$

Hence

$$dN_0(\psi_0) = \frac{N_0}{\zeta\left(\frac{1}{\eta_\lambda}\right)} \sin \psi_0 \, d\psi_0. \tag{8}$$

We can now find N at any point "l" as in the previous argument by replacing the pitch distribution given in (2) by that in (8) except that the upper limit is now given by $\sin^2 \Psi_0 = 1/\eta_\lambda$.

That is

$$N = \frac{N_0}{\zeta(1/\eta_\lambda)} \phi \cos l \, [(1 - \eta \sin^2 \psi_0)^{1/2}]_{\Psi_0}^0$$

$$= N_0 \, \phi \cos l \, \zeta \left(\frac{\eta}{\eta_\lambda} \right) \Big/ \zeta \left(\frac{1}{\eta_\lambda} \right) \tag{9}$$

where $\zeta \left(\frac{\eta}{\eta_\lambda} \right) = 1 - \left(1 - \frac{\eta}{\eta_\lambda} \right)^{1/2}$ and use has been made of (5).

An approximation can be obtained by noting

$$\zeta(\delta) \approx \tfrac{1}{2}\delta + \tfrac{1}{8}\delta^2.$$

Hence for $\eta_\lambda \gg 1$ and $\eta_\lambda \gg \eta$:

$$N = N_0 \eta \phi \cos l. \tag{10}$$

This approximation is good to within about 10 per cent provided $\eta_\lambda/\eta > 2\frac{1}{2}$ or $\sec^6\lambda/\sec^6 l > 2$ or $R > 1{\cdot}25$.

The distributions derived have been expressed in terms of N_0 since this quantity (as a function of R_0 or λ) is the one most readily found from whistler and pulsation studies. However, the $N_0(\lambda)$ distribution is derivable if we assume a distribution for N_λ, the electron density in the upper ionosphere.

Suppose

$$N_\lambda = N_E \cos \lambda.$$

Substituting in (7)

$$N_0 = \frac{N_E}{\phi_\lambda} \zeta\left(\frac{1}{\eta_\lambda}\right)$$

$$\approx \frac{N_E}{2\phi_\lambda \eta_\lambda} \text{ for } \lambda > 25°$$

Or in terms of $R_0 (R_0 > 1{\cdot}25)$:

$$N_0 \approx \frac{N_E}{2R_0^3(4 - 3/R_0)}. \tag{11}$$

3. Discussion

3.1. *Assumptions*

The theory is valid provided (i) that the geomagnetic field is approximately dipole, (ii) that collisions and (iii) gravitational forces can be neglected, and (iv) that the electrons (and protons) are supplied mainly from near the earth's surface. We will consider each of these assumptions separately.

3.1.1. *Dipole field.* Recent data from the space probe Pioneer V (Coleman *et al.*, 1960) indicates that the field extends out to about 14 earth's radii. Vestine and Sibley (1959) find that the field lines connecting the auroral zones ($R_0 \sim 6$) are not seriously distorted by solar streams, even during auroral displays. This indicates the dipole field is valid out to about 10 radii.

3.1.2. *Collisions.* As pointed out in the Introduction, collisions in the regions of highest collision frequency, the source regions, are effectively taken into account by the theory. In an exosphere of protons and electrons only collisions of electrons with protons are important since elastic collisions between like particles involve only velocity exchange and the much heavier protons are not greatly effected by collisions with electrons. Assuming a temperature of about 10,000°K in the source regions, the thermal velocity of an electron would be around 10^8 cm/sec. The time taken for one trip along the line of force $\lambda = 70°$ (say) would be about 100 sec. The effective average density $\bar{N}$ ($\bar{N}s \equiv \int N ds$) along this line is about 80 cm^{-3} so that at this temperature the effective average collision frequency will be about 2×10^{-4} sec^{-1}. Thus the probability of an electron suffering a collision during a single trip would be about 1 in 50. Collisions would involve pitch changes and so

change the theoretical pitch distribution slightly. In the equilibrium condition this effect could be allowed for by a weak source in the equatorial plane giving rise to a small and essentially constant additive term (equation 3).

3.1.3. *Gravitational forces.* These can be neglected if the maximum gravitational potential energy is much less than the kinetic energy of the particles. This condition is met for temperatures in the source regions of ~2°K for electrons and ~4000°K for protons. CHAPMAN (1959) suggests that the temperature of the exosphere

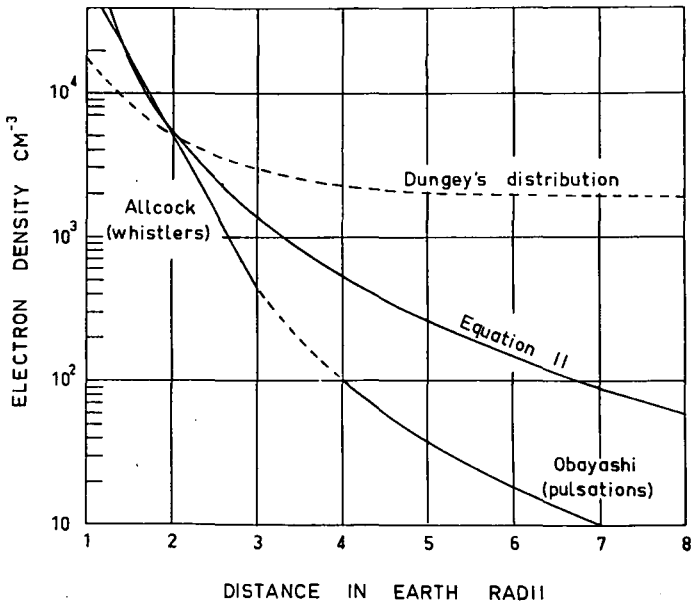

Fig. 1. Electron density along a radius in the equatorial plane.

ranges from 30,000°K at heights around 1000 km to about 200,000°K where the exosphere merges into interplanetary space. Thus it is likely that the condition is met for both electrons and protons.

3.1.4. *Source points.* JOHNSON (1959) has shown that the electrons etc. making up the exosphere must be of telluric (terrestrial) rather than solar origin. Hence the source will be the ionosphere where appreciable ionization is taking place. The theory developed above strictly requires that the "surface of the earth" be the ionosphere and so the "radius of the earth" be the radius of the ionosphere. This will effect slightly the units of R and R_0 and the definition of λ.

3.2. *Computed distributions*

The electron density in the equatorial plane (N_0) as a function of radial distance (R_0) was computed from (11) for $N_E = 2 \times 10^5$ cm^{-3}. This value of N_E, the average electron density of the source region above the equator, is consistent with experimental measurements of the noon maximum density of the ionosphere (N_{max}) at the equator (CROOM *et al.*, 1960) of ~20×10^5 cm^{-3} and values N/N_{max} ~0·2 at ~800 km (presumably the source region) found by satellite experiments (GARRIOTT, 1960). This is shown in Fig. 1 together with DUNGEY'S (1954) theoretical

distribution $N \propto \exp(2{\cdot}5/R)$ scaled to give agreement at 2 earth's radii and the experimental distribution of ALLCOCK (1959) from whistler studies for the range 1·2–3 earth's radii, and by OBAYASHI (1958) from pulsation studies for the range 4–7 earth's radii. When compared with the experimental curve we find a discrepancy which is small for $R_0 < 2$, nearly a factor of ten for $R_0 \sim 7$, but decreasing at greater distances [using OBAYASHI'S extrapolation $N = \exp(17{\cdot}5/R_0)$].

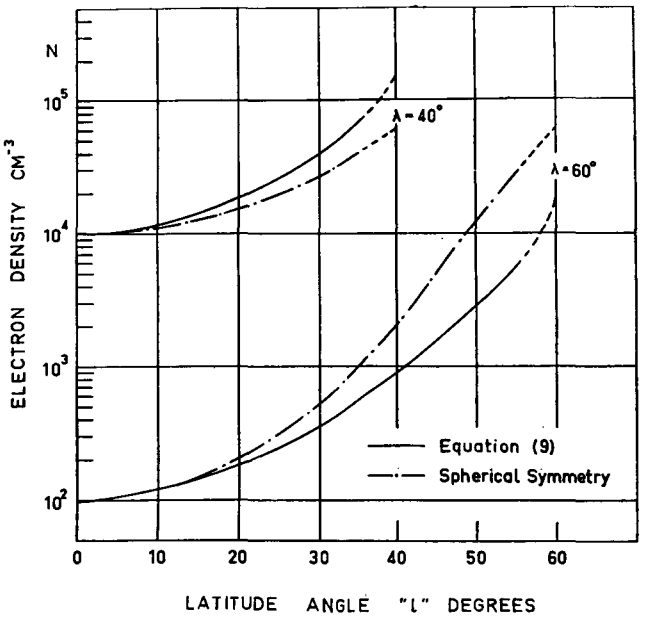

Fig. 2. Electron density along a line of force.

The distributions along lines of force $\lambda = 40°$ and $\lambda = 60°$ were computed from (9) using values of N_0 of 10,000 cm^{-3} and 100 cm^{-3} respectively taken from the whistler–pulsation experimental curve. These are shown in Fig. 2 together with distributions computed from the experimental curve on the assumption that the electron density is distributed with spherical symmetry about the earth. The dashed portions of the curves correspond to extrapolations into regions within 1000 km. The fact that the discrepancies between the two types of distribution change sign between $\lambda = 40°$ and $\lambda = 60°$ suggest that the spherical symmetry distribution may be a reasonable approximation for longitudinal propagation studies within this range of λ. However, for $\lambda < 60°$, $\phi \cos l \approx 1$ and so provided also $R > 1{\cdot}25$, we have from (10) $N \approx \eta N_0$ or $N \propto H$. Hence in this region the "whistler" mode (longitudinal extraordinary mode at frequencies much less than the gyro frequency) refractive index, being proportional to N/H, is approximately constant.

Values of electron density (N) were computed for a large number of points (λ, l) for lines up to $\lambda = 80°$ from values of N_0 taken from the experimental $N_0(R_0)$ whistler–pulsation curve. For $\lambda > 65°$ values of *effective* N_0 were obtained by

extrapolation. For the longer lines of force ($\lambda > 70$) it was assumed that the theory would remain a reasonable approximation for $R < 10$ even though the line of force equations may not hold for $R > 10$. Contours of electron density or *isopycs* are shown in a plane containing the geomagnetic axis in Fig. 3. The line of force $\lambda = 70°$ is shown for reference. Presumably the contours close over the axis poles. This suggests considerable extensions of electron density in the direction of the axis.

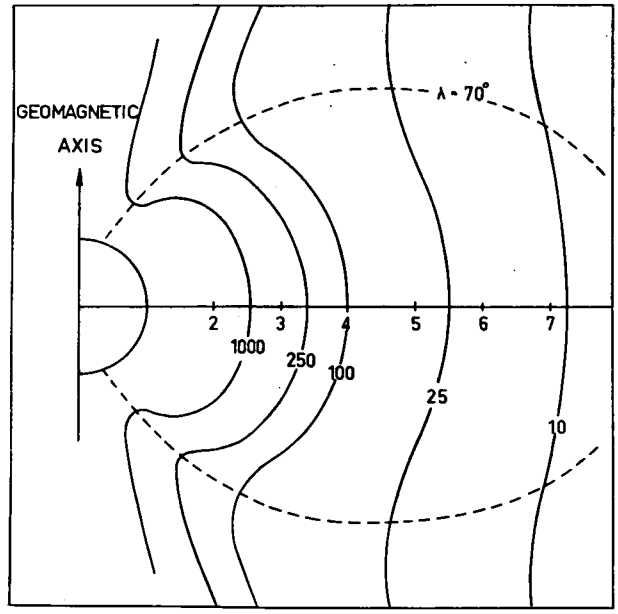

Fig. 3. Contours of electron density (isopycs) in a plane containing the geomagnetic axis.

4. Conclusions

The distribution of electron (and proton) density along a line of force has been derived (equation 9). At latitudes less than 60° and heights greater than about 2000 km ($R > 1{\cdot}25$) the electron density is approximately proportional to the magnetic field strength ($N/N_0 = H/H_0$). The density distribution of "aurora" or "magnetic storm" particles has also been derived (equation 3). The latter expression approximates to $N = N_0$ for latitudes less than about 60°. The electron density distribution in polar coordinates has been derived graphically (Fig. 3). At low latitudes the distribution is approximately spherically symmetrical, but at high latitudes departures from this are great, tending towards constancy along radii. This suggests considerable extensions of electron density above the geomagnetic poles.

Acknowledgements—The writer expresses his appreciation to Professor G. Newstead of the Department of Electrical Engineering and Dr. K. B. Fenton of the Department of Physics, University of Tasmania, and to Dr. W. G. Baker, Officer in Charge, Ionospheric Prediction Service, for helpful discussions and suggestions.

NOTE ADDED IN PROOF

IT HAS SINCE been pointed out to the writer by Dr. J. H. PIDDINGTON and Dr. F. S. JOHNSON that satellite orbit data give temperatures of 1000–1500°K at heights around 400–700 km (HARRIS and JASTROW, 1959) so that the assumption of 10,000°K in the source regions is around seven or eight times too high. If these low temperatures applied throughout the exosphere, collision frequencies would be some twenty times greater. The electron density distribution will be largely controlled by the distribution of the much heavier protons which may not be seriously affected by electron collisions, but at these low temperatures thermal protons would have insufficient energy to neglect gravitional and geocentrifugal effects. This difficulty might be resolved by placing the source regions at a much greater height where the effective gravitional potential energy is lower and where the temperature may be much higher. The same equations derived above will describe this case provided quantities are redefined as discussed in Section 3.1.4.

On the other hand the writer has also been informed since (by Professor R. A. HELLIWELL) of a distribution of electron density out to 5 earth radii obtained from nose whistler measurements (SMITH, 1960). This distribution was found to fit a "gyrofrequency" model: $N = Kf_H\phi_\lambda^{-1}$, where K is constant. Our distribution can be put in this form from (10) and (11) where

$$K = \frac{N_E\phi \cos l}{2(f_H)_\lambda} \approx \frac{N_E}{2(f_H)_\lambda}.$$

For $R_0 > 1{\cdot}25$ and l and $\lambda < 60°$, K is "constant" to within about 50 per cent. The two distributions can be closely matched throughout this region if the value of N_E suggested in Section 3.2 is reduced by a factor of about three.

REFERENCES

ALFVEN H.	1950	*Cosmical Electrodynamics*, p. 4. Clarendon Press, Oxford.
ALLCOCK G. MCK.	1959	*J. Atmosph. Terr. Phys.* **14**, 185.
CHAPMAN S.	1959	*J. Atmosph. Terr. Phys.* **15**, 43.
CHAPMAN S. and SUGIURA M.	1956	*J. Geophys. Res.* **61**, 485.
COLEMAN P. J., SONNETT C. P., JUDGE D. L. and SMITH E. J.	1960	*J. Geophys. Res.* **65**, 1856.
GROOM S., ROBBINS A. and THOMAS J. O.	1960	*Nature, Lond.* **185**, 902.
DUNGEY J. W.	1954	*The Physics of the Ionosphere*, p. 229. Physical Society London.
GARRIOTT O. K.	1960	*J. Geophys. Res.* **65**, 1139.
GOLD T.	1959	*Nature. Lond.* **183**, 355.
HARRIS I. and JASTROW R.	1959	*Planet. Space Sci.* **1**, 20.
JOHNSON F. S.	1959	*Nature, Lond.* **184**, 1787.
OBAYASHI T.	1958	*Rep. Ionos. Res. Japan* **12**, 301.
SMITH R. L.	1960	Stanford Electronics Laboratory, Techn. Rept. No. 6
VESTINE E. H. and SIBLEY W. L.	1959	*Planet. Space Sci.* **1**, 285.

NOTE ADDED TO REPRINT

R. L. Dowden
Ionospheric Prediction Service, Hobart, Tasmania

The shape of the isopycs (Fig. 3) is drastically dependent on the No (Ro) model used. Since (11) agrees very well with Smith's data for $N_E = 6 \times 10^4$ cm^{-3} these curves have been redrawn on the following basis:

$$N = \frac{N_E}{2} \cdot \frac{\eta\,\phi}{\eta_\lambda\,\phi_\lambda} \cdot \cos l \qquad \text{from (10) and (11)}$$

$$= \frac{N_E}{2R^3} \cdot \frac{\phi^2 \cos l}{4 - \frac{3}{R}\cos^2 l} = \text{const. for each curve}$$

This is shown in Fig. 4. Horns of Fig. 3 near $\lambda = 70^\circ$ are now removed. Since N_λ is not really zero at the poles, the polar dip ($l > 70^\circ$, say) of Fig. 4 will also be affected. "H" is a curve of constant gyro frequency.

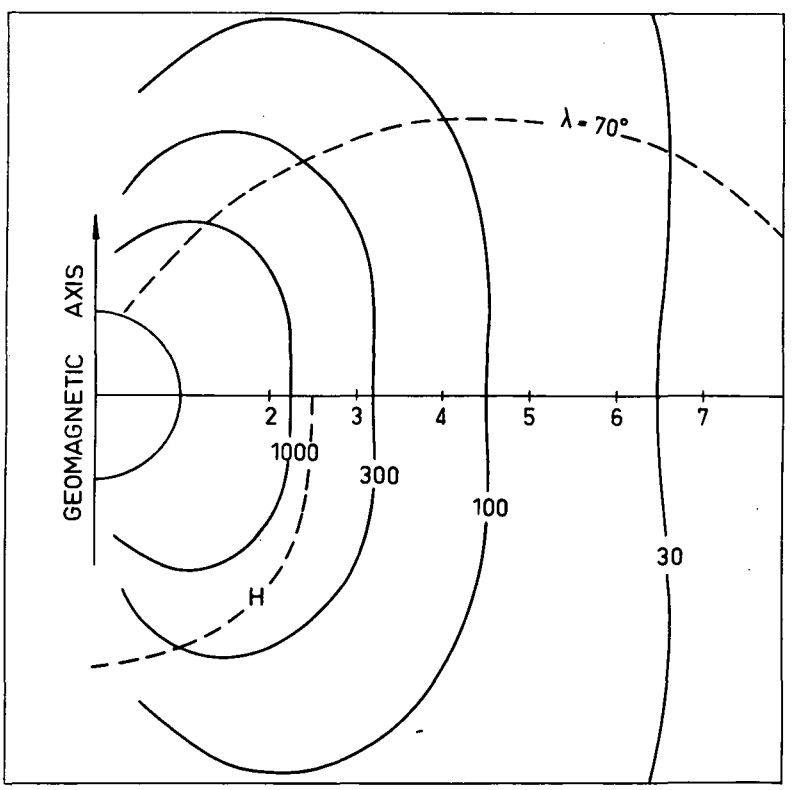

Fig. 4

JOURNAL OF GEOPHYSICAL RESEARCH VOLUME 67, No. 6 JUNE 1962

Theory of Generation of Exospheric Very-Low-Frequency Noise (Hiss)

R. L. DOWDEN

Ionospheric Prediction Service and University of Tasmania
Hobart, Tasmania, Australia

Abstract. The traveling wave tube amplification process proposed by Gallet and Helliwell is considered in greater detail. Account is taken of the spiral motion of particles traveling in the magnetic field, the interaction distance for which amplification at any one frequency can occur, and the slowing down of the stream particles by the wave amplification process. It is shown that narrow band bursts of hiss can be generated by weak electron streams of even very broad velocity and pitch distribution. The center frequency of such a band is characteristic of the terminating latitude of the line of force of generation. Stronger streams produce an overload effect giving rise to wide and very wide bands. Narrow bands can be produced at other frequencies by streams of narrow velocity and pitch distribution.

Introduction. The phenomenon treated here is that continuous type of exospheric emission variously called VLF noise, exospheric noise, geomagnetic noise, and hiss. It usually appears as band-limited white noise in the frequency range of about 1 to 10 kc/s. Hiss occurs in a broad band or in one or more narrow bands. The narrow bands usually have bandwidths of around 1 kc/s, though narrower bands occur [*Helliwell and Carpenter,* 1961]. Hiss occurs in bursts of two main types [*Ellis,* 1959]. The most common type, 'isolated burst,' is typical of magnetically quiet conditions. These bursts are narrow band, usually 1–2 kc/s, centered at about 4 kc/s. Though detectable at relatively low latitudes the vast majority of these have been shown to occur at geomagnetic latitudes greater than 50° [*Ellis,* 1960]. The center frequency, bandwidth, and intensity of the hiss remain remarkably constant over the duration of these bursts, which is generally about an hour. The second type occurs as an extended series of hiss bursts or 'noise storms.' In contrast, these show considerable intensity and bandwidth variations. All major magnetic storms are accompanied by noise storms [*Ellis,* 1959]. Generally, the bandwidth increases with magnetic activity. During severe disturbances very wide band bursts covering the range from about 100 c/s to over 200 kc/s can occur [*Dowden,* 1962*a*].

Hiss shows a strong correlation with airglow [*Duncan and Ellis,* 1959] and aurora [*Martin, Helliwell, and Marks,* 1960]. Rocket and satellite observations have shown that streams of electrons produce aurora [*McIlwain,* 1960] and airglow [*O'Brien, Van Allen, Roach, and Gartlein,* 1960]. It seems likely that these streams also produce hiss, though experiments to test this have yet to be reported.

Several mechanisms have been suggested [*Ellis,* 1957, 1959; *Allcock,* 1957; *MacArthur,* 1959; *Gallet and Helliwell,* 1959] capable of producing noise in this frequency range. However, none of these attempts to account for all the features outlined above. The most promising approach is the selective amplification process analogous to the traveling wave tube (TWT) proposed by Gallet and Helliwell. In this an electron stream provides amplification at frequencies for which the phase velocity of the amplified wave is equal to velocity of the stream. Both electrons and wave were assumed to travel exactly along the direction of the magnetic field.

Gallet's TWT process can be generalized by removing the restriction that the electrons travel exactly down the field line. In general, the electrons will spiral down the field lines. The pitch of the spiral at any position along the field line is determined by the principle of invariance of magnetic moment. For the low-energy particles required for this process (at most, a few kev) the radii of gyration will be much smaller than the extent of the wave front. Thus it is the component of particle velocity down the field

line or 'guiding center' velocity that must be equated to the longitudinal component of the wave phase velocity.

The analogy of this process with the traveling wave tube is perhaps closer than envisaged by Gallet and Helliwell. Since their work was published, it has been established by several people that field-aligned columns of ionization can occur in the exosphere [*Smith,* 1960], and these produce a strong wave guide action in the very-low-frequency range [*Smith, Helliwell, and Yabroff,* 1960]. A longitudinal magnetic field is often introduced into traveling wave tubes to focus the electron beams, and it is the guiding center velocity of the electrons that determines the amplification. As for the laboratory TWT, a (signal) longitudinal electric field is required for interaction with the stream. As was pointed out by Gallet and Helliwell, a substantial longitudinal component of electric field will exist in the exospheric TWT. It is the phase velocity of this component that is important, but for simplicity we will assume that this is c/n, where n is the refractive index of the medium for strict longitudinal propagation in the extraordinary mode below the gyrofrequency (whistler mode). Thus for guiding-center velocity $\beta_d c$ the condition for amplification is

$$n\beta_d = 1$$

In addition to this, we assume that, as for the laboratory TWT, the amplification in decibels or nepers is proportional to the distance in wavelengths along the field line for which amplification is possible at any one frequency. In the treatment given below the physical processes of amplification are not considered further.

Many of the writers referred to above described mechanisms for the production of chorus type phenomena rather than hiss. These discrete VLF emissions differ from the phenomenon considered here in ways other than their discreteness [*Helliwell and Carpenter,* 1961]. A mechanism for the production of these discrete emissions, very different from that considered here, is described by the writer elsewhere [*Dowden,* 1962*b*].

Amplified Frequencies. From the condition

$$n\beta_d = 1$$

and the refractive index for whistler-mode propagation

$$n^2 = 1 + p^2/f(h - f)$$

$$n^2 \gg 1$$

We find by solving for f

$$f = \frac{h}{2}\left[1 \pm \left(1 - \frac{4\beta_d{}^2 p^2}{h^2}\right)^{1/2}\right]$$

where

p is the plasma frequency,
h is the gyrofrequency,
f is the amplified frequency, and
n is the refractive index.

This is essentially the expression derived by *Gallet and Helliwell* [1959]. If a model of the exosphere is assumed, this expression can be put in a form in which, for a given line of force, the latitude angle coordinate is the only variable. To do this we assume that, at least along the lines of force considered here, the magnetic field is a dipole and the electron density varies in a way previously derived [*Dowden,* 1961]. Thus

$$h = \eta h_0$$

$$p^2 = p_0{}^2\, \eta\phi \cos l \quad \text{for} \quad R > 1.25$$

$$\beta_d{}^2 = \beta^2(1 - \eta \sin^2 \psi_0)$$

where

$\eta = \phi \sec^6 l$,
$\phi = (1 + 3 \sin^2 l)^{1/2}$,
l is the latitude angle coordinate,
R is the radius vector in earth radii,
ψ is the pitch angle, and
subscript 0 refers to values in the equatorial plane.

We assume here that the energy loss of any particle through amplification of the wave will be sufficiently small to regard the particle speed βc as constant. The effects of appreciable energy loss will be considered in a later section. Substituting these expressions, we find

$$f = \frac{\eta h_0}{2} \cdot \left\{1 \pm \left[1 - \frac{4\beta^2 p_0{}^2}{h_0{}^2} \cos^7 l(1 - \eta \sin^2 \psi_0)\right]^{1/2}\right\} \tag{1}$$

It will be seen later that the frequency given by the minus sign is the more interesting. This

can be put in a form containing relatively slowly varying functions, which is more suitable for computation. We define

$$a = 4\beta^2 p_0^2/h_0^2$$
$$x = a \cos^7 l(1 - \eta \sin^2 \psi_0)$$
$$\gamma = (2/x)[1 - (1 - x)^{1/2}]$$

Then

$$f^- = (\eta h_0/2)[1 - (1 - x)^{1/2}]$$
$$= \frac{\beta^2 p_0^2}{h_0} \gamma \cdot \phi \cos l(1 - \eta \sin^2 \psi_0) \qquad (2)$$

Frequencies as a function of the latitude angle l have been computed for particles of various speeds and pitch angles traveling along the line of force that terminates at geomagnetic latitude 50°. A smooth join to an ionosphere similar to that used by *Gallet and Helliwell* [1959] has been made at a height of 2000 km above the surface of the earth. The results of this are shown in Figure 1. Except for the effect of the ionosphere, the shape of these curves would be very similar for lines of force terminating at other latitudes. Only a change in frequency scale is required. The important parameter affecting the shape is a. It is seen that in many cases the amplified frequency is fairly constant over great distances. This follows from (2), for $\phi \cos l$ stays within 15 per cent of unity for $l < 60°$, γ rapidly approaches unity for small values of x, and the term containing the pitch angle is fairly constant except near the mirror points. Of even greater interest are those regions for which variation of these terms nearly cancels out, producing very nearly constant frequencies over great distances. At these frequencies amplification will be great. We will consider this in greater detail.

Interaction distance. For appreciable interaction at any *one* frequency we require not only that the wave phase and particle guiding center velocities be equal, but also that this condition should hold effectively over some appreciable distance s.

Suppose that initially ($s = 0$) the condition $n\beta_d = 1$ holds exactly at some frequency, but further on, owing to changes in the guiding-center velocity of the medium, the particle stream slowly overtakes the wave. The stream (guiding-center) velocity relative to the wave is thus

$$\Delta v = \frac{c}{n}(n\beta_d - 1)$$

In time dt

$$d(\Delta s) = \Delta v \cdot dt \qquad ds = c/n \cdot dt$$
$$\therefore\ d(\Delta s) = (n\beta_d - 1)\, ds$$

Now

$$(n\beta_d - 1) = \int_0^s (n\beta_d)' \cdot ds$$

where

$$(n\beta_d)' = \frac{\partial}{\partial s}(n\beta_d)_{f\ const.}$$

Hence

$$\Delta s = \int_0^s \int_0^s (n\beta_d)' \cdot ds \cdot ds$$

In the region of interest, that is, on one of the curves defined by (1), the condition $n\beta_d = 1$ holds at all points, changes in the medium or stream velocity being exactly balanced by changes in frequency f.

Thus

$$\frac{d}{ds}(n\beta_d) = 0$$

Hence

$$\frac{\partial}{\partial s}(n\beta_d)_{f\ const.} = -\frac{\partial}{\partial s}(n\beta_d)_{f\ varying}$$

Now

$$n\beta_d = p\beta_d[f(h - f)]^{-1/2} \quad \text{for} \quad \beta^2 \ll 1 (n^2 \gg 1)$$

$$\therefore\ -\frac{\partial}{\partial s}(n\beta_d)_{f\ varying}$$
$$= \frac{\frac{1}{2} p\beta_d [f(h - f)]^{-1/2} \cdot \left(h \cdot \frac{df}{ds} - 2f \cdot \frac{df}{ds}\right)}{f(h - f)}$$

Hence

$$\frac{\partial}{\partial s}(n\beta_d)_{f\ const.} = \frac{1}{2f} \cdot \frac{h - 2f}{h - f} \cdot \frac{df}{ds}$$

since $n\beta_d = 1$. Since Δs must be small (at least $< \lambda/2$) throughout the interaction distance s, then s is given by the integration limits

$$\frac{\lambda}{2} > \Delta s = \int_0^s \int_0^s (n\beta_d)' \cdot ds \cdot ds$$
$$= \frac{1}{2} \int_0^s \int_0^s \left(\frac{1}{f} \cdot \frac{h - 2f}{h - f} \cdot \frac{df}{ds}\right) ds \cdot ds \qquad (3)$$

where λ is the wavelength.

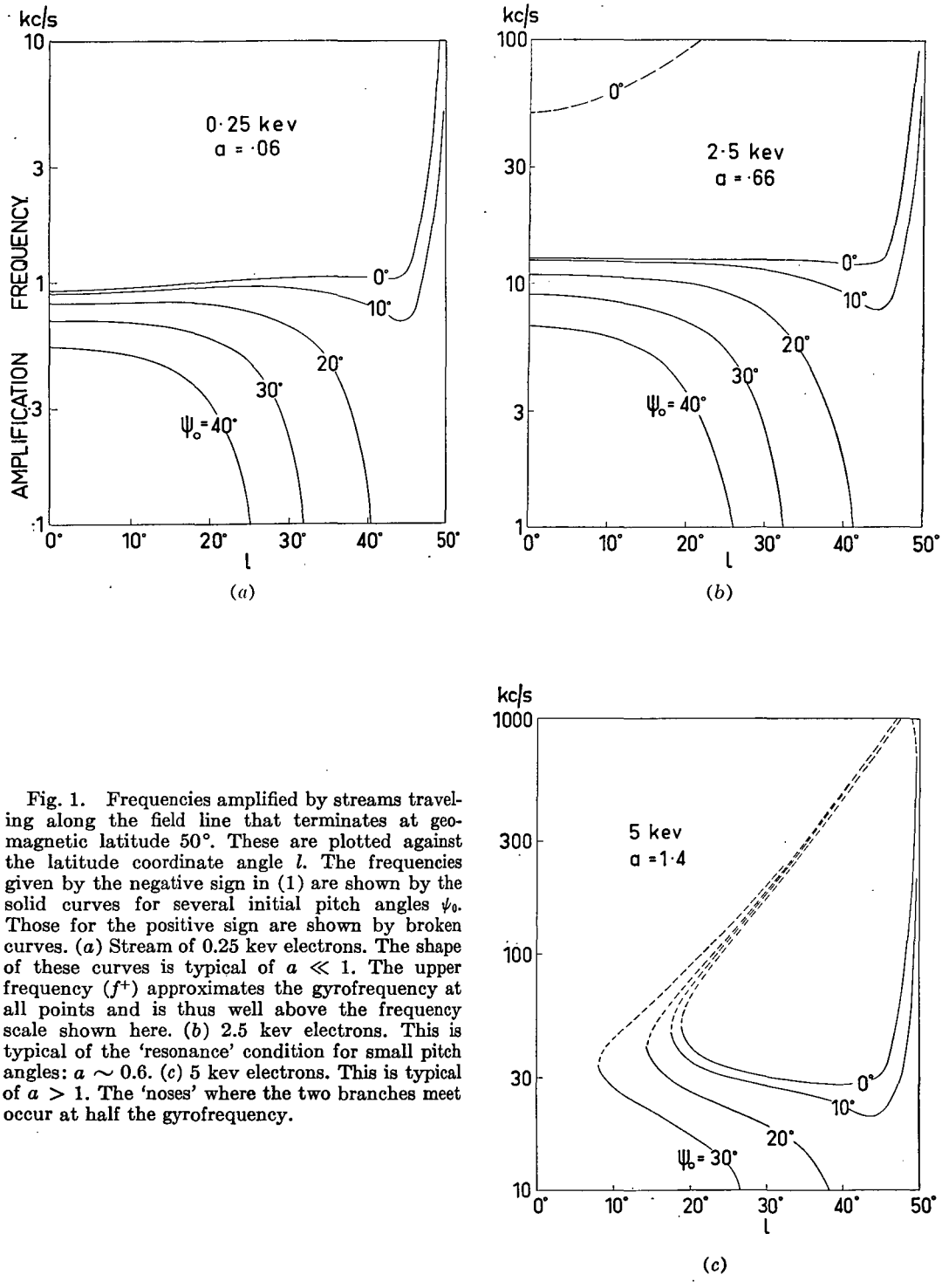

Fig. 1. Frequencies amplified by streams traveling along the field line that terminates at geomagnetic latitude 50°. These are plotted against the latitude coordinate angle l. The frequencies given by the negative sign in (1) are shown by the solid curves for several initial pitch angles ψ_0. Those for the positive sign are shown by broken curves. (*a*) Stream of 0.25 kev electrons. The shape of these curves is typical of $a \ll 1$. The upper frequency (f^+) approximates the gyrofrequency at all points and is thus well above the frequency scale shown here. (*b*) 2.5 kev electrons. This is typical of the 'resonance' condition for small pitch angles: $a \sim 0.6$. (*c*) 5 kev electrons. This is typical of $a > 1$. The 'noses' where the two branches meet occur at half the gyrofrequency.

This shows that amplification will not be appreciable at the frequency given by the plus sign (f^+) in (1) for two reasons; first, because df/ds is usually large (Fig. 1) and, second, because $(h - f)$ is generally quite small. At the points where the two curves join (Fig. 1c) $h - 2f$ is zero, but also df/ds is infinite. Consequently, the high-frequency branch will not be considered further.

Thus, considering only the low-frequency branch, we differentiate (1) with respect to l and make the γ substitution

$$\frac{1}{f}\frac{df}{dl} = \tan l\left\{6 + \frac{3\cos^2 l}{\phi^2} - \frac{7 + \eta\left(\frac{3\cos^2 l}{\phi^2} - 1\right)\cdot\sin^2\psi_0}{(1 - \eta\sin^2\psi_0)(2 - \gamma)}\right\} = L \quad (4)$$

From the line of force equations for a dipole field

$$\frac{ds}{dl} = R_0\phi\cos l \quad (5)$$

The resulting expression containing s can be simplified by noting that $\phi\cos l \sim 1$ for $l < 60°$ and, in the region of interest (high amplification) the term

$$(h - 2f)/(h - f)$$

is also close to unity. Thus from (3), (4), and (5) we have

$$\frac{2\,\Delta s}{R_0} \simeq \int_{l_1}^{l_2}\int_{l_1}^{l} L\,dl\,dl \quad (6)$$

$$s/R_0 \simeq l_2 - l_1$$

We assume that, as in the TWT process, the amplification (in decibels or nepers) is proportional to the interaction distance measured in wavelengths, s/λ. In those cases for which s is sufficiently small, the integration range $l_2 - l_1$ is also small, so that over this range the integral L in (6) will be approximately constant. Thus

$$\frac{2\,\Delta s}{R_0} \simeq L\cdot\tfrac{1}{2}(l_2 - l_1)^2 = \frac{\lambda}{R_0}$$

in the limiting case ($\Delta s = \lambda/2$).

Then, since

$$\lambda = \frac{c}{nf} = \frac{\beta_d c}{f}$$

$$\left(\frac{s}{\lambda}\right)^2 \simeq \frac{2f}{\beta_d c}\cdot\frac{R_0\phi\cos l}{L} \quad (7)$$

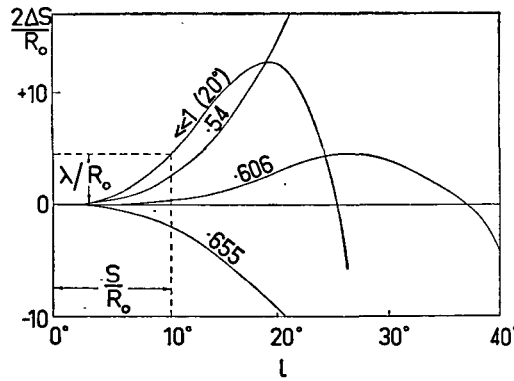

Fig. 2. Calculation of s/λ. Equation 6 is plotted for three values of a near 0.6 for $\psi_0 = 0$, and for $a \ll 1$ for $\psi_0 = 20°$.

However, in the more interesting cases where s is large, (6) must be integrated. Curves giving $2\Delta s/R_0$ as a function of l are shown in Figure 2 for some of the cases which give relatively large values of s. For a given curve the value s/λ is found by selecting a range of l that has a range of $2\Delta s/R_0$ equal to λ/R_0. This range of l is then s/R_0, as is shown in Figure 2. It is seen that for very small pitch angles the highest values of s/λ are found for $a \sim 0.6$. For larger pitch angles these are found at lower values of a. No particles of pitch angle ψ_0 much greater than 20° have large s/λ values.

The parameter s/λ as a function of frequency for particles of very small pitch angle traveling along the line of force terminating at geomagnetic latitude 60° is shown in Figure 3. Particles of greater pitch angle will have a s/λ curve showing a smaller and broader maximum occurring at lower frequencies. For other lines of force the essential change in the s/λ curve is the frequency scale, the maximum occurring (from equation 2) at

$$f \simeq ah_0/4 \simeq 0.15h_0$$

This relation is also shown in Figure 3.

The theory derived so far shows that, if a particle stream is confined to a narrow tube of force and if this stream is 'weak' so that very high amplification is required, a narrow band of noise (hiss) can be produced even though the stream contains a wide spectrum of particle velocities and pitch angles. This occurs because only a very narrow range of particle velocities and pitches can give the necessary amplification.

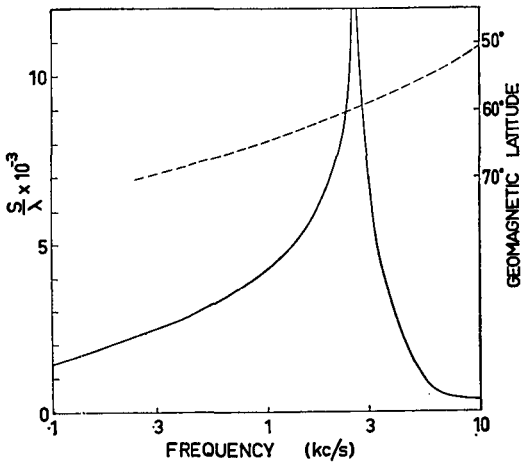

Fig. 3. Interaction parameter s/λ for stream particles of small pitch guided along the field line terminating at geomagnetic latitude 60°. At other latitudes frequencies will scale so that maximum s/λ occurs at the frequency given by the dashed curve.

Thus we have explained the observed occurrence of narrow band, 'quiet,' isolated bursts. The theory further predicts that the frequency at which these bursts occur is a function of the terminating latitude of the line of force. There is not sufficient experimental evidence as yet to prove this one way or the other: some observations indicate that lower frequencies occur at higher latitudes as has been predicted by *Gustafsson, Egeland, and Aarons* [1960]; others [*Outsu and Iwai*, 1961] seem to indicate the reverse.

Energy loss. As for the laboratory TWT, we expect the amplification (in nepers) to be proportional to s/λ. Thus the amplified power is

$$P = b \exp(\alpha s/\lambda) \tag{8}$$

where b and α are constants. The constant b is thus the power before amplification, or at least that generated at the beginning of the amplification process. The constant α controls the rate of amplification. This must be some function of the properties of the stream.

If b (in Wm^{-2} c/s^{-1}) is not a strong function of frequency, then, from (8), the s/λ curve in Figure 3 has the shape of a logarithmic plot of generated noise intensity with frequency. However, from (2) the noise power in any given small band of frequency is produced by particles of a corresponding small range of velocities and pitches. Clearly, the noise power produced in this band cannot exceed the kinetic power (K) of the corresponding particles. Thus

$$P < K$$

This 'overload' condition is probably more restrictive than this, so we write it as

$$P \leq P_m = AK \tag{9}$$

where A is a factor as yet undetermined. Thus in general there will be an overload plateau region of relatively constant intensity, provided, of course, that neither A nor K is a strong function of frequency. This will be reached for a given value of α when the intensity given by (8) reaches that given by (9). Then for all values of s/λ as given in Figure 3 greater than the critical value (from equations 8 and 9)

$$(s/\lambda)_{crit} = 1/\alpha \log_e (AK/b) \tag{10}$$

the intensity will be given by (9).

Consequently 'weak' streams for which the rate of amplification (α) is small will produce narrow band hiss, and 'strong' streams (large α) will produce wide or very wide band hiss. The peak intensity for all will be given by (9), so that unless A or K is a strong function of α, the main effect of varying degrees of amplification rate should appear in the bandwidth rather than in intensity. If α is related to magnetic activity, then this explains why the peak intensity of hiss bursts occurring during magnetically quiet periods is of the same order as that during disturbed conditions, but in general the bandwidth increases with magnetic activity from around 1 kc/s for 'isolated bursts' [*Ellis*, 1959] to over 100 kc/s during severe disturbances [*Dowden*, 1962*a*].

It is difficult to make quantitative estimates, since little is known of the relevant quantities. We can get some idea of the amplification required in the following way. The observed peak intensities of hiss after allowing for propagation losses [*Dowden*, 1962*a*] are of the order of $AK = 10^{-10}\ Wm^{-2}$ (c/s)$^{-1}$. If the amplification is large we require only a very crude idea of the initial noise intensity b. For Cerenkov emission [*Ellis*, 1957] this would be of the order of $b = 10^{-19}$ Wm^{-2} (c/s)$^{-1}$. Then from (8) it is seen that about 20 nepers of amplification would be required. From (10) and Figure 3, $\alpha = 2 \times 10^{-3}$ would be required for a narrow band burst of

hiss and $\alpha = 2 \times 10^{-2}$ for a wide band burst. Although this amplification is very high compared with laboratory TWT practice, the values of amplification rate α required here are very conservative.

We also need to see if the kinetic energy of electron streams is adequate to explain the observed hiss intensities, that is, if the required values of A in (9) are reasonable. Rocket measurements [*McIlwain*, 1960] have been made in an electron stream that produced a quiescent auroral glow and so might be taken as typical. Within the range of measurement (3 to 30 kev) the stream kinetic energy flux in watts per square meter per unit energy interval (kev) was found to fit the expression

$$K = 5 \times 10^{3} E \exp(-E/5) \qquad (11)$$

E in kev. At around 2 kc/s, from (2), amplification will be produced by 0.5 kev electrons, and an energy interval of 1 ev will correspond to a frequency interval of about 4 c/s. So assuming that the above expression (11) is valid down to 0.5 kev, the stream kinetic 'intensity' is

$$K \simeq 6 \times 10^{-7} W m^{-2} (\text{c/s})^{-1}$$

From (9) and the observed intensity quoted above, $A \sim 10^{-4}$. Even if this extrapolation of (11) is a very crude approximation, it seems that there will be sufficient energy, that is, $A < 1$. For the laboratory TWT the efficiency is around 10 per cent; that is, $A \sim 0.1$. However, we would expect much lower values for the exosphere because, within the much longer iteration distances of several thousand wavelengths required, a relatively small loss of kinetic energy would destroy synchronism.

Discussion. The theory explains the main characteristic of hiss: that it appears as band-limited white noise. The expression (9) suggests that within this band the intensity will be relatively uniform but outside the band the intensity (8) drops exponentially. Bandwidths from very narrow to very wide are possible without requiring special velocity and pitch distributions of the stream particles. The bandwidth of the noise increases with the 'strength' of the stream, which seems in agreement with the observation that bandwidth increases with magnetic activity. Very strong streams requiring only short distances of interaction to reach overload power could produce noise at all the frequencies in Figure 1 simultaneously and so produce the very wide band bursts. Short streams some 1000 km long in the direction of the field. having high values of α and a narrow spectrum of velocities, would amplify the frequencies along one of the curves in Figure 1 in sequence. These could produce the 'quasi-constant tones' and the TWT 'hooks' as proposed by *Gallet and Helliwell* [1959].

We would expect 'isolated bursts' to be produced by weak streams. If these generally occur in geomagnetic latitudes from about 50° to 65° then the corresponding center frequencies (broken curve in Figure 3) should range from about 1 to 10 kc/s. Thus 4-kc/s bursts should occur at around 55° to 60°. The experimental evidence so far obtained seems to allow this, though there is not sufficient data to provide a test.

On the other hand, narrow band noise not conforming to this frequency-latitude relation could be produced by streams of narrow energy (velocity) and pitch distributions. *McIlwain* [1960] found that a stream which produced a strong visible aurora consisted of practically monoenergetic electrons. A stream having more than one such energy distribution could produce more than one narrow band of noise. Multiple narrow bands could also be produced by weak streams of uniform velocity distribution if several occurred in slightly different latitudes simultaneously. Thus, as seen from Figure 3 (broken curve), center frequencies differing by a factor of 2 can be produced by streams less than 5° of latitude (~500 km) apart. In the same way the finite width of streams would set a limit to the narrowness of the amplified band. However, satellite measurements at a height of a few hundred kilometers [*O'Brien, Van Allen, Roach, and Gartlein*, 1960] show that some streams are as narrow as 25 km (traversed by the satellite in 3 sec).

It may appear to the reader that this theory rests on the assumption that detailed expressions can be extracted from a theoretical model which might not be truly representative of the real exosphere. However, provided the electron density *along the field line* varies *smoothly* in a manner not greatly different from the model used, the essential qualitative results of this theory should still hold. Similarly the qualitative results may not be greatly affected should

subsequent study of the exospheric TWT mechanism require some modification to the amplification condition $n\beta_d = 1$.

Acknowledgment. I am indebted to Professor G. R. A. Ellis of the Physics Department, University of Tasmania, for suggesting this work initially and for giving many helpful criticisms and suggestions.

References

Allcock, G. McK., A study of the audio-frequency radio phenomenon known as 'dawn chorus,' *Australian J. Phys., 10,* 286–298, 1957.

Dowden, R. L., A theoretical model of electron density along a geomagnetic line of force in the exosphere, *J. Atmospheric and Terrest. Phys., 20,* 122–130, 1961.

Dowden, R. L., Wide band bursts of V.L.F. radio noise ('hiss') at Hobart, *Australian J. Phys., 15,* 114–119, 1962*a*.

Dowden, R. L., Doppler-shifted cyclotron radiation from electrons: a theory of very-low-frequency emissions from the exosphere, *J. Geophys. Research, 67* (5), 1962*b*.

Duncan, R. A., and G. R. Ellis, Simultaneous occurrence of subvisual aurorae and radio noise bursts on 4.6 kc/s, *Nature, 183,* 1618–1619, 1959.

Ellis, G. R., Low frequency radio emission from aurorae, *J. Atmospheric and Terrest. Phys., 10,* 302–306, 1957.

Ellis, G. R. A., Low frequency electromagnetic radiation associated with magnetic disturbances, *Planetary and Space Sci., 1,* 253–258, 1959.

Ellis, G. R. A., Directional observations of 5 kc/s radiation from the earth's outer atmosphere, *J. Geophys. Research, 65,* 839–843, 1960.

Gallet, R. M., and R. A. Helliwell, Origin of very low frequency emissions, *J. Research NBS, 63D,* 21–27, 1959.

Gustafsson, G., A. Egeland, and J. Aarons, Audio-frequency electromagnetic radiation in the auroral zone, *J. Geophys. Research, 65,* 2749–2758, 1960.

Helliwell, R. A., and D. L. Carpenter, Whistlers-west IGY-IGC synoptic program, *SEL Final Rept.,* Stanford University, March 20, 1961.

MacArthur, J. E., Theory of the origin of the very low frequency radio emission from the earth's exosphere, *Phys. Rev. Letters, 2,* 491–492, 1959.

McIlwain, Carl E., Direct measurement of particles producing visible auroras, *J. Geophys. Research, 65,* 2727–2747, 1960.

Martin, L. H., R. A. Helliwell, and K. R. Marks, Association between aurorae and V.L.F. hiss observed at Byrd Station, Antarctica, *SEL Tech. Rept. 1,* Stanford University, April 29, 1960.

O'Brien, B. J., J. A. Van Allen, F. E. Roach, and C. W. Gartlein, Correlation of an auroral arc and a subvisible monochromatic 6300 A arc with outer-zone radiation on November 28, 1959, *J. Geophys. Research, 65,* 2759–2766, 1960.

Outsu, J., and A. Iwai, SEA and hiss associated with great bursts of solar radio emission in November, 1960, 3, Hiss, *Proc. Research Inst. of Atmospherics, Nagoya Univ., 8,* 13, 1961.

Smith, R. L., The use of nose whistlers in the study of the outer ionosphere, *SEL Tech. Rept. 6,* Stanford University, July 11, 1960.

Smith, R. L., R. A. Helliwell, and I. W. Yabroff, A theory of trapping of whistlers in field-aligned columns of enhanced ionization, *J. Geophys. Research, 65,* 815–823, 1960.

(Manuscript received December 11, 1961; revised March 22, 1962.)

Doppler-Shifted Cyclotron Radiation from Electrons: A Theory of Very Low Frequency Emissions from the Exosphere

R. L. DOWDEN

Ionospheric Prediction Service and University of Tasmania
Hobart, Tasmania, Australia

Abstract. Cyclotron radiation from electrons in the exosphere spiraling along a line of force *away* from the observer will appear at a frequency less than the local gyrofrequency. An electron traveling from the observer's hemisphere to the opposite hemisphere will radiate a decreasing frequency until it crosses the equator, and thence an increasing frequency. Propagation conditions and various particle speeds give frequency-time spectra similar to those observed. A method of scaling electron speeds and the field lines in which they occur from observed data is described. Tests of the theory are discussed.

Introduction. Very low frequency emissions occur in the audiofrequency region and show association with magnetic disturbance. It is generally thought that they are generated in the exosphere or upper ionosphere by fast charged particles. Two main types occur: 'hiss,' a continuous white noise that can occur in broad or narrow bands; and 'chorus,' which is made up of rising and falling tones or whistles. Only the chorus type is considered here. This phenomenon sometimes occurs as quite separate discrete whistles showing definite and repeatable forms on frequency-time spectrographs. These have been described by many workers as 'falling tones,' 'hooks,' 'risers,' and 'pseudo noses.' Examples of these are shown in Figure 1 (after *Helliwell and Carpenter* [1961]).

The first theory explaining the frequency-time shape of some of these was given by *Gallet and Helliwell* [1959]. They suggested that, when the particle speed $\beta_d c$ was equal to the wave velocity c/n at some frequency, energy from the particle would be fed to the wave in a process analogous to that of the traveling wave tube (TWT).

Thus from the condition

$$n\beta_d = 1$$

and the refractive index

$$n^2 = 1 + p^2/[f(h - f)]$$

$$n^2 \gg 1$$

they found

$$f = \frac{h}{2}\left[1 \pm \left(1 - \frac{4\beta_d{}^2 p^2}{h^2}\right)^{1/2}\right]$$

where h is the gyrofrequency, p is the plasma frequency, and $\beta_d c$ is the component of particle velocity along the magnetic field line. (This is a more general form. They considered particles traveling exactly along the field line.)

This was applied to 'hooks' having a slowly descending frequency followed by a rapid rise. On this theory the first part would be produced in the exosphere and the rapid rise in the upper ionosphere.

MacArthur [1959] considered Doppler-shifted cyclotron radiation from protons. Protons gyrating at frequency H will appear at a much higher frequency f if they are rapidly approaching the observer, where

$$f = H/(1 - \beta_d n)$$

He showed that this approximated to the TWT expression. Essentially this is because for $H/f \ll 1$, $n\beta_d \simeq 1$. The same process was also considered by *Murcray and Pope* [1960*a*]. However, they used the refractive index at frequency H rather than that at f and consequently obtained a different expression. This was corrected in a later work [*Murcray and Pope*, 1960*b*].

Murcray and Pope [1960*a*, 1961] pointed out an advantage of the proton gyration theory over the TWT theory: a quantitative estimate of radiation can be made. On the other hand, such an estimate made by *Santirocco* [1960] indicated that *proton* radiation would be much too small for detection unless [*Murcray and Pope*, 1961] enormous numbers of protons radiate coherently.

However, the situation is different for radiation from gyrating *electrons*, since the emitted

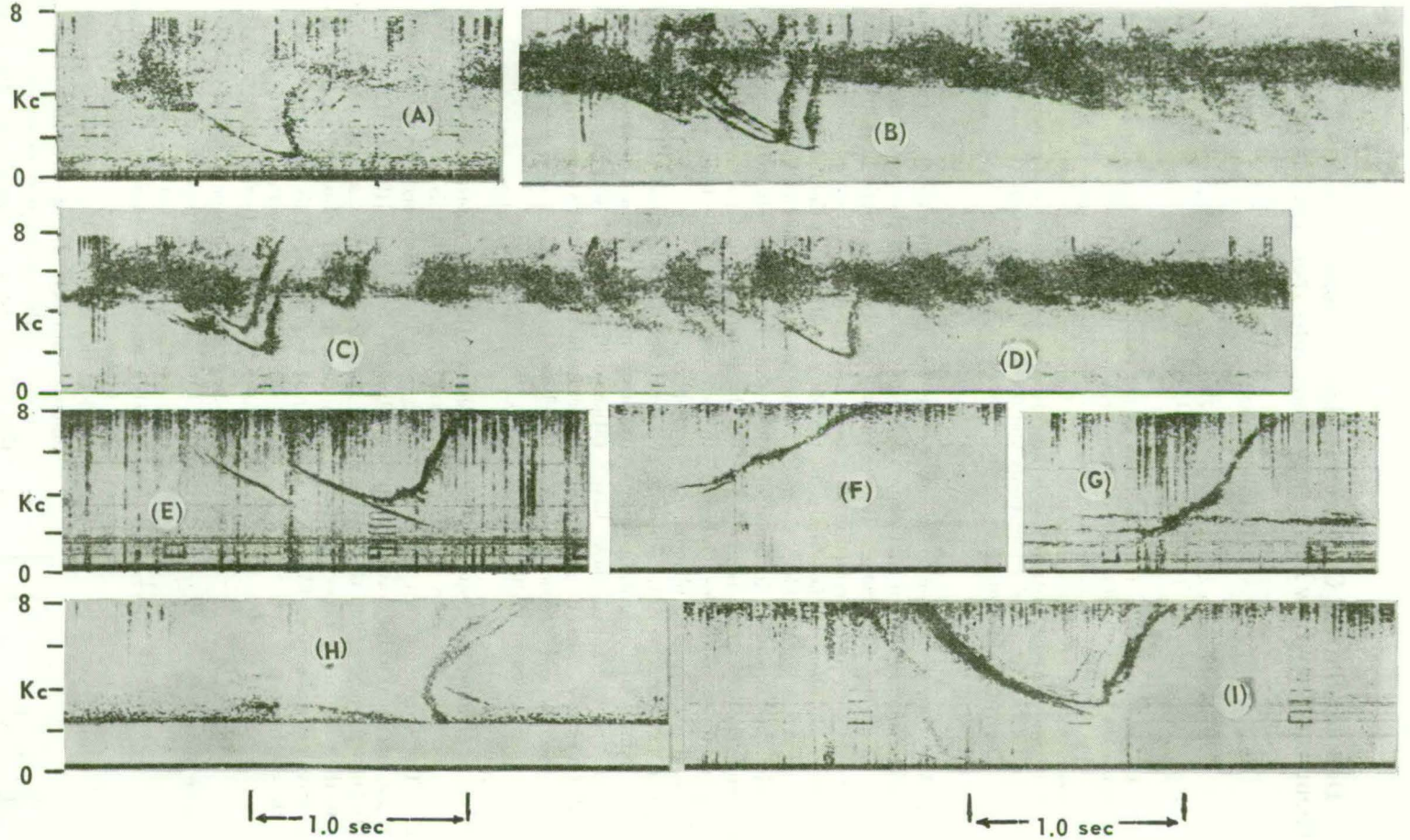

Fig. 1. Spectrograms of discrete VLF emissions (after *Helliwell and Carpenter* [1961]). Falling tones appear in *e*, quasi-constant tones in *g*, and risers in *f* and *g*. The other forms are probably all hooks.

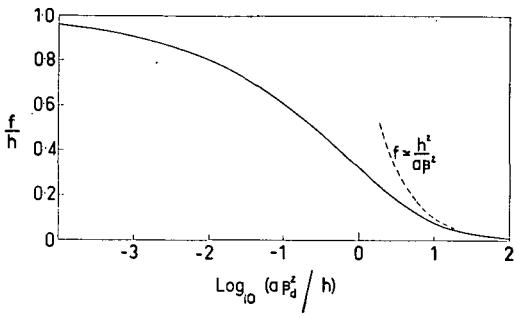

Fig. 2. Graph of equation 3 for finding emitted frequency.

power is inversely proportional to the square of the particle mass. Thus we would expect the radiation power from electrons to be greater than 3 million times that from protons, other factors being the same.

Theory. Suppose that an electron (or rather a small bunch of electrons) is traveling in a helix about a line of force of the earth's magnetic field. Suppose that it is traveling *away* from the observer's hemisphere with velocity component along the line of force of $\beta_d c$. Thus the rotating electron (or bunch) is an oscillator of frequency h moving away from the observer at velocity $\beta_d c$ in a medium for which the *observed* frequency f travels at velocity c/n.

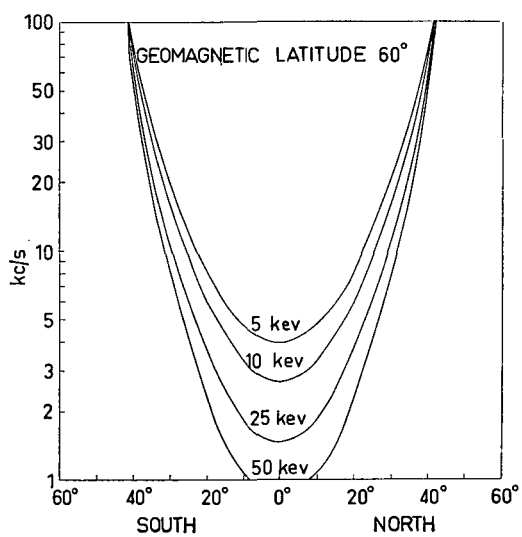

Fig. 3. Frequency emitted by an electron of the energies shown as a function of position (latitude angle). All four electrons have mirror points at 41°.

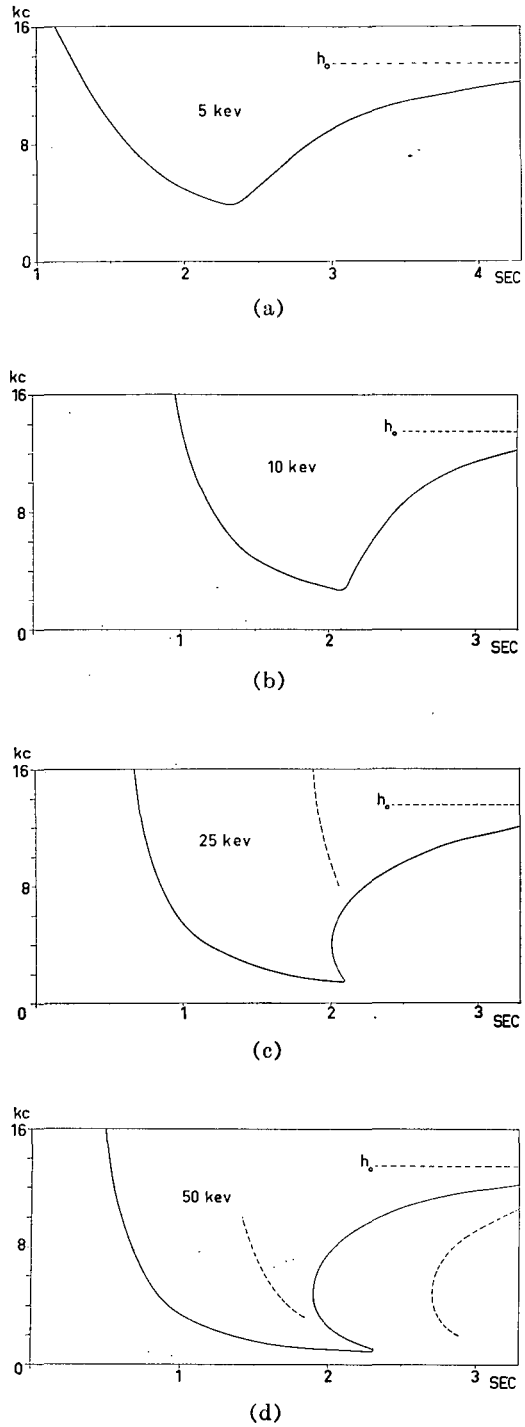

Fig. 4. Frequency-time (dispersions) curves for the electrons considered in Figure 3. These should be compared with the observed spectrograms in Figure 1.

TABLE 1. Mirror Oscillation Periods of the Electrons Considered in Figure 3

Energy, kev	Period, sec
5	2.56
10	1.82
25	1.28
50	0.81

Thus

$$f = h/(1 + \beta_d n)$$

where

$$n^2 \simeq p^2/[f(h - f)] \quad \text{for} \quad n^2 \gg 1$$

Hence

$$(h - f)^3 = p^2 \beta_d{}^2 f$$

Smith [1960] has shown that a model of electron density distribution in the exosphere for which the electron density is everywhere proportional to the gyrofrequency fits his nose whistler data rather well. Theoretical considerations by *Dowden* [1961] lead to a distribution that approximates to this gyrofrequency model.

Thus $p^2 = ah$, where $a \simeq 1$ Mc/s [*Smith*, 1960]

$$\therefore (h - f)^3 = a\beta_d{}^2 fh \qquad (1)$$

This is difficult to evaluate algebraically except for $f \ll h$, when

$$f \simeq h^2/a\beta_d{}^2 \qquad (2)$$

However (1) can be put in the form

$$\frac{(1 - f/h)^3}{f/h} = \frac{a\beta_d{}^2}{h} \qquad (3)$$

A plot of $a\beta_d{}^2/h$ versus f/h permits f to be found, given $\beta_d{}^2$ and h. This is shown in Figure 2. The approximation 2 is seen to be valid only for $a\beta_d{}^2/h > 20$.

Values of f have been found from Figure 2 for electrons of energies 5, 10, 25, and 50 kev traveling along the line of force terminating at geomagnetic latitude 60°. The position of a point on this field line is determined by the latitude angle l. The emitted frequency as a function of latitude angle is shown in Figure 3. The helical pitch (ψ_0) of all these electrons is 20° in the equatorial plane, so that mirror points occur in each hemisphere at $l = 41°$. The

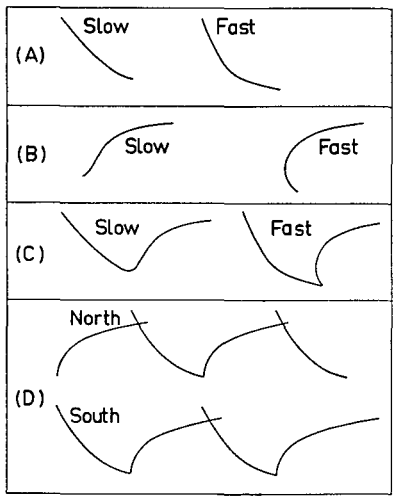

Fig. 5. Types of discrete emission that can be produced by this process. (*A*) Bunch injected at midpoint (equatorial plane), mirrored in *observer's* hemisphere, and scattered at midpoint (falling tone or pseudo whistler). (*B*) Bunch injected at midpoint and either absorbed near the mirror in the *opposite* hemisphere or mirrored, and scattered, at the midpoint (riser for slow bunch, pseudo nose for fast). (*C*) Bunch injected at midpoint, mirrored in observer's hemisphere, and survived one transit through midpoint to pass into opposite hemisphere (hook). (*D*) Medium-speed bunch injected at midpoint, mirrored in southern hemisphere, then northern, southern, northern, and finally scattered at the midpoint. In the northern hemisphere a riser, a hook, and a falling tone are observed; in the southern, two hooks. Synchronized spectrograms from conjugate points would look like this.

parameter β_d is calculated for invariance of magnetic moment:

$$\beta_d{}^2 = \beta^2(1 - \eta \sin^2 \psi_0)$$

where

$$\eta = (1 + 3 \sin^2 l)^{1/2} \sec^6 l$$

Suppose that these electrons make one trip from the mirror point in the observer's hemisphere to the mirror point in the opposite hemisphere. We need to find how frequency would vary with time as observed on the earth's surface at the base of this line of force. Such frequency-time curves can be found by summing the time delay due to the finite velocity of the electron (T_e) and that due to the finite group velocity of the wave (T_g).

$$T = T_e + T_g$$

TABLE 2. Hazards and Relative Occurrence

Class and Types	Hazards: Mirrors	Hazards: Source Region Transits	Observed* Relative Abundance
Chorus			403
(B) Risers	0	0	178
psuedo noses			7
(A) Falling tones	1	0	21
(C) Hooks	1	1	15
(D) Multiple forms	2 or more	1 or more	—

* From *McInnes* [1961].

where

$$T_g = \int \frac{ds}{V_g} = \frac{a^{1/2}}{2cf^{1/2}} \int \frac{h^{3/2}}{(h - f)^{3/2}} \cdot ds + \frac{D(\text{ionosphere})}{f^{1/2}}$$

and

$$T_e = \int \frac{ds}{V_e} = \frac{1}{\beta c} \int \frac{ds}{(1 - \eta \sin^2 \psi_0)^{1/2}}$$

Integration is carried out over the path, and the integrals were evaluated numerically. The resulting frequency-time curves are shown in Figure 4. The time $T = 0$ is defined as that instant when the electron passes through the equatorial plane toward the observer's hemisphere. It could thus be the time of injection into the line of force. Note that for the 5-kev electron the time scale starts 1 second after this.

Discussion. The frequency-time curves in Figure 4 show good agreement with the observed hooks in Figure 1. If the electron bunch only makes half of the mirror-to-mirror trip, which might happen if the source of the bunch (probably near the equatorial plane) is also a sink, then only half of the full hooks will be observed. If this half trip was confined to the observer's hemisphere only, the falling part (falling tone) would be observed. This might be mistaken for a whistler in some circumstances. Trips confined to the opposite hemisphere would give rise to the other half: risers (*f* and *g* in Fig. 1) and pseudo noses.

On the other hand, at times several complete trips might take place before the bunch is lost.

TABLE 3. Deduced Latitude and Energy of the Electrons Producing Nosed Hooks in Figure 1

Event in Figure 1	Latitude	Energy, kev
a	62°	7
d	62°	5
h	62°	25

This would give rise to a series of hooks of similar shape separated in time by the period of oscillation of the bunch between mirrors. For the faster particles in Figure 4 this is indicated by the curved broken lines. The oscillation periods are given in Table 1. An observer in the opposite hemisphere near the conjugate point would observe the same series of hooks, but since radiation is observed only when the bunch is traveling *away* from this observer he will observe this series shifted in time by half a period. Thus a northward-going bunch sends a hook to the southern observer, then, when returning on its southward trip, sends a hook to the northern observer. This conjugate point test of the theory was suggested to the author by G. R. A. Ellis.

The types of emission described above are illustrated in Figure 5. A bunch tends to be scattered by turbulent magnetic fields in the source region (probably near the equatorial plane) and to be absorbed by collisions near the mirror points. Thus we would expect the relative frequency of occurrence of the various types of emission to decrease with the number of mirrors and source-region transits required for each type. Thus 'quasi-vertical' or 'typical' chorus, and risers, which are required to survive no such hazards, should be the most common. In Table 2 the number of hazards for each type (as listed in Fig. 5) is compared with the observed relative frequency of occurrence (from *McInnes* [1961]). Nosed forms seem to be relatively rare, probably because low particle speeds occur more frequently than high. The observed order of abundance is otherwise as expected.

It can be seen from Figure 4 that when circumstances (fast particles, high latitudes) give rise to a nose similar to the nose whistler, the nose frequency is about one-third of the minimum gyrofrequency (h_0, shown by broken line). This allows calculation of the terminal latitude (λ) of the line of force along which the bunch is

guided:

$$\cos \lambda = (h_0/870)^{1/6} \qquad h_0 \text{ in kc/s}$$

The one-sixth power makes latitude evaluation reasonably accurate even for very rough estimates of h_0. The minimum frequency (f_0) can also be scaled from an observed hook. Substitution of h_0 and f_0 into equation 1 immediately gives the value of β_d^2 in the equatorial plane. The pitch will be smallest in the equatorial plane, so that, except for large pitch angles, $\beta_d^2 \simeq \beta^2$. The energy of the electrons in kev is then given by

$$E = 250\beta^2 \quad \text{kev}$$

Estimates of λ and E for the three hooks in Figure 1 showing well-developed noses (*a, d, h*) are given in Table 3.

It is interesting to compare this theory with that of the TWT. In the exosphere, for a gyrofrequency model of electron density and for fairly slow particles, the latter gives rise to a constant or slowly changing frequency. It is only when the particle (or bunch) penetrates the ionosphere that the frequency increases rapidly. Thus the TWT theory explains narrow-band hiss, 'quasi-constant tones,' and hooks having a fairly constant frequency first part and a rapidly increasing second part. A nose might be produced with this mechanism if the TWT hook is reflected back along the line of force and observed in the opposite hemisphere. The hook shown in Figure 1(*H*) might be of this type. On the other hand, the theory presented here produces all the forms entirely in the exosphere. In addition, it can explain the other hooks shown in Figure 1. The TWT theory will not produce multiple hooks from successive particle mirroring, since particles having mirror points in or below the ionosphere will not survive. It seems, then, that both mechanisms operate. The TWT theory produces some of the observed forms with relatively slow particles (1 kev or less) of small pitch angle (for hooks). Our theory produces other forms with faster particles, which may have greater pitch angles. In both theories noses are produced by propagation and so can be used to determine the line of force associated with the particles. The above comments on the TWT theory also apply to MacArthur's gyrating proton mechanism.

Conclusions. The qualitative frequency-time form of many exospheric emissions is explained by this theory. Further, the theory does not require ionospheric effects to explain part of this form, as does the TWT type mechanism. In addition to explaining characteristics already observed, it predicts further points that would provide a test for the theory. Since radiation is produced only from electrons traveling *away* from the observer, local precipitation effects (aurora, absorption, X rays) will tend to occur in the hemisphere opposite that from which the radiation is observed. Observation of more than one similar hook produced by bunches making more than one trip would show that the hooks were generated in a region whose mirroring is possible (exosphere) and would give an independent measure of particle velocity to check the theory. Simultaneous observations at both ends of a line of force (conjugate point experiment) would be useful for checking this.

Acknowledgment. I am indebted to Professor G. R. A. Ellis, Physics Department, University of Tasmania, for many suggestions and discussions.

References

Dowden, R. L., A theoretical model of electron density along a geomagnetic line of force in the exosphere, *J. Atmospheric and Terrest. Phys., 20,* 122–130, 1961.

Gallet, R. M., and R. A. Helliwell, Origin of very low frequency emissions, *J. Research NBS, 63D,* 21–27, 1959.

Helliwell, R. A., and D. L. Carpenter, Whistlers-west IGY-IGC synoptic program, *SEL Final Rept.,* Stanford University, March 20, 1961.

MacArthur, J. W., Theory of the origin of the very low frequency radio emissions from the earth's exosphere, *Phys. Rev. Letters, 2,* 491–492, 1959.

McInnes, B. A., A study of ionospherics at Macquarie Island, *Australian J. Phys., 14,* 218–233, 1961.

Murcray, W. B., and J. H. Pope, Doppler shifted cyclotron frequency radiation from protons in the exosphere, *Phys. Rev. Letters, 4,* 5–6, 1960*a*.

Murcray, W. B., and J. H. Pope, Radiation from protons of auroral energy in the vicinity of the earth, *J. Geophys. Research, 65,* 3569–3574, 1960*b*.

Murcray, W. B., and J. H. Pope, Energy fluxes from the cyclotron radiation model of V.L.F. radio emission, *Proc. IRE, 49,* 811–812, 1961.

Santirocco, R. A., Energy fluxes from the cyclotron radiation model of V.L.F. radio emission, *Proc. IRE, 48,* 1650, 1960.

Smith, R. L., The use of nose whistlers in the study of the outer ionosphere, *SEL Tech. Rept. 6,* Stanford University, July 11, 1960.

(Manuscript received November 17, 1961.)

(*Reprinted from Nature, Vol.* 195, *No.* 4846, *pp.* 1085–1086, *September* 15, 1962)

Cyclotron Theory of Very-Low-Frequency Discrete Emissions

IT was recently shown[1] that the Doppler shifted cyclotron radiation from receding electrons would give the observed frequency-time shape of discrete very-low-frequency emissions. A further development enables information about these electrons to be deduced from this shape. Thus, electron energy (E), initial helical pitch angle (ψ_0), geomagnetic field line of occurrence (λ), and the exosphere electron density parameter[2], 'scale frequency' (f_a), are obtained from four parameters (two frequencies and two times) scaled from a spectrogram of the emission. Full details of this process will be published elsewhere.

As a demonstration, consider the 'hook' shown in Fig. 1*a*. The location of three points in the frequency-time plane unambiguously requires $E = 150$ keV, $\psi_0 = 68{\cdot}6°$, $\lambda = 61{\cdot}4°$ and $f_a = 527$ kc/s. To test the theory, 25 points were calculated from first principles using this information. The curve through these points is shown in Fig. 1*b*. Comparison shows excellent agreement.

The theory[1] explains other types of discrete emissions as special cases of 'hooks'. In particular, the theory predicted a repetitive type of emission not previously recognized. This occurs when the electron bunch survives several hemisphere to hemisphere traverses or 'bounces' between magnetic mirror points. The emission appears as a succession of similar hooks separated by the bounce period of the electrons. It is readily distinguished from whistler mode echoes of a single hook since successive hooks are not progressively more dispersed according to their order in the sequence. Since the observable radiation is unidirectional the hooks are received in opposite hemispheres alternately, that is, the sequence observed in one hemisphere is displaced half a bounce period from that observed in the other. This effect distinguishes the predicted emission from some other effect such as periodic injection of electrons.

Observation of this predicted emission showing a bounce period consistent with E, ψ_0, and λ scaled from the shape would be a crucial test of the theory both qualitatively and quantitatively.

A sequence which was probably of this predicted type was recently discussed[3]. It appeared as two

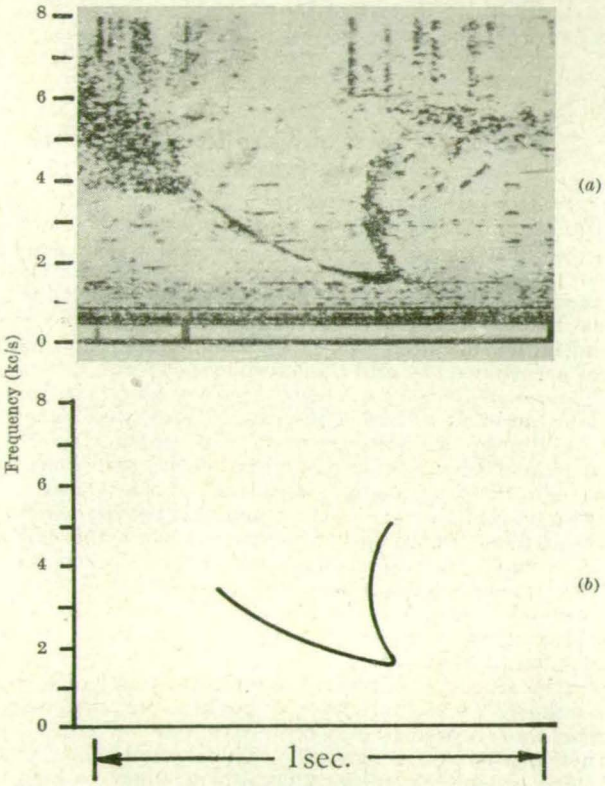

Fig. 1. *a*, 'Hook' recorded at Seattle, on September 23, 1957, at 2035 : 28 U.T. (after Helliwell and Carpenter, ref. 6) ; *b*, as calculated from the theory (ref. 1) for $E = 150$ keV, $\psi_0 = 68{\cdot}6°$, $\lambda = 61{\cdot}4°$ and $f_a = 527$ kc/s

bursts of 5–6 kc/s noise (presumably parts of a single hook) seen three times. It was observed in both hemispheres, not simultaneously, but alternately as explained here. Since only a narrow frequency band was observed the progressive dispersion criterion could not be applied. However, the recurrence period was consistent with a bounce period for electrons of typical energies as deduced from other hooks, but only a half to a third of typical whistler mode echo, delay times at this frequency. On the other hand, in a reply[4], Helliwell pointed out that whistler delay times can be sufficiently small during magnetic storms so that in this case the echo possibility cannot be ruled out.

I have since noticed four clear-cut examples published by Gallet[5]. In each of these there was a striking lack of progressive dispersion despite the

Table 1. Comparison of Observed Recurrence Period (P_0) with that Calculated (P_c) from E, ψ_0 and λ deduced from the Frequency-Time Shape

Sequence No.	No. of hooks in each sequence	Energy (E) (keV)	Helical pitch ψ_0	Geomagnetic latitude λ	Calculated period P_c (sec.)	Observed period P_0 (sec)
1	3	14	70°	59°	1·2	1·6
2	6	8	62°	59°	1·7	1·6
3	2	15	72°	59°	1·1	1·6
4	3	5	48°	59°	2·1	1·6

considerable frequency extent of the hooks and the relatively large number of separate hooks (six, in one sequence). Gallet[5] remarked on this at the time. Table 1 shows E, ψ_0 and λ deduced from the shape of one of the hooks for each sequence. The expected bounce periods calculated from E, ψ_0 and λ are shown as P_c and the observed periods (as measured by Gallet) are shown as P_0. The spectrograms as published[5] are rather small for accurate scaling so that the probable error in P_c is rather large. However, the general agreement is quite good.

The electron cyclotron theory gives excellent agreement with the observed frequency-time shape of discrete emissions. In addition, the predicted periodic emission is shown to occur and with periods reasonably close to those predicted. Verification of the theory not only clears up a mystery of long standing but also justifies the use of spectrograms of emissions for finding information about the electrons which produce them. Large numbers of such spectrograms were recorded during the International Geophysical Year.

I thank Prof. G. R. A. Ellis for advice.

R. L. Dowden

Ionospheric Prediction Service,
University of Tasmania,
Hobart, Tasmania.

[1] Dowden, R. L., *J. Geophys. Res.*, **67**, 1745 (1962).
[2] Dowden, R. L., *Nature* (in the press).
[3] Dowden, R. L., *Nature*, **195**, 64 (1962).
[4] Helliwell, R. A., *Nature*, **195**, 64 (1962).
[5] Gallet, R. M., *Proc. Inst. Rad. Eng.*, **47**, 211 (1959).
[6] Helliwell, R. A., and Carpenter, D. L., *Whistlers-West I.G.Y.–I.G.C. Synoptic Program* S.E.L., Final Rep., March 20, 1961 (Stanford University).

Printed in Great Britain by Fisher, Knight & Co., Ltd., St. Albans.

(*Reprinted from Nature, Vol.* 195, *No.* 4836, *p.* 64 *only, July* 7, 1962)

Very-Low-Frequency Discrete Emissions received at Conjugate Points

In a recent article[1] describing a geomagnetic conjugate point experiment an accurately synchronized pair of spectrograms was shown. As shown in Fig. 1 of that article a sequence of six noise bursts in the 5–6 kc./s. frequency region was observed at both Knob Lake, Canada (68° N., geomagnetic), and at Byrd Station, Antarctica (70° S., geomagnetic); but the sequence began at Knob Lake 0·8 ± 0·1 sec. before it began at Byrd.

However, close inspection of Fig. 1 indicates that in each case the sequence is not six separate bursts but a pair of bursts seen three times. In support of this it will be noticed that the shapes and separation of the two bursts in each pair are similar and in each case the first burst occurs at a slightly higher frequency than the second. Furthermore, the time separation between successive pairs (using the time-scale provided) is 1·6 ± 0·1 sec., which is just twice the delay between Knob Lake and Byrd. Thus at intervals of 0·8 sec. this pair of bursts appeared alternately at Knob Lake and Byrd.

This phenomenon cannot be due to successive reflexions in opposite hemispheres of electromagnetic energy because the observed time delays are too short. Whistler observations in these latitudes show 5 kc./s. propagation times between 1·5 and 2·5 sec. for a single hemisphere to hemisphere trip[1]. Even then these times refer to lower latitudes because geomagnetic field lines terminating at latitudes greater than about 62° do not allow 5 kc./s. propagation of this type[2]. Thus if this phenomenon were due to whistler type echoes the delays would be several times longer.

However, such a sequence of alternate reception at conjugate points was predicted in a theory proposed by me[3] for the production of very-low-frequency discrete emissions. In fact such a conjugate point experiment was suggested as a test for the theory.

According to this theory Doppler-shifted cyclotron radiation is emitted by a small cloud or bunch of electrons spiralling along a field line. Only the downward-shifted frequency can propagate so that radiation is only emitted backwards. If the bunch should survive several trips along the field line from hemisphere to hemisphere, being reflected at the ends by

magnetic mirror effect, then an observer at each end of the field line would receive an emission each time the bunch was travelling away from him. Thus for each observer the time between successive emissions would be the complete (there and back) oscillation period of the cloud and the delay between the sequences observed in opposite hemispheres would be half this period[3].

The complete oscillation period of 1·6 sec. from Fig. 1 (ref. 1) would correspond to 60 keV. electrons (for minimum helical pitch angles of 20°) if the guiding field line was that connecting the two observing stations or 15 keV. electrons if the guiding field line was typical of those (around 60°) producing nose whistlers observed at Byrd[2]. These electron energies deduced from the oscillation period (15–60 keV.) are close to those (5–25 keV.) required by my theory to produce the detailed frequency-time shape of observed discrete emissions[3].

I thank Prof. G. R. A. Ellis, of the Physics Department, University of Tasmania, for advice.

R. L. Dowden

Ionospheric Prediction Service
and Department of Physics,
University of Tasmania,
Hobart.

[1] Lokken, J. E., Shand, J. A., Wright, Sir C. S., Martin, L. H., Brice, N. M., and Helliwell, R. A., *Nature*, **192**, 319 (1961).
[2] Smith, R. L., *The Use of Nose Whistlers in the Study of the Outer Ionosphere* (Stanford Electronics Laboratory, 1960).
[3] Dowden, R. L., *J. Geophys. Res.*, **67**, 1745 (1962).

Printed in Great Britain by Fisher, Knight & Co., Ltd., St. Albans.

Author's Reply to the Preceding Discussion

R. L. DOWDEN

Ionospheric Prediction Service, Hobart, Tasmania

Brice has devised a method of testing one of the features of my [*Dowden*, 1962*a*] electron cyclotron theory of discrete VLF emissions: that the sequence of emitted frequencies is spatially symmetric about the top of the magnetic field line (geomagnetic equatorial plane). He has derived testing parameters which should be equal to unity for any sequence of successive whistler mode echoes of a hook beginning with the zero order or nonreflected hook. When this test was applied to four such sequences this parameter was of the order of three, quite significantly not unity. Brice concludes that my theory therefore cannot explain these hooks.

Now, using Brice's notation, it can easily be shown from his equation 2 that for symmetrical generation the theory predicts:

$$T_n - T_n' = (2n + 1)(T_0 - T_0') \qquad (1)$$

If these difference times are calculated from his Table 1, it will be seen that they are clearly not in the predicted ratio 1:5:9 for the first sequence and 1:3 for the other three.

On the other hand, it is rather striking that these ratios are none the less in a logical order. They are quite close to 3:7:11 for the first sequence and 3:5 for the other three. This suggests that in each sequence the first trace observed by Brice was not the zero-order, or non-reflected, hook but the first-order, or once-reflected, hook. Then each of Brice's tabulated values of n should be increased by one. Now we can resolve this by measuring the times between any two traces in a sequence at f_I and f_0. These are the propagation times for the appropriate number of complete hemisphere to hemisphere hops. Thus, using the first and third of the traces in Brice's Figure 1 we find $8\tau_0 = 4.10$ sec and $8\tau_1 = 3.72$ sec. Thus from Brice's equation 1, $T_0 - T_0' = 2(\tau_0 - \tau_1) = 0.095$ sec. This is approximately one-third the value tabulated by him. Consequently, for the first sequence at least we have clearly demonstrated that the first trace observed is the first-order, or once-reflected, hook. Thus, for this sequence Brice's tabulated values of n should be increased by one, and his testing parameters should be calculated from his equation 4. This is shown in Table 1.

Without having recourse to the original

TABLE 1

n	T_n, sec	T_n', sec	$T_n - T_n'$, sec	Predicted $T_n - T_n'$ Ratios	$\frac{n-1}{3}\cdot\frac{T_1 - T_1'}{T_n - T_1}$	$\frac{n-1}{3}\cdot\frac{T_1 - T_1'}{T_1' - T_n'}$
0	Not observed		0.095	1		
1	0.39	0.05	0.34	3		
3	0.57	−0.14	0.71	7	1.3	1.2
5	0.75	−0.31	1.06	11	1.3	1.3
0	Not observed		*	1		
1	0.16	0.03	0.13	3		
2	0.22	−0.03	0.25	5	0.7	0.7
0	Not observed		*	1		
1	0.35	0.02	0.33	3		
2	0.42	−0.07	0.49	5	1.6	1.2
0	Not observed		*	1		
1	0.17	0.02	0.15	3		
2	0.22	−0.03	0.25	5	1.0	1.0

* These missing values could be obtained from the original spectrograms.

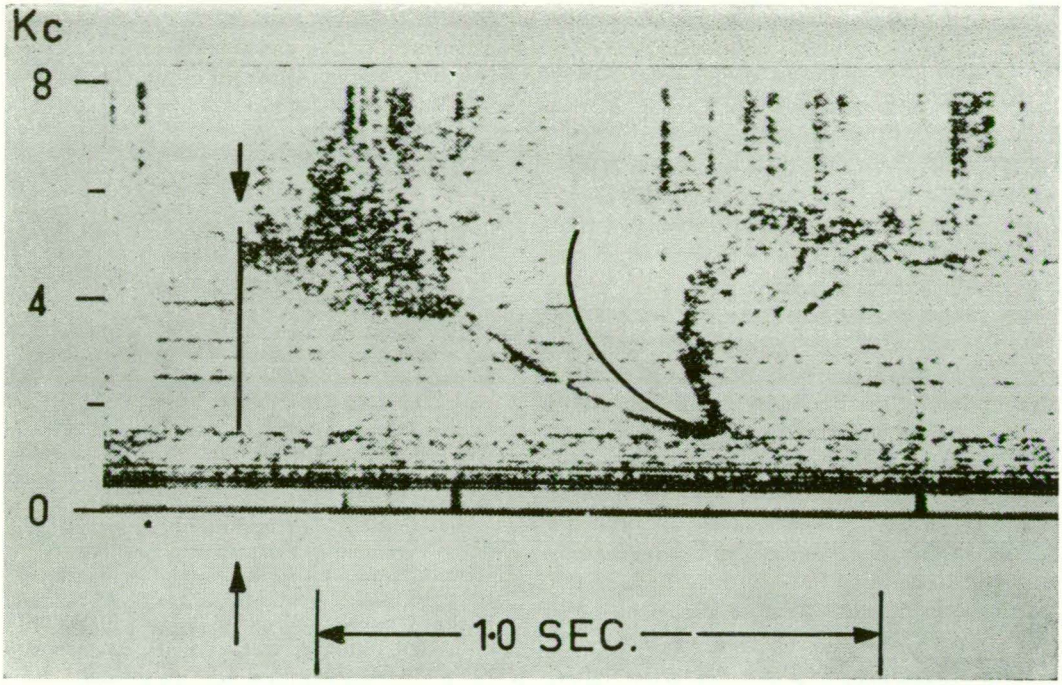

Fig. 1. Hook recorded at Seattle on September 23, 1957, at 20h 35m 28s UT (after *Helliwell and Carpenter* [1961]). Superimposed on this is a computed nose whistler originating from a hypothetical impulse at the top of the field line at the time shown by the arrow. Note that this computed curve is in the center of the hook at all frequencies.

spectrograms for the other three sequences, we cannot here make similar statements about these other three. Brice's statement that 'this ambiguity is removed if the hook and echo are observed at conjugate stations' is not strictly true. Although the zero order signals must have been reflected somewhere near one of the conjugate stations, they could have been missing from the spectrograms or at least not recognized as such for a variety of reasons.

However, we can say that Brice's first sequence unambiguously demonstrates the symmetry aspect of my theory in both the predictions that the $T_n - T_n'$ ratios should be close to 1:3:7:11 (from equation 1) and that his testing parameters should be close to unity. The other three sequences fit the theory if the same interpretation of n applies to these also (Table 1). Furthermore, this can easily be checked from the spectrograms as shown above for the first sequence. It should be noted that the remaining discrepancies in $T_n - T_n'$ and his testing parameter values are easily accounted for by errors in scaling the times T_n and T_n' of about 0.01 to 0.02 sec. This is quite reasonable since the widths of the traces are some 0.05 to 0.1 sec., as is seen in his Figure 1.

Another test of the symmetry aspect of my theory is now presented. It is a consequence of this symmetry feature [*Dowden*, 1962*b*] that the observed frequency-time distribution of a hook should be symmetrically spaced (in time) about a half-dispersed nose whistler. In other words, at any frequency the midpoint in time between the two branches of a hook should lie on a curve corresponding to the whistler mode dispersion of a hypothetical wide-band impulse originating at the top of the field line at the instant of generation of the lowest frequency. This is also the instant at which the emitting electron bunch passes through this point.

Consider the hook shown in Figure 1. Superimposed on this is the nose whistler originating from a hypothetical impulse at the top of the field line at the instant shown by the arrow. The frequency-time shape of this nose whistler was calculated from a function given by *Smith and Carpenter* [1961] which they have shown accu-

rately represents this shape. The frequency-time scale adopted corresponds to a nose frequency (f_n) of 4.60 kc/s (latitude of end point 61.4°) and a short whistler delay time (t_n) at this frequency of 1.64 seconds. This (f_n, t_n) is typical of moderately disturbed conditions [*Carpenter*, 1962] when generation of hooks is likely. Careful measurement of Figure 1 shows that this curve is accurately in the center of the hook at all frequencies as predicted.

It is interesting to note from this second test that the 'symmetry curve' or 'equivalent half short whistler' of any hook allows direct measurement of f_n (as in Figure 1) or estimation (when the nose does not appear) by the *Smith and Carpenter* [1961] techniques mentioned by Brice. These same techniques allow estimation of t_n for nonreflected hooks. Thus, in principle hooks give the same propagation information as whistlers. In addition, f_n locates the path of the emitting bunch, and $\frac{1}{2}t_n$ gives the instant the bunch passed through the top of this path. More convenient methods of scaling f_n and t_n, as well as methods for deducing electron energy and helical pitch angles, are given elsewhere [*Dowden*, 1962*b*]. Thus all the relevant information about the emitting electrons can be deduced from a spectrogram of a hook. Tests of other predictions of my theory are published elsewhere [*Dowden*, 1962*c*].

References

Carpenter, D. L., New experimental evidence of the effect of magnetic storms on the magnetosphere, *J. Geophys. Research, 66*, 2582–2586, 1961.

Dowden, R. L., Doppler-shifter cyclotron radiation from electrons: A theory of very low frequency emissions from the exosphere, *J. Geophys. Research, 67*, 1745–1750, 1962*a*.

Dowden, R. L., Method of measurement of electron energies and other data from spectrograms of VLF emissions, *Australian J. Phys.*, in press, 1962*b*.

Dowden, R. L., The cyclotron theory of VLF discrete emissions, *Nature*, in press, 1962*c*.

Helliwell, R. A., and D. L. Carpenter, Whistlers—west IGY-IGC synoptic program, *SEL Final Rept., Stanford University*, March 20, 1961.

Smith, R. L., and D. L. Carpenter, Extension of nose whistler analysis, *J. Geophys. Research, 66*, 2582–2586, 1961.

(Received July 12, 1962.)

Reprinted from the
AUSTRALIAN JOURNAL OF PHYSICS
VOLUME 15, NUMBER 1, PAGES 114–119, 1962

WIDE-BAND BURSTS OF V.L.F. RADIO NOISE (HISS) AT HOBART

By R. L. Dowden

WIDE-BAND BURSTS OF V.L.F. RADIO NOISE (HISS) AT HOBART*

By R. L. DOWDEN†

[*Manuscript received August* 15, 1961]

Summary

Wide-band bursts of radio noise from the upper ionosphere or exosphere have been observed at frequencies from 100 c/s to 250 kc/s. The observed intensity [Wm^{-2} $(c/s)^{-1}$] ranges from nearly 10^{-9} at 100 c/s to 10^{-19} at 250 kc/s. However, the intensity at the source (above the ionosphere), deduced by subtracting the losses suffered in the ionosphere and below the ionosphere, shows a relatively flat spectrum at a level of the order of 10^{-10} Wm^{-2} $(c/s)^{-1}$.

I. INTRODUCTION

V.L.F. noise, also known as " hiss " or geomagnetic noise, is audio-frequency radio noise originating in the upper ionosphere or exosphere which tends to occur at times of aurora and geomagnetic activity (Ellis 1959). It usually occurs in bursts of minutes or hours' duration. These bursts are usually narrow band (a few kilocycles bandwidth) centred at around 5 kc/s (Ellis 1959). Sometimes, particularly at times of strong geomagnetic disturbance, very wide-band bursts occur (Ellis 1959 ; Dowden 1960). Some very wide-band bursts have been observed covering a range of from less than 5 kc/s to more than 200 kc/s (Dowden 1960). Later observations (this paper) have followed these wide-band bursts down to less than 100 c/s so it seems likely that occasionally bursts spread over the range from 100 c/s or less to a few hundred kc/s—a frequency ratio of several thousand.

This paper examines the ground level intensities recorded at several spot frequencies (125, 240, 410, 760 c/s, 1·8, 4·3, 9·0, and 230 kc/s) during wide-band bursts observed at Hobart. The corresponding intensities at an arbitrary level above most of the ionosphere (550 km) are deduced from considerations of the losses affecting the wave from that level to the observing point.

II. EXPERIMENTAL

(*a*) *Techniques*

The receiving systems were broadly similar to those described elsewhere (Ellis 1959). A vertical loop antenna fed a wide-band amplifier followed by a narrow-band pass amplifier for each channel. Special techniques were used to avoid spurious effects of atmospherics and other impulsive noise.

In one recording system the detected outputs were applied to the vertical deflection plates of a C.R.O. During an impulse the C.R.O. spot would be deflected well off scale but between impulses the spot would be deflected only by

* Presented at the Conference on the Sun-Earth Environment, Brisbane, May 24–26, 1961.

† Ionospheric Prediction Service, University of Tasmania, Hobart.

continuous signal. When such a display is photographed by slowly moving film the continuous level between impulses is readily apparent.

The second system was developed by Ellis (1959) for recording on a pen recorder. This also records only the continuous level between impulses. In this method the detected outputs were applied to a partially unidirectional integrator. This had a long time constant of many tens of seconds for increases in signal but a very short time constant of some milliseconds for signal decreases. The system is thus the reverse of a peak-reading voltmeter.

Both systems give strong discrimination (of about 40 dB) against atmospherics even when the " mark-space " ratio of atmospherics is very high. In some cases both recording systems were used on the one frequency channel.

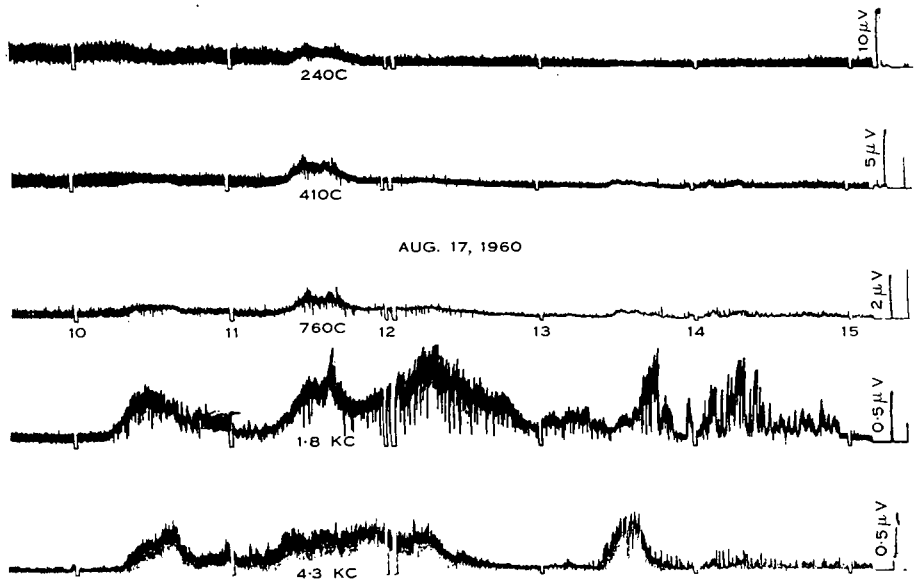

Fig. 1.—Typical wide-band (*c.* 1130 L.T.) and narrow-band bursts.

Further discrimination from any spurious effects follows from the nature of the phenomena studied. That shown in Figure 1 is fairly typical. The smooth rise and fall of amplitude during bursts, the duration of bursts (order of an hour), and the relative infrequency of bursts (around 10 per month), make the phenomena readily distinguishable from steady background noise or man-made bursts of interference.

Two basic methods of intensity calibration were used. In the first the loop antenna was replaced by a signal generator or noise generator of the same impedance. Burst intensities were then deduced from this receiver sensitivity calibration and the effective height of the loop antenna calculated from measurement of its physical dimensions. The second method gave direct calibration by generating a known field strength in the vicinity of the antenna from a remote auxiliary loop. Both methods gave consistent results. The calibration and reading accuracy (about 10%) was more than adequate for the argument presented in this paper.

Only six recording channels were available so that simultaneous recordings were not made at all eight frequencies mentioned above. However, there was sufficient frequency overlap to suggest that the wide-band bursts measured mainly at the higher frequencies were similar to those measured mainly at the lower frequencies.

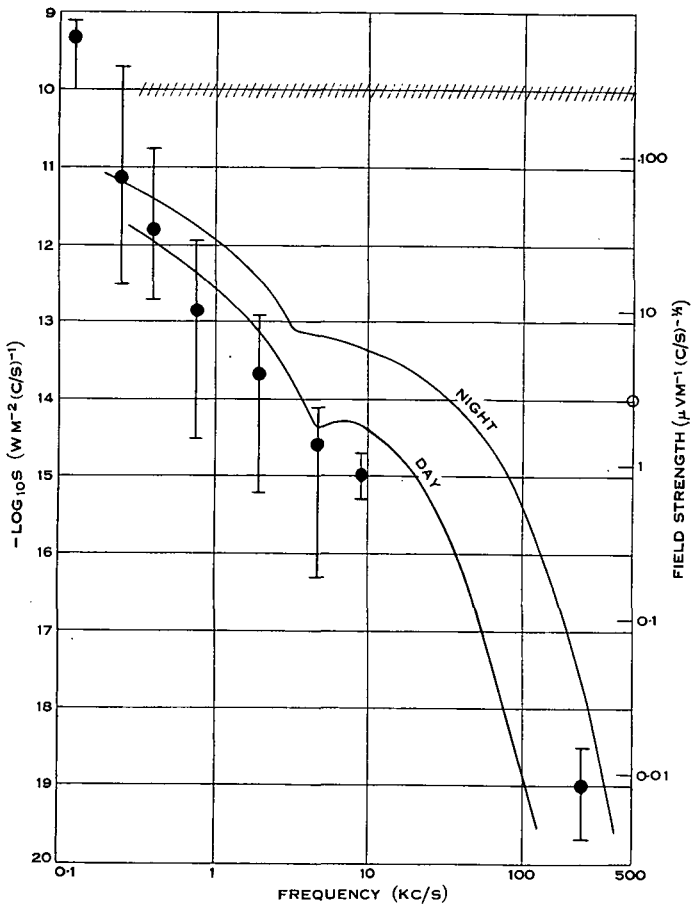

Fig. 2.—Medians and spread of peak intensities of observed wide-band bursts. Curves are expected ground intensities for a " white " source above the ionosphere at the hatched level [10^{-10} Wm^{-2} $(c/s)^{-1}$]. The right-hand ordinate is field strength.

Two sweep-frequency analysers covering the ranges 40–500 c/s and 400 c/s to 6 kc/s, though of less sensitivity and of restricted use for intensity measurement, were used to check the interpretation of the fixed-frequency records.

(*b*) *Observations*

Twenty-five wide-band bursts recorded over a period of about 15 months are considered here. Figure 1 shows one of these recorded on the five frequencies operating at the time. Other narrow-band bursts at around 2 and 5 kc/s are

seen on the same record. The median intensities and the spread of intensities recorded is shown plotted in Figure 2. Medians for 125 c/s and for 9·0 and 230 kc/s may not be truly representative, as less than five values were obtained for each. The burst signal to background noise ratio was best around the middle of the band (20 dB at 5 kc/s) but worsened in both directions to about 5 dB at 100 c/s and 10 dB at 200 kc/s.

III. Discussion

Although there is no strong evidence to indicate the level at which V.L.F. noise is produced, we will assume here that it is above most of the ionosphere, that is, above (say) 550 km. Directional and spaced observations (Ellis 1960; Dowden 1961) show that V.L.F. noise bursts often appear to be coming from virtual sources of quite small areas on the Earth's surface. Consequently we adopt the model that the burst is generated in a relatively narrow tube of force somewhere above the ionosphere, is then piped down through the ionosphere in the " whistler mode ", and radiated out under the ionosphere in the two-surface (Earth or ocean and ionosphere) waveguide to the observer. We require, then, the losses suffered in these two modes.

The Earth-ionosphere waveguide losses have been calculated by Watt and Maxwell (1957) for frequencies from 1 to 100 kc/s. Curves are given of field strength versus frequency for propagation over day-time and night-time sea-water paths of various distances for a unit " white " point source. In our case the distance between the virtual source and the observing point is not known for each burst but a typical median value can be estimated along the following lines.

Suppose all sources were point sources and that they were randomly distributed about Hobart. We consider an annular area centred on Hobart at distance r, width $\mathrm{d}r$, and area $\mathrm{d}A$. We define the probabilities: $p_s(r, \mathrm{d}r)$ of a source occurring within this annular area; $p_0(r, \mathrm{d}r)$ of it being observed at Hobart if it did occur; and $p_{0s}(r, \mathrm{d}r)$ of an *observable* source occurring within this area (within r and $r+\mathrm{d}r$). It follows:

$$\begin{aligned} p_s(r,\mathrm{d}r) &\propto \mathrm{d}A \propto r.\mathrm{d}r \\ p_0(r,\mathrm{d}r) &\propto \text{intensity on arrival at Hobart} \\ &\propto \mathrm{e}^{-\alpha r}/r \end{aligned}$$

where α = attenuation coefficient for the Earth-ionosphere waveguide mode.

$$\begin{aligned} p_{0s}(r,\mathrm{d}r) &= p_s(r,\mathrm{d}r)\cdot p_0(r,\mathrm{d}r) \\ &= \mathrm{e}^{-\alpha r}\cdot \mathrm{d}r. \end{aligned}$$

We define a median range $\bar{r}$ such that

$$\int_0^{\bar{r}} p_{0s}(r,\mathrm{d}r) = \int_{\bar{r}}^{\infty} p_{0s}(r,\mathrm{d}r),$$

that is

$$\frac{1}{\alpha}[\mathrm{e}^{-\alpha r}]_{\bar{r}}^{0} = \frac{1}{\alpha}[\mathrm{e}^{-\alpha r}]_{\infty}^{\bar{r}}.$$

Hence

$$\mathrm{e}^{-\alpha\bar{r}} = \tfrac{1}{2}.$$

The attenuation coefficient, α, is strongly frequency dependent, but typical values are around 3 dB per 1000 km (Watt and Maxwell 1957) so that the typical range ($\bar{r}$) will be around 1000 km.

Suppose instead the sources were very large so that everywhere in the vicinity of Hobart was essentially uniformly illuminated by each burst. We consider the same annular area described above. The total power intercepted by this annulus is proportional to its area,

$$dP_s(r) \propto r.dr,$$

Transmission over distance r to Hobart would decrease this by a factor $e^{-\alpha r}/r$, so that the power observed at Hobart from this area (from ranges r to $r+dr$) is then

$$dP_{0s}(r) = K.e^{-\alpha r}.dr,$$

K being a constant of proportionality. We define the median range $\bar{r}$ as that range within which half of the observed power occurs. Then

$$K\int_0^{\bar{r}} e^{-\alpha r}.dr = K\int_{\bar{r}}^{\infty} e^{-\alpha r}.dr.$$

Hence the same argument as that above leads to $\bar{r} \approx 1000$ km.

Selection of the $\bar{r}=1000$ km day and night curves of Watt and Maxwell gives us the below-ionosphere losses for the frequency range 1–100 kc/s. Those for frequencies outside this range are estimated by extrapolation.

The attenuations for whistler mode propagation through the ionosphere were obtained from curves by Helliwell (1958) using a model day-time ionosphere from 80 to 550 km given by Francis and Karplus (1960). Night-time attenuations were estimated from this model by disregarding the ionosphere below 100 km. The values found are roughly consistent with whistler mode echo observations (Dowden 1959) at 17 kc/s and observations of 512 kc/s signals from the ground made by a receiver carried in a rocket to a height of over 400 km (Mechtly and Bowhill 1960).

The losses for propagation through the ionosphere (whistler mode) and below the ionosphere (waveguide) are combined and plotted in Figure 2 for day and night conditions. We have assumed a " white noise " source of intensity 10^{-10} Wm^{-2} $(c/s)^{-1}$ at a level of 550 km. The curves thus represent the expected intensity at an observing station on the ground about 1000 km from the point immediately below the source. The accuracy of these curves deteriorates towards both ends of the frequency scale. The treatment used above breaks down at the low end because the distances involved approach a wavelength. At the high frequencies the attenuations are so large that small errors in the estimation of parameters become important. Both ends will suffer from the extrapolations.

It is seen from Figure 2 that the expected " ground level " spectrum resulting from this flat or " white " source spectrum fits the observed intensities to an order of magnitude or so, although an intensity proportional to wavelength

might give a better fit at the low frequency end. The main point emerging from this study is that much of the very strong frequency dependence of observed intensities is accounted for by attenuation.

Intensities of over 10^{-14} Wm^{-2} $(c/s)^{-1}$ at 512 kc/s have been observed at a height of 400 km by Mechtly and Bowhill (1960). This is a lower limit (receivers overloaded) and so consistent with our results. On the other hand, at frequencies above 900 kc/s, at times when the ionosphere above Hobart is transparent, ground level intensities (due to cosmic noise) of only 2×10^{-19} Wm^{-2} $(c/s)^{-1}$ are observed (Ellis 1957). This is some nine orders of magnitude less than our value. However, it must be remembered that very wide-band bursts are rare and occur only during very severe disturbances, whereas the ionosphere is transparent at low frequencies only during very quiet conditions. Nevertheless, this does show that, at least at the higher frequencies, a continuous high background level does not exist.

IV. Acknowledgments

The author is indebted to Professor G. R. A. Ellis of the Physics Department, University of Tasmania, for many interesting discussions, criticisms, and suggestions, and to Mr. G. T. Goldstone of the Ionospheric Prediction Service, Hobart, for building, operating, and maintaining the equipment.

V. References

Dowden, R. L. (1959).—*Nature* **183**: 385–6.
Dowden, R. L. (1960).—*Nature* **187**: 677–8.
Dowden, R. L. (1961).—*J. Geophys. Res.* **66**: 1587–8.
Ellis, G. R. A. (1957).—*J. Geophys. Res.* **62**: 229–34.
Ellis, G. R. A. (1959).—*Planet. Space Sci.* **1**: 253–8.
Ellis, G. R. A. (1960).—*J. Geophys. Res.* **65**: 839–43.
Francis, W. E., and Karplus, R. (1960).—*J. Geophys. Res.* **65**: 3593–600.
Helliwell, R. A. (1958).—Low frequency propagation studies, Part I. ASTIA Document No. AD110184 (Stanford University).
Mechtly, E. A., and Bowhill, S. A. (1960).—*J. Geophys. Res.* **65**: 3501.
Watt, A. D., and Maxwell, E. L. (1957).—*Proc. Inst. Radio Engrs., N.Y.* **45**: 787–94.

Printed by C.S.I.R.O., Melbourne

Simultaneous Observations of VLF Noise ('Hiss') at Hobart and Macquarie Island

R. L. DOWDEN

Ionospheric Prediction Service and the University of Tasmania
Hobart, Tasmania, Australia

Ellis [1960] showed that individual bursts of VLF radio noise associated with geomagnetic disturbances (also called 'hiss' or 'geomagnetic noise') are often fed into the ionosphere-earth waveguide structure at fairly well defined points. The geographical position of these virtual sources can be located by comparing noise intensities of three different stations [*Ellis*, 1961]. For each pair of stations there will exist a family of curves defined by

$$(r_2/r_1) \exp [-\alpha(r_1 - r_2)] = R$$

where R (a constant of each curve) is the ratio of the power intensities observed from a noise source distant r_1, r_2, respectively, from stations 1 and 2, and where α is the attenuation coefficient.

Data were obtained for the pair of stations Hobart–Macquarie Island at the two frequencies 4.3 and 9.3 kc/s for the 10 weeks from December 26, 1959, to March 3, 1960. Bursts recorded at both stations are listed in Table 1. It should be noted that the sensitivity of the receiver at Macquarie Island was much lower than that at Hobart, particularly at 9 kc/s. Only those bursts observed at both stations were considered. This tended to exclude 4-kc/s components that were not stronger at Macquarie Island and 9-kc/s components which were not very much stronger at Macquarie Island.

A map of the area showing Hobart and Macquarie Island, the auroral zone (hatched arc), and constant R curves for attenuation coefficients of 10 db/1000 km (full line curves) and 2 db/1000 km (dashed) corresponding to 4 kc/s and 9 kc/s propagation, respectively, is given in Figure 1. A 4-kc/s source occurring on the Hobart–Macquarie Island line would appear 10 db weaker at both stations if it were shifted

TABLE 1. Simultaneous Noise Bursts

Date	Universal Time	4 kc/s Intensity $Wm^{-2}(c/s)^{-1} \times 10^{16}$			9 kc/s Intensity $Wm^{-2}(c/s)^{-1} \times 10^{16}$		
		Hobart	M. I.	Ratio	Hobart	M. I.	Ratio
Jan 14	0500–1000	30	650	22			
15	2040	30	14	0.5			
Feb 1	1630	1.2	4.8	4			
2	1630–1715	1.2	1.2	1			
3	0450–1400	8.5	170	20	1.2	480	400
3	2125	13	120	3			
4	0200–1900	4.8	330	70	0.5	330	660
5	0530	2.1	19	9	<0.5	210	>400
6	0130	2.1	19	9	0.3	270	900
6	2330	0.5	19	36			
9	1315	3.3	480	140	0.3	270	900
19	2045	0.3	13	45	<0.13	120	>1000
19	2100	0.8	30	36	0.2	210	1000
26	1600	0.3	2.1	7	1.1	<3.3	<3
29	2235–2310	2.1	8.4	4			
Mar 1	2130	2.1	19	9			

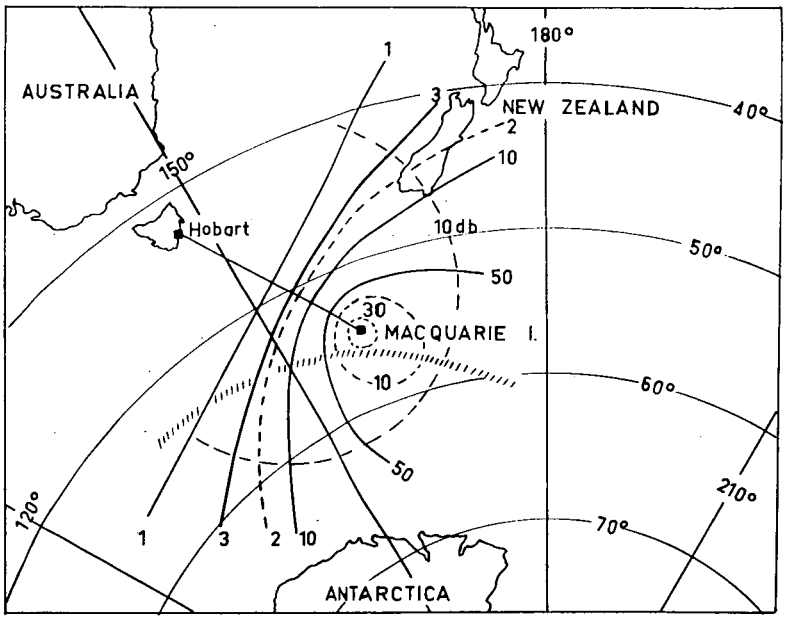

Fig. 1. Map of area showing constant intensity ratio curves for attenuation coefficients of 10 db per 1000 km (full-line curves) for 4 kc/s, and of 2 db per 1000 km (dashed) for 9 kc/s. The hatched arc is the auroral zone. Coordinates are geographic.

along a curve of constant intensity ratio to the dash semicircle marked '10 db.'

Independent 'fixes' of individual bursts are not possible without data from another pair of stations. All but one of the observed 9-kc/s components must have occurred well inside the R = 30 ring (Fig. 1). Little can be said about the positions of the 4-kc/s components except that they occurred on the appropriate curves and probably within the 10-db semicircle. However, two important points emerge. First, at 9 kc/s only sources of a few kilometers in extent could produce intensity ratios of 1000 even if the sources occurred overhead at Macquarie Island. This shows that some sources at least have very narrow dimensions. Second, it is immediately apparent from Figure 1 that for all but one (February 26) of the eight bursts observed at both frequencies, the source positions for the two components could not have coincided. In fact, the distances between these two source positions varied from at least 100 to 500 km.

Acknowledgments. This work also represented part of the research program of the Australian National Antarctic Research Expeditions at Macquarie Island. I wish to thank Mr. R. Levick for operating the Macquarie Island equipment, Mr. G. T. Goldstone for operating the Hobart equipment, and Professor G. R. A. Ellis, Physics Department, University of Tasmania, for much criticism and stimulating discussion.

References

Ellis, G. R. A., Directional observations of 5 kc/s radiation from the earth's outer atmosphere, *J. Geophys. Research, 65*, 839–843, 1960.

Ellis G. R. A., Spaced observations of the low frequency radiation from the earth's upper atmosphere, *J. Geophys. Research, 66*, 19–23, 1961.

(Received January 16, 1961.)